Technological Driving Forces and Barriers for the Dissemination of Degassing Technology in the Oil Industry

- The case of the DONG degassing plant

Master Thesis by
Thor-Bjørn Ottosen

UNIVERSITAS ROSKILDENSIS · IN TRANQUILLO MORS · IN FLUCTU VITA ·

DONG energy

Fact sheet

Title:	Technological Driving Forces and Barriers for Dissemination of Degassing Technology Within the Oil Industry
Subtitle:	The case of the DONG Degassing plant
Author:	Thor-Bjørn Ottosen
Hand-in date:	28th of February 2013
Supervisors:	Bent C. Jørgensen, *Physics* Ole Hertel, *Tek-Sam main supervisor* Anders Christian Hansen, *Tek-Sam secondary supervisor*
Module:	Integrated experimental master thesis (K-IES)
Department:	Department of Science, Systems and Models, Department of Environmental and Spatial Change
University:	Roskilde University

Abstract

This thesis examines the effect of installing the DONG degassing plant in 2009. The evaluation focuses on the environmental, technical and economic aspects of the technology. The effect of the degassing plant on the environment is evaluated through a tracer release experiment using acetylene(C_2H_2) as a trace gas to determine the change in emission as a result of installation of the degassing plant. This is used as a basis for modelling the VOC concentration distribution on the northern hemisphere using the DEHM model. The concentration data are subsequently used in a 1-D RCM for modelling the change in radiative forcing as a result of the installation of the DONG degassing plant.
The technical aspect is evaluated through a determination of the inherent availability and the energy-production relationship determined from production data.
The economic aspect is evaluated through a cost-benefit analysis with stakeholders being respectively the users of the oil pipe and the society.
Due to the small amount of measurements performed in the present project, the environmental effect of the installation of the DONG degassing plant remains inconclusive. Based on earlier measurements the modelling show a concentration change as a result of the change in emission of up to $10^{-4} ppm$ with the majority concentrated around Fredericia.
The inherent availability is shown to have been 96% in the period from the installation of the plant to August 2012, approaching 98% over time. The energy per produced to offgas is shown to be 0.58 $^{MWh}/_{ton}$.
The net present value of the installation of the degassing plant is shown to be approximately zero for the users of the oil pipe and positive for the society.

Nomenclature

BAT	Best Available Technique
BREF	BAT Reference
CBA	Cost-Benefit Analysis
CRDS	Cavity Ring-Down Spectrometer
CTM	Chemical Transport Model
DEHM	Danish Eulerian Hemispheric Model
DG	Directorate General
DIAL	DIfferential Absorption LIDAR
EFRT	External Floating Roof Tanks
ELV	Emission Limit Value
EPA	Environmental Protection Agency
GP	Gothenburg Protocol
GVA	Gross Value Added
HP	High Pressure
IPPC	Integrated Pollution Prevention and Control
LIDAR	LIght Detection And Ranging
LP	Low Pressure
MTBF	Mean Time Between Failures
MTTR	Mean Time To Repair
NCEP	National Centers for Environmental Protection
NECD	National Emissions Ceiling Directive

NMVOC	Non-Methane VOC
PAH	Polycyclic Aromatic Hydrocarbons
RCM	Radiative-Convective Model
RCM	Reliability-Centered Maintenance
RF	Radiative Forcing
RMSE	Root Mean Square Error
RVP	Reid Vapor Pressure
SCADA	Supervisory Control And Data Acquisition
TEU	Treaty on the European Union
TFEU	Treaty on the Functioning of the European Union
TOA	Top Of Atmosphere
UNECE	United Nations Economic Commission for Europe
VOC	Volatile Organic Compounds
WACC	Weighted Average Cost of Capital
WGS	World Geodetic System
WTA	Willingness To Accept
WTP	Willingness To Pay

Short table of contents

Contents

Chapter 1

Introduction

Since today's society is based on a fossil fuel economy in the form of cars and fossil fuel fired power plants, the oil industry has emerged over the 20^{th} century to supply the fuel needed for the economy. The oil industry structure is presented in schematic form on fig. 1.1. As can be seen, the oil industry is divided into an upstream section and a downstream section (sometimes supplied with a midstream section). The upstream section consists of a department related to exploration and production and a department related to crude oil transportation and storage. The downstream section consists of three departments related to respectively: upgrading and refining, product transportation and storage, and distribution and marketing. For the oil to reach the consumers in the form of gasoline, it has to pass all departments illustrated on fig. 1.1 from left to right. Moreover, a range of activities support the main activities just described. These are illustrated above or below the center-line of the figure. When a well is drilled in an oilfield the oil flows freely, known as "continuous flow". It is possible to slow down the production, but very difficult to stop the flow completely (Van Vactor, 2010, p. 110 & 117–122). However, the demand for oil is fluctuating, resulting in the need to store the oil in the production chain.
The present project will focus on the department related to crude oil transportation and storage, and the focus will be on the environmental impact resulting from these industrial activities.
For the storage process, various types of storage tanks have been used throughout the industry. As crude oil consists of a range of molecules ranging from methane as the smallest to large Polycyclic Aromatic Hydrocarbons(PAH), the lightest components of the crude oil will evaporate at atmospheric temperatures. This process is known as "separation", since oil and gas are separated. Since the evaporation rate of a liquid in a closed container is proportional to the vapor space (see section 4.1 for more info), the oil industry has reduced the evaporation of Volatile Organic Compounds(VOC) through the use of external floating-roof tanks, a construction which is illustrated in fig. 1.2. To minimize evaporation from the rim of the floating roof various types of sealant are used. Due to the wind and thereby the resulting pressure difference across the rim seal an emission will occur. Other emission mechanisms include thermal deformation of the tank shell, tank shell deformation due to liquid head (Nassar, 2012),

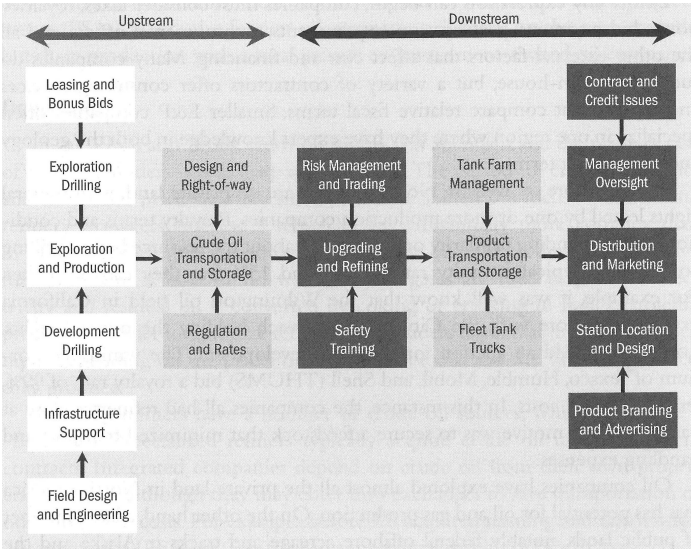

Figure 1.1: Schematic overview of the oil industry(Van Vactor, 2010, p. 119)

breathing losses, solubility losses, and wicking of the liquid (U.S. Environmental Protection Agency, 1995). The VOC's are mainly alkanes of length one to seven (Spectrasyne Ltd, 2009), and directly or indirectly these compounds are greenhouse gases (see chapter 6 for more info). Moreover, they also constitute a problem for the health of the surrounding population.

Although the amount of evaporation per cubic meter of transported crude oil is very small, considering that approximately 90% of the Danish crude oil is passing through the nine storage tanks used at the DONG oil terminal (comparison of DONG Oil Pipe (2010) and Larsen (2010)), the Fredericia oil terminal still generates a considerable amount of atmospheric emissions.

As can be seen in figs. 1.3a and 1.3b, the emissions from the Fredericia oil terminal are one of the large sources within the fugitive sector, with respect to both Non-Methane VOC (NMVOC) and methane.

The fugitive sector is responsible for 12% of the national NMVOC emission and 2% of the national methane emission, based on numbers from 2009 (Plejdrup, 2012), which is the year the degassing plant was commissioned. The numbers for the Fredericia terminal are calculated numbers.

Comparing to other sources of NMVOC and methane, the emission from the Fredericia terminal is approximately 20% of the NMVOC emission and approximately 150% the methane emission from the total road transport in Denmark, based on numbers from 2006 (comparison of Plejdrup (2012) and Winther (2008)), which is before the installation of the degassing plant.

Comparing to public electricity and heat generation, the emission from the Fredericia terminal is approximately 20% for methane and approximately 200% for NMVOC respectively, based on numbers from 2008 (comparison of Plejdrup (2012) and Nielsen et al. (2010)). Again, the numbers are from before the installation of the degassing plant.

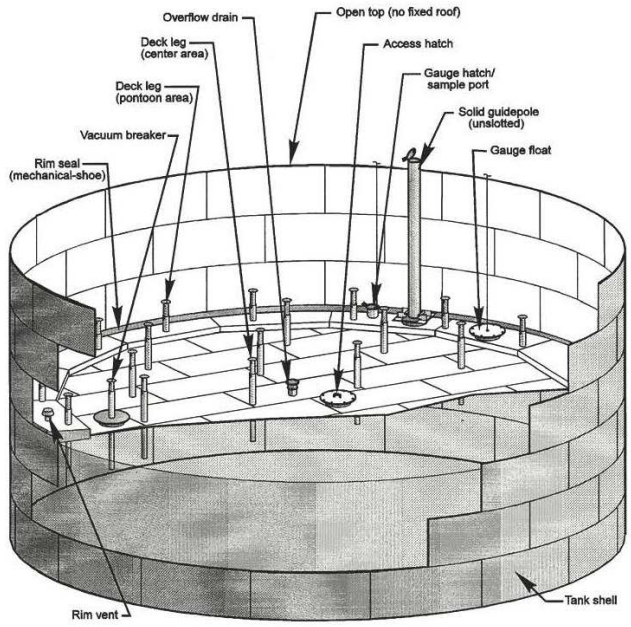

Figure 1.2: Schematic drawing of an external floating roof tank(U.S. Environmental Protection Agency, 1995, p. 7.1-43)

This means that the Fredericia oil terminal is a large single source of emissionss with respect to both NMVOC and methane[1].
The emission is a result of the production of crude oil in the Danish part of the North Sea. Since the oil production is expected to continue for the next few decades the emissions can likewise be expected to continue (Larsen, 2010).
To reduce the emissions from the Fredericia Oil Terminal, DONG[2] decided to install a degassing plant, which was inaugurated in 2009 (more details on the background for the installation and the preceding analyses in section 2.2).

The degassing plant at the Fredericia Oil Terminal is quite unique, since there are only a few of its kind in the world. When making the initial design, the engineers had to travel to Oman where a similar plant has been built. This means that very little research has been done on this issue, thus from a research point of view, the implications of using the technology are interesting.
As described in section 2.3, large industrial facilities are supposed to use the best available technique (BAT) to obtain an environmental permit. To guide the industrial facilities in the determination of BAT, a series of BAT Reference (BREF) documents has been published by the Joint Research Center.
The degassing technology as described in this report is neither mentioned in the BREF on Emissions from Storage (the European IPPC Bureau, 2006) nor in

[1]This exposition is based on the numbers supplied to the municipalities by DONG Oil Pipe A/S. An alternative calculation of the emissions will be presented in section 8.1.1 meaning that these proportions will change.
[2]Meaning DONG Oil Pipe A/S.

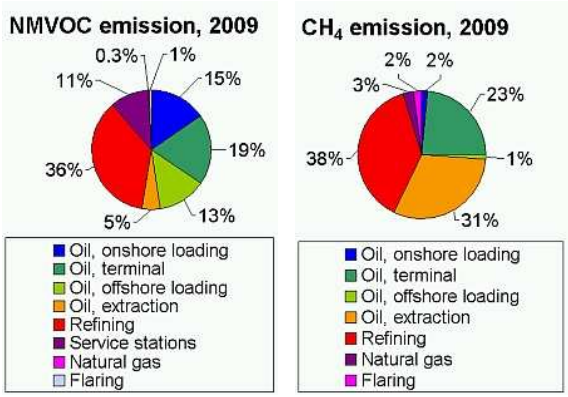

(a) Distribution of NMVOC-emission sources in the fugitive sector in Denmark in 2009

(b) Distribution of CH_4-emission sources in the fugitive sector in Denmark in 2009

Figure 1.3: The relative size of the sources of NMVOC and CH_4 in the fugitive sector in Denmark in 2009Plejdrup (2012).

the BREF on Best Available Techniques for Mineral Oil and Gas Refineries (the European IPPC Bureau, 2003a) although it contains sections on emissions from EFRTs.

The BREF on Mineral Oil and Gas Refineries is, at the time of writing, subject to revision, and the present research should be seen as a contribution to this process. At the time of writing there are no plans for revision of the BREF on emissions from storage.

The degassing technology is closely related to the vapor recovery technology, the main principle of which is illustrated in fig. 1.4. However, where degassing is "actively" making the oil evaporate through e.g. applying a vacuum or heating the oil, vapor recovery is a system to collect vapors generated "passively" as a result of tankage operation.

After the installation of the degassing plant, a survey to document the environmental effect of the plant was undertaken in September/October 2009, using a DIfferential Absorption LIDAR system to determine the emission of methane(CH_4), Non-Methane VOC (NMVOC)(C_2+), and benzene (C_6H_6), as a representative for the PAH fraction (Spectrasyne Ltd, 2009). Since this survey was undertaken shortly after the inauguration of the degassing plant, the results might not be representative of the longer term operation of the facility. Moreover, the crude oil flow through the system has been declining since the installation of the degassing plant, meaning that the preconditions for the degassing plant have changed (DONG Oil Pipe, 2012). Furthermore as part of a good practice, a long term evaluation of the degassing plant should be undertaken. Since Spectrasyne Ltd (2009) is solely an environmental evaluation, a need for a more interdisciplinary evaluation arises. It is thus the aim of this report to supply this evaluation.

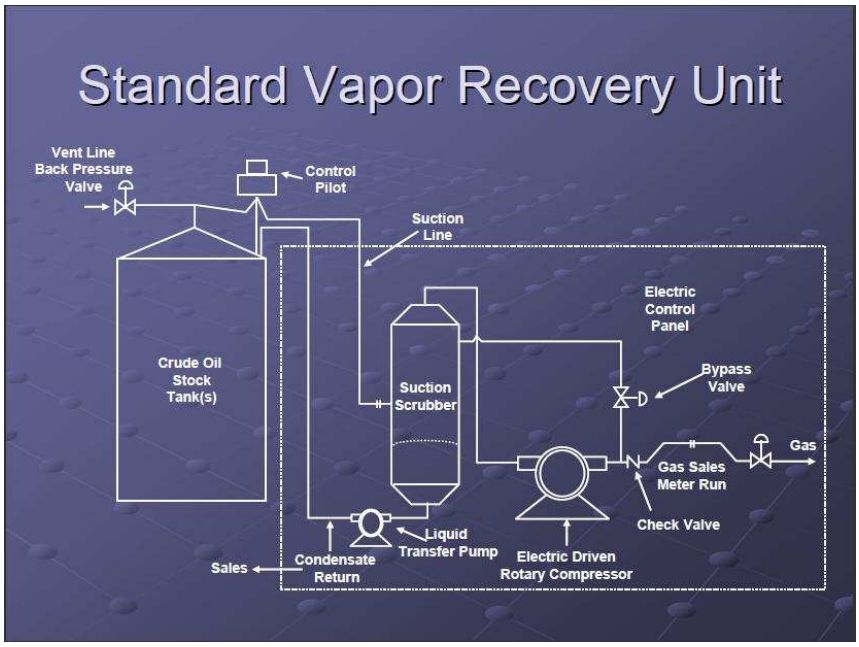

Figure 1.4: Schematic drawing of a vapor recovery system for a fixed roof tank (`www.vaporrecoveryunits.net`)

1.1 Research question

The project will be written from the point of view of the DONG degassing plant, as a representation of degassing technology in general.
The framework of the project will be the possibility of disseminating this technology to the general oil industry, and whether or not this is a likely and/or desirable future outcome.
The underlying assumption is, the economical incentives hypothesis, stating that "technological innovation [and as a result technological diffusion] takes place in response to economic incentives" (Smith, 1990, p. 6) (comment in brackets added by the author).
This simplified view of technological diffusion is, of course, complicated by the lack of information, which means that technological diffusion is, in reality, not such a linear process.
Based on this framework, the research question of this project will be:

> **What are the environmental, technical, and economical driving forces and barriers, related to the degassing technology itself, for dissemination of degassing technology, exemplified by the DONG degassing plant, in the global oil industry?**

The aim of this project is thus to evaluate the effect of the plant in a holistic manner. The focus on environmental, technical and economical aspects of this plant is also in line with the approach taken in the regulation (the European

IPPC Bureau, 2006, p. 112).
The research question of this report can be elaborated on in the following way:

- As described in section 2.2, the degassing plant was expected to obtain an environmental effect as a result of a certain amount of expenditure. The degassing plant is thus an environmental initiative, and analysing the environmental effect of the degassing plant is thus a prime focus of the project. The environmental part can be split into the following subsidiary goals:
  - As a first subsidiary goal, the aim of the environmental part of the project is to analyse the positive effect, which the installation of the degassing plant had, in the form of reduced emissions from the storage tanks, and the influence of the operating mode of the tanks on said emissions.
  - Moreover, the second aim of this project is to analyse the effect of the degassing plant on the greenhouse effect in the form of negative radiative forcing[3] (the arguments for this choice are presented in section 1.2).
- Since this project is based on an interdisciplinary approach, looking at the technical aspect of the degassing plant will be important. The technical part will aim at determining the achieved availability and the energy/production relationship of the degassing plant. These two factors were chosen, due to the fact that they are quantifiable from the available production data, as opposed to e.g. safety and working environment. Moreover, the availability and the energy/productions relationship are assumed to be the most important driving forces for technological dissemination.
- The economical aspect will aim at analysing the economic effect of the the degassing plant, seen from the perspectives of the users of the oil pipe (the oil producing companies) and the society.
- It is furthermore the aim of the project to analyse the errors and uncertainties, related to the above mentioned analyses, and their influence on the the validity of the conclusion.

1.2 Project scope

During the research process of this report, certain choices about the direction of the project had to be made. In the following section the arguments for these choices will be presented:

[3] "The radiative forcing of the surface-troposphere system due to the perturbation in or the introduction of an agent(say, a change in greenhouse gas concentrations) is the change in net(down minus up) irradiance (solar plus longwave; in Wm^{-2}) at the tropopause AFTER allowing for stratospheric temperatures to readjust to radiative equilibrium, but with surface and tropospheric temperatures and state held fixed at the unperturbed values" (Original emphasis) (Ramaswamy et al., 2001, p. 353).

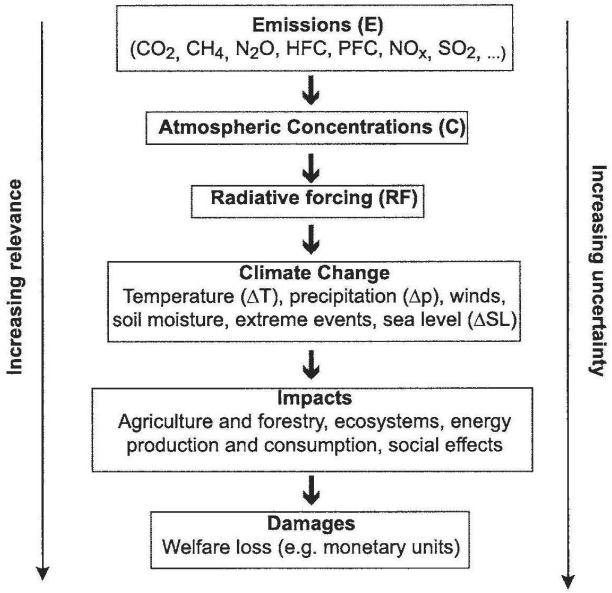

Figure 1.5: Cause-effect chain of emissions to climate change. For simplicity it is assumed that all climate effects happen through radiative forcing. The author is however aware of other impact routes e.g. changes in vegetation structure causing climatic effects resulting directly from changes in carbon dioxide concentration Fuglestvedt et al. (2003).

- The effect of VOCs on human health is not investigated in the current project. There are adverse health effects of Polycyclic Aromatic Hydrocarbons (PAH) and benzene (Carlsen, 2009), but benzene as a representative of the aromatic fraction is only emitted in small amounts (approximately 0.2% of the emission before the installation of the degassing plant and approximately 0.5% of the emission after the installation of the degassing plant according to Spectrasyne Ltd (2009)) compared to the alkanes from the Fredericia storage terminal (Spectrasyne Ltd, 2009).
  The alkanes, especially ethane (Carlsen, 2009), also have negative health effects. Moreover alkanes can react with NO_x and in this way act as an ozone precursor. This posses a health issue, since ozone is toxic to humans and plants (Williams and Koppmann, 2007). However, since little is known about the connection between the atmospheric concentration of alkanes and the effect on the public health, an assessment of the consequences for the public health of the installation of the degassing plant would be very complicated and time demanding and is therefore left out of the project.
  Moreover, a focus on public health would make the atmospheric chemistry of VOCs a very important aspect in the project. This is especially true because the reaction rate for the specie in consideration becomes very important for the concentration modelling and thus for the health impact. As described in section 6.1, the atmospheric chemistry is one of the largest

sources of uncertainties in atmospheric dispersion models. Therefore, and since this project is not a chemistry-project, this is an additional argument for leaving the health aspect of the problem out of the project. The health aspect is however taken into account in chapter 8 but only indirectly in the form of unit prices for emissions.

- The effect of the installation of the DONG degassing plant on the greenhouse effect is assessed through a calculation of the negative change in radiative forcing resulting from the change in emission. This choice is made as a balance between certainty and relevance as illustrated in fig. 1.5.
  Moreover, moving towards increasing relevance on the cause-effect chain also means increasing complexity in calculation. Radiative forcing is a first-order indicator of the effect of a specific emission on the climate "without the need for complex and computationally demanding climate models" (Fuglestvedt et al., 2003, p. 275).
  To obtain an accurate picture of the effect of a climatic perturbation, a lot of different processes would have to be taken into account in the modelling process e.g. radiative processes, feedback mechanisms, ocean currents, etc. There are uncertainties related to the parametrisation of all these processes. The more processes included in a climate model the larger the uncertainties of the model, but the greater the relevance, as illustrated in fig. 1.5.
  When studying very small climatic perturbations, the uncertainties of the model quickly become larger than the perturbation itself, meaning that no climate signal can be detected. As such, radiative forcing is a well suited choice of climate indicator since it permits calculation using less complex modelling approaches and thereby smaller uncertainties. In this context no assumptions are made about the efficacy[4] of the calculated forcing (Fuglestvedt et al., 2010, p. 4656).

1.3 Target group

The target group of this project is other researchers in the field benefiting from the exploration of a new research area within atmospheric emissions and from the description of the experimental design that could be used for other cases. Researchers in climate change might also benefit with respect to the interplay between atmospheric emissions and climate science. A third group who might benefit from this report would be decision makers in the oil industry with respect to knowledge about the advantages and disadvantages of degassing technology. Readers of chapters 4 to 6 are expected to have a certain background knowledge of mathematics, since mathematics like differential equations and integration by parts are used without further explanation. Moreover, a fundamental knowledge of the physics of the greenhouse effect and fundamental thermodynamics is assumed in these chapters.

[4]The effect of a specific radiative forcing in relation to the effect of the forcing of a CO_2 doubling (Fuglestvedt et al., 2010, p. 4656).

1.4 Overview of the report

In chapter 2 the problem analysis of the present situation is presented. The focus here will be: an interdisciplinary exposition of the legislation, the technical background of the construction of the plant, and the Danish oil transport system, of which the DONG degassing plant is a part. Moreover, a review of previous research in the field will be given in this chapter.
Chapter 3 will cover the methods used in the project.
The theory used, as a basis for the understanding of the evaporation process and as a basis for the modelling and experiment, is presented in chapter 4.
The details of the atmospheric and climate modelling are presented in chapter 6.
In chapter 5, the design, including modelling of the setup used to measure the emission from an EFRT, is explained. Moreover, the results of the various sub-experiments are presented. As part of this, a simple Gaussian plume modelling of the emission from one of the tanks at the Fredericia Oil Terminal is performed. This model was presented and the used code developed as part of the course "Air pollution – models and management" and, as such, doesn't represent new work performed in connection with the present project. This part of the model is therefore not described in any further detail.
The technical analysis, consisting of both the availability and the energy/production relationship, is performed in chapter 7.
The economical analysis is presented in chapter 8.
The report is concluded in chapter 9.

As part of this project, the designed setup had to be installed at the Fredericia Oil Terminal. In order to obtain permission to install the equipment, a safety approval had to be obtained from the operator of the terminal. In order to describe the experimental work in a compressed form and in a form to be understood by people without an academic degree, an experiment description was produced. As an illustration of the logistical challenges related to this project the experiment description is attached in appendix A.
In order to minimise the amount of appendices, the source code developed in relation to this project is attached on a cd. To ease the readability of the report, important equations are marked with a box around the equation.

Chapter 2

Background

This chapter will account for the regulatory and the physical environment, in which the degassing plant is operating, plus the history of the decision process leading to the present situation. This is important in order to provide an understanding of the cause and development of the emission and what solutions would be feasible in relation to the problem.
Moreover, this serves as a foundation for the understanding of why the preferred solution was chosen and as a benchmark with which to compare the analyses presented in chapters 5, 7 and 8.
A review of previous work in the field is also presented in this chapter to put the present study into context.

2.1 The Danish crude oil transport system

As the DONG degassing plant is part of the larger crude oil transport system, a short overview is given here with the purpose of providing an understanding of the process.
Most of the produced crude oil from the Danish sector in the North Sea passes the oil pipe from the platform Gorm E ending at the oil terminal in Fredericia. The oil is pumped from Gorm E, passing through a 220 km offshore pipeline, ending at the Filsø onshore pumping station. Subsequently the oil passes through a 110 km onshore pipeline ending at the Fredericia oil terminal. The oil is owned by a range of companies[1], according to the production from the individual fields and distribution of ownership, and transported by DONG Oil Pipe A/S.
The transport of the natural gas from the producing fields takes place in a separate system consisting of a gas transport pipeline from the Tyra rig to Nybro gas treatment plant. The locations of the rigs and the pipelines are illustrated on figure 2.1.

[1] Mærsk Olie og Gas A/S, Shell, Chevron, DONG E&P Nor, DONG E&P DK and Bayerngaz.

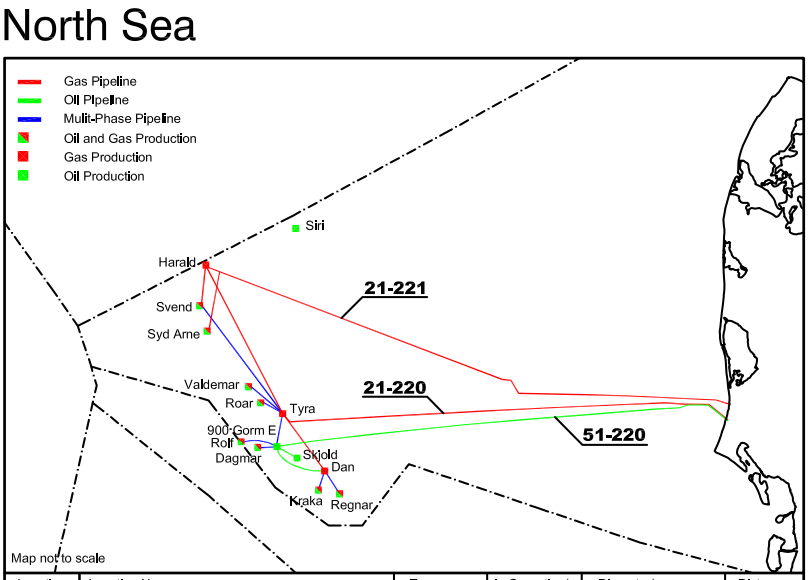

Location Map ID	Location Name	Type	In Operation/ Notes	Diameter/ Pressure	Distance Km
21-220	**North Sea Gas Pipeline**		1984	**30" /138 bar**	**214**
21-221	**Syd Arne - Nybro Søledning**		1999	**24" /150 bar**	**285**
-	**Tyra - Harald (Operated by Mærsk)**		-	**24" /138 bar**	**77**
51-220	**North Sea Oil Pipeline**			**20" /95 bar**	**220**
900	Gorm E	Platform	1984		

Figure 2.1: Map of the major oil fields and the oil- and gas pipelines in the danish sector of the north sea (Map courtesy of DONG Naturgas A/S).

2.1.1 Gorm E

The Gorm E pumping platform is operated by Mærsk Oil and owned by DONG Oil Pipe A/S. Gorm E consists of seven pumps to provide the pressure needed to generate a reasonable flow in Fredericia, where a pressure valve is located to prevent gas from being created at the high points of the oil pipe.
Before entering the export pumps, the oil goes through a separation process located at other parts of the Gorm platform, as illustrated in fig. 2.2. The oil first passes a high pressure (HP) separator operating at 8–10 bar, then a low pressure (LP) separator operating at 1–1.5 bar, and lastly a separator called V-3601, located at the Gorm E sector of the platform, operating at 1 bar. The average retention time in the separators is 20–30 seconds (Jensen, 2012). A separator uses the difference in density between oil and water, and the fact that light components of the oil will evaporate as a result of thermodynamic conditions to separate oil, gas, and water (water and gas being produced as by-products in the oil production).
The gas separated in the HP and LP separators is exported to Nybro gas treatment plant via the Tyra platform. The gas separated in V-3601 is led to the flare, however this amount is small compared to the gas separated in the HP and LP separators (Jensen, 2012). According to the use permit, the gas has to have

an RVP (Reid Vapor Pressure) of 0.83 bar, which has been settled according to assessments of the emissions from the storage tanks at the terminal.

As the oil flow has been decreasing over the recent years, the Filsø pumping station is mostly running in bypass mode. Moreover, no process equipment related to stabilisation of the oil is located at the Filsø pumping station, and it will thus not be described in any further detail.

2.1.2 Fredericia oil terminal

The Fredericia oil terminal is operated by A/S Dansk Shell. The degassing plant is located here, so the oil is further stabilised before entering the external floating roof storage tanks. The gas separated from the crude oil in the degassing unit, is subsequently sold to the refinery and used as fuel gas. The refinery is located next door and is owned and operated by Shell Fredericia.
When exported from the storage tanks, the oil is either transferred to the Shell Fredericia refinery for refining or exported over the Fredericia harbour. The transport equipment from the oil terminal to the harbour is owned by Shell Fredericia. Fredericia Harbour owns the area where the exporting facilities are located.
The degassing plant is constructed as a large (approximately $1250m^3$) horizontal two-phase separator (COWI, 2006). The principle of a two-phase separator is illustrated in fig. 2.3. The oil is pumped into the degassing vessel V-9601, and the average retention time is roughly 20 minutes, which is considerably longer than for the separators at the platform.
The vessel is designed to withstand a vacuum of 0.2 bar, but the actual applied vacuum is 0.1 bar (Christensen, 2006). This vacuum is applied by a compressor, hereafter the gas is compressed and transported to the discharge separator V-9602. In this vessel the gas is cooled, whereupon it is exported to the Shell refinery fuel gas system. Condensate from the gas/liquid separator V-9602 is drained back to V-9601. A combination of valves ensures that the compressor runs at a constant level, meanwhile keeping the oil level and vacuum level in V-9601 constant (Ørum Nielsen, 2008).
The degassing plant is equipped with a pressure sensor to measure the pressure in the degassing vessel, a mass flow meter to measure the amount of exported offgas to Shell, and a set of oxygen meters to measure the oxygen content of the exported gas since oxygen in the exported gas possesses a safety hazard.

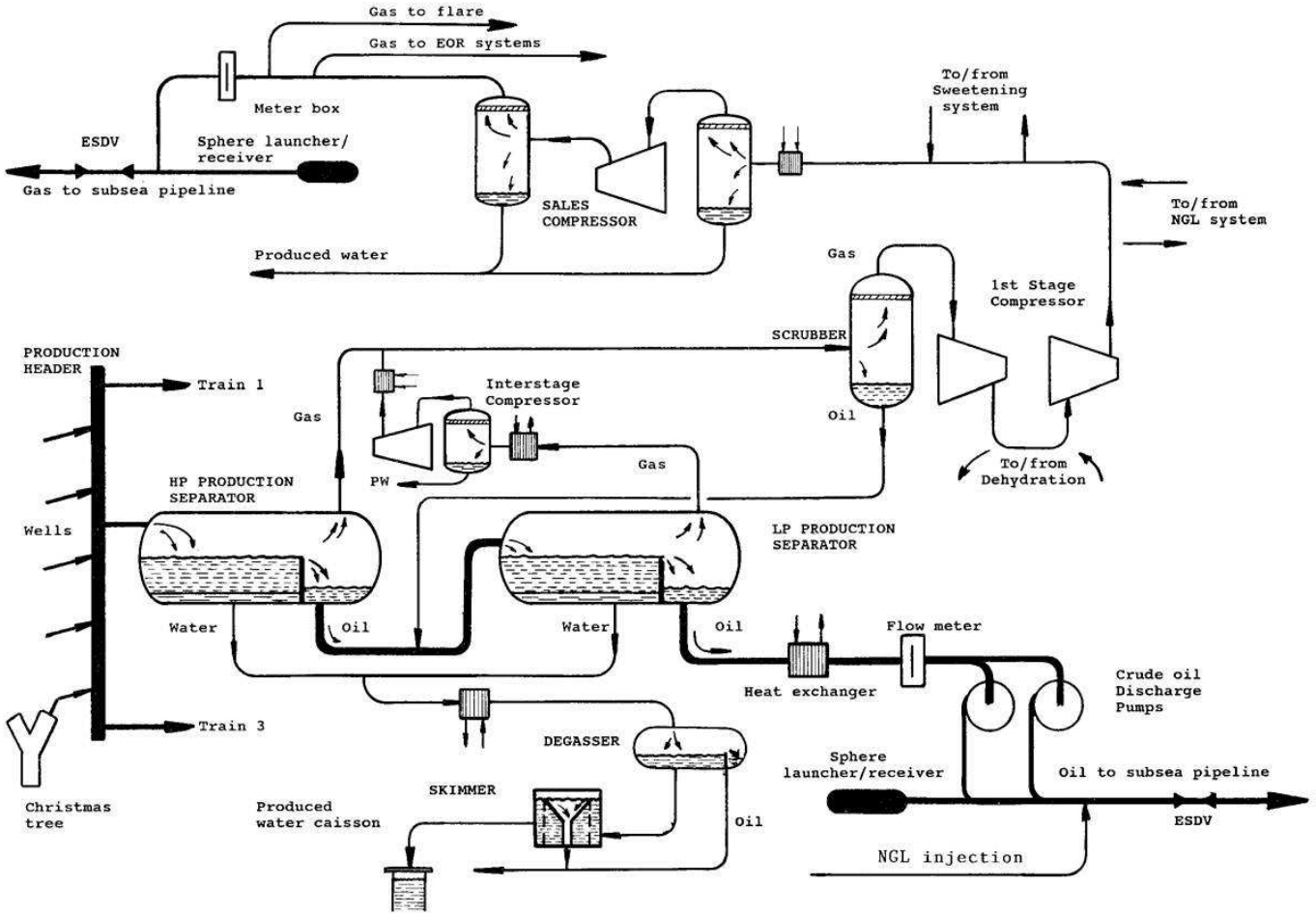

Figure 2.2: Illustration of the separation principle applied at the Gorm E rigMaersk Olie og Gas A/S (2012).

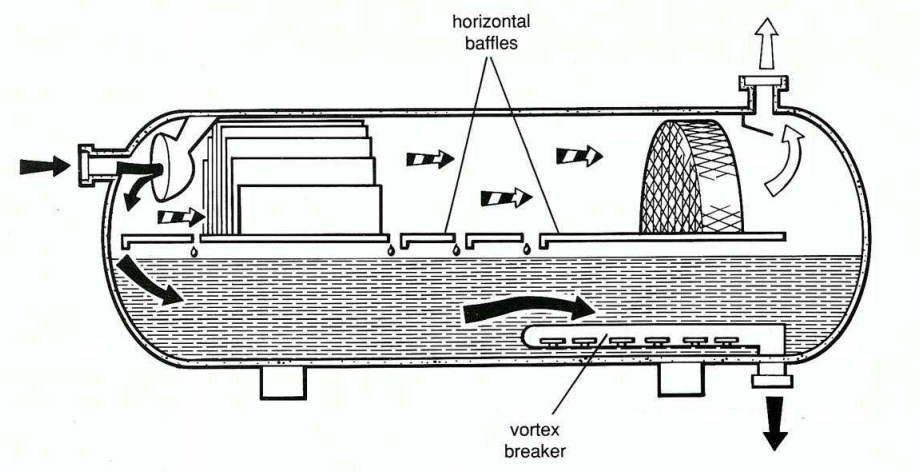

Figure 2.3: Illustration of the working principle of a two-phase separatorMaersk Olie og Gas A/S (2012).

2.2 The preconditions for the construction of the degassing plant

The historical development, leading to the construction of the DONG degassing plant in 2009, was a relatively long process to reduce the VOC emissions from the petroleum activities in Fredericia. In the years 1996-1999 an experimental vapor recovery unit was installed at the harbour.
The municipalities demanded, in the year 2000 environmental permit, that Shell Fredericia analyse how reductions in the emissions from the harbour area could be made. In 2001, as part of the routine maintenance of the crude oil storage tanks at the Fredericia oil terminal, Motherwell Bridge Ltd did an inspection of the tank roofs. The results of this investigation indicated large amounts of gas trapped beneath the floating roofs. This was concluded due to the dishing of the roofs plus oil seeping onto the roof through welding cracks and so forth. This posed both an environmental and a safety issue (Higgins and Johnstone, 2001).
In the fall of 2001 the first emission measurement was performed by Spectrasyne Ltd using LIDAR technology. These measurements indicated potential problems with the stabilisation equipment offshore. After investigating the cause of the high emissions, changes were made on the platform and a new LIDAR measurement was requested (Spectrasyne Ltd, 2009).
In 2003 the tax municipalities rejected the application of duty exemption of the district heat coming from the vapor recovery unit, which made the project unprofitable.
Prior to the decision on the construction of the degassing plant, a number of reports threw light on various aspects of the degassing plant. In the following sections these reports are briefly summarized.

2.2.1 Emissions Study – Legislative Review

The report (Smyllie, 2003) is a review of the relevant legislation that the authorities could use to demand DONG Oil Pipe to reduce the emissions from the Fredericia oil terminal. The aim of the report is to answer the question, "Why should capital be invested to minimise VOC emissions?" (Smyllie, 2003, p. 1). The question is answered through an assessment of the relevance of the available legislation to the case of DONG Oil Pipe:

The Gothenburg Protocol

The United Nations Economic and Social Council (UNECE) Gothenburg Protocol (GP) aims at reducing the acidification and ground level ozone through establishment of national emission ceilings for NO_x, VOC and ammonia. Since Denmark is a signatory to the protocol, Denmark is obliged to reduce the emissions of VOC by 52% in the period 1990 to 2010.
Furthermore there are industry specific environmental limit values, however, these are assessed not to apply to DONG, since they are mainly related to industries falling under the European Commission Solvent Emissions Directive. Moreover, a cost per ton of VOC, for the last abatement measure in order to meet the national emission ceiling limit, is provided corresponding to DKK 2111/t.
All of this leads to the conclusion that it is likely that the authorities would demand a reduction in the VOC emissions from the Fredericia terminal to meet the national emission ceiling, also considering that the abatement cost falls close to the stated figure. However, it is also possible that this could be met through other policy measures, as this has not been discussed with the Danish Environmental Protection Agency.

The National Emissions Ceiling Directive

Apart from the UNECE GP the European Union has agreed on the National Emissions Ceiling Directive (NECD). The NECD and UNECE GP emissions ceiling for VOC for Denmark are the same, and it is thus considered complementary legislation (Smyllie, 2003, p. 6).

The IPPC Directive

In Smyllie (2003), it is stated that in the EU the IPPC directive is the primary piece of legislation controlling emissions from certain industrial activities. For the analysis it is assumed that the Fredericia oil terminal falls under the IPPC directive, or if not, would be required to follow the principles of BAT. The essence of BAT being that techniques to improve the environmental performance are used, as long as they are not imposing disproportionate costs to the operator (Smyllie, 2003, p. 9).
The IPPC directive works through a system of certification where the industrial installations have to apply for an environmental permit regularly. Moreover, a set of guidelines are produced, describing what the best available technique is in certain circumstances, however, no directly applicable benchmarks, mass emission limits, or emission limit values are presented in these guidelines. The

IPPC Directive concludes that, "There is no clear statement that would require DONG to reduce emissions, but there are possible clauses that could be interpreted in a way to require DONG to reduce emissions" (Smyllie, 2003, p. 13).

The fact that the measured emissions are significantly higher than the reported emissions, means that the authorities might require DONG to reduce the emissions from the actual level to the reported level.

2.2.2 Emissions Reduction Study at the Fredericia Terminal

In this report (Smyllie et al., 2003), the options for reducing the emissions of VOC are analysed with respect to technical and economical criteria. To reduce the emissions from the tanks, two types of approaches are identified in the draft BREF note on Emissions from storage (the European IPPC Bureau, 2002), the BREF note for the chemical sector on treatment of waste gas (the European IPPC Bureau, 2001), the CONCAWE BREF document for refineries (Alfke et al., 1999), and the EC DG report on controlling emissions from ships (Rudd and Hill, 2001). The two approaches are:

- Stabilisation before the crude oil enters the tanks.
- Tank doming with gas collection and treatment.

It is argued in the report that tank doming is not a technically viable solution since tank doming creates a vapor space above the floating roof tank. Since the development of vapors from the crude oil is determined by the atmospheric temperature, the speed of the vapor development is hard to control. Moreover vapor is only created when filling the tank, which means it will be dependent on the operational state of the tank.
However, the largest problem with this solution is that the vapor space expands as the tank is emptied. To fill out this vapor space, gas has to be pumped into the tank. In order not to create a fire hazard, the gas has to be either nitrogen or VOCs from a source e.g. a vapor return line from the harbour. However, since a vapor return line would have to be run under the sea and at 5–6 meters depth in places, this would make the option prohibitively expensive.
Lastly, doming only one tank would mean that all crude oil had to pass this tank before entering the terminal meaning that the operational flexibility of the terminal would be greatly reduced. Contrary to this, doming all tanks would correspond to one tank being out of service for a period approaching 18 months. Considering the above mentioned arguments, it is concluded that tank doming is not a feasible solution.
Considering the option of stabilisation, "DONG has been advised that further stabilisation offshore cannot be achieved" (Smyllie et al., 2003, p. 1). This means, that some form of stabilisation at the Fredericia Oil Terminal has to be developed. This has the advantage that it is a controlled stabilisation of the crude as opposed to the uncontrolled stabilisation in the tank doming option. Moreover, stabilising the crude oil at the terminal means that the gas is not mixed with other gases in the process, thus less process intensive purification

would be needed.
After the crude oil has been stabilised, a range of options for the use of the offgas was considered:

- Generating combined heat and power using a gas turbine.
  Advantage:
  Gas turbines can achieve high energy efficiencies.
  Disadvantages:
  Gas turbines have to be operated at constant load for maximum efficiency. Moreover, in periods of low offgas flow from the degassing plant, supply fuel would have to be used either from the refinery or from another source. The gas produced in the refinery is significantly different from the offgas produced in the degassing plant. This would make the substitution between the two fuel types difficult.
  Lastly, utilising the heat in the Fredericia district heating scheme would require quite a bit of pipework to be done and this would make the solution expensive.

- Power generation using a gas turbine.
  Advantage:
  Simpler solution since no pipework to utilise the excess heat has to be laid out.
  Disadvantage:
  Lower energy efficiency.

- Combined heat and power using a gas engine.
  Advantage:
  One of the main advantages of using gas engines over gas turbines is that the load of gas engines can be adjusted such that a high energy efficiency can be obtained over a wider range of gas flows.
  Disadvantages:
  Gas engines have lower availability than gas turbines due to their greater complexity. This means that more money has to be spent on maintenance in this solution as compared to a solution with gas turbines.
  Using the excess heat from gas engines, requires the same pipework as described above for gas turbines. However, for gas engines the heat has to be disposed of in some way, meaning that in the three months of the year where the district heating system doesn't need any input, the heat has to be disposed of through large radiators, thus creating extra expenses for the project.

- Power generation using a gas engine.
  Advantage:
  Simpler solution since no pipework to utilise the excess heat has to be laid out.
  Disadvantage:
  Lower energy efficiency.

- Steam generation.
  After a discussion of the technical possibilities of this solution the report

concludes, "Steam boilers offer a good synergy between the refinery and the terminal and therefore represents a good solution that would represent BAT"(Smyllie et al., 2003, p. 55)

- Destruction of emission by ground flare.
  Advantage:
  The report states that an elevated flare will not be a possibility due to the visibility of the flare. Since the flare will burn with a smoky flame, it is unlikely to be accepted by the municipalities. However, a ground flare represents a simple and inexpensive solution.
  Disadvantage:
  There might be difficulties in reaching the emission limit values with respect to CO and NO_x using a ground flare.

- Destruction of emission by thermal oxidiser.
  Advantage:
  Better chance of meeting emission limit values.
  Disadvantage:
  Thermal oxidisers are usually used to handle gas with low concentrations of organic vapor. This means that this option is neither practical nor economical.

- Destruction of emission by thermal oxidizer and heat generation for district heating.
  Advantage:
  Some of the thermal energy could be recovered if using a hybrid thermal oxidiser and ground flare thus obtaining a higher energy efficiency.
  Disadvantage:
  Again this would require pipework to connect to the Fredericia district heating system thus making the project more expensive.

- Supply fuel gas to refinery.
  Advantage:
  This would be the simplest (and therefore possibly cheapest) solution among the solutions considered.
  Disadvantage:
  The report states that the refinery had stated that supplying additional fuel would result in a risk of increased flaring. The refinery gas balance is made such as to minimize the need to flare and this has been agreed upon by the municipalities. The report states, "For the purpose of this study it has been assumed that simply supplying the refinery with fuel gas is not viable (...)"(Smyllie et al., 2003, p. 56).

In this way, the various possibilities for collecting and using the gas are reviewed.

Through the lifetime of the refinery it goes through a number of maintenance cycles. After each cycle the refinery is shut down for maintenance, where, among others, catalysts are replaced in a process known as "regeneration". In the period approaching regeneration the refinery produces extra gas, which is the reason for the conclusions stated above. After regeneration the gas production drops,

making extra gas intake possible. This leads to the decision of stabilising the crude before entering the tanks and exporting the separated gas to the Shell refinery.

2.2.3 VOC Emissions in the Fredericia Area

The aim of the report (Gullick et al., 2005) is to investigate the impact of installation of a degassing unit on the terminal and on the harbour emissions. In order to model the impact of the degassing plant, a number of crude oil samples are collected at the Fredericia Oil Terminal. These are subsequently analysed to represent the evaporation behaviour in Hysys, a program used for chemical engineering simulation. The oil sampling is only representative for the crude oil arriving at the Fredericia terminal during the sampling period and does not account for any seasonal or other variation.
The results of the Hysys model are then used in combination with the US EPA TANKS model that simulates the emission from storage tanks based on an input of the chemical composition of the stabilised liquid in the tank in combination with a range of parameters representing the state of the tank. The liquid is stabilised to -0.2 barg[2]. Moreover, the simulation is based on the terminal design flow. The TANKS model is mainly developed for reporting emissions to the municipalities. Therefore, it is only accurate for the total emission and for the species most important in regulation such as benzene and toluene. The simulated emissions are subsequently compared with the measured emissions reported in Spectrasyne Ltd (2002). The results show a 99% reduction for the eight DONG tanks, in use at the time, from 7751 t/y to 88.2 t/y.

2.2.4 DONG Terminal Degassing Plant Operating Pressure Review

As a further detailing of the report (Gullick et al., 2005), the report (Smyllie et al., 2005) aims at describing the quantity of gas produced, the impact the loss to fuel gas will have on the quantity of oil, and the residual emissions from tank and ship loading, as a function of degassing pressure. Moreover, this is converted into a managerial economics analysis through multiplying the produced gas by a fixed gas price of DKK 805/t gas. The diminished oil production is multiplied with respectively 20 $/bbl[3], 30 $/bbl, and 40 $/bbl to analyse the effect of variations in oil price. The electricity used by the degassing plant is multiplied by a price of DKK 0.5/kWh. Furthermore, the analysis rests on a number of assumptions:

- Stabilisation to 1.0 bara[4] is representative of the current situation. This scenario is thus not recalculated.
- Operating the degassing plant in a mode between 0.6 bara and 1.0 bara is not considered to effect the capital expenditure on the facility.
- The capital investment has been assumed to be DKK 60 million.

[2]Relative pressure in *bar* as compared to atmospheric pressure.
[3]bbl = blue barrel, ≈ 159L
[4]bara = bar absolute – measured pressure + atmospheric pressure

- It is assumed that the Shell refinery has the capacity and need to take all the fuel gas produced in the degassing plant.
- It is assumed that the current emissions to the atmosphere are lost anyway, and so should not be counted as lost crude revenue.
- The operating costs are assumed to be DKK 5,061,100/y based in Gullick et al. (2005).

In order to produce the vacuum required to separate the oil and gas, a certain amount of power consumption has to be used. To calculate this, Hysys is used to determine the power consumption needed to produce a certain degassing pressure, and the results are shown in table 2.1. These numbers will be used for comparison with the technical analysis presented in chapter 7 and the economical analysis presented in chapter 8.
The results of the study are shown in figs. 2.4 and 2.5. The emissions reported on the figures are larger than the ones presented earlier since the emissions in the figures include emission reductions obtained at the harbour as a result of the installation of the degassing plant. In fig. 2.5 a project lifetime of 15 years and a 6% discount rate has been assumed in order to annualise the prices.
From fig. 2.4 it can be seen that most of the emission is reduced at an operating pressure of 0.9 bara. Moreover, as the pressure is further decreased, the expenses, in the form of lost crude oil revenue, increase faster than the incomes, in the form of revenue from gas sales. From fig. 2.5, the connection between oil price and degassing operating pressure can be seen. It is clearly seen that the higher the oil price the more important the degassing operating pressure becomes.

2.2.5 Environmental permit

The municipalities, in what was Vejle Amt, had to give an environmental permit to the degassing plant, before the operation could start. Two documents describe this process namely Christensen 2005 and Christensen 2006.
In Christensen 2005 the municipalities' assessment, of whether the DONG degassing plant produces the accepted reduction of VOC emissions, is described. It is the municipalities' opinion that the project will have a very high environmental impact. The optimal pressure in the degassing plant is, however, dependent on the crude oil composition, which has been determined with a great degree of

Degassing pressure (Bara)	Power (kW)
0.90	64.7
0.85	90.0
0.80	120.0
0.75	156.1
0.60	323.9

Table 2.1: Excerpt from table of power consumption as a function of degassing pressure based on (Smyllie et al., 2005, p. 11).

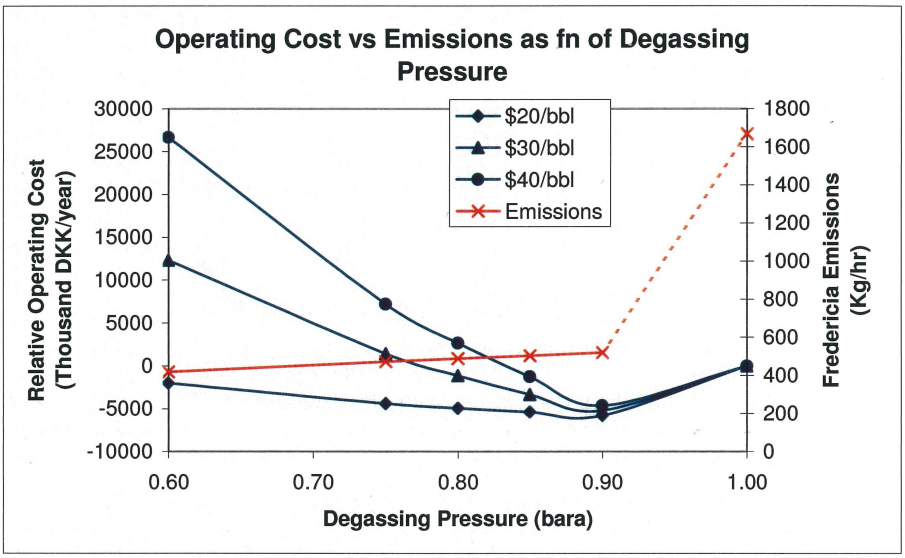

Figure 2.4: Operating costs and emission as a function of degassing pressure (Gullick et al., 2005).

uncertainty and possible seasonal variations are not known.
It is recommended that the operational pressure will always be at least 0.1 bar vacuum. The municipalities assessment' is based on the EU commission's material related to the implementation of the Gothenburg Protocol, where a price of up to 1800 Euro for one ton VOC emission abatement is presented. These numbers are based on calculations for gasoline and are as such not directly comparable. Most VOC reductions will however be possible for a price of less than 500 Euro (3750 DKK) per ton VOC. Compared to a price of 3200 DKK for the DONG degassing plant, it is concluded that, "it is socioeconomic sound to invest in VOC-reduction using DONGs planned Degassing Plant" (translation by the author). Later on it is concluded, "it is the municipalities assessment, that the described Degassing Plant project should be realised as soon as possible, since the expenses to VOC-reduction are fair in relation to the achieved reduction"(translation by the author). It can thus be seen that the economics of the VOC-reduction played a very important role in the municipalities assessment of the DONG Degassing plant.

In the environmental permit (Christensen, 2006) the requirements to the degassing plant are specified. The requirements are:

- The pressure in the degassing vessel should always be at least 0.9 bara.
- Latest one year after installation, DONG has to measure the total VOC emission from the terminal. The method and time has to be agreed with the control authorities.

Due to the difficulties of determining the VOC content in the oil, no requirements for the amount of removed VOC are set. The requirements are, however, that as

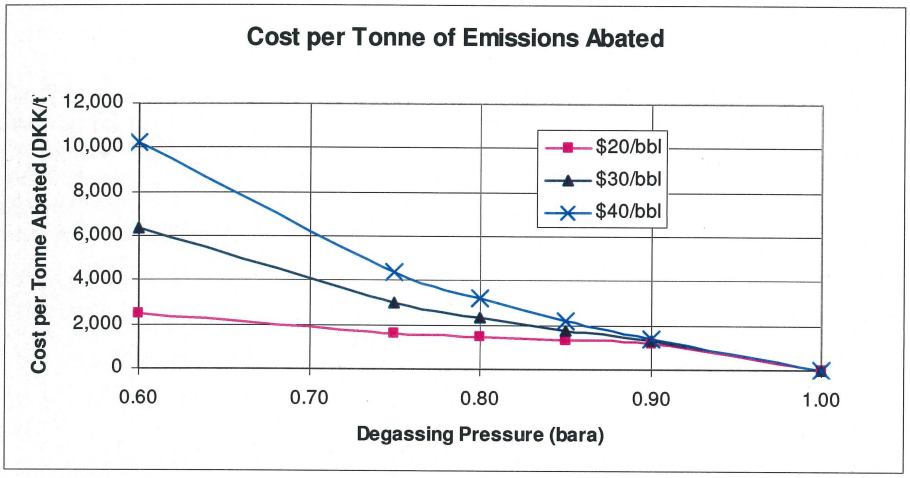

Figure 2.5: Annual cost per tonne emission abated (Gullick et al., 2005).

much VOC as possible is removed considering the design of the plant. Moreover, it is stated that the expected downtime is approximately 2%. DONG is required to inform the municipalities about downtime and the causes for downtime.

2.3 Regulation of emissions of VOC

The following section will describe the mechanisms used for regulating emissions of VOC. Since most of the emission regulation takes place at the EU level, the section will start with an introduction to the types of regulation and the nature of EU law in section 2.3.1. This is to ease the understanding through a description of the framework surrounding the important directives with respect to VOC. The important directives are thus described in sections 2.3.2 to 2.3.4.

2.3.1 Introduction to regulation in the EU

When describing EU law, the two key points of interest are: to what degree the law is binding, and whether the law is directly applicable in the individual member states, or whether it has to be implemented in the national legislation to be effective.
In the EU, the framework for the law making process is stated in the treaties[5] agreed upon by the heads of state and confirmed through national constitutional processes leading to treaty ratification. The framework describes in which areas the EU has competencies to regulate, and which areas are left to the member states (TFEU article 3-6). A policy area can either be:

- Regulated exclusively by the EU as e.g. customs policy.
- Regulated by shared competencies between the EU and the individual member states as e.g. environmental policy,
- Regulated by the individual member states supported by the EU as in e.g. tourism policy (Weatherill, 2010, p. 28–35).

Two fundamental principles surround EU law: Supremacy and direct effect. The two principles are established by the EU court. The principle of supremacy means that if an EU regulation and a national regulation on the same topic exists in a member state, the legal document adopted by the EU shall have supremacy over the legal document adopted by the member state. This is also stated in the Lisbon treaty but only as a declaration, which means it isn't legally binding. Moreover, it is stated in an annex to the declaration that although it is not included in the treaty, it is still existing and is a reality as case-law[6].
The principle of direct effect means that as soon as a legislation act is agreed upon in the EU, it is in force in the member states (Weatherill, 2010, p. 82). As opposed to e.g. national law in Denmark, when interpreting the EU legal documents, it is only the text in the documents themselves that forms the basis of the interpretation (Moe, 2011, p. 310)
The EU legislation acts can take five different forms (TFEU Article 288) (Weatherill, 2010, p. 30):

- A regulation is a document directly agreed upon by the EU, which is directly applicable in all member states. Thus a regulation need not have any national implementation in the member states in order to exist.

[5]The latest being the Treaty on European Union (TEU) and the Treaty on the Functioning of the European Union (TFEU). The two treaties are commonly known as the Lisbon Treaty.
[6]Law based on court rulings.

- A directive is legally binding in all member states, but must be transformed into national legislation by the national parliaments. It is up to the national parliaments to decide the form and method through which the directive is implemented. The transposition must be completed normally within two years and must comply fully with all the main elements of the directive (Clemmensen et al., 2007, p. 92). The Commission verifies that the member states implement the directives timely and correct (Moe, 2011, p. 312).
- A decision is legally binding. A decision need not be addressed to all member states.
- Recommendations and opinions are not legally binding

In the EU and in most industrialised countries the environmental regulatory framework has five main stages:

- The law.
- Standards for the use of technologies and/or standards for the environmental quality.
- Licenses or permits to allow industrial facilities to operate
- Monitoring of compliance with the law and the license.
- Enforcement of the law and conditions included in the license. In the EU, the enforcement of the law is delegated to the member states (Moe, 2011, p. 313).

In the EU, the law consists of the treaties. This is in the environmental area supplemented with respectively the IPPC Directive (96/61 EC), the NEC Directive (2001/81/EC), and the air quality directive (2008/50/EC). The license or permit is a tool to link every single industrial activity to the law and is thus the implementation of the law. The monitoring is the follow-up check to make sure the license, and thereby the law, is obeyed. Enforcement is enacted when non-compliance is observed (Clemmensen et al., 2007, p. 92).

2.3.2 The IPPC Directive

The following section is based on (Clemmensen et al., 2007, p. 91-101). In the European Union, industrial activities account for a large part of the environmental impact. Since the environmental area is an area subject to shared responsibility between the EU and the individual member states, it means that the small and medium sized companies are regulated by the member states, whereas the large industrial installations are regulated by the EU. A range of sectors with potentially high environmental impact is listed in Annex I of the directive. The industrial activities listed in Annex I are prohibited until they have obtained an environmental license. This is to make sure that the environmental authorities are not met with an existing situation, where large investments are needed to modify or change an established industrial installation due to environmental

reasons.
The IPPC Directive is based on the principles stated in the EU treaty (Article 174):

- The Principle of prevention.
- The Principle of intervention at the source.
- The Polluter Pays Principle.
- The Precautionary Principle.

The environmental license is granted by what, in the directives terminology, is called the Competent Authority as a reference to the institution implementing the regulation. In the IPPC Directive it is stated that the Competent Authority should in the licensing procedure make sure that (IPPC directive article 3):

- The necessary measures are taken in order to prevent pollution particularly through the application of BAT.
- Waste production is avoided or waste is recovered when produced and – if technically and economically impossible – is disposed of while avoiding or reducing any impact on the environment.
- Energy is used efficiently.
- Measures are taken to prevent accidents and limit their consequences.
- Measures are taken to avoid risk of pollution and return the site of operation to a satisfactory state, when activities are definitively closed down.

Apart from the overall objectives as stated above, the Directive formulates six key principles to guide the granting of environmental permits:

- The integrated approach means that the competent authority has to view the relationship between the industrial installation and the environment as a whole. This is to prevent a reduction in one type of emission leading to an increase in another type of emission. Moreover, aspects like energy efficiency, noise, and safety can be taken into account in the regulation.
- Conditions formulated as Emission Limit Values (ELV). Where appropriate, the conditions of the environmental permit shall be formulated as a mass based emission limit, that may not be exceeded during one or more time periods.
- The use of BAT when setting environmental permit conditions.
- Periodical review and update of the permit. This means that as technology develops, the definition of what constitutes BAT will change. Moreover the permit will be reviewed in the case of:
  - The pollution caused by the industrial installation is of such significance that a new environmental permit containing new limit values is needed.

  - Substantial change in what constitutes BAT has happened, making significant reductions possible without imposing excessive costs.
  - The operational safety of the process requires other techniques to be used.
  - New provisions from the Community or national legislation demands it.

- The public's right to participate in the decision making process is a central principle in the IPPC Directive. This is implemented through the public having access to:
  - The permit applications in order to give opinions.
  - The permits.
  - The results of the monitoring of releases
  - the European Pollutant Emission Register

Best Available Technique

Since the concept of BAT is a key concept in the IPPC directive, the meaning will be elaborated ON in the following section. BAT as defined by the IPPC Directive is not to be understood as a prescription of the use of a specific technique. Rather BAT has to be determined on a case by case basis taking into account the technical characteristics of the installation (Article 9,4). Bat is defined in the Directive in the following way:

> "(...) the most effective and advanced stage in the development of and their methods of operation which indicate the practical suitability of particular techniques for providing in principle the basis for emission limit values designed to prevent and, where that is not practicable, generally to reduce emissions and the impact on the environment as a whole" (Article 2.11)

Where *available*

> "techniques shall mean those developed on a scale which allows implementation in the relevant industrial sector, under economically and technically viable conditions, taking into consideration the costs and advantages, whether or not the techniques are used or produced inside the Member State in question, as long as they are reasonably accessible to the operator" (Article 2,11).

BAT can both be determined for the individual industrial installation and at the sector level. When defining what is considered BAT, the likely costs and benefits of the technique shall also be taken into account.
To support the Competent Authority in deciding what is considered as BAT at a given time, the Commission has established the European IPPC Bureau at DG (Directorate General) Joint Research Center to collect information on BAT in various sectors and facilitate the exchange of knowledge between the member states.

The outcome of this process is a series of BAT Reference (BREF) documents with the aim of supporting the Competent Authority in formulating BAT requirements. The BREFs are not legally binding documents, but function to support the determination of BAT requirements.
"The definition of what constitutes "economically and technically viable" techniques is somewhat unclear in the directive"(Clemmensen et al., 2007, p. 100). In practice, the Competent Authority should, in dialogue with representatives from the industry, examine the viability of the proposed processes to arrive at an acceptable definition of BAT, which is achievable by the installations. Reference to worldwide examples should also be considered in the examinations.

In Denmark, the IPPC Directive is implemented through the environmental protection act (Moe, 2011, p. 36). The environmental permit is in the specific case granted by the Environmental Protection Agency's local office, since the Fredericia terminal is a complicated industrial plant (Moe, 2011, p. 332).

2.3.3 The National Emissions Ceiling directive

With the aim of limiting acidification, euthrophication, and tropospheric ozone, the European Parliament and the European Council published the National Emissions Ceiling directive (2001/81/EC) November 27, 2001. The directive is targeted the emissions of SO_2, NO_x, VOC, and NH_3. The argument for the Directive is the Gothenburg Protocol to which, all the member states are parties. The directive sets binding national emission limits for the compounds mentioned, and the emission limits have to be reached in 2010 and 2020 respectively.
All member states have to supply national emission inventories and emission prognoses, for the years leading up to 2010, to the Commission, to document the path to reaching the goals stated by Directive. Exchange of information between the member states, on how the emission limits are reached, will take place if the Commission decides to do so (Basse, 2007, p. 58–59).

In Denmark, the Environmental Protection Agency has to supervise that the emissions don't exceed the emission ceilings. Moreover, it is the Environmental Protection Agency's job to develop strategies for limiting the national emissions to below the limits stated in the directive (NEC-bekendtgørelsen, 2011).
In the governmental strategy on clean air (Poulsen, 2008), it is stated that the national emission ceiling for 2010 with respect to VOC[7] is exceeded by approximately 3.5%. It is furthermore stated that new analyses of the VOC emissions will reveal whether or not new initiatives are needed. The main sources of anthropogenic VOC emission are stated to be solvents use, traffic, and individual solid fuel combustion. In the strategy, current and future initiatives are presented to reduce the emissions of VOC from traffic and individual solid fuel combustion, but not in relation to solvent use, although, it is stated as the largest source of VOC. With respect to traffic, the initiatives include, among others, duty exemption for hydrogen cars and electric cars. With respect to individual solid fuel combustion, the strategy is to promote cleaner technology both in Denmark and in the EU. Lastly, an unravelling of the available emission

[7]When VOC is used in the report the meaning is NMVOC.

prognoses will be performed to analyse the possibilities for complying with the NEC Directive.

2.3.4 The Air Quality Framework Directive

The Air Quality Framework Directive (1996/62/EC) is relevant in this context, since it sets concentration limits for tropospheric ozone to be implemented by September 9 2003. As explained in section 4.3, NMVOC acts as an ozone precursor, and as such, one possible way to reduce tropospheric ozone is to reduce the emission of NMVOC.
The Air Quality Framework Directive is a "framework directive" meaning that it sets up a set of rules for how various types of air emission are supposed to be regulated and leaves the Council to decide the details through daughter directives. The main argument for the Air Quality Framework Directive is to prevent negative health impacts of inhalation of the specified compounds. The fundamental principles for the strategy initiated by the directive is stated in article 1 as:

- define and establish objectives for ambient air quality in the Community designed to avoid, prevent or reduce harmful effects on human health and the environment as a whole,
- assess the ambient air quality in Member States on the basis of common methods and criteria,
- obtain adequate information on ambient air quality and ensure that it is made available to the public, inter alia by means of alert thresholds,
- maintain ambient air quality where it is good and improve it in other cases.

The Air Quality Framework Directive defines competencies and deadlines for when the EU institutions should have developed daughter directives to the Directive (Article 4). The Directive states that the member states shall specify zones or agglomerations where the concentration limit values stated in the daughter directives are exceeded.
The size of the zones are not defined in the Directive meaning that the zone size is highly variable across the union (Basse, 2007, p. 47). Furthermore the member states have to prepare compliance plans for the zones with exceedingly high concentrations. Both setting up concentration limit values and compliance with the set limit values will be based on a combination of measurements and modelling.
Since, for the time being, it is not seen as technically possible to fulfil the long-term environmental goals to comply with the WHO (World Health Organisation) limits, preliminary environmental goals are set for acidification and pollution by tropospheric ozone plus instruments to make a compliance with the environmental goals possible have to be developed (Basse, 2007, p. 60).

In the governmental strategy from 2008 on clean air (Poulsen, 2008), it is acknowledged that the concentration limit which has to be complied with in

2020 is exceeded, however no initiatives are presented to reduce the ozone concentration until 2020.
With respect to both the Air Quality Framework Directive and the National Emissions Ceiling Directive, the strategy promotes cleaner technology through governmental investment. It is stated that DKK 7 mio. is reserved in the period 2007–2009 to develop technologies to reduce the air emissions. Moreover, through the globalisation pool DKK 144 mio. is reserved to strategic research in cleaner technology, among others, for the clean air research area. It is, however, not stated whether any of these investments will be directed towards reductions in the emissions of VOC.

2.4 Previous work in the field

As stated earlier, the DONG degassing plant is one of only a few in the whole world. This means, that no studies are published similar to the present study. However, there have been a few studies on evaluation of emissions and emission reduction technology from oil terminals and refineries. These studies are reviewed in the following section. Moreover, as stated earlier, Spectrasyne Ltd studied the effect of the installation of the DONG degassing plant through a series of measurements performed in July 2002 (before the installation of the degassing plant) and between 29 September and 5 October 2009 (shortly after the installation of the degassing plant) respectively. These measurements are likewise reviewed in this section. Since Spectrasyne Ltd (2009) is the closest related study to the present, and the reporting to the municipalities and parts of the present study are based on these measurements, more space is devoted to this study.
The review of previously published articles is not claimed to be comprehensive, but to cover the major works in the area. The studies are found using respectively ISI Web of Knowledge and Google Scholar with key words such as "VOC", "emission", "refinery", and "oil terminal". The articles are reviewed chronologically:

2.4.1 Atmospheric concentrations of saturated and aromatic hydrocarbons around a Greek oil refinery

In Kalabokas et al. (2001), the ambient air concentrations of hydrocarbons were measured in the vicinity of a Greek refinery in order to compare the concentration with other areas subject to anthropogenic atmospheric emissions. The measurements were performed in weekly campaigns distributed over the season in the year 1997. During these weekly campaigns, measurements were collected four times a day. The measurements were taken using chemical methods, where samples were taken on site and later analysed in the laboratory. Kalabokas et al. (2001) shows a seasonal variation in the concentration of both the saturated and aromatic hydrocarbons and a diurnal variation in the saturated hydrocarbons. Since this trend correlates with the trend in temperature, it is suggested that the main source of saturated hydrocarbon emissions result from evaporation. The results are subsequently compared to Rappenglück et al. (1998) and Hatzianestis et al. (1996), where concentration measurements are performed in an urban and suburban area which is influenced by emissions from traffic. It is concluded that the concentrations in the area around the refinery are low compared to the concentrations in the areas influenced by traffic.
In this study, it is noticeable that concentrations are measured as opposed to emissions. This is probably due to the inherent difficulties in measuring/modelling emissions. Moreover, concentrations are the important parameters when performing regulation with respect to human health, as described in section 2.3. However, when only measuring concentrations, it is impossible to separate the quantity originating from the refinery as opposed to other sources. Moreover, concentrations are very much influenced by the local meteorological conditions. Meteorological measurements are performed in the study, but there is no indi-

cation as to whether or not the conditions, under which the measurements are taken, represent typical conditions or not. Lastly this study does not relate the concentration measurements to the operational conditions at the refinery.

2.4.2 Ambient volatile organic compound (VOC) concentrations around a petrochemical complex and a petroleum refinery

Inspired by Kalabokas et al. (2001), Cetin et al. (2003) is measuring the ambient air VOC concentrations in the vicinity of a petrochemical complex and a refinery in Turkey in order to estimate the concentration contribution resulting from the industrial activities. In this study, the samples were again collected on site and chemically analysed in the laboratory. The samples were collected unevenly spaced over the year from September 2000 to September 2001. The results show VOC concentrations 4-20 times higher than measured at a suburban site (Cetin, 2002). Cetin et al. (2003) also shows a seasonal variation and hypothesises that this might be due to increased evaporation from fugitive sources due to increased temperatures.
It is noteworthy that the measurements are performed in the vicinity of two industrial plants as opposed to Kalabokas et al. (2001), where the study area only contains one plant. All other things being equal, this should lead to increased concentrations. Moreover, the measured concentrations are likewise influenced by the operational and maintenance conditions of the industrial plants, but this is not touched upon in the article. Meteorological measurements are also performed in this study, but whether or not they represent typical conditions is not touched upon either.

2.4.3 Volatile organic compound concentrations in ambient air of Kaohsiung petroleum refinery in Taiwan

Lin et al. (2004) is, as far as the author is aware, the first published study of its kind where spectroscopic methods were used for concentration determination. The aim of the study was to measure the ambient air concentrations of NMVOC in the vicinity of the Kaosiung refinery in Taiwan using the chemical methods also employed by Kalabokas et al. (2001) and Cetin et al. (2003) and UV-DOAS (Ultra-Violet Differential Optical Absorption Spectroscopy) and to evaluate the reliability of the UV-DOAS technique. The measurements were performed between 28 April and 4 May 2001 at various locations at the refinery area. Since the samples were collected over such a short time period, Lin et al. (2004) are cautious about drawing conclusions on the concentrations resulting from the refinery, however it is concluded that the refinery is a potential source of hydrocarbon concentrations in the nearby areas. The results show good correlation between the chemical sampling method and the spectroscopic method and further research in the spectroscopic technique is encouraged.

2.4.4 Organic liquid storage tanks volatile organic compounds (VOCs) emissions, dispersion and risk assessment in developing countries: The case of Dar-es-Salaam City, Tanzania

Jackson (2006) is a model study of the emission and concentration resulting from the petroleum storage areas in Dar-es-Salaam City, Tanzania. The study uses the US EPA TANKS model (U.S. Environmental Protection Agency, 1995) to calculate the annual emissions resulting from the petroleum storage facilities. The input data to the model (such as tank type, level of maintenance, tank content etc.) comes from the tank storage companies, and the meteorological data comes from Tanzania meteorological agency. The results of the TANKS model is subsequently fed into the CALPUFF model (Atmospheric Studies Group, 2012) to calculate the resulting concentrations as a result of atmospheric dispersion. It is concluded that the losses resulting from atmospheric emissions are small compared to other losses in the companies. This is probably also influenced by the fact that the study is performed in a developing country. The concentrations resulting from the dispersion modelling are compared to international limit values and it is concluded that the concentrations are below the limit values. However, the input to the CALPUFF model is only the emission from the tank storage companies, and especially since traffic is not included, the actual concentrations might be much higher. A risk assessment based on the calculated concentrations is also performed based on multiplication of the concentration with weights representing children and adult exposure to benzene respectively. The cancer risk is calculated to be above the WHO guidelines.
Since no measurements are performed in this study, it is difficult to assess the validity of the modelling approach. Actual measurements might have served as both calibration with respect to the input to the modelling and as validation of the actual results. On the other hand, Jackson (2006) is the first study trying to quantify emissions as opposed to concentrations.

2.4.5 Investigation of volatile organic compound (VOC) emission in oil terminal storage tank parks

In Paulauskiene et al. (2009), VOC emissions from a tank farm in Lithuania are measured using the same chemical measurement technique as Kalabokas et al. (2001) and Cetin et al. (2003). The studied tank farm consists of fixed-roof tanks and internal floating roof tanks which makes emission measurements easier, since the source is a point source as opposed to a diffuse source. This also means that the study is not directly comparable to the present study. The samples were taken over nine days within the tank farm area. Paulauskiene et al. (2009) is the first study to examine the effect of the technical properties of the individual tanks. It is found that for fixed roof tanks, the maximum evaporation appears when the oil level is low. Moreover, the effect of different types of sealing systems is studied, and the use of appropriate sealing is encouraged.

2.4.6 Introduction of cleaner production in the tank farm of the Pancevo Oil Refinery, Serbia

Jovanovic et al. (2010) studied the effect of emission reduction maintenance on a series of storage tanks at the Pancevo Oil Refinery in Serbia in the years 2004 to 2008. The tanks were either retrofitted or domed in order to reduce VOC emissions. The assessment of this use of new technology is done using the US EPA TANKS model (U.S. Environmental Protection Agency, 1995) with input coming from the refinery and meteorological data coming from the Serbian meteorological office. The effect is assessed to be a reduction of total VOC emission of 37.6% and specifically for benzene a reduction of 62.7%. The modelling is backed up by concentration measurements from a nearby measurement station operated by the municipalities showing a benzene concentration decrease of 58%. It is argued that this concentration decrease is caused only by the reductions from the refinery, since the tank farm reconstruction was the only major environmental activity in the period. The dispersion of the emission from the refinery to the measurement station was not modelled in the study, which would have further fortified the argument.

2.4.7 Fugitive Hydrocarbon Emission Survey of 8 Crude Oil Storage Tanks at DONG, Fredericia

Spectrasyne Ltd (2009) differs markedly from all the other studies in two ways: Firstly, by using only spectroscopic measurement methods for measuring the emissions from the tanks, secondly, by relating the measurements to the operational phase of the tanks thus combining atmospheric measurements with technical analysis.

Spectrasyne Ltd (2009) comprises the emission measurements performed to fulfill the requirements stated in the environmental permit (Christensen, 2006). The report is a summary report covering the measurements performed in respectively 2001, 2002, and 2009, and as such functions as an environmental evaluation of the degassing plant.

The measurement technique used is a DIAL system only, since, according to Spectrasyne Ltd (2009), the DIAL technique has improved and is now one of the leading technologies for concentration measurements. To measure emissions, the concentrations and plume area from the DIAL are combined with external wind speed and wind direction measurements. The details of this are not described in the report. The precision of this system is stated to be +5% to -15%, but the validation experiments are not described in enough detail and are not referenced such that the correctness of these figures can be assessed. The DIAL system measures either methane and bezene emissions or C_2+ and benzene emissions and is switching between these modes every 45 minutes. The benzene emissions are measured as representatives of the aromatic fraction. To provide a speciation of the C_2+ emission, a series of sorption tube measurements are performed as well.

As stated, measurements were performed in 2001, 2002, and 2009. In 2001 the tanks were measured in as-found condition. However, it became evident that the operational mode of the tanks had a large influence on the emissions.

Large emissions occurred especially during filling of the tanks. Moreover, the measurements were influenced by the waste soil site located west of the tank at the time. After these measurements, DONG performed an analysis of the cause of the high emissions measured, and the cause was located in technical problems at the North Sea platforms. These problems were subsequently solved and a new measurement series requested.
The second set of measurements was performed in July 2002 and differed from the first set of measurements in two ways: Firstly, the waste soil site was not used during the measurement period, secondly, the measurements were planned such as to catch all five operational modes of the tanks: Filling, top dip, run down, intermediate standing, and bottom dip. The measurements were not performed on the same tank due to practicality and to cover the various tanks in the terminal.
The third set of measurements was performed at the end of September and beginning of October 2009 after the installation of the degassing plant. For the third set of measurements, the soil waste site was abandoned, but upwind measurements were still checked before the actual measurements. The measurements were again collected as to represent the various operational modes of the tank.
As can be seen on table 2.2, the filling operational mode is covered on more tanks than any of the other operational modes. This is due to the fact that the filling mode was identified as having particularly high emissions during the 2002 measurements due to turbulence generation in the beginning of the filling operation.
The results of the measurements are shown on fig. 2.6. The results are obtained by averaging the DIAL measurements, subsequently multiplying with the time factors supplied by the site, and multiplying with 8 tanks. As can be seen the emission reduction between 2002 and 2009 is 53% for methane and 79% for NMVOC. This difference is assumed to result mainly from the installation of the degassing plant.
Spectrasyne Ltd (2009) is the most detailed and precise of the reviewed studies since it carefully analyses the influence of the operational mode of the tanks on the emissions. However, as is indicated in the report, the meteorological conditions also influence the emission, especially with respect to wind penetration of the seals e.g. at top dip. It is also concluded that the emission reduction in reality might be slightly greater due to "wind speed differences" (Spectrasyne

	Bottom Dip	***Filling***	***Top Dip***	***Static***	***Rundown***
T9801 (Out of Commission)					
T9802	x	x	x		x
T9803		x	x		x
T9804	x	x	x		
T9805	x	x		x	
T9806	x	x			

Table 2.2: Tanks and operational modes covered during the 2009 measurements (Spectrasyne Ltd, 2009, p. 7)

2001 Data

Condition	Time Factor	CH4 (kg/h)	C2+ (kg/h)	Benz-ene (kg/h)
Bottom Dip				
Scan Weighted Mean		7.6	6.7	0.20
Time Factored	49%	**3.7**	**3.3**	**0.10**
Top Dip				
Scan Weighted Mean		77.3	92.0	0.46
Time Factored	22%	**16.7**	**19.9**	**0.10**
Filling				
Scan Weighted Mean		201.8	298.6	1.04
Time Factored	12%	**25.1**	**37.2**	**0.13**
Outflow				
Scan Weighted Mean		*	22.4	0.13
Time Factored	6%	**1.2**	**1.5**	**0.01**
Intermediate				
Scan Weighted Mean		41.5	28.1	0.44
Time Factored	11%	**4.5**	**3.0**	**0.05**
Total per tank (sum of time factored figures)		**51.2**	**64.8**	**0.38**
All 8 tanks		**410**	**519**	**3.05**

2002 Data

Condition	Time Factor	CH4 (kg/h)	C2+ (kg/h)	Benz-ene (kg/h)	VOC(d) (kg/h)
Bottom Dip					
Scan Weighted Mean		7.4	13.5	0.12	13.6
Time Factored	49%	**3.6**	**6.6**	**0.06**	
Top Dip					
Scan Weighted Mean		50.3	102	0.31	102
Time Factored	22%	**10.9**	**22.0**	**0.07**	
Filling					
Scan Weighted Mean		130	204	0.31	204
Time Factored	12%	**16.2**	**25.3**	**0.04**	
Rundown					
Scan Weighted Mean		24.0	27.1	0.16	27.2
Time Factored	6%	**1.6**	**1.8**	**0.01**	
Intermediate					
Scan Weighted Mean		7.8	19.4	0.10	19.5
Time Factored	11%	**0.8**	**2.1**	**0.01**	
Total per tank (sum of time factored figures)		**33.0**	**57.8**	**0.18**	**58.0**
All 8 tanks		**264**	**462**	**1.48**	**464**

2009 Data

Condition	Time Factor	CH4 (kg/h)	C2+ (kg/h)	Benz-ene (kg/h)	VOC(d) (kg/h)
Bottom Dip					
Scan Weighted Mean		7.6	5.6	0.05	5.7
Time Factored	49%	**3.7**	**2.7**	**0.02**	
Top Dip					
Scan Weighted Mean		25.3	19.7	0.24	20.0
Time Factored	22%	**5.5**	**4.3**	**0.05**	
Filling					
Scan Weighted Mean		36.3	24.4	0.27	24.7
Time Factored	12%	**4.5**	**3.0**	**0.03**	
Rundown					
Scan Weighted Mean		12.9	14.2	0.16	14.4
Time Factored	6%	**0.8**	**0.9**	**0.01**	
Intermediate					
Scan Weighted Mean		9.0	9.7	0.06	9.7
Time Factored	11%	**1.0**	**1.0**	**0.01**	
Total per tank (sum of time factored figures)		**15.5**	**12.0**	**0.13**	**12.1**
All 8 tanks		**124**	**96.2**	**1.01**	**97.2**

Figure 2.6: Results of the 2001, 2002 and 2009 measurements (Spectrasyne Ltd, 2009, p. 16)

Ltd, 2009, p. 17) between 2002 and 2009. Since the 2002 measurements were performed in July, and the 2009 measurements were performed at the end of September, there might also have been a temperature (and eventually a pressure) difference between the two sets of measurements, however this is not considered in Spectrasyne Ltd (2009).
The results presented in fig. 2.6 are average emissions measured. However, these average results cover significant variations among the individual measurements. Especially during filling operations, where the emissions are reported to be high, are results reported between 14.5 $^{Kg}/_{h}$ and 43.2 $^{Kg}/_{h}$ for C_2+ and between 2.4 $^{Kg}/_{h}$ and 98.0 $^{Kg}/_{h}$ for methane. These differences are considerably larger than the reported uncertainties related to the instrumentation, but without any apparent explanation to the differences.
Moreover, the run down measurements are not performed at actual run down, but instead as a gravity mediated transfer of oil between two tanks. This means, that the run down rate is slower than at actual run down. It is difficult to assess whether this has any influence on the achieved measurements.
It would also be worth looking into the influence of the operational history of the tanks, since the measurements performed are not full operational cycles performed at one tank, but an operational cycle pitched together from several measurements, sometimes with considerable time intervals in between the measurements.
Lastly, the measurements are performed quite close to the tanks depending on the wind direction and speed. Whether the measurements always only cover one tank, or whether there is an influence from the surrounding tanks, is hard to assess on the present base. Moreover, there might be effects resulting from the measurements being performed in the tank wake.
Several of the other studies have found seasonal and diurnal variations in the emissions. Since all the measurements in Spectrasyne Ltd (2009) are performed within a few days, it is impossible to detect such a variation in the study. This is however not tantamount to the fact that a seasonal and/or diurnal variation is non-existing.

2.4.8 Review summary

As can be seen from this short literature review, there has been a tendency towards: going from concentration measurements towards emission measurements, and from chemical measurement methods towards spectroscopic measurement methods. Moreover, two separate lines of research have developed in this field: one focusing on the technical aspect and using a modelling approach, and one focusing on the air emission aspect using measurements. Due to this separation, there is still a lack of knowledge on what the determining factors are with respect to the magnitude of the emissions.
Although technical aspects are analysed in Paulauskiene et al. (2009) and most notably in Spectrasyne Ltd (2009), e.g. the effect of the operational history of the tank and the large variations measured during filling indicates a basis for further research. Comparing the results of the TANKS modelling of the DONG terminal, as described in section 2.2.3, to the measured results shown in fig. 2.6, which is one of the only published comparisons of the TANKS model

with measurements, the model reports an expected annual emission of 88 $^{t}/_{year}$, and the measurements show an annual emission of 1929 $^{t}/_{year}$. This shows that the model results are roughly a factor of 20 smaller than the measurements. The reason for this discrepancy is not immediately apparent, however it indicates that relying on the model alone can lead to large misjudgements in the estimates. Seen from a regulatory point of view, it is apparent from this short review that the knowledge base in this area is flimsy.

Chapter 3

Method

This section will explain the used methods in the project. A technology assessment naturally takes point of departure in the concept of "quality" or "goodness" of a technology. "Quality can be defined qualitatively as the amount by which the product satisfies the users' (customers') requirements" (Ebeling, 1997, p. 6). The main objective of the degassing plant is as described in section 2.2 to reduce the emissions from the floating roof storage tanks to levels below acceptable emission limit values, and an evaluation of the technology against this goal is performed in the environmental analysis as described in section 3.3. Subsequently the objective of the degassing plant is to perform this task at as low a cost as possible. An evaluation of the degassing plant against this objective is performed in section 3.2. Two factors influencing the cost of the plant to an acknowledgeable level is the electricity use and the maintenance costs. Thus the objective of achieving an emission reduction in a cost-effective way is related to the technical/operational state of the degassing plant. The operational performance with respect to energy use and availability is analysed in section 3.4. Since the scientific theoretical base of the project has influence on the way the analysis is performed, the first section is devoted to an elaboration on that. This is then followed by an explanation of the economic method used, the environmental method used, and the technical method used.

3.1 Scientific theoretical base

To argue for the choice of method the starting point will be theory of science. In the following the chosen theory of science will be explained and arguments for the validity of the chosen theory of science will be presented.

This project is based on the theory of weak welfarism as presented by Adler and Posner (Adler and Posner, 2006, p. 53). Weak welfarism states that:

> "the morally required choice for a given actor, public or private, in a given choice situation, depends on the balance of $\{W, F_1, F_2, \ldots, F_m\}$, where W is overall welfare, F_i are other considerations, and $m \geq= 0$".

This means that overall welfare is a morally relevant decision criteria along with other criteria, not that overall welfare is morally decisive. Moreover Adler and Posner 2006 provide no indications on how to balance overall welfare against other considerations.

3.1.1 Definition of welfare

Arguing that overall welfare has moral value rests on defining the term "welfare". This section will review different definitions of welfare and argue for the definition used in this report:
Adler and Posner present three views on the definition of welfare: The mental-state view aims at finding some "attribute of experiences or mental-states, such that a person P is better off in O_1 than in O_2 if and only if his experiences in the two outcomes differ with respect to that attribute" (Adler and Posner, 2006, p. 29). This type of approach reduces the definition of welfare to a function of solely our mental state. If a person is in the same mental state in two different situations, then her welfare must be the same according to this definition. According to the mental-state view of welfare, this is true regardless of the other ways in which the two situations might differ. According to Adler and Posner, this is not a reasonable assumption, since much evidence exist indicating "many of the things individuals care about and strive for don't affect mental well-being very much" (Adler and Posner, 2006, p. 31).
The objective-good accounts of welfare tries to compile a list of goods representing different dimensions of welfare. This list is then supposed to be equally valid to all people in the world. This is an important fact in this approach since what is welfare for a specific person can differ from what she desires or believes to be good (Adler and Posner, 2006, p. 32). This approach has the flaw that the individual might not prefer some element on the list of goods. Something that the individual doesn't want and never comes to want can't improve the individuals welfare.
The last approach is known as the preference-based view of welfare. The preference-based view states that a situation is better for an individual if the individual actually prefers that situation over another situation. According to Adler and Posner two important criticisms can be raised against the preference-based view of welfare. The first criticism comes from the fact, that people can prefer states that don't improve their welfare because their preferences are "evil, ignorant, adaptive or otherwise misshapen" (Adler and Posner, 2006, p. 33). This is known as the problem of non-ideal preferences. The second criticism comes from people having preferences intuitively unrelated to their own lives. This could be preferences for things happening far away from the person or preferences for things that the person never gets to hear about. This is known as the problem of disinterested preferences (Adler and Posner, 2006, p. 35).
Following the approach presented by Adler and Posner this report will use the restricted preference-based account of welfare, meaning that welfare is defined by people's preferences, however, only preferences that survives idealization and who are self-interested should be given value. This approach raises the following problems: Conflicting interests, meaning that a person can have preferences that are inconsistent and/or changing preferences over time for example:

> "Jane might prefer watching TV to reading but have a second-order preference for reading over TV. Jane wishes she were the kind of person who preferred reading. Is she benefited by watching TV or not?" (Adler and Posner, 2006, p. 37)

Another problem is known as the problem of appropriate idealization, meaning the procedure by which non-ideal preferences should be laundered (as in the case of evil, ignorant, adaptive or otherwise misshapen preferences). The last problem is the definition of self-interest, meaning the procedure by which disinterested preferences should be laundered. Adler and Posner do not direct answers to these challenges. Nevertheless using the restricted preference-based account of welfare as an ideal and bearing the above mentioned criticisms in mind can be argued to be an appropriate approach, and it will be the approach chosen in this project.

3.1.2 Interpersonal welfare comparisons

The argument that overall welfare has moral value rests on the assumption that interpersonal welfare comparisons are possible. Interpersonal welfare comparison, means that the amount of welfare two persons have can be compared. If interpersonal welfare comparisons are impossible the conception overall welfare has no meaning. Taking a pragmatic approach, governmental decision makers are frequently faced with policy choices where the winners and loosers are not the same. Sometimes these choices might be rendered indeterminate, but most often the choice is made to the advantage of some group in society. This shows that interpersonal comparisons are in fact an integrated part of all kinds of regulation and thus it can be argued that interpersonal welfare comparisons, despite a doubtful ethical foundation, do occur (Adler and Posner, 2006, p. 42). Adler and Posner continues to review specific approaches to interpersonal comparisons and the interested reader is referred to (Adler and Posner, 2006, p. 43–52). That interpersonal welfare comparisons are possible is thus a central assumption to this project.

3.1.3 The moral relevance of overall welfare

Thus having defined the term welfare and argued for the possibility of interpersonal welfare comparisons paves the way for the concept overall welfare. The moral value of overall welfare, and thus the case for weak welfarism is based in the Pareto principle. "The Pareto principle holds that a project (including a regulation) is desirable if it makes at least one person better off while making no one worse off"(Adler and Posner, 2006, p. 5). "Among serious scholars of morality, the Pareto principle is far and away the most widely accepted moral axiom. Virtually all welfare economists and many, probably most, moral philosophers endorse it"(Adler and Posner, 2006, p. 55). Since a Pareto superior project is increasing overall welfare, and since a Pareto superior project is desirable it means that overall welfare has moral value. Thus by embracing overall welfare along with other aspects weak welfarism has moral relevance and is thus the scientific theoretical approach chosen in this project.
As an alternative to the Pareto principle, the Kaldor-Hicks criterion is often

mentioned. Since very few real world projects can survive a Pareto-test, the Kaldor-Hicks criterion is often used as argument for overall welfare. The Kaldor-Hisck standard says, "that a project is desirable if it makes the winners better off by an amount sufficient to overcompensate the losers, if the losers could be compensated through a costless lump-sum transfer" (Adler and Posner, 2006, p. 21). The various defences for this criterion is discussed in (Adler and Posner, 2006, p. 22) and the interested reader is referred to this. It is concluded that "because Kaldor-Hicks is, taken as a moral principle, unsound (...)" (Adler and Posner, 2006, p. 22) this criterion can not be used to argue for the value of overall welfare.

3.1.4 Methodological approach

With reference to the aim of the project the project will evaluate the DONG degassing plant using an interdisciplinary approach. This is as well in line with the theory of weak welfarism stating that a number of considerations should be given value. The three sub-analysis of the project will use three specific methodological approaches:
The economical part will approach the degassing plant through a welfare economics approach, where an approximation for overall welfare change (change in costs and benefits) as a result of the installation of the degassing plant is evaluated. Since valuating certain aspects of environmental and technical benefits from the installation of the degassing plant is very complicated this will not be part of the evaluation of overall welfare but instead figure as separate analysis.
The environmental part will approach the degassing plant through the interplay between theory, models and experiments. In this respect a distinction between "phenomena-theory", "method-theory" and "instrument-theory" will be made. The phenomena-theory will be presented in chapter 4 and deals with explaining the mechanism behind evaporation and climate effects of the VOC emission from the Fredericia terminal. The method-theory deals with theory related to the used method, where concepts and mechanisms needed to understand the used methods will be explained. This will be the case in the section on reliability engineering theory in section 3.4.2. The instrument-theory is related to the instruments used in the experiment, and as such will be presented in section 5.2.2.
The technical part will approach the degassing plant through an explanatory modeling approach (Hodges, 2009), where certain aspects of the degassing plant are represented in simplified statistical models to explain certain aspects of the functioning of the plant.

3.2 Economical analysis

The economical analysis will consist of a cost-benefit analysis (CBA) of the degassing plant. The reason for the choice of CBA is that CBA is an approximation for overall welfare (Adler and Posner, 2006, p. 154). Moreover CBA takes into consideration a large set of welfare effects, which has the opportunity of accurately tracking overall welfare. This is possible since "the marginal utility of money, for a given individual in a given scenario, is the marginal utility of whichever marketed good or service (or combination thereof) has the maximum marginal utility at that point. Thus variability in the marginal utility of money can be expected to be less than that of particular goods and services, even important ones. For example, the initial units of food an individual purchases are vitally important; otherwise she starves. But at some point, once the individual is sufficiently fed, consumption of $1 more in food would bring less utility than the expenditure of the $1 on something else. Up to that point, the marginal utility of $1 equals the marginal utility of $1 in food; after that point, the marginal utility of food drops (...)" (Adler and Posner, 2006, p. 97). Since money have different marginal utility depending on the wealth of the person receiving them, CBA will have some inherent inaccuracies due to its use of money as a common metric. This can be taken into account by either a separate distributive analysis or by applying distributive weighting to the WTP/WTA functions (Adler and Posner, 2006, p. 24 & 157). This will be kept in mind during the analysis. CBA also has the advantage of limiting the use of normative choices. This improves the transparency of the analysis, which is advantageous.

3.2.1 Discussion of the economic methodological approach

In the article "Cost-benefit analysis: New foundations on shifting sand" (Sinden et al., 2009) the approach described by Adler and Posner is reviewed. Adler and Posners reply to the critique is presented in the article "New foundations of cost-benefit analysis: A Reply to Professors Sinden, Kysar and Driesen" (Adler and Posner, 2009). The criticism, the reply, and the influence on the economic methodological approach will be elaborated on in this section.

In Sinden et al. 2009 the rigorous approach to moral philosophy taken by Adler and Posner is praised. Whereas earlier CBA proponents claim that "that welfarism provides the correct moral philosophy to guide public policy, that welfare is an individualistic and monistic concept, and that willingness-to-pay valuations correctly transform welfare impacts into monetary units for policy analysis" (Sinden et al., 2009, p. 51). As presented above Adler and Posners approach is a different one compared to earlier CBA proponents. Moreover the moral philosophy approach as presented in Adler and Posner 2006 is characterized as "specific and scrupulous throughout" (Sinden et al., 2009, p. 52).
As stated above, Adler and Posner states that CBA is an imperfect proxy for overall welfare. Sinden et al. 2009 however, raises the question, that just because a decision procedure tracks overall welfare in theory, it may not do so in practice. Since Adler and Posner 2006 is a highly theoretical book, the disparity between overall welfare and CBA cannot be determined, but have to be left for the

empirics. Moreover a number of weaknesses associated with CBA may eventually mislead decision makers rather than enlighten them (Sinden et al., 2009, p. 58). This is acknowledged by Adler and Posner 2009, however as they rhetorically ask: "To what extent are competing administrative decision procedures also subject to these difficulties?" (Adler and Posner, 2009, p. 76).
A number of other administrative decision procedures has been proposed as competitive to CBA, most notably Cost-Effectiveness Analysis. In CEA the environmental benefit is not valuated, but compared to expences used to achieve the required reduction. This is useful for comparing different alternatives with either a specified environmental benefit or with a cost per unit of each alternative. It is not possible to discount future values in CEA, which makes this approach more suitable for short-term projects where discounting is not as important. Moreover, when using this approach for evaluating a single project as is the case in this report, an external economic accept criteria is necessary for comparison with the result of the CEA. This in reality turns it into a CBA, where the environmental benefits of a specified project are valuated through an external economic accept criteria. In this case, the transparency of a CBA is larger than a CEA and is thus the preferred approach.
According to Miljøstyrelsen - Stab & Strategi (2005) there is general agreement within the central authorities on the relevance of using CBA. Moreover, as stated in section 2.2 the environmental economics was an important argument for the municipalities' assessment of the degassing plant before the construction of the plant.
A number of criticisms has been raised about how CBA has been performed in Denmark. The following list is based on Miljøstyrelsen - Stab & Strategi (2005):

- The fact that only preferences in the danish population is included in CBA has been a subject of critique. This is especially relevant when talking about transboundary pollution and climate change. However, as long as a standardized procedure is followed in all performed CBAs, the intercomparison between different projects are ensured. Moreover the present CBA is not to be seen as an absolute measure of the net present value of the DONG degassing plant, but rather as an indication of whether or not the construction of the degassing plant was an economically sound decision, whence the use of uncertainty calculations.

- The use of a discount rate for discounting future effects as opposed to present has as well been a subject of criticism, but again, as long as the same discount rate is used for all environmental project assessments, the intercomparability of the different projects are ensured.

- When evaluating an existing practice against a change in practice in some cases, the expenditure on the existing facilities has been regarded as sunk costs, which has been a subject of criticism. In this project the degassing plant is evaluated as if it was a new project in line with the procedure described in Miljøministeriet (2010).

- When environmental initiatives are financed based on collection of taxes, a tax distortion loss appears because the general activity in society is

decreasing as a result of increased tax collection. The size of the tax distortion loss has been surrounded by debate, however since the DONG degassing project is not financed by the state but by a private company, it is the author's opinion that this is not relevant to the present project.

- The valuation of environmental goods has been a subject of critique. The approach chosen in this project follows the principles described in Miljøministeriet (2010). The standard prices for the emission of methane and NMVOC will be used in the assessment. Moreover careful examination of how these standard prices are produced will be produced, and an assessment of the validity of the supplied prices will be performed. Furthermore uncertainty analysis will be performed in order to analyse the sensitivity of the obtained results.

3.2.2 Cost-Benefit Methodology

To be able to compare this analysis to other environmental/climate initiatives a consistent methodology has to be followed. The present analysis methodology is based on Miljøministeriet (2010). In the following, the methodological issues related to the cost-benefit analysis will be explained, but the details of the calculations will be postponed to chapter 8.
In line with the research question the present analysis will evaluate the economics of the installation of the DONG degassing plant. The installation of the degassing plant is characterised as a "direct measure" and as such performing a CBA is simpler compared to a "managerial measure". Since the DONG degassing plant is already a reality the performed CBA can be characterized as an "ex post" analysis. However, the lifetime of the degassing plant is far from over, and a certain amount of projection into the future will be included in the analysis. The present CBA is as such a mixture between an "ex ante" and an "ex post" analysis. As described in Miljøministeriet 2010, p. 45 an "ex post" analysis is useful for illuminating the economic consequences of the DONG degassing plant and for comparison with the expectations set up before the installation of the plant.
The scenario including the degassing plant will be compared to what is called a "business as usual" scenario. This means that apart from the installation of the degassing plant all other things (e.g. the oil price) will proceed as if the degassing plant didn't exist.
According to the pipelines act §3 (Rørledningsloven, 2011) the users of the oil pipe have to pay an amount covering the capital costs of the oil pipe including the terminal and pump facilities and an amount covering any other expences related to the operation of the pipeline. Moreover it is stated, that all users of the pipeline have to pay an amount corresponding to 5% of the value of the production of the crude oil apart from the above described payments. Of this payment 95% goes to the state and the last 5% goes to DONG Oil Pipe A/S. According to §3 in the executive order on payment of crude oil and condensate (Betalingsbekendtgørelsen, 2010), the payment of the 5% fee is repealed at July 9, 2012 for users covered by the hydrocarbon tax law about taxation of income from the sole right concession. This basically means, that

the 5% fee is no longer charged.
Since as a consequence of the above expounded regulation, the installation of the degassing plant will only have minor economic influence on DONG Oil Pipe A/S, it is natural to analyse the economic effect to the degassing plant seen from the users of the pipeline's perspective. Moreover the economic effect of the degassing plant will be analysed seen from the society's perspective. "The society" is in this context defined as the widest possible definition, including all costs and benefits resulting from the degassing plant, no matter to who they occur. This is relevant seen from a planning context, where the result of this analysis can be used for recommendations on whether or not the technology should be in more widespread use.

Consequence description

According to Miljøministeriet 2010, p. 58 when performing a CBA it should be considered whether other consequences than allocation consequences should be incorporated in the analysis. However, referring to section 1.2 only allocation consequences are considered in this analysis.
Following the recommendations in Miljøministeriet 2010, p. 71 all domestic economic and environmental consequences are included in the analysis. Moreover the international environmental consequences is included in the analysis, since, as described in section 2.3, both methane and NMVOC is covered by international environmental agreements.
The time horizon for the analysis will first follow the designed lifetime of the degassing plant corresponding to 15 years from the commission in 2009. Moreover since a new oil field (the Hejre oil field) is being commissioned in 2015(Hansen, Hansen), a new degassing plant will be constructed (Hougaard, 2012). The influence of this "artificially" shortened lifetime on the economics of the degassing plant will subsequently be analysed. As a way of considering a wide range of environmental and economic impacts the consequence scheme as presented in Miljøministeriet 2010, p. 9 is used as a checklist to make sure every relevant aspect is included in the analysis and that nothing is counted twice.

Valuation

The valuation of the costs and benefits follows the procedure described in Miljøministeriet (2010). The details of the individual calculations are postponed to chapter 8. The present CBA is performed in nominal prices. This means, that input in the form of fixed prices are converted to nominal prices using the GVA-deflator (Gross Value Added) obtained from Energistyrelsen (2011).

Discounting

When the analysis is performed from the perspective of the users of the oil pipe, the company WACC (Weighted Average Cost of Capital) obtained from DONG Oil Pipe A/S is used. When the analysis is performed from the perspective of the society, the discount rate specified by the ministry of finance is used. This approach is in line with the methodology specified in Miljøministeriet (2010).

Risk and uncertainty

According to Miljøministeriet (2010), "the result of the welfare economic analysis should always be reported to the decision makers in a way reflecting the degree of uncertainty not creating a false feeling of precision"(Miljøministeriet, 2010, p. 28). In this case, the uncertainties in the analysis are reported as a respective "best-case" and "worst-case" scenario. This is chosen since a large number of the inputs to the analysis e.g. the inputs from Larsen (2010) are supplied without indications of reasonable uncertainties or even better distributions of uncertainties. Since it would require a lot of work to try to establish these uncertainties in this project, this is left out.

3.3 Environmental analysis

Using figure 1.5 on page 7 as a model for the structure of the environmental analysis of the degassing plant and the storage tanks, the environmental analysis will start with the most certain but least relevant parameter (the emission(E)), gradually moving towards less certainty and increasing relevance:

1. The change in emission as a result of the installation of the degassing plant will be determined through an experiment as described in section 3.3.1.

2. Based on the determined emission, the atmospheric concentration will be modeled with the DEHM(Danish Eulerian Hemispheric Model) model.

3. These concentrations will subsequently be used as input parameters for the 1-D RCM (Radiative-Convective Model) to calculate the change in radiative forcing as a result of the installation of the degassing plant as described in section 3.3.2.

3.3.1 Determination of the emission source strength

The change in emission source strength will be assessed through an experimental study, with the aim of measuring the change in emission from an oil storage tank as a result of the installation of the degassing plant. The arguments for the choice of method will be presented here, whereas the details of the experimental design will be presented in chapter 5
In the BREF document on General Principles of Monitoring (the European IPPC Bureau, 2003b) potential monitoring techniques, among them the tracer release technique used in this study, are reviewed. It concludes that the technical working group "could not agree conclusions over several issues, especially regarding harmonisation of monitoring procedures" (the European IPPC Bureau, 2003b, p. 68). Therefore a specialised procedure is developed for the present experiment.
The fundamental assumption of the experiment is, that under similar conditions the tanks that have not been measured will have a similar emission. This assumption is based on the agreement between DONG and Shell stating that Shell has to maintain the storage tanksShell (1995). Moreover almost all of the tanks at the DONG oil terminal has been out for inspection in the years 2008 to 2010. This means, that the state of maintenance of the tanks should be equal.
The emission source strength will be determined through a series of tracer-release experiments inspired by API (1990); Eklund (1999); Galle (1999); Lamb et al. (1995); Thoma et al. (2008); US DoD ESTCP (2008); US EPA (2007). When performing the LIDAR measurements in 2001/2002, Spectrasyne found that the operational mode of the tank had a large influence on the emission. Therefore the experiments will be conducted to measure the five operational modes of the tanks (Bottom Dip, Filling, Top Dip, Intermediate Static, Rundown) as identified by Spectrasyne Ltd (2009) with and without the degassing plant. The experiments consist of releasing a chemically inert trace gas in a way accurately simulating the geometry of the emission source. The trace-gas used is acetylene(C_2H_2) and the source gas is methane(CH_4) as a representative for the

total VOC emission. By measuring both the source compound concentration and the trace gas concentration in a point, a distance from the source as illustrated on figure 3.1, it is possible to calculate the emission through the following relationshipLamb et al. (1995):

$$\frac{Q_{\mathrm{CH_4}}}{Q_{\mathrm{C_2H_2}}} = \frac{C_{\mathrm{CH_4}}}{C_{\mathrm{C_2H_2}}} \tag{3.1}$$

Where Q_{x} is the emission of the respective compound and C_{x} is the concentration of the respective compound above background. The gas used in this case is acetylene(C_2H_2) since the used measurement apparatus a Picarro G2203 Cavity RingDown Spectrometer is designed for measuring CH_4 and C_2H_2 simultaneously with a high temporal resolution. Moreover methane is the most abundant compound in the emission, which makes it easy to measure preciselySpectrasyne Ltd (2009). The total VOC emission including NMVOC will be calculated based on the relationship between methane and NMVOC as detected by Spectrasyne Spectrasyne Ltd (2009).
The position of the measurement instrument will be determined from data gathered from an anemometer installed on site combined with a calculation of the overlap of the plume from the surrounding tanks performed in GIS. See section 5.2.1 for more information.

3.3.2 Determination of the effect on the greenhouse effect

Inspired by Chang and Park (2004); Jonson et al. (2002); Myhre et al. (2007, 2003); Valks and Velders (1999) After determining the source strength this will be used as input data to the DEHM model, which is a large scale model, coupled with the 1-D RCMMacKay and Khalil (1991) model for calculating the radiative balance. The emission will be tagged to be able to turn down the source in accordance with the installation of the degassing plant.

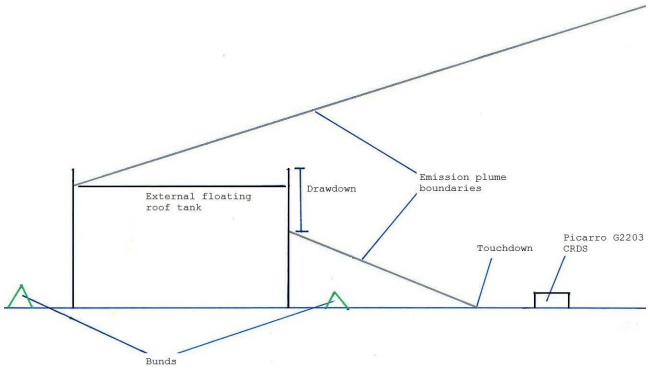

Figure 3.1: Schematic drawing of the measurement setup

3.4 Technical analysis

The technical analysis will consists of two sub-analysis: An analysis of the energy/production relationship and an analysis of the inherent availability. These concepts are chosen since they are important indicators of the way the degassing plant has been running since the installation.

3.4.1 Analysis of the energy/production relationship

The energy/production relationship as a function of time is defined as (Morvay and Gvozdenac, 2008, p. 91):

$$PI_{Pt} = \frac{E_t}{P_t} \tag{3.2}$$

Where PI_{Pt} is the performance indicator, E_t is the energy as a function of time and P_t is the offgas amount as a function of time. As stated in section 2.1 the energy of the degassing plant is approximately constant, whereas the offgas amount is variable leading to variations in the energy/production relationship. Since there is no direct measurement of the energy used in the degassing plant, the used energy will be calculated indirectly by making a scatter plot of the gross flow versus energy consumption on a monthly basis of the time period from the last upgrade of the system finished in 2001 to the installation of the degassing plant in May 2009. These data will be obtained from the DONG Oil Pipe monthly report database. Next a linear regression of the flow versus energy use data will be performed to determine the energy/flow relationship before the installation of the degassing plant. The same procedure is applied to the monthly data for the period after the installation of the degassing plant until August 2012. The approximate energy consumption of the degassing plant can thus be calculated as the average difference between the two regression lines. To obtain a more accurate fit a seasonal variation is fitted to the residual of the linear regression for the period prior to the installation of the degassing plant. The fundamental assumption in this operation is that the relationship between flow and energy use for the terminal is constant except for a seasonal variation and the installation of the degassing plant during the examined period. The average energy/production relationship can thus be calculated. The data on offgas amount will be obtained from the DONG monthly report database.
The uncertainties in the analysis is examined through a visual inspection of the residual plot between the fitted energy consumption and the measured energy consumption. Moreover the histogram of the residual will be drawn and evaluated visually. The mean and the standard deviation of the residual will be calculated as a way to quantify the uncertainties related to the fitting procedure, and the influence on the energy/production relationship will be calculated.

3.4.2 Availability analysis

The availability of the degassing plant is examined in the availability analysis. In order to provide a foundation for the empirical analysis some central concepts and formulas are introduced in the section Reliability engineering theory. The used methodology based on the theory is then presented in the section Reliability engineering method.

Reliability engineering theory

Three central concepts from the discipline "reliability engineering" will be used in the availability analysis. These are thus introduced in the following and their application in the analysis expounded:

> "**Reliability** is defined to be the **probability** that a component or system will perform a required function for a given period of time when used under stated operating conditions." (Original emphasis) (Ebeling, 1997, p. 5)

Two aspects are central to this qualitative definition of reliability. First of all it is defined according to the purpose of the technology. This means, that without an unambiguously stated function of the technology, the concept of reliability becomes useless. Second of all, the reliability is only specified for the conditions of "stated operating conditions". This implies that the reliability of a specific component or system is not affected by intended or unintended maluse.

> "**Maintainability** is defined to be the probability that a failed component or system will be restored or repaired to a specified condition within a period of time when maintenance is performed in accordance with prescribed procedures." (Original emphasis) (Ebeling, 1997, p. 6)

Central in this definition is the concept of "prescribed procedures" which covers the way maintenance is to be performed as well as the availability of resources to be used during maintenance e.g. people, spare parts, tools etc.

> "**Availability** is defined as the probability that a component or system is performing its required function at a given point in time when used under stated operating conditions." (original emphasis) (Ebeling, 1997, p. 6)

This definition is deceivingly close to the definition of reliability, however, where availability is the probability that a component is currently running although it might have failed earlier, reliability is only considering the probability of a component running after a specified length of time or other time unit (e.g. batch, cyclus etc.). Again the availability is only defined as long as the component or system is used under stated operating conditions, thus taking precautions against intended or unintended maluse.
Availability can be quantitatively defined in various ways, depending on the scope of the analysis and the object under investigation (see Ebeling 1997, p. 254–257 for a discussion of possible definitions). For the present analysis the inherent availability is chosen as the definition, since it is the simplest of the definitions presented. This is the case because it is based only on the failure- and repair time distribution, as opposed to some of the more complicated definitions. The definition of inherent availability is (Ebeling, 1997, p. 255):

$$A(T) = \frac{\text{MTBF}}{\text{MTBF+MTTR}} \tag{3.3}$$

Where $A(T)$ is the time dependent inherent availability, MTBF is the mean time between failure, and MTTR is the mean time to repair. The MTBF and MTTR will be defined in the following.

Since the study object of this project is a repairable system, the relevant parameter for the description of uptime will be the failures. Analysing the operating time of the degassing plant, the occurrence times of the failures can be denoted by $T_1, T_2 \ldots$. Let T_k be the random variable representing the time to the kth failure with $T_0 = 0$ and let $X_i = T_k - T_{k-1}$ be the random variable representing the operating time between failure $k-1$ and k. Then $T_k = \Sigma_{i=1}^{k} X_i$ and $E(T_k) = \Sigma_{i=1}^{k} E(X_i)$, where E denotes the expected value of the function. $E(X_i)$ is then denoted the mean time between failures (MTBF).

In a similar way as the above presented analysis for uptime, important conceptions from the analysis of downtime will be used in the analysis.
If T is again defined as a continuous random variable representing the time to repair a failed component or system. For such a variable it is possible to define a probability density function $h(t)$, representing the shape of the repair distribution. The cumulative distribution function $H(t)$ is then defined as:

$$\Pr\{T \leq t\} = H(t) = \int_0^t h(t')dt' \tag{3.4}$$

Since $h(t)$ is the distribution function the MTTR, Mean Time To Repair can be calculated as(Ebeling, 1997, p. 191-192):

$$MTTR = \int_0^\infty th(t)dt = \int_0^\infty (1 - H(t))dt \tag{3.5}$$

The maintenance philosophy at the Fredericia oil terminal as administered by A/S Dansk Shell, is following the Reliability-Centered Maintenance(RCM) principle (Michaelsen[1] personal communication). The RCM principle is deviating from earlier types of maintenance philosophies, where time was believed to be the sole factor of the probability of failure. Following the RCM principle failures are prevented through a combination of strategies leading to a reduction in downtime (NASA, 2008). This means that analyzing the availability of the degassing plant solely in terms of the MTBF and the MTTR is an adequate description. More complicated definitions of availability would include preventive maintenance times, but following the RCM principle, preventive maintenance doesn't impart downtime on the system.

Reliability engineering method

To calculate the MTBF and MTTR a definition of respectively failure and normal operational mode is necessary.
The available data to construct this definition are the offgas mass flow as a function of time and the pressure in the degassing vessel as a function of time. These data are obtained from the DONG SCADA-system, and corrected for dataloss through filling in the gaps with data from Shell DCS. In the case of small datalosses, linear interpolation is used, and in case of failure based on

[1]Miklos Michaelsen, Operations supervisor DONG Oil Pipe

visual interpretation of the time series the gaps are filled with zeroes. The data are obtained as temporal averages with resolution of one hour since 1st of May 2009 until 1st of October 2012. This means, that there will be a group of short failures that cannot be observed in the time series. The procedure prescribed below is constructed to compensate for this.
The definition of respectively failure and normal operations is constructed fisrt based on a visual inspection of a 3D-histogram of the available operational data, meaning the offgas mass flow and the pressure in the degassing vessel. The modes of respectively operation and failure will thus appear as peaks in the 3D-histogram, since normally the amount of time spent in either normal operations or failure, will be larger than the time spent on transition between the operational modes. The definition is then defined based on the mean and standard deviation of respectively the offgas mass flow and the pressure in the degassing vessel.
Next the time series is sorted in respectively failure and non-failure. The failures are subsequently manually inspected. For each detected potential failure, the "electrolog", the logging system of the operator, was consulted for incidences that could account for the detected failure. If outer circumstances e.g. shutdown on the platform or that the refinery could not receive the gas, the incidence was not registered as a failure. Moreover it was assessed whether an incidence should be registered as two closely located failures or as one long failure. If both the measured offgas mass flow and the measured pressure in the degassing vessel had left the failure criteria in between the two incidences, it was classified as two closely located failures. If only either the mass flow or the pressure had left the failure criteria, it was classified as one long failure.
Following the approach of Ebeling 1997, p. 31, the cumulative number of failures was fitted using a piecewise linear function, consisting of a burn-in period with a steeper slope and a useful life with a gentler slope. This is line with NASA 2008, p. 4-7 stating that "Complex items frequently demonstrate some infant mortality, after which their failure probability increases gradually or remains constant, and a marked wear-out age is not common". The point of transition from burn-in period to useful life was also fitted. The residual between the fit and the data was subsequently inspected, and the mean and standard deviation of the residual was calculated to assess the uncertainty.
The repair time distribution was first plottet as a function of time to assess whether or not there would be a temporal trend in the data. Since this was not the case, a histogram of the repair times was drawn, and based on a visual inspection an exponential distribution was fitted. The uncertainty within this part of the procedure was not evaluated, due to very few data points. The fitted MTBF and MTTR are thus inserted in eq. (3.3). The uncertainty in the inherent availability resulting from the calculated uncertainty on the MTBF is subsequently calculated.

Chapter 4

Theory

This chapter is divided into three sections.
The section on evaporation theory is what was termed ”phenomena-theory” in the method section. The purpose is to provide a fundamental understanding of the physics of the evaporation from an EFRT and the governing physical processes.
The section on meteorology will explain the fundamental concept of atmospheric stability, which is used in the modelling in chapter 5.
The section on climate will focus on the chemical interactions between VOC and other atmospheric constituents and forms part of the basic understanding for the modelling performed in chapter 6.

4.1 Evaporation theory

As a starting point for understanding the emissions from the EFRTs in Fredericia, the theory of evaporation of petroleum fluids is considered. This is chosen as a basis for understanding the evaporation process taking place in the storage tanks and thus the mechanisms controlling the size of the emissions.
Since the author has been unable to locate any published results on modelling the physics of the evaporation from EFRT, this section is patched together from theory on the evaporation of water and evaporation of oil spills at sea. Lastly, reflections on the differences between the evaporation from an EFRT and the above mentioned patch elements are presented. Moreover, since ”the fundamental physics of evaporation is not well understood” (Fingas, 1996, p. 5), this section may appear more fragmented than the other theory sections.

4.1.1 Kinetics and thermodynamics of gases

The term ”evaporation” used in this report is at the micro-level a competing process of evaporation and condensation. At equilibrium, the rate of evaporation balances the rate of condensation. If the rate of evaporation is larger than the rate of condensation, a net evaporation of molecules will occur, which is what is termed ”evaporation” in the other sections of this report.

The fundamental mechanism controlling the theoretical maximum rate of evaporation is the kinetic movement of gas at the liquid-gas interface. The following derivation rests on these assumptions:

- Any gas consists of separate particles called molecules. In a pure gas they are alike.
- The molecules move about in all directions.
- The pressure caused by the movement of the molecules is the only one existing in the gas, when it is in the ideal state.
- The molecules are not infinitely small. Thus they collide with one another.
- The speed of the gas molecule is distributed according to a Maxwell-Boltzmann distribution.
- As a first approximation, the gas behaves as an ideal gas.

The number of molecules striking a unit area of surface in a gas pr. unit time can be calculated as:

$$\phi_0 = \tfrac{1}{4} n \bar{c} \tag{4.1}$$

Where n is the number of molecules of gas pr. unit volume, and $\bar{c}$ is the mean molecular speed. Assuming that the speed of the gas follows a Maxwell-Boltzmann distribution:

$$P(c)dc = 4\pi \sqrt{\left(\tfrac{m}{2\pi kT}\right)^3} e^{-\frac{mc^2}{2kT}} c^2 dc \tag{4.2}$$

Where $P(c)dc$ is the probability that a given molecule will have the speed c in the interval dc, m is the molecular mass, k is Boltzmann's constant and T is the absolute temperature of the gas. Solving for the average speed:

$$\bar{c} = \int_0^\infty cP(c)dc = 4\pi \sqrt{\left(\tfrac{m}{2\pi kT}\right)^3} \int_0^\infty c^3 e^{-\frac{mc^2}{2kT}} dc \tag{4.3}$$

$$\int_0^\infty c^3 e^{-\frac{mc^2}{2kT}} dc = \tfrac{1}{2}\Gamma(2) \left(\tfrac{2kT}{m}\right)^2 = \tfrac{1}{2} \left(\tfrac{2kT}{m}\right)^2 \tag{4.4}$$

$$\bar{c} = 4\pi \sqrt{\left(\tfrac{m}{2\pi kT}\right)^3} \tfrac{1}{2} \left(\tfrac{2kT}{m}\right)^2 \tag{4.5}$$

$$= \sqrt{16\pi^2 \tfrac{m^3}{8\pi^3 k^3 T^3} \tfrac{1}{4} \tfrac{16k^4T^4}{m^4}} = \sqrt{\tfrac{8kT}{\pi m}} \tag{4.6}$$

Where Γ is the gamma function. The number of gas molecules pr. unit volume is calculated from the ideal gas equation:

$$n = \tfrac{\bar{p}}{kT} \tag{4.7}$$

Where $\bar{p}$ is the average pressure of the gas. Inserting these two results in eq. (4.1) yields:

$$\phi_0 = \tfrac{1}{4} \tfrac{\bar{p}}{kT} \sqrt{\tfrac{8kT}{\pi m}} \tag{4.8}$$

$$= \bar{p} \sqrt{\tfrac{1}{16} \tfrac{1}{k^2T^2} \tfrac{8kT}{\pi m}} \tag{4.9}$$

$$= \bar{p} \sqrt{\tfrac{1}{2kT\pi m}} \tag{4.10}$$

$$\phi_0 = \tfrac{\bar{p}}{\sqrt{2kT\pi m}} \tag{4.11}$$

The mass flux of molecules across the gas-liquid interface is defined as:

$$J_m \equiv m\phi_0 = \frac{m\bar{p}}{\sqrt{2kT\pi m}} \tag{4.12}$$

$$= \frac{1}{\frac{1}{\bar{p}m}\sqrt{2kT\pi m}} \tag{4.13}$$

$$= \frac{1}{\frac{1}{\bar{p}}\sqrt{\frac{2kT\pi m}{m^2}}} \tag{4.14}$$

$$= \frac{1}{\frac{1}{\bar{p}}\sqrt{\frac{2kT\pi}{m}}} \tag{4.15}$$

$$= \bar{p}\sqrt{\frac{m}{2kT\pi}} \tag{4.16}$$

$$= \bar{p}\sqrt{\frac{M}{2RT\pi}} \qquad R = \frac{kM}{m} \tag{4.17}$$

Thus for a pure liquid e.g. water evaporating into a perfect sustained vacuum the theoretical maximum evaporation rate will be:

$$w_e = p_{\mathrm{tr}}\sqrt{\frac{M}{2RT_{\mathrm{tr}}\pi}} \tag{4.18}$$

Where w is the evaporation rate in $\frac{Kg}{m^2 s}$, M is the molar mass of the substance in $\frac{Kg}{\mathrm{mol}}$, R is the universal gas constant, T_{tr} is the absolute temperature in K at the interface, and p_{tr} is the saturation vapor pressure in $\frac{N}{m^2}$. When performing experiments an "evaporation coefficient" (E) is multiplied to this equation to account for experimental imperfections (Jones, 1992, p. 5-6 & 37).
The saturated vapor pressure of a liquid is highly dependent on temperature. This is due to the increase in the number of molecules with higher kinetic energy at higher temperature. This means that the vapor pressure of a liquid is always rising with temperature. The vapor pressure dependency on temperature is controlled by the Clausius-Clapeyron relation:

$$p_{\mathrm{tr}} = e^{-\frac{\Delta H_{\mathrm{vap}}}{RT}+C} \tag{4.19}$$

Where ΔH_{vap} is the molar heat of vaporization and C is a constant. The molar heat of vaporization is strongly connected to the intermolecular forces in the liquid thus stronger intermolecular forces means a larger heat of vaporization (Chang, 2008, p. 409-410).
For condensation the same derivation as presented above for evaporation is valid. The rate of condensation is proportional to the vapor pressure in the vapor space above the liquid following this relationship:

$$w_c = p_{\mathrm{min}}\sqrt{\frac{M}{2RT_{\mathrm{v}}\pi}} \tag{4.20}$$

Where p_{min} is the vapor pressure in the vapor region, and T_v is the absolute temperature in the vapor region. This means that as soon as the liquid starts to evaporate, if the vacuum above the liquid is no longer sustained, the net evaporation rate will gradually slow down since the evaporation rate is constant, and the condensation rate is increasing, until an equilibrium is reached, as illustrated in fig. 4.1 (Jones, 1992, p. 37).

4.1.2 Boundary-layer effects

In the last section, the theory of evaporation in a low vacuum was explained. If the evaporation, however, takes place in the presence of a gas which is chemically inert to the liquid, the evaporation is observed to occur at a much lower rate than predicted from the kinetic theory of gases.
The following section is based on Dayton (1998). The lower net evaporation rate is explained by the generation of a boundary layer next to the liquid surface through which the liquid vapor has to diffuse, and the fact that rate of diffusion is much lower than the rate of evaporation in vacuum. When reaching the outer boundary of the boundary layer, the vapor is removed by the convection happening in the vapor space outside the boundary layer.

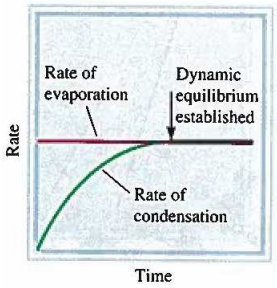

Figure 4.1: Illustration of the time development of the evaporation rate and the condensation rate (Chang, 2008, p. 409).

Since the experiments, paving the way for this theoretical work, were made with a wire in a chamber, the following derivation will take place in cylindrical geometry. The derivation is equally valid in plane geometry. The diffusion from a wire can be calculated as:

$$q = 2\pi r D \frac{dc}{dr} \tag{4.21}$$

Where q is the diffusion from the wire pr. unit length in $\frac{g}{ms}$, r is the wire radius, D is the diffusion coefficient, and c is the concentration of liquid vapor molecules in the boundary layer. The diffusion coefficient is defined as:

$$D = \frac{1}{3} v_a L \tag{4.22}$$

Where v_a is the average velocity of the vapor molecules, and L is the mean free path of the vapor molecules. Moreover the following relation is valid:

$$\eta = \frac{1}{3} \rho v_a L \tag{4.23}$$

Where η is the viscosity of the gas and ρ is the density of the gas. Combining these two equations yields:

$$D = \frac{\eta}{\rho} \tag{4.24}$$

This means that the diffusion coefficient is inversely proportional to the pressure. Inserting this result into eq. (4.21):

$$q = \frac{Ar}{P} \frac{dc}{dr} \tag{4.25}$$

Where A is a constant of proportionality. Assuming the radius of the wire to be a and the radius of the boundary layer to be b and solving this equation using

separation of variables:

$$\frac{q}{A}P\frac{1}{r}dr = dc \tag{4.26}$$

$$\frac{q}{A}P\int_b^a \frac{1}{r}dr = \int_b^a dc \tag{4.27}$$

$$maP\int_b^a \frac{1}{r}dr = \int_b^a dc \qquad m = \frac{q}{Aa} \tag{4.28}$$

$$maP\log\left(\frac{a}{b}\right) = c_a - c_b \tag{4.29}$$

$$m = \frac{c_a - c_b}{aP\log\left(\frac{a}{b}\right)} \tag{4.30}$$

Where m is the rate of evaporation. This shows that the rate of evaporation is constant with respect to time. Moreover, since the convection is determining the concentration at the edge of the boundary layer, the amount of convection outside the boundary layer will determine the rate of evaporation.

4.1.3 The evaporation of oil spills

Fingas (1996) experimentally examined the evaporation of crude oil in the laboratory. Since crude oil is a mixture of a range of compounds, the evaporation rate will not be constant with respect to time although the temperature, pressure, and vapor space are kept constant as illustrated in fig. 4.2. Fingas (1996) examines the evaporation with time of a range of oils and refined products, fits a range of equations to the data, and compares the coefficient of determination to find the best fit of the simplest equation. The petroleum mixtures consisting of only a few hydrocarbons yield a best fit to a square root function with time, whereas mixtures consisting of more than seven components evaporate as a logarithmic function with time.
Furthermore, Fingas (1996) finds that the evaporation of crude oil is not boundary layer limited. This is concluded on the basis that the evaporation is not increased by any significant amount as a result of increasing wind speed (Fingas, 1996, p. 68) and on the basis that the evaporation rate is increasing as a result of increasing oil mass (Fingas, 1996, p. 87). "[However,] These conclusions [independence of wind speed] are not at present generally accepted in the field of oil spill modeling, and run counter to most prior work in this area" Reed et al. (1999) (Text in square brackets added by the author). The observed independence of the boundary layer for oils is explained by the fact that the saturation concentration for most crude oil components is much larger than the evaporation rate. This means that the saturation limit is never reached for crude oil evaporation.

4.1.4 Section summary and theory-derived hypothesis

The following consequences can be drawn from these sections on evaporation theory:

- From section 4.1.1, it was shown that the evaporation is proportional to the surface area. This means that when storing crude oil in an EFRT the surface area is reduced as opposed to e.g. a fixed roof tank.

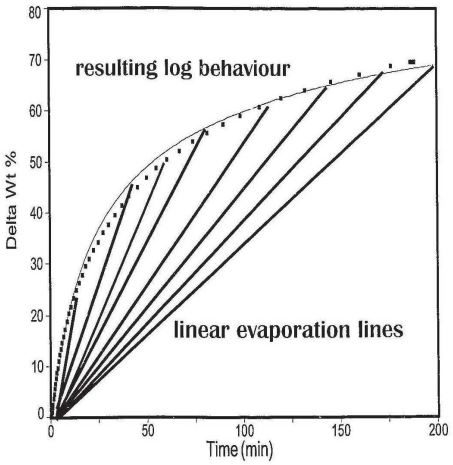

Figure 4.2: Illustration of the principle behind the time development of evaporation of crude oil consisting of a range of components with constant evaporation rates(Fingas, 1996, p. 63)

- The boundary layer theory presented in section 4.1.2 showed a relationship between the evaporation rate and pressure, meaning a larger atmospheric pressure would lead to a smaller evaporation rate. This hypothesis can be tested if comparing experiments performed under various pressures. Moreover, the concentration at the outer edge of the boundary layer is controlled by the wind speed, meaning, a larger wind speed will lead to a lower concentration at the outer edge and thus a higher rate of evaporation. A higher wind speed is also causing a lower pressure on the tank roof surface due to the Bernoulli effect. Both of these effects will influence the evaporation rate in a positive direction, thus a higher wind speed should lead to a higher evaporation rate.

- In 4.1.3 the hypothesis that the evaporation rate is not boundary layer limited was presented. This can be tested if the wind speed dependency turns out to be false. Moreover, it was shown that the evaporation rate of the total crude oil was strongly dependent on time. This can, however, not be tested in the experiment since only one component out of the VOC mixture is measured as a tracer for the VOC distribution. This is because the chemical composition of the VOC emission will change over time.

4.2 Meteorology

This section will explain the meteorological theory and the quantities used in the interpretation of the experimental results. The focus will be on the concept of atmospheric stability.
Fundamental to the discussion of air movement is the concept of an "air parcel". An air parcel is "a hypothetical mass of air that may deform as it moves vertically in the atmosphere" (Seinfeld and Pandis, 2006, p. 767). The following derivation is based on (Seinfeld and Pandis, 2006, p. 9 & 722-730). The concept of an air parcel is useful, as long as the exchange of molecules across the borders of the parcel is small compared to the total number of molecules in the air parcel. To describe the temperature profile of the atmosphere let the air parcel rise vertically along the z-axis. Furthermore, it is assumed that the air parcel at all times is in thermodynamic equilibrium with the surrounding atmosphere. The energy of the air parcel is thus described by the first law of thermodynamics:

$$dU = dQ + dW \tag{4.31}$$

Where dU is the change in the internal energy of the air parcel as it rises, dQ is the heat input to the system, and dW is the external work done on the system. As the air parcel rises through the atmosphere, its volume expands as a result of the declining pressure. This means that the external work done on the system amounts to $-pdV$, where p is the pressure in the air parcel, and V is the volume of the air parcel. Invoking the differential ideal gas law:

$$d(pV) = \frac{mRdT}{M_{\text{air}}} \tag{4.32}$$

Where m is the mass of the air parcel, R is the gas constant, T is the absolute temperature, and M_{air} is the molar mass of the air. Applying the product rule for differentials to the left side of equation 4.32 yields:

$$d(pV) = pdV + Vdp \tag{4.33}$$

This means that the expression for external work done on the system can be written as:

$$dW = vdP - \frac{mRdT}{M_{\text{air}}} \tag{4.34}$$

When an air parcel rises through the atmosphere, the expansion is accommodated by a negligible exchange of heat across the borders of the air parcel, thus $dQ = 0$. By definition, the internal energy of the air parcel is $dU = C_v dT$, where C_v is the heat capacity at constant volume meaning that the first law of thermodynamics can be written as:

$$C_v dT = Vdp - \frac{mRdT}{M_{\text{air}}} \tag{4.35}$$

$$= \frac{mRT}{M_{\text{air}}p}dp - \frac{mRdT}{M_{\text{air}}} \tag{4.36}$$

Dividing both sides of equation 4.36 by dT:

$$c_v = \frac{mRT}{M_{\text{air}}p}\frac{dp}{dT} - \frac{mR}{M_{\text{air}}} \quad \Leftrightarrow \quad (4.37)$$

$$c_v + \frac{mR}{M_{\text{air}}} = \frac{mRT}{M_{\text{air}}p}\frac{dp}{dT} \quad \Leftrightarrow \quad (4.38)$$

$$\frac{c_v + \frac{mR}{M_{\text{air}}}}{\frac{mRT}{M_{\text{air}}p}} = \frac{dp}{dT} \quad \Leftrightarrow \quad (4.39)$$

$$\frac{\frac{mRT}{M_{\text{air}}p}}{c_v + \frac{mR}{M_{\text{air}}}} = \frac{dT}{dp} \quad \Leftrightarrow \quad (4.40)$$

Assuming the pressure dependency with height of the atmosphere to be described by the hydrostatic equation and assuming a constant temperature in the atmosphere:

$$\frac{dp(z)}{dz} = -\rho(z)g \quad (4.41)$$

Applying the ideal gas law on the atmosphere:

$$\rho(z) = \frac{M_{\text{air}}p(z)}{RT_a} \quad (4.42)$$

Inserting this in equation 4.41:

$$\frac{dp(z)}{dz} = -\frac{M_{\text{air}}gp(z)}{RT_a} \quad (4.43)$$

Using the chain rule for differentials with equation 4.43 on equation 4.40:

$$\frac{dT}{dz} = -\frac{mg}{c_v + \frac{mR}{M_{\text{air}}}} \quad (4.44)$$

$$= -\frac{g}{\hat{c}_v + \frac{R}{M_{\text{air}}}} \quad (4.45)$$

Where $\hat{c}_v$ is the heat capacity at constant volume pr. unit mass. Noting that $\hat{c}_v + \frac{R}{M_{\text{air}}} = \hat{c}_p$, where $\hat{c}_p$ is the heat capacity at constant pressure pr. unit mass leads to:

$$\frac{dT}{dz} = -\frac{g}{\hat{c}_p} \quad (4.46)$$

The quantity $\frac{g}{\hat{c}_p}$ is known as the "dry adiabatic lapse rate" denoted by Γ and is the temperature change for a parcel of dry air rising adiabatically through the atmosphere.
Rewriting equation 4.40 in terms of $\hat{c}_v$ and $\hat{c}_p$:

$$\frac{dT}{dp} = \frac{(\hat{c}_p - \hat{c}_v)\frac{T}{p}}{\hat{c}_p} \quad (4.47)$$

Multiplying the nominator and the denominator of the fraction by $\hat{c}_v$ and using the definition $\gamma = \frac{\hat{c}_p}{\hat{c}_v}$:

$$\frac{dT}{dp} = \frac{\gamma - 1}{\gamma}\frac{T}{p} \quad (4.48)$$

Integrating equation 4.48 from z_1 to z_2 using separation of variables:

$$\int_{z_1}^{z_2} \tfrac{1}{T} dT = \tfrac{\gamma-1}{\gamma} \int_{z_1}^{z_2} \tfrac{1}{p} dp \qquad \Leftrightarrow \qquad (4.49)$$

$$\ln(T(z_2)) - \ln(T(z_1)) = \tfrac{\gamma-1}{\gamma} \ln(p(z_2)) - \ln(p(z_1)) \qquad \Leftrightarrow \qquad (4.50)$$

$$\ln\left(\tfrac{T(z_2)}{T(z_1)}\right) = \tfrac{\gamma-1}{\gamma} \ln\left(\tfrac{p(z_2)}{p(z_1)}\right) \qquad \Leftrightarrow \qquad (4.51)$$

$$\ln\left(\tfrac{T(z_2)}{T(z_1)}\right) = \ln\left(\left(\tfrac{p(z_2)}{p(z_1)}\right)^{\frac{\gamma-1}{\gamma}}\right) \qquad \Leftrightarrow \qquad (4.52)$$

$$\tfrac{T(z_2)}{T(z_1)} = \left(\tfrac{p(z_2)}{p(z_1)}\right)^{\frac{\gamma-1}{\gamma}} \qquad (4.53)$$

Assuming an air parcel somewhere in the atmosphere in the state T, p. This air parcel is now brought dry adiabatically to the surface and reaches the pressure p_0. This air parcel will now have a temperature called the potential temperature(θ):

$$\theta = T\left(\tfrac{p_0}{p}\right)^{\frac{\gamma-1}{\gamma}} \qquad (4.54)$$

Manipulating equation 4.54 and differentiating with respect to z:

$$\ln(\theta) = \ln(T) + \ln\left(\left(\tfrac{p_0}{p}\right)^{\frac{\gamma-1}{\gamma}}\right) \qquad \Leftrightarrow \qquad (4.55)$$

$$\ln(\theta) = \ln(T) + \tfrac{\gamma-1}{\gamma} \ln\left(\tfrac{p_0}{p}\right) \qquad \Leftrightarrow \qquad (4.56)$$

$$\ln(\theta) = \ln(T) + \tfrac{\gamma-1}{\gamma} \ln\left(p_0 - p\right) \qquad \Leftrightarrow \qquad (4.57)$$

$$\tfrac{d}{dz}\ln(\theta) = \tfrac{d}{dz}\ln(T) + \tfrac{d}{dz}\tfrac{\gamma-1}{\gamma} \ln\left(p_0 - p\right) \qquad \Leftrightarrow \qquad (4.58)$$

$$\tfrac{d}{d\theta}\tfrac{d\theta}{dz}\ln(\theta) = \tfrac{d}{dT}\tfrac{dT}{dz}\ln(T) + \tfrac{d}{dp}\tfrac{dp}{dz}\tfrac{\gamma-1}{\gamma} \ln\left(p_0 - p\right) \qquad \Leftrightarrow \qquad (4.59)$$

$$\tfrac{1}{\theta}\tfrac{d\theta}{dz} = \tfrac{1}{T}\tfrac{dT}{dz} + \tfrac{\gamma-1}{\gamma}\tfrac{1}{p}\tfrac{dp}{dz} \qquad \Leftrightarrow \qquad (4.60)$$

In an atmosphere satisfying the dry adiabatic condition, $\frac{dT}{dz} = -\Gamma$ meaning that $\frac{d\theta}{dz} = 0$. This is known as an atmosphere in neutral stability. Under these assumptions $\theta = T_0$ and $T = T_0 - \Gamma z$. Inserting these conditions in 4.60 yields:

$$\theta = T + \Gamma z \qquad (4.61)$$

The above derivation was based on the assumption of a dry adiabatic atmosphere. Due to local meteorological conditions such as radiative cooling and wind causes the atmosphere to deviate from the dry adiabatic condition and thus from the neutral stability. If the atmosphere has a non-adiabatic lapse rate(Λ) and assuming that the atmospheric temperature profile is:

$$T_a = T_0 - \Lambda z \qquad (4.62)$$

Inserting this result in equation 4.43 on page 62:

$$\tfrac{dp(z)}{dz} = -\tfrac{M_{\text{air}} g p(z)}{R(T_0 - \Lambda z)} \qquad (4.63)$$

Again using the chain rule on equation 4.40 on page 62 yields the following temperature dependency on height:

$$\frac{dT}{dz} = \frac{mg\frac{T(z)}{t_0-\Lambda z}}{c_v+\frac{mR}{M_{\text{air}}}} \quad \Leftrightarrow \tag{4.64}$$

$$\frac{dT}{dz} = -\frac{\Gamma T(z)}{t_0-\Lambda z} \quad \Leftrightarrow \tag{4.65}$$

Integrating equation 4.65 from z_0 to z:

$$\frac{1}{T(z)}\frac{dT}{dz} = -\Gamma\frac{1}{t_0-\Lambda z} \quad \Leftrightarrow \tag{4.66}$$

$$\int_{z_0}^{z}\frac{1}{T(z)}\frac{dT}{dz}dz = -\Gamma\int_{z_0}^{z}\frac{1}{t_0-\Lambda z}dz \quad \Leftrightarrow \tag{4.67}$$

$$\int_{z_0}^{z}\frac{1}{T(z)}\frac{dT}{dz}dz = \frac{\Gamma}{\Lambda}\int_{t_0}^{t_0-\Lambda z}\frac{1}{u}du \quad u = t_0-\Lambda z \quad du = -\Lambda dz \quad \Leftrightarrow \tag{4.68}$$

$$\ln(T(z)) - \ln(T_0) = \frac{\Gamma}{\Lambda}\left(\ln(T_0-\Lambda z) - \ln(T_0)\right) \quad \Leftrightarrow \tag{4.69}$$

$$\ln\left(\frac{T(z)}{T_0}\right) = \frac{\Gamma}{\Lambda}\ln\left(\frac{T_0-\Lambda z}{T_0}\right) \quad \Leftrightarrow \tag{4.70}$$

$$\ln\left(\frac{T(z)}{T_0}\right) = \ln\left(\left(\frac{T_0-\Lambda z}{T_0}\right)^{\frac{\Gamma}{\Lambda}}\right) \quad \Leftrightarrow \tag{4.71}$$

$$\frac{T(z)}{T_0} = \left(\frac{T_0-\Lambda z}{T_0}\right)^{\frac{\Gamma}{\Lambda}} \quad \Leftrightarrow \tag{4.72}$$

$$T(z) = T_0\left(\frac{T_0-\Lambda z}{T_0}\right)^{\frac{\Gamma}{\Lambda}} \quad \Leftrightarrow \tag{4.73}$$

$$T(z) = T_0\left(\frac{T_a(z)}{T_0}\right)^{\frac{\Gamma}{\Lambda}} \quad \Leftrightarrow \tag{4.74}$$

An adiabatic air parcel moving in a non-adiabatic atmosphere will experience an acceleration proportional to the difference in density of the air parcel(ρ) and that of the surrounding air(ρ_a):

$$a = \frac{g(\rho_a-\rho)}{\rho} \tag{4.75}$$

Using the ideal gas law:

$$a = \frac{g(T_a-T(z))}{T(z)} \tag{4.76}$$

Rewriting the expression for the acceleration and inserting equation 4.74 into the expression yields:

$$a = g\left(\frac{T(z)}{T_a}-1\right) \quad \Leftrightarrow \tag{4.77}$$

$$a = g\left(T(z)T_a^{-1}-1\right) \quad \Leftrightarrow \tag{4.78}$$

$$a = g\left(\frac{T(z)}{T_0}\left(\frac{T_a}{T_0}\right)^{-1}-1\right) \quad \Leftrightarrow \tag{4.79}$$

$$a = g\left(\left(\frac{T_a}{T_0}\right)^{\frac{\Gamma}{\Lambda}}\left(\frac{T_a}{T_0}\right)^{-1}-1\right) \quad \Leftrightarrow \tag{4.80}$$

$$\boxed{a = g\left(\left(\frac{T_a}{T_0}\right)^{\frac{\Gamma}{\Lambda}-1}-1\right)} \tag{4.81}$$

It is thus shown that the acceleration or deceleration of a moving air parcel is determined by the ratio $\frac{\Gamma}{\Lambda}$. This defines the concept of atmospheric stability. If the air parcel is accelerated by the buoyancy force of the surrounding atmosphere, it is known as an unstable atmosphere. If the air parcel is slowed down by the buoyancy force the atmosphere, it is called stable. If no acceleration due to buoyancy is experienced, the atmosphere is characterized by the dry adiabatic lapse rate and is called a neutral atmosphere.
In order to measure the atmospheric stability, a quantity called the Monin-Obukhov length is introduced (Seinfeld and Pandis, 2006, p. 862):

$$L = \frac{-\rho c_p T_0 u_*^3}{\kappa g \bar{q_3}} \tag{4.82}$$

Where, ρ is the air density, c_p is the heat capacity at specific pressure, T_0 is the surface temperature, κ is von Karman's constant, g is the acceleration of gravity, and $\bar{q_3}$ is the turbulent heat flux. Where the turbulent heat flux is:

$$\bar{q_3} = \rho c_p \overline{u_3' \theta'} \tag{4.83}$$

Where u_3' is the fluctuating wind component in the vertical direction, and θ' is the fluctuating component of the potential temperature. The relationship between the Monin-Obukhov length and the atmospheric stability is illustrated on fig. 4.3. The advantage of the Monin-Obukhov length is that all the quantities are measurable. As such, this is a tool to measure the atmospheric stability.

L		Stability Condition
Small negative	$-100\text{ m} < L < 0$	Very unstable
Large negative	$-10^5\text{ m} \leq L \leq -100\text{ m}$	Unstable
Very large (positive or negative)	$\lvert L \rvert > 10^5\text{ m}$	Neutral
Large positive	$10\text{ m} \leq L \leq 10^5\text{ m}$	Stable
Small positive	$0 < L < 10\text{ m}$	Very stable

Figure 4.3: The connection between the Monin-Obukhov length and the atmospheric stability (Seinfeld and Pandis, 2006, p. 862).

4.3 Climate

This section is based on Collins et al. (2002). The main atmospheric removal of organic compounds is through the reaction with OH radicals. The rate of removal depends on the the OH concentration distribution, the concentration distribution of the organic compound (RH), and the rate coefficient of equation 4.84:

$$\mathrm{OH} + \mathrm{RH} = \text{oxidation products} \tag{4.84}$$

Often this reaction produces peroxy radicals($\mathrm{RO_2}$) which proceed through the following reaction sequence yielding nitrogen dioxide ($\mathrm{NO_2}$), ozone($\mathrm{O_3}$), carbonyl products and a hydroperoxy radical($\mathrm{HO_2}$):

$$\mathrm{RO_2} + \mathrm{NO} = \mathrm{NO_2} + \mathrm{RO} \tag{4.85}$$

$$\mathrm{RO} + \mathrm{O_2} = \mathrm{HO_2} + \text{carbonyl products} \tag{4.86}$$

$$\mathrm{NO_2} + h\nu = \mathrm{NO} + \mathrm{O} \tag{4.87}$$

$$\mathrm{O} + \mathrm{O_2} + \mathrm{M} = \mathrm{O_3} + \mathrm{M} \tag{4.88}$$

Where M is a catalyst. In situations of high concentrations of NO the $\mathrm{HO_2}$ radicals are destroyed through the following reaction:

$$\mathrm{HO_2} + \mathrm{NO} = \mathrm{NO_2} + \mathrm{OH} \tag{4.89}$$

Thus leading to no loss of atmospheric hydroxyl radicals. However, in conditions of low concentration of NO other reaction pathways will destroy the hydroperoxy radical such as:

$$\mathrm{HO_2} + \mathrm{HO_2} + \mathrm{H_2O} = \mathrm{H_2O_2} + \mathrm{O_2} + \mathrm{H_2O} \tag{4.90}$$

$$\mathrm{RO_2} + \mathrm{HO_2} = \mathrm{ROOH} + \mathrm{O_2} \tag{4.91}$$

$$\mathrm{HO_2} + \mathrm{O_3} = \mathrm{OH} + \mathrm{O_2} + \mathrm{O_2} \tag{4.92}$$

The reaction pathways under conditions of low NO concentration will lead to a build up of organic compounds in the atmosphere, and as the OH radicals are not there to remove them, they build up further. This is also valid for methane, meaning that a release of NMVOC will result in an increase in methane concentrations as a result of the above described mechanism.

Chapter 5

Experiment

As stated in section 3.3, the aim of the experiment is to determine the change in emission from storage tank T9805 as a result of the different modes of operation with and without the degassing plant.
The experiment is divided into several sub-experiments, each dealing with a specific phase in the design and execution of the experiment:

Design and test of the tracer-release system: The tracer-release system forms a vital part of the experiment. Therefore section 5.1 is devoted to the design and testing of the accuracy of the tracer-release system.

Tracer-release experiment The actual experiments performed at the Fredericia oil terminal. This is described in section 5.2.

5.1 Design and test of the tracer-release system

The aim of this sub-experiment is the construction of a tracer-release system to create a constant controlled release of acetylene with a geometry and flow characteristic accurately simulating the methane emission.

5.1.1 Design

The VOC emission from the tank is diffuse and assumed equally spread along the rim of the tank. To adequately mimic the VOC emission, the tracer is released from 20 release points along the rim of the tank as illustrated on figure 5.1. The choice of 20 resembles a balance between simulating a continuous release and the practicality of constructing and assembling the setup. The diameter of the tank is approximately 50m and the distance from the side of the tank to the tank-side of the nearest tank is 70m, the distance between the tank side and the CRDS instrument has to be at least 100m for the measurements not to be biased of the one side of the tank as opposed to the other. Using the law of cosines means that the distance between the release points is 7.82m meaning that the distance to the measuring instrument is more than a factor of 10 greater. This means that the geometry of the controlled release will simulate the continuous release of VOC as a good approximation.

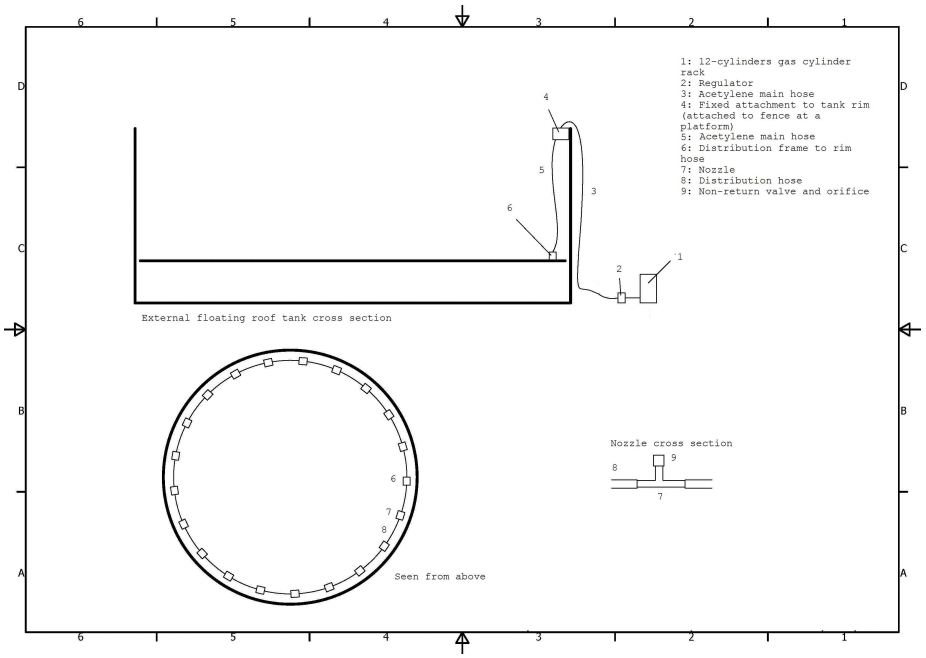

Figure 5.1: Schematic drawing of the tracer-release system.(Drawing by: Torben Rasmussen modified by the author.)

To minimize the uncertainties when applying equation A.1 on page 205 the flow of trace gas has to be as constant as possible. As it is reported by the gas supplier, that using a regulator will yield as constant gas flow as the pressure in the gas cylinder drops, a regulator is used. The assumption of constancy is tested in the laboratory as described in section 5.1.3 and 5.1.4.
To minimize the risk of dust and other impurities entering the acetylene-hose and thus posing a safety risk non-return valves are used upstream of the orifice. The gas is released horizontally through the nozzles to avoid giving the trace gas a vertical speed not present in the VOC emission, and thus not simulating the emission from the tank. The nozzle is illustrated on figure 5.2.

As an initial estimate for the size of the controlled release the emission used in US DoD ESTCP (2008) of 0.2 g/s was used. US DoD ESTCP (2008) uses a distance of 200m from release to detector, and have a minimum detection level of 3ppb for acetylene. The Picarro G2203 CRDS instrument used in this study has a minimum detection limit of 600ppt. Moreover solving equation 5.64 for the release needed to yield a concentration of 1.2ppb at at distance of 200m yields a maximum release for stability class A and B of 0.18g/s. Thus it is concluded, that a release of 0.2g/s will yield a measurable acetylene concentration when performing the experiments described in section 5.2.

5.1.2 Flow-theory

The pneumatics of the setup will be explained in this section. The section is organized so that the equations for the flow through the major individual flow

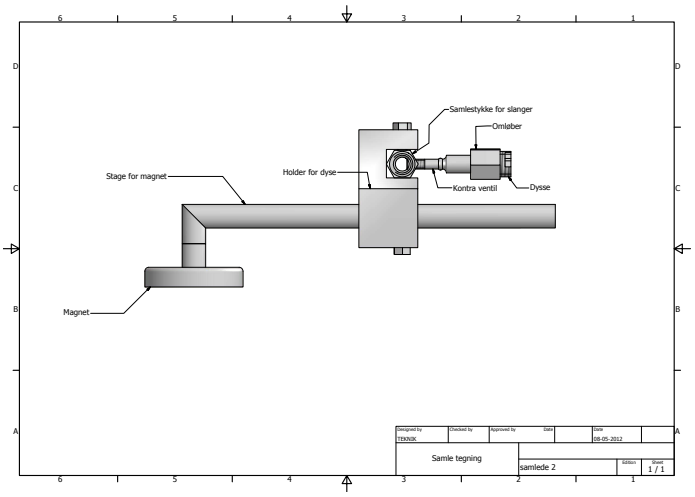

Figure 5.2: Illustration of the nozzles used in the experiment. Figure by Værkstedet.

elements will be derived first. The pressure drop in the non-return valves and fittings is assumed negligible. The structure of these sections will be according to the way the flow experiences it from the gas bottle rack to the release to the atmosphere. Afterwards the formulas for the flow through the fundamental elements will be combined and a numerical calculation to calculate the flow and pressure in the individual flow elements will be presented. This will be the foundation for the argumentation of the validity of the design.

Flow in a hose

When the flow in a hose is laminar and incompressible, the friction force is determined by the shear between the gas and the wall. The shear is defined as the force working perpendicular to the movement of the gas. When the flow is laminar, the flow will move in layers and there will be a shear between the layers. Experimentally it can be determined, that for a layer of thickness dy is influenced by a shear force (τ), the following relationship is valid:

$$\tau = -\eta \frac{dv}{dy} \tag{5.1}$$

Where η is the viscosity of the liquid and v is the velocity of the liquid. For a liquid moving at constant speed, the following force equilibrium can be set up:

$$\Delta P \pi r^2 = \left(-\eta \frac{dv}{dr}\right) 2\pi r L \quad \Leftrightarrow \tag{5.2}$$

$$\frac{dv}{dr} = -\frac{\Delta P}{2\eta L} r \quad \Leftrightarrow \tag{5.3}$$

$$\int \frac{dv}{dr} = -\int \frac{\Delta P}{2\eta L} r \quad \Leftrightarrow \tag{5.4}$$

$$v = -\frac{\Delta P}{4\eta L} r^2 + C \quad \Leftrightarrow \tag{5.5}$$

Where r is the distance from the center of the hose to a position located in the radial direction, ΔP is the pressure difference between the two sides of a fluid

element, L is the length of the fluid element and C is a constant. The constant is determines by setting the velocity at the cross-sectional perimeter to zero:

$$v = \frac{\Delta P}{4\eta L}\left(R^2 - r^2\right) \tag{5.6}$$

Integrating with respect to the perimeter area (A) to obtain the volume flow in the hose:

$$q_v = \int v dA \qquad \Leftrightarrow \tag{5.7}$$

$$q_v = \int_0^R v(2\pi r)dr \qquad \Leftrightarrow \tag{5.8}$$

$$q_v = \frac{\Delta P \pi}{2\eta L}\int_0^R \left(R^2 - r^2\right) r dr \qquad \Leftrightarrow \tag{5.9}$$

$$q_v = \frac{\Delta P \pi}{2\eta L}\left[\frac{1}{2}R^2 r^2 - \frac{1}{4}r^4\right]_0^R \qquad \Leftrightarrow \tag{5.10}$$

$$q_v = -\frac{\Delta P \pi R^4}{8\eta L} \qquad \Leftrightarrow \tag{5.11}$$

$$\tag{5.12}$$

Converting from volume flow to throughput by multiplying by the average pressure and converting from radius to diameter yields:

$$\boxed{Q = \frac{\pi d^4}{128\eta l}\bar{P}(P_u - P_d)} \tag{5.13}$$

Where $\bar{P}$ is the average pressure in the hose, P_u is the upstream pressure and P_d is the downstream pressure. This expression will be used in the numerical calculation described in section 5.1.6.

Flow through the orifice

This section is based on (American Society of Mechanical Engineers, 1971, pp. 47). In fluid dynamics there are two governing equations. The continuity equation representing the conservation of mass and the energy equation representing the conservation of energy. For flow through an orifice two areas are defined: The diameter before the orifice designated A and the diameter in the orifice designated a. The continuity equation can be written as:

$$\rho_1 A V_1 = \rho_2 a V_2 \Leftrightarrow V_1 = \frac{\rho_2}{\rho_1}\frac{a}{A}V_2 \tag{5.14}$$

Where V_1 is the velocity of the flow before the orifice, V_2 is the velocity after the orifice and ρ is the density of the gas. The energy equation can be written as:

$$(u_{k2} + u_{i2}) - (u_{k1} + u_{i1}) = (p_1 - p_2) + \rho g\,(h_1 - h_2) + q_H \tag{5.15}$$

Where u_k is the kinetic energy of the fluid, u_i is the internal energy of the fluid, p is the static pressure, g is the gravitational acceleration, h is the height of the fluid above a datum and q_H is the heat transferred to or from the gas. Invoking the following assumptions:

- The flow is horizontal: $h_1 = h_2$.

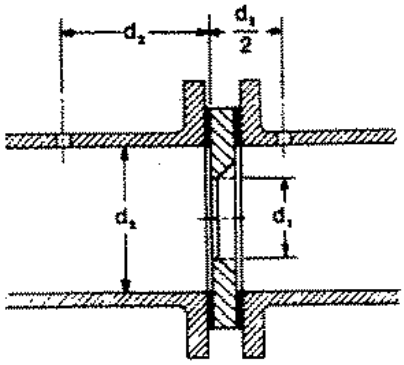

Figure 5.3: Illustration of the inner diameter(d) and the outer diameter(D) of a square-edged orifice(Crane Co, 1999, p. A-20)
.

- In flowing from section A to a the fluid performs no external work.
- The flow does not fluctuate with respect to time and the flow is anywhere normal to the pipe axis.
- There is no transfer of heat between the fluid and the pipe: $q_H = 0$.

Moreover the calculations are first performed for incompressible flow. Under these assumptions the continuity equation and the energy equation becomes:

$$AV_1 = a_V 2 \tag{5.16}$$

$$u_{k1} + p_1 = u_{k2} + p_2 \tag{5.17}$$

Because the velocity is constant across the flow profile, the kinetic energy pr. volume is:

$$u_k = \tfrac{1}{2}\rho V^2 \tag{5.18}$$

Inserting equation 5.18 in equation 5.17 yields:

$$\tfrac{1}{2}\rho V_1^2 + p_1 = \tfrac{1}{2}\rho V_2^2 + p_2 \tag{5.19}$$

Isolating V_1 in the continuity equation, inserting in the energy equation and solving for V_2:

$$\tfrac{1}{2}\rho \left(\tfrac{a}{A}\right)^2 V_2^2 + p_1 = \tfrac{1}{2}\rho V_2^2 + p_2 \tag{5.20}$$

$$p_1 - p_2 = \tfrac{1}{2}\rho V_2^2 \left(1 - \left(\tfrac{a}{A}\right)^2\right) \tag{5.21}$$

$$V_2^2 = \frac{p_1 - p_2}{\frac{1}{2}\rho\left(1-\left(\frac{a}{A}\right)^2\right)} \tag{5.22}$$

$$V_2^2 = 2\frac{p_1 - p_2}{\rho}\frac{1}{1-\left(\frac{a}{A}\right)^2} \tag{5.23}$$

The factor $\left(\frac{a}{A}\right)^2$ can be replaced by the diameters as long as the orifice is circular denominated $\beta^4 = \left(\frac{d}{D}\right)^4$. Inserting into equation 5.23 and converting to an

expression for mass:

$$m_T = \rho a V_2 \tag{5.24}$$

$$= a\sqrt{2\rho(p_1 - p_2)}\sqrt{\frac{1}{1-\beta^4}} \tag{5.25}$$

The above equation was developed under the assumption of incompressible flow. Since the experiment is working with gas, the flow is compressible. The energy equation is thus restated in the form:

$$\frac{V_1^2}{2} + \frac{p_1}{\rho_1} + u_{i1} = \frac{V_2^2}{2} + \frac{p_2}{\rho_2} + u_{i2} \tag{5.26}$$

Introducing the definition of enthalpy(H) pr. volume for a fluid:

$$H = u_i + pv \tag{5.27}$$

Where v is the specific volume of the gas defined as the inverse of the density. Applying this definition in equation 5.26:

$$H_1 - H_2 = \frac{V_2^2}{2} - \frac{V_1^2}{2} \tag{5.28}$$

The assumption of no transfer of heat between the pipe and the gas, means that the process of flow through the orifice is adiabatic, for which the following equation is valid:

$$p_1 v_1^\gamma = p_2 v_2^\gamma = c' \tag{5.29}$$

Where c' is a constant. If it is assumed that the used gas behaves like an ideal gas, equation 5.28 becomes:

$$H_1 - H_2 = \int_{p_1}^{p_2} v dp \tag{5.30}$$

Invoking equation 5.29:

$$H_1 - H_2 = c' \int_{p_1}^{p_2} p^{-\frac{1}{\gamma}} dp \tag{5.31}$$

Solving this equation knowing $\int_a^b x^n dx = \frac{b^{n+1} - a^{n+1}}{n+1}$:

$$H_1 - H_2 = c' \left(p_2^{\frac{\gamma-1}{\gamma}} - p_1^{\frac{\gamma-1}{\gamma}} \right) \frac{\gamma}{\gamma-1} \tag{5.32}$$

$$= c' \left(p_2^{\frac{\gamma-1}{\gamma}} \left(\frac{p_1}{p_1}\right)^{\frac{\gamma-1}{\gamma}} - p_1^{\frac{\gamma-1}{\gamma}} \right) \frac{\gamma}{\gamma-1} \tag{5.33}$$

$$= c' p_1^{\frac{\gamma-1}{\gamma}} \frac{\gamma}{\gamma-1} \left(1 - r^{\frac{\gamma-1}{\gamma}} \right) \tag{5.34}$$

Where $r = \frac{p_2}{p_1}$. Putting this result back into the equation for the change in kinetic energy pr. mass:

$$\frac{V_2^2}{2} - \frac{V_1^2}{2} = c' p_1^{\frac{\gamma-1}{\gamma}} \frac{\gamma}{\gamma-1} \left(1 - r^{\frac{\gamma-1}{\gamma}} \right) \tag{5.35}$$

Since $c' = v_1 p_1^{\frac{1}{\gamma}}$ inserting this into the expression yields:

$$\frac{V_2^2}{2} - \frac{V_1^2}{2} = p_1 v_1 \frac{\gamma}{\gamma-1}\left(1 - r^{\frac{\gamma-1}{\gamma}}\right) \tag{5.36}$$

Calculating the mass flow in the same way as the incompressible solution:

$$m = AV_1\rho_1 = aV_2\rho_2 \tag{5.37}$$

Using equation 5.29 in the form $\frac{\rho_2}{\rho_1} = r^{\frac{1}{\gamma}}$:

$$V_1 = V_2\left(\frac{a}{A}\right) r^{\frac{1}{\gamma}} \tag{5.38}$$

Inserting this into equation 5.36 yields:

$$\frac{V_2^2}{2} - \frac{V_2^2\left(\frac{a}{A}\right)^2 r^{\frac{2}{\gamma}}}{2} = p_1 v_1 \frac{\gamma}{\gamma-1}\left(1 - r^{\frac{\gamma-1}{\gamma}}\right) \tag{5.39}$$

$$V_2^2\left(1 - \left(\frac{a}{A}\right)^2 r^{\frac{2}{\gamma}}\right) = \frac{2p_1}{\rho_1}\frac{\gamma}{\gamma-1}\left(1 - r^{\frac{\gamma-1}{\gamma}}\right) \tag{5.40}$$

$$V_2 = \left(\frac{\frac{2p_1}{\rho_1}\frac{\gamma}{\gamma-1}\left(1-r^{\frac{\gamma-1}{\gamma}}\right)}{1-\left(\frac{a}{A}\right)^2 r^{\frac{2}{\gamma}}}\right)^{\frac{1}{2}} \tag{5.41}$$

Inserting this into equation 5.37 and using the fact $\rho_2 = \rho_1 r^{\frac{1}{\gamma}}$ yields the steady mass flow:

$$m_T = a\left(\frac{2p_1\rho_1 r^{\frac{2}{\gamma}}\frac{\gamma}{\gamma-1}\left(1-r^{\frac{\gamma-1}{\gamma}}\right)}{1-\left(\frac{a}{A}\right)^2 r^{\frac{2}{\gamma}}}\right)^{\frac{1}{2}} \tag{5.42}$$

This can be further modified using $p_1 = \frac{p_1-p_2}{1-r}$ and $\beta^2 = \frac{a}{A}$:

$$m_T = a\left(\frac{2(p_1-p_2)\rho_1 r^{\frac{2}{\gamma}}\frac{\gamma}{\gamma-1}\left(\frac{1-r^{\frac{\gamma-1}{\gamma}}}{1-r}\right)}{1-\beta^4 r^{\frac{2}{\gamma}}}\right)^{\frac{1}{2}} \tag{5.43}$$

Rewriting this in the same form as 5.25:

$$m_T = a\sqrt{\frac{2(p_1-p_2)\rho_1}{1-\beta^4}}\left(r^{\frac{2}{\gamma}}\left(\frac{\gamma}{\gamma-1}\right)\left(\frac{1-r^{\frac{\gamma-1}{\gamma}}}{1-r}\right)\frac{1-\beta^4}{1-\beta^4 r^{\frac{2}{\gamma}}}\right)^{\frac{1}{2}} \tag{5.44}$$

The last expression is usually called the expansion factor (Y):

$$Y = \left(r^{\frac{2}{\gamma}}\left(\frac{\gamma}{\gamma-1}\right)\left(\frac{1-r^{\frac{\gamma-1}{\gamma}}}{1-r}\right)\frac{1-\beta^4}{1-\beta^4 r^{\frac{2}{\gamma}}}\right)^{\frac{1}{2}} \tag{5.45}$$

Due to friction, the actual flow rate through the orifice will be less than calculated by 5.44. To compensate for that, an additional factor C is introduced in the equation:

$$m = \frac{\pi d^2}{4} \frac{C}{\sqrt{1-\beta^4}} \sqrt{2\rho_1(p_1 - p_2)} Y \tag{5.46}$$

The second expression if often replaced by the flow coefficient $K = \frac{C}{\sqrt{1-\beta^4}}$:

$$\boxed{m = \frac{\pi d^2}{4} K \sqrt{2\rho_1(p_1 - p_2)} Y} \tag{5.47}$$

This formula will in the following sections be used for fitting the flow-pressure relationship of the constructed nozzles and in the numerical calculation of the flow in the set-up.

5.1.3 Setup

To measure the flow and the temporal variation in the flow a mechanical flowmeter was constructed as illustrated on figure 5.4. This was chosen since measuring the flow through an orifice of 0.2mm requires very advanced instrumentation, which for the present purpose was deemed unnecessary.
The setup consists of a tub with water and a 2m long translucent plastic cylinder open in the end below the water level and sealed in the end above the water level. When applying a vacuum to the plastic cylinder, water is sucked from the tub into the cylinder. Before the experiment starts, the water level in the cylinder is marked on the side of the cylinder with a permanent marker. Moreover the room temperature and pressure are recorded using a M+S 1010 digital manometer and KD AK-688 digital thermometer. When a pressure is applied to the nozzle rising bubbles will form from the orifice. When the pressure is adjusted with the pressure reducing valve and the manometer, the nozzle is placed under the opening of the cylinder and the time is started. After a defined period of time the new water level is marked on the cylinder. When the experiment is over, the nozzle is removed from the opening of the cylinder at the exact time before the mark made to get a more precise marking of the final height. When the nozzle is removed from the opening, the water height in the tub is marked as well. By measuring the distance between the first and the second mark the average flow over a certain time period can be calculated in the following way:

Calculating the volume(V) as a result of time:

$$V(t) = \frac{dh_t}{dt} \cdot \pi \cdot r^2 + V_{\text{init}} \tag{5.48}$$

Where $\frac{dh_t}{dt}$ is the change in height measured from the top of the cylinder over the defined time period, r is the inner radius of the cylinder being 4cm and V_{init} is the volume before the start of the defined period.
Since the force of gravity is still working on the water above the water level of the tub, a vacuum has to exist in the cylinder corresponding to the pressure from the water column of height from the water level in the tub to the water level in the cylinder. This quantity is known as (h_b). The pressure inside the cylinder (P_{ins}) is thus calculated in the following way:

$$P_{\text{ins}} = P_{\text{out}} - h_b(t) \cdot g \cdot \rho \tag{5.49}$$

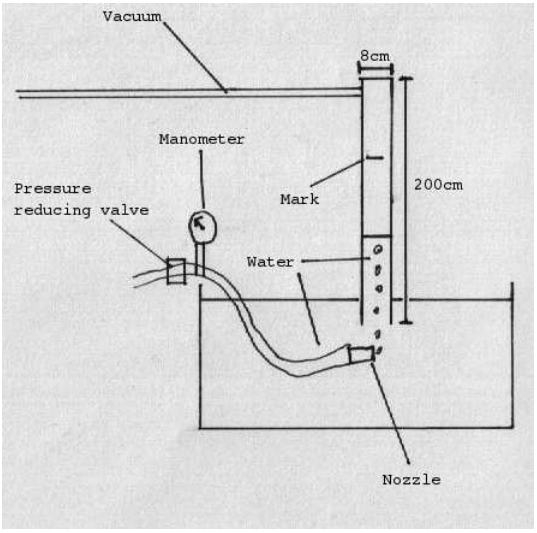

Figure 5.4: Schematic drawing of the mechanical flow meter

Where P_{out} is the room pressure, g is the gravitational constant taken to be $9.82\frac{m}{s^2}$ and ρ is the density of water taken to be $1000\frac{kg}{m^3}$.
Using the ideal gas law it is now possible to calculate the molar gas flow as s function of time($n(t)$):

$$n(t) = \frac{P_{\text{ins}}V(t)}{RT} \tag{5.50}$$

Where R is the gas constant taken to be $0.082057\frac{L\cdot\text{atm}}{K\cdot\text{mol}}$ and T is the temperature in Kelvin converted by adding 273.15 to the measured temperature. By multiplying with the molar density of the gas, it is possible to calculate the flow of gas as s function of time. By setting marks for short periods of time it is possible to detect changes in flow as a function of time.

5.1.4 Execution

The setup described in section 5.1.3 was used for three different experiments, which will be described individually:

Experiment 1 – Average flow and constancy

This experiment was performed on several nozzles and orifices to measure the average flow through the orifice and the constancy of the flow through the pressure reducing valve.
This was done using the procedure described in section 5.1.3 with a defined time period of 15 minutes following the approach of Galle (1999). After every minute a new mark was made on the cylinder due to a balance between getting a high temporal resolution and practicality. Three examples of the results from this experiment can be seen on figure 5.5. The tested nozzles are numbered sequentially in the order they are tested first time. After performing the first six measurement series the pressure reducing valve broke down. This means, that Nozzle 2 is tested with the old setup, whereas Nozzle 1 and 6 are tested

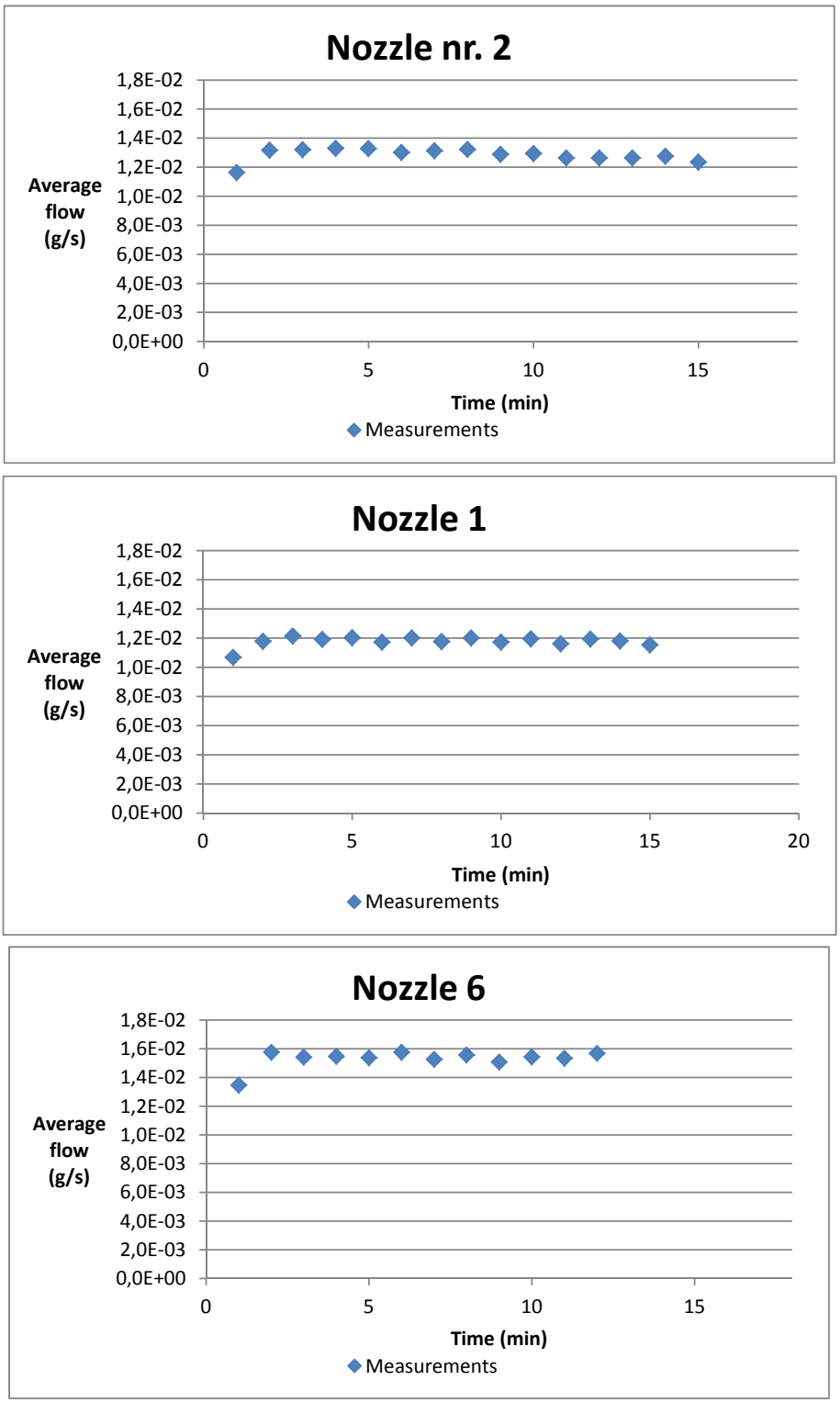

Figure 5.5: Examples of results from Experiment 1.

on the setup with a replaced pressure reducing valve. On the same time the flow-manometer was replaced with one with a resolution of 0.1bar as opposed to the old one with a resolution of 0.5 bar. This means, that the experiments performed with Nozzle 1 and 6 are considerably more precise.
Several things can be seen from the data. The variation in flow from minute to minute is very small respectively 1.40% and 1.29% root mean square with respect to the average for Nozzle 1 and 6 (excluding the first minute due to the large systematic deviation in all the measurement series). The average however is 30% larger for Nozzle 6 compared to Nozzle 1, which probably can be assigned to the d^2 factor in equation 5.47. This is not testable since the orifice diameter is not measurable to a precision of 0.01mm.

Experiment 2 – Flow-pressure relationship

To test the pressure dependency of the flow through the nozzle as presented in equation 5.47, a measurement series was performed. The water level in the cylinder was adjusted to a fixed position using the vacuum. The pressure was set and time was allowed for the flow to adjust to the new settings. A five minute measurement was made, where the first minute interval and the five minutes interval was marked on the cylinder. The pressure was subsequently raised by 0.1bar and the whole procedure was repeated covering the interval between 0.1bar and 1.5bar.
The reason for measuring for five minutes was to be able to exclude the first minute that always deviates much without much loss of data. Moreover measuring for a longer time period gives a better signal to noise ratio. Lastly since this experiment had to be repeated many times the time period was not to be longer than necessary to provide a good signal to noise ratio. The results are shown in figure 5.6. A nonlinear fit of equation 5.47 was made to the data. The fitted parameters was the diameter of the hole and the friction coefficient. The initial estimates were 0.2mm for the hole diameter as this was the construction specification and 0.6 for the friction coefficient based in reading off the graph in (Crane Co, 1999, p. A-20). The fitted diameter is $0.215mm$ and the fitted friction coefficient is 0.6761.

5.1.5 Sources of error

The declining trend seen in the measurement series of Nozzle 2 on figure 5.5 has almost disappeared after changing the pressure reducing valve and the manometer. Whereas the coefficient of determination for a linear fit to Nozzle 2 is 0.79 the corresponding coefficient is 0.23 for Nozzle 1 and 0.05 for Nozzle 6. This is probably due to leakages in the former pressure reducing valve as observed by the lab technicians during the replacement.
The flow of the first minute of every measurement series is systematically on the average 11.5% lower than the following minutes. The reason is believed to be the time it takes for the bubbles formed at the nozzle to rise to the top of the cylinder. This means that there is a time lag from the start of the experiment to any flow materialising as a change in water level. This is measured to be

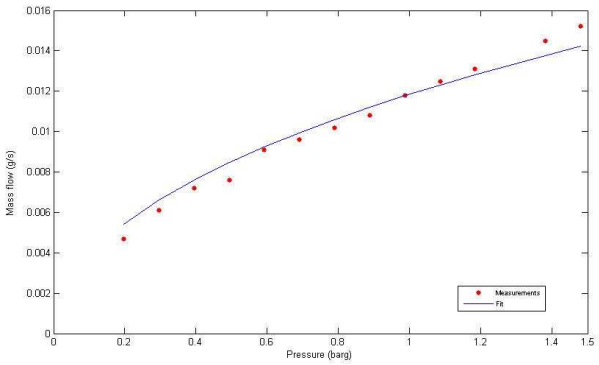

Figure 5.6: The flow-pressure relationship of Nozzle 6

approximately corresponding to the size of the discrepancy.

5.1.6 Numerical calculation of the set-up

To calculate the variation in pressure and the resulting variation in flow along the line of the set-up a numerical solution of the governing flow equations was performed.

Design of calculation

The set-up is an example of what is called a "branching flow"Sleigh and Goodwill (1998). The calculation was performed with a data point at every hose fitting. This means that the continuity equation has to be obeyed at every data point. This results in 21 equations with 21 unknowns, one for each hose in the system. For each hose in the system the following equation was solved:

$$m_{\text{in}} = m_{\text{out}} \tag{5.51}$$

Where m is the mass flow. The hoses were numbered such that the main hose was number 1, the hoses in the right branch was number 2-11 and the hoses in the left branch was number 11-21. Likewise the input pressure was called P_{in}, the pressure at the T-piece was P_1, the pressures in the right branch was P_2-P_{11} and in the left branch P_{12}-P_{21}. The nozzles in the right branch was called $a1$-$a10$ and in the left branch $b1$-$b10$. The naming convention is illustrated in fig. 5.7 This means, that the formulas for the hoses in e.g. a-branch will be:

$$\begin{aligned}
\rho_h Q_h - \rho_{12} Q_{12} - Qua_1 - \rho_3 Q_3 &= 0 && (5.52)\\
\rho_2 Q_2 - Qua_1 - \rho_4 Q_4 - Qua_2 &= 0 && (5.53)\\
\rho_3 Q_3 - Qua_2 - \rho_5 Q_5 - Qua_3 &= 0 && (5.54)\\
&\vdots \\
\rho_8 Q_8 - Qua_7 - \rho_{10} Q_{10} - Qua_9 &= 0 && (5.55)\\
\rho_9 Q_9 - Qua_8 - Qua_{10} &= 0 && (5.56)
\end{aligned}$$

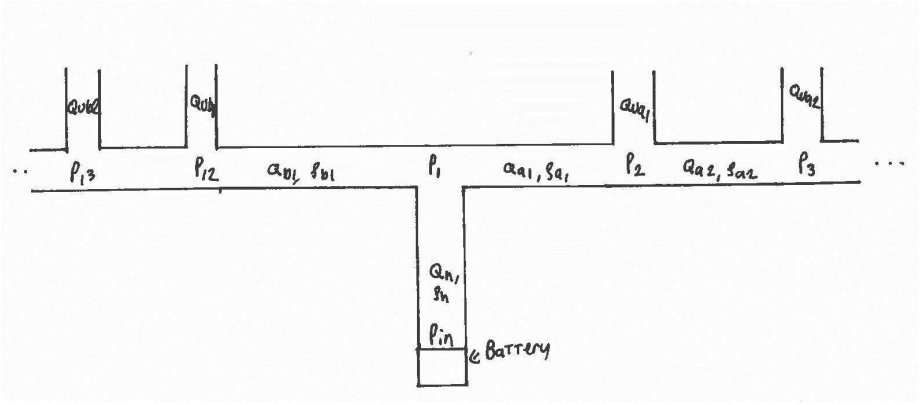

Figure 5.7: Illustration of the naming convention used in the numerical calculation.

Where ρ_x is the density divided by the average pressure in the hose, Q_x is the throughput in units of pressure times volume flowLivesey (1998) calculated from eq. (5.13), in the individual hose and Qua_x is the mass flow from the individual nozzle represented by the fitted equation in Experiment 2. ρ_h and Q_h is respectively the density divided by the average pressure and the throughput of the main hose. The density of a gas can be calculated according to the ideal gas equation as described in eq. (4.42) on page 62. The continuity equation for the main hose is calculated according to:

$$\rho_h Q_h - \rho_2 Q_2 - \rho_{12} Q_{12} = 0 \tag{5.57}$$

The equations are set up in the same way for the *b*-branch. These equations was solved using the *fsolve* MatLab-function.
To determine the tracer release rate the total flow(m) is calculated as the sum of all the nozzles:

$$m = \sum_{n=1}^{n=10} Qua_n + \sum_{n=1}^{n=10} Qub_n \tag{5.58}$$

In order to secure a homogeneous release along the branches and thereby no difference between one side of the tank and the other. the relative deviation(σ) is calculated between the first nozzle in a branch and the last nozzle in a branch, since it it expected to be where the largest deviation is. This is calculated according to the following formula:

$$\sigma_a = \frac{Qua_1 - Qua_{10}}{Qua_1} \tag{5.59}$$

The filling time used as the minimum release length is calculated by the length of the hose divided by the velocity of the flow in the hose and summing up for the hoses in series:

$$t = \frac{L_h}{v_h} + \frac{L_{a1}}{v_{a1}} + \frac{L_{a2}}{v_{a2}} + \ldots + \frac{L_{a10}}{v_{a10}} \qquad v_{ax} = \frac{m_{ax}}{\rho_{ax} A} \tag{5.60}$$

Where L_h is the length of the main hose, L_{ax} is the length of hose number x in branch a, v_{ax} is the velocity of the flow in hose number x in branch a, m_{ax} is

the mass flow in hose number x in branch a, ρax is the density in hose number x in branch a and A is the cross-sectional area of the hose. The filling time calculated in this way is an approximate filling time, since it is calculated at steady state.
To ensure the assumptions of laminar and incompressible flow, the Reynolds number and Mach number for all the hoses are calculated. Reynolds number of the individual hoses is calculated according to the formulaLivesey (1998):

$$Re = \frac{4MQD_h}{RTB\eta} \tag{5.61}$$

Where $D_h = D$ is the hydraulic diameter of the hose, B is the cross-section perimeter and η is the viscosity of the gas.
The Mach number is calculated according to the following formula:

$$Ma = \frac{v_{ax}}{v_s} \tag{5.62}$$

Where Ma is the Mach number and v_s is the speed of sound.
To determine the nozzle diameter required to give the design flow of $0.2\frac{g}{s}$, the diameter was added as a fit parameter in a separate calculation. This means that another equation has to be added to the system:

$$\sum_{n=1}^{n=10} Qua_n + \sum_{n=1}^{n=10} Qub_n - 0.2 \cdot 10^{-3} = 0 \tag{5.63}$$

The procedure was repeated in a loop with input pressures ranging from 0.1 barg to 1.5 barg to decide the input pressure used. Moreover the effect of temperature was examined by doing the calculations at respectively $5°C$ and $25°C$ as the expected maximum and minimum temperature. The effect of changing atmospheric pressure was examined by performing the calculation at respectively $980hPa$ and $1030hPa$ as representing the expected maximum and minimum atmospheric pressure.

Results

An example of the results from a calculation is shown in table 5.1. The settings for the calculation are chosen such that the atmospheric pressure is expected to be on average 1013hPa and the average temperature to be $15°C$. Moreover as will be shown, the input pressure and orifice diameter is the same as in the actual experiment.
As can be seen from the table, the pressure drop from the battery to the end of the line is very small. That is very acceptable, since it means a smaller variation in the tracer release rate, which can be seen from column 4. The release rate has to be as constant as possible for detecting small changes in the actual emissions. Moreover it can be seen that the pressure in the data points is symmetric when comparing $P_2 - P_{11}$ to $P_{12} - P_{21}$ corresponding to the a- and b-branch. The results of the numerical calculation with varying pressure are shown in table 5.2. For the assumptions of Hagen-Poiseuilles law to be valid the flow has to be laminar and incompressible. The transition from laminar to turbulent flow takes place at the critical Reynolds number $Re_{\text{crit}} = 2300$Livesey (2004). This means,

Data point:	Value (barg):	Data point:	Value $\left(\frac{g}{s}\right)$:
P_1	0.5990		
P_2	0.5990	Qua_1	0.0163
P_3	0.5990	Qua_2	0.0163
P_4	0.5990	Qua_3	0.0163
P_5	0.5989	Qua_4	0.0163
P_6	0.5989	Qua_5	0.0163
P_7	0.5989	Qua_6	0.0163
P_8	0.5989	Qua_7	0.0163
P_9	0.5989	Qua_8	0.0163
P_{10}	0.5989	Qua_9	0.0163
P_{11}	0.5989	Qua_{10}	0.0163
P_{12}	0.5990	Qub_1	0.0163
P_{13}	0.5990	Qub_2	0.0163
P_{14}	0.5990	Qub_3	0.0163
P_{15}	0.5989	Qub_4	0.0163
P_{16}	0.5989	Qub_5	0.0163
P_{17}	0.5989	Qub_6	0.0163
P_{18}	0.5989	Qub_7	0.0163
P_{19}	0.5989	Qub_8	0.0163
P_{20}	0.5989	Qub_9	0.0163
P_{21}	0.5989	Qub_{10}	0.0163

Table 5.1: Results of calculation with $P_{\text{in}} = 0.6barg$, atmospheric pressure $P_{\text{atm}} = 1013hPa$, t=15°C, d=0.35mm

that the pressure lower than 0.7 barg, and thus the maximum tracer release rate will be $0.35\frac{g}{s}$. As a safety margin an input pressure of 0.6 barg is chosen. Choosing an orifice diameter of $0.35mm$ will yield a tracer release rate larger than the design criteria, which is desirable. Moreover seen from a practical point of view, an orifice diameter of $0.35mm$ will be easier to construct in a homogeneous way compared to a smaller orifice diameter.
As can be seen from the table, the assumption of incompressible flow is satisfied at all pressures. The criteria for the flow to be treated as incompressible is $Ma < 0.3$Livesey (1998).
It is also shown in table 5.2 that the variation in tracer release rate as a function of pressure drop in the hoses is negligible.
Lastly it is shown that the tracer release length has to be at least 910 seconds corresponding to approximately 15 minutes.

Pressure (P) (barg)	Total flow (m) $\left(\frac{g}{s}\right)$	Relative deviation (σ) (%)	Filling-time (t) (s)	Min d mm	Re_h	Ma_h
0.1	0.14	0.0378	1491	0.44	882	0.0012
0.2	0.19	0.0223	1156	0.36	1240	0.0015
0.3	0.23	0.0161	1028	0.33	1509	0.0017
0.4	0.27	0.0126	964	0.30	1732	0.0018
0.5	0.30	0.0103	929	0.29	1925	0.0019
0.6	0.33	0.0086	910	0.28	2096	0.0019
0.7	0.35	0.0074	900	0.27	2251	0.0019
0.8	0.37	0.0064	896	0.26	2393	0.0019
0.9	0.39	0.0056	896	0.25	2525	0.0019
1.0	0.41	0.0050	899	0.24	2647	0.0019
1.1	0.43	0.0045	904	0.24	2763	0.0019
1.2	0.45	0.0040	911	0.24	2872	0.0019
1.3	0.46	0.0037	919	0.23	2975	0.0019
1.4	0.48	0.0033	928	0.23	3073	0.0019
1.5	0.49	0.0031	938	0.22	3167	0.0018

Table 5.2: Result of numerical calculation of flow in the set-up. Atmospheric pressure $P_{\text{atm}} = 1013hPa$, t=15°C, where Re_h and Ma_h are respectively the Reynolds number and the Mach number for the flow in the main hose.

5.2 Tracer-release experiment

5.2.1 Set-up

As can be seen from fig. 5.8, the study area is characterised by a complex geometry. Tank T9805 as marked with red on the figure, is located as part of a tank farm meaning that the emissions from the tank is likely to be mixed with emissions from the surrounding tanks and the refinery. Moreover all tanks are located in pits, as a safety measure to contain the oil in case of tank leakage, in combination with the tank farm geometry means that an accurate description of the emission from Tank T9805 is very complicated.
To determine where to locate the CRDS in order to measure the emission from tank T9805 and still minimise the signal from the surrounding tanks a simple Gaussian plume modeling approach was chosen. The Gaussian plume model with total reflection as presented in (Seinfeld and Pandis, 2006, p. 918) calculates the concentration as:

$$C(x,y,z) = \frac{q}{2\pi u \sigma_y \sigma_z} \left(e^{-\left(\frac{z-h_s}{2\sigma_z}\right)^2} + e^{-\left(\frac{z-h_s}{2\sigma_z}\right)^2} \right) e^{-\left(\frac{y}{2\sigma_y}\right)^2} \tag{5.64}$$

Where $C(x,y,z)$ is the concentration of an emitted compound as a function of position in meters, q is the emission in gs^{-1}, u is the wind speed, σ is the dimensionless dispersion parameter in the y or z direction and h_s is the release height. This was implemented in FORTRAN and afterwards exported to ArcGIS, since ArcGIS contains a number of preprogrammed tools suited for geographic geometric analysis. In the geometric analysis only the emission plumes from tank T9806 and T9804 apart from tank T9805 (see fig. 5.8) was included for

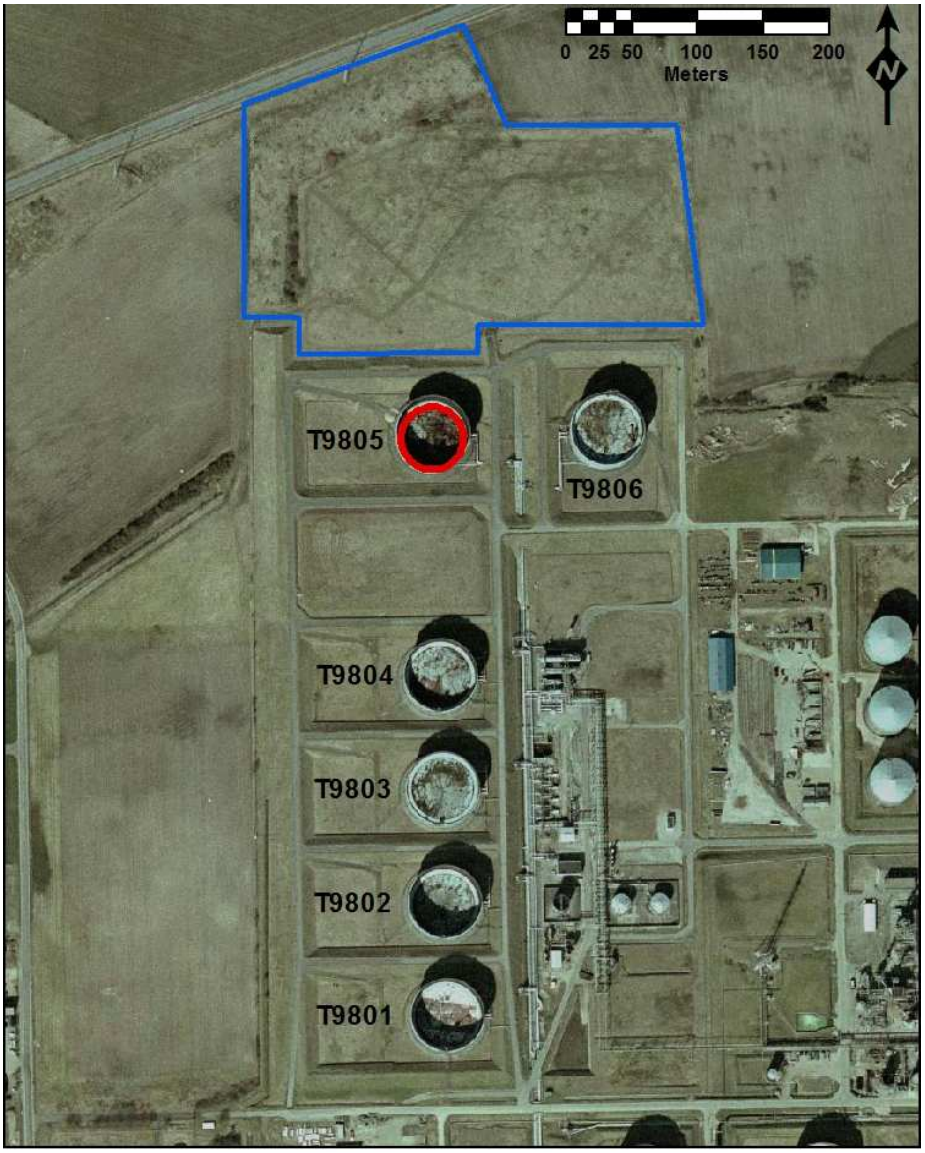

Figure 5.8: Orthophoto of the Fredericia oil terminal(Source: KMS). The numbers of the individual tanks are written in black. The tank studied in this project is marked with red. The area where the measurements are to be taken is marked with blue.

simplicity and because it was assumed that the other tanks were located so far away that, due to atmospheric dilution of the emission, their signal was negligible. The emission plumes from the three tanks and the overlap of the emission plumes, for every wind direction from south to west with one degree interval and an average wind speed of 5 m/s, was calculated using the ArcGIS ModelBuilder and Python scripting. Afterwards the largest possible axis parallel rectangle, within the plume from tank T9805 but outside the overlap region from tank T9806 and T9804 in a distance between 100m and 250m from the tank rim was calculated and the gps-coordinates of the rectangle in the coordinate system WGS84 (World Geodetic System) was calculated. The aim was thus to position the CRDS within this delineated rectangle using the concomitant GPS. An example of the graphical visualisation of one such calculation can be seen in fig. 5.9.

An excerpt of the data are shown in tables 5.3a to 5.3d. The area of the largest possible axis parallel rectangle as a function of wind direction is plotted in figs. 5.10a to 5.11b. To discriminate between which wind directions to perform measurements and which to rule out the area of the largest possible axis parallel rectangle was used. Since the spatial resolution of a GPS (depending on location and circumstances) is $> 10m$ a rectangle area of a few hundred m^2 was used as discrimination limit.

As can be seen on fig. 5.10a, for the stability class A and B the area of the largest possible axis parallel rectangle is decreasing until a wind direction of approximately 245°. This is a consequence of the chosen geometry. Since the Gaussian plume is approximately elliptical, as the plume is rotated and the rectangle is not rotated along, the largest possible axis parallel rectangle will decrease. When the wind direction changes past 245° the geometry of the largest possible rectangle changes as illustrated in figs. 5.12a and 5.12b. The geometry for the western wind directions is independent of the influence from the other tanks as a function of wind direction. For all wind directions the area of the largest possible axis parallel rectangle is larger than $4000m^2$ and as such it should be possible to obtain a signal from Tank T9805 without interference from the two nearby tanks in all the considered wind directions. Moreover the results for this stability class contains the largest areas compared to all the other wind directions.

For the case of stability class C as illustrated on fig. 5.10b the area is slightly decreasing between 180° and 200° thus to increase reaching a peak at a wind direction around 220°. This is a result of the fact that at this wind direction the interference from the plume of tank T9804 has disappeared and only a minimal area of the plume from tank T9806 is overlapping the plume from Tank T9805. Again the area of the largest possible axis parallel rectangle is stabilizing at wind directions more westerly than 245° as a result of the same effect as for stability class A and B. The conditions where reliable measurements would easiest be obtained appears to be with a wind direction around 220°. However, as with stability class A and B, it appears that it should be possible to obtain reliable measurements in all the considered wind directions since the area is larger than $4000m^2$ for all considered wind directions. For stability class C the areas have on average declined indicating a larger overlap from the surrounding tanks as compared to stability class A and B.

Wind direction (°)	LLx	LLy	URx	URy	Size(m^2)
180	55.5968769	9.7390157	55.5981341	9.7408217	15849
190	55.5968754	9.7395888	55.5980629	9.7412937	14132
200	55.5968653	9.7401522	55.5979605	9.7416782	11659
210	55.5967961	9.7406187	55.5977843	9.7419987	9513
220	55.5966505	9.7410967	55.5976142	9.7422541	7755
230	55.5965531	9.7412851	55.5973146	9.7424775	6350
240	55.5964246	9.7414883	55.5970557	9.7426268	5040
250	55.5955187	9.7418799	55.5968757	9.7423773	4500
260	55.5952950	9.7418759	55.5965938	9.7423953	4519
269	55.5950939	9.7418645	55.5963760	9.7424030	4636

(a) Largest axis parallel rectangle for the respective wind direction in stability class A and B.

Wind direction (°)	LLx	LLy	URx	URy	Size(m^2)
180	55.5976917	9.7387946	55.5981215	9.7409176	6565
190	55.5976372	9.7394796	55.5980500	9.7414950	5983
200	55.5974720	9.7401326	55.5979676	9.7418205	5954
210	55.5971227	9.7407472	55.5978538	9.7421930	7429
220	55.5966704	9.7411651	55.5975771	9.7424853	8358
230	55.5964375	9.7414757	55.5972909	9.7425986	6676
240	55.5962991	9.7416296	55.5969650	9.7427120	5045
250	55.5956554	9.7418786	55.5967354	9.7424501	4187
260	55.5954245	9.7418708	55.5964504	9.7424767	4235
269	55.5952266	9.7418670	55.5962306	9.7424698	4125

(b) Largest axis parallel rectangle for the respective wind direction in stability class C.

Wind direction (°)	LLx	LLy	URx	URy	Size(m^2)
180	55.5980642	9.7388329	55.5981375	9.7388568	12
190	55.5968526	9.7398279	55.5974655	9.7401522	1349
200	55.5974713	9.7402885	55.5981420	9.7408791	2733
210	55.5971755	9.7409378	55.5979703	9.7417364	4394
220	55.5968699	9.7414837	55.5977207	9.7425405	6256
230	55.5963867	9.7415445	55.5971916	9.7427408	6726
240	55.5961602	9.7417543	55.5969024	9.7427463	5131
250	55.5957728	9.7418809	55.5966146	9.7426542	4496
260	55.5955266	9.7418803	55.5963435	9.7426799	4519
269	55.5953352	9.7418777	55.5961310	9.7426893	4473

(c) Largest axis parallel rectangle for the respective wind direction in stability class D.

Wind direction (°)	LLx	LLy	URx	URy	Size(m^2)
180	0.0000000	0.0000000	0.0000000	0.0000000	0
190	55.5978461	9.7397853	55.5982140	9.7398462	139
200	55.5974287	9.7405092	55.5981582	9.7408501	1678
210	55.5971458	9.7411601	55.5979551	9.7417598	3332
220	55.5969088	9.7417098	55.5976732	9.7426427	4959
230	55.5967038	9.7421141	55.5973416	9.7432454	5060
240	55.5963937	9.7424741	55.5970463	9.7436158	5223
250	55.5960024	9.7422260	55.5965285	9.7436527	5314
260	55.5956822	9.7424186	55.5962830	9.7437185	5501
269	55.5954543	9.7423637	55.5960094	9.7437481	5430

(d) Largest axis parallel rectangle for the respective wind direction in stability class E and F.

Table 5.3: Excerpt of data from the geographic geometric analysis.

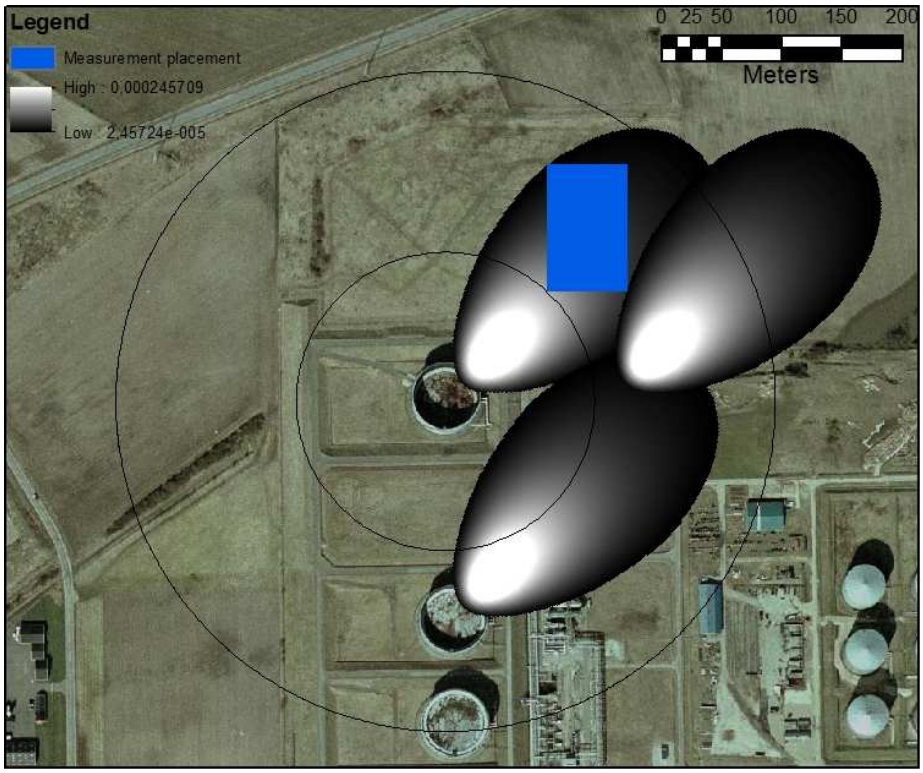

Figure 5.9: Example of the results of the Gaussian plume calculation. Data calculated for 225° wind direction and stability class A and B.

The results for stability class D shown on fig. 5.11a resembles the results for stability class C, however, the peak at a wind direction around 220° is sharper. Moreover the area of the largest possible axis parallel rectangle is almost zero at a wind direction of 180° and gradually increasing reaching a maximum of a little more than $7000m^2$, which again is smaller than the maximum of stability class C. That the initial areas of the largest possible axis parallel rectangles are almost zero means that measurements will not be taken in wind directions between 180° and approximately 190°.

For stability class E and F as shown on fig. 5.11b the overlap has increased even further. This is seen from the areas being zero for wind directions between 180° and 190° and thus gradually increasing. This means, that for this stability class measurements will not be taken for wind directions between 180° and roughly 200°. From 190° the area of the largest possible axis parallel rectangle is increasing until a wind direction of 220°, whereupon the area stabilizes fluctuating around a value of approximately 5000°. For this atmospheric stability class the area of the largest possible axis parallel rectangle stabilizes at relatively southern winds. As illustrated on fig. 5.12 the overlap between the emission plumes from the surrounding tanks ceases at relatively southern winds compared to the other stability classes. This is the cause of the stability in the graph of the area as a function of wind direction.

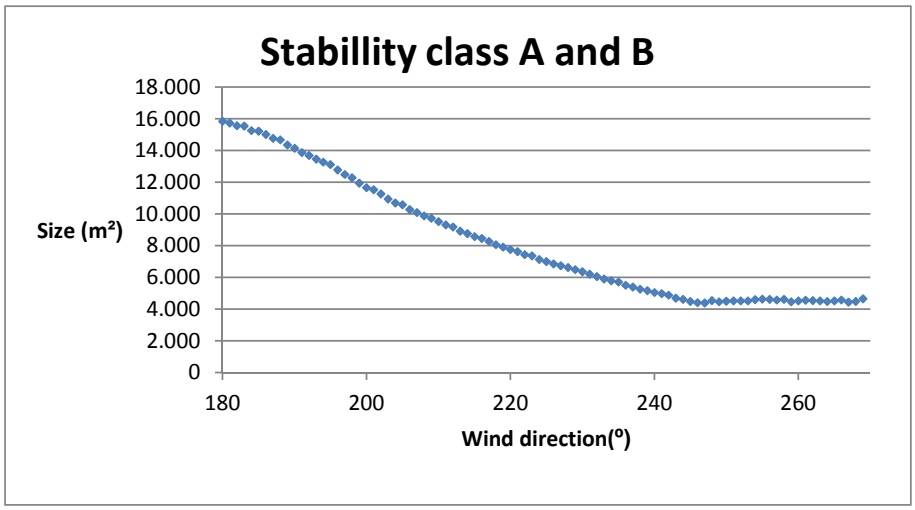

(a) Graph of data from the geometric analysis for stability class A and B

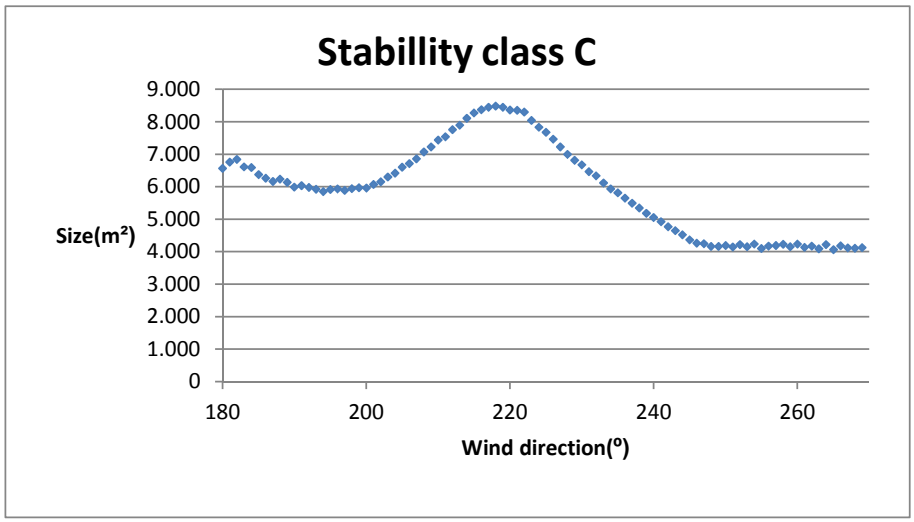

(b) Graph of data from the geometric analysis for stability class C

Figure 5.10: Graphs of area of largest possible axis parallel rectangle for stability class A and B and C.

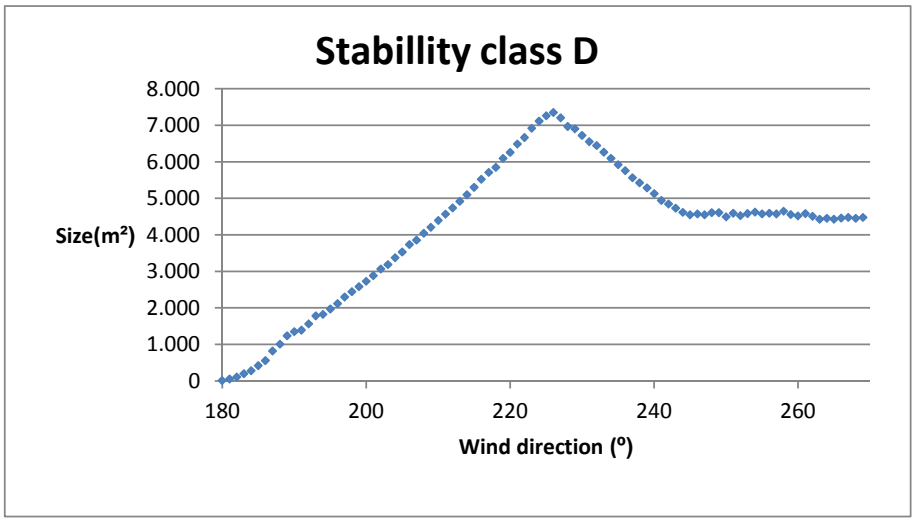

(a) Graph of data from the geometric analysis for stability class D

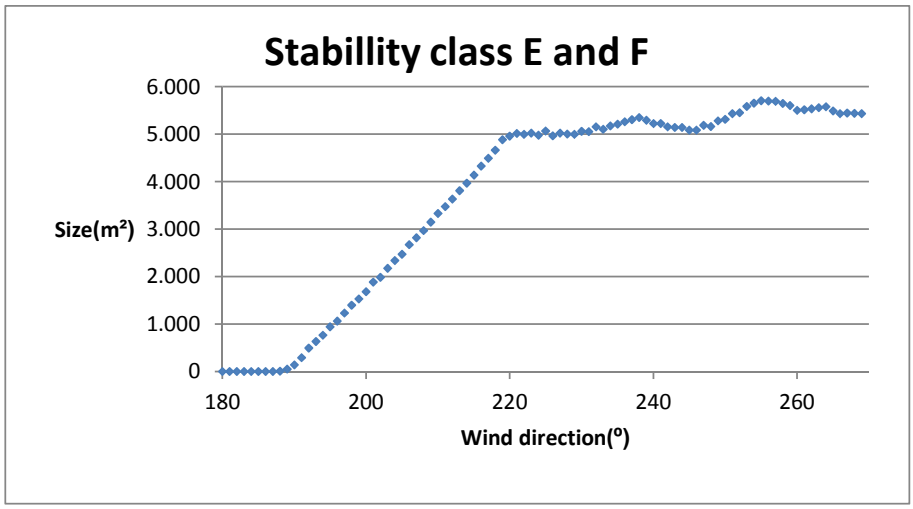

(b) Graph of data from the geometric analysis for stability class E and F

Figure 5.11: Graphs of area of largest possible axis parallel rectangle for stability class D and E and F.

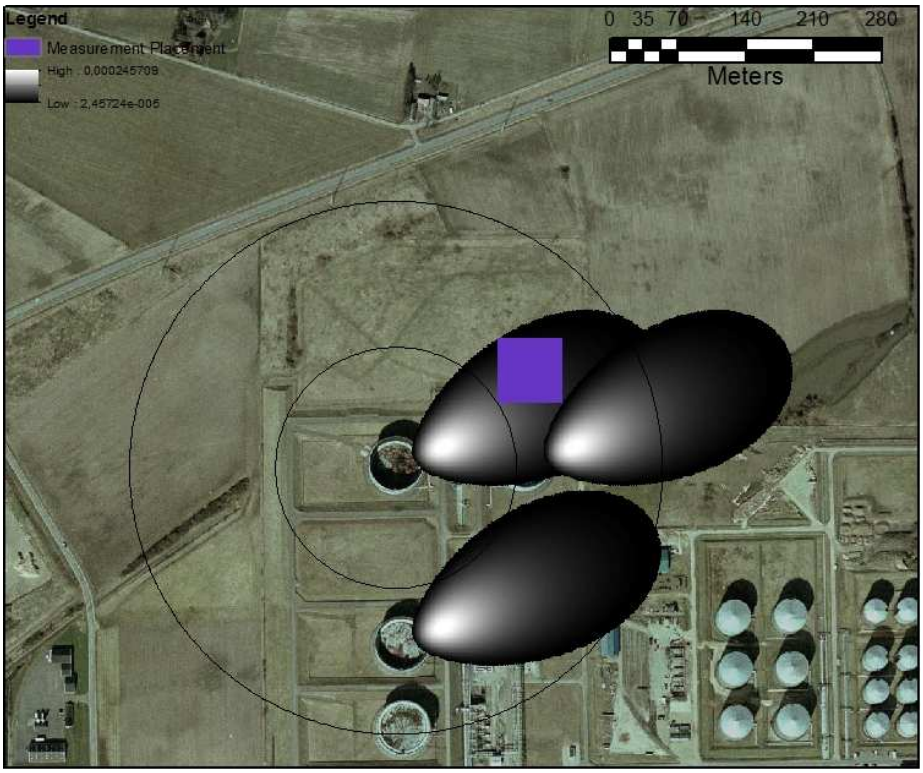

(a) Results of the Gaussian plume calculation. Data calculated for 245° wind direction and stability class A and B.

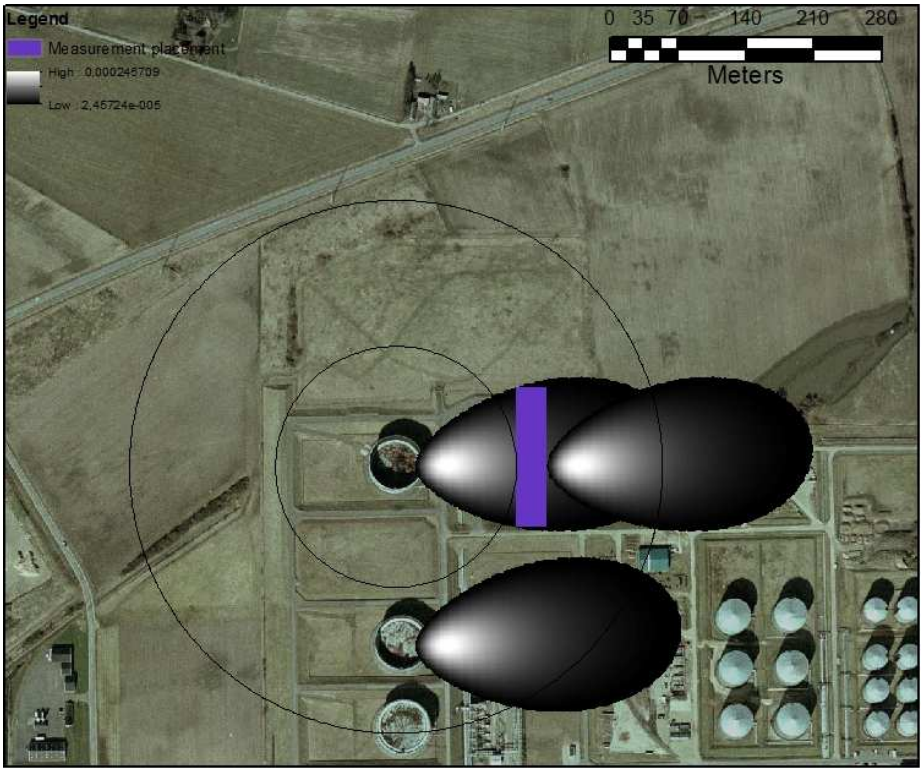

(b) Results of the Gaussian plume calculation. Data calculated for 265° wind direction and stability class A and B.

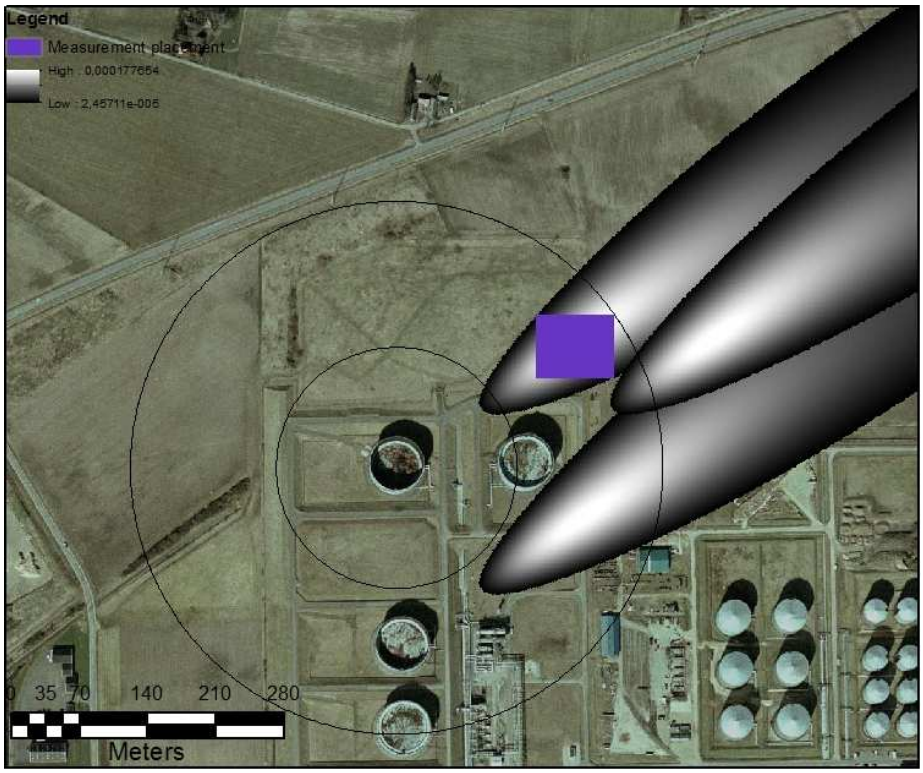

Figure 5.12: Results of the gaussian plume calculation for stability class E and F for a wind direction of 235°.

5.2.2 Instrumentation

Sonic Anemometer

To aid in determining the initial position of the CRDS and as an aid in determining appropriate averaging times and sorting the obtained data a Metek uSonic-3 Scientific sonic anemometer was installed at the field north of the Fredericia terminal.
The working principle of a combined sonic anemometer and thermometer is a set of combined sound wave emitters/receivers aligned opposite each other. As shown below, the travel time of a sound pulse between a set of emitters/receivers depends on the wind speed and the temperature. Thus a measurement of the travel times between the emitters/receivers allows a fast determination of wind speed and temperatureSozzi and Favaron (1996):
As seen from figure fig. 5.13 the two travel times depend on the geometry of the sonic and the wind speed as follows(Kaimal and Finnigan, 1994, p. 247):

$$t_1 = \frac{d}{c\cos(\gamma) - v_d} \tag{5.65}$$

$$t_2 = \frac{d}{c\cos(\gamma) + v_d} \tag{5.66}$$

By measuring the two travel times independently and taking the difference between the reciprocals, the wind speed parallel to the axis joining the set of

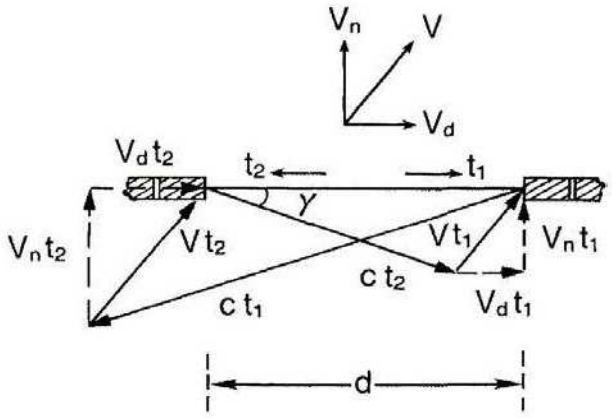

Figure 5.13: Illustration of the sound ray geometry of a pair of emitters/receivers. γ is the angle between the line joining the emitters/receivers and the apparent propagation of the sound pulse from E/R no. 2 to E/R no. 1, d is the distance between the two emitters/receivers c is the velocity of sound, V is the velocity of the wind, t_1 is the travel time from E/R no. 2 to E/R no. 1, and t_2 is the travel time from E/R no. 1 to E/R no. 2(Kaimal and Finnigan, 1994, p. 247).

emitters/receivers(v_d) can be determinedSozzi and Favaron (1996):

$$\frac{1}{t_1} - \frac{1}{t_2} = \frac{c\cos(\gamma) - v_d}{d} - \frac{c\cos(\gamma) + v_d}{d} = \frac{2V_d}{d} \quad \Leftrightarrow \quad (5.67)$$

$$V_d = \frac{d}{2}\left(\frac{1}{t_1} - \frac{1}{t_2}\right) \quad \Leftrightarrow \quad (5.68)$$

Thus by aligning three non-parallel sets of emitters/receivers the three-dimensional wind speed can be determined. The temperature is determined by looking at the sum of the travel times:

$$\frac{1}{t_1} + \frac{1}{t_2} = \frac{c\cos(\gamma) - v_d}{d} + \frac{c\cos(\gamma) + v_d}{d} = \frac{2c\cos(\gamma)}{d} \quad (5.69)$$

As seen from fig. 5.13 $\gamma = \sin^{-1}\left(\frac{V_n}{c}\right)$. Substituting this expression into eq. (5.69) yields:

$$\frac{1}{t_1} + \frac{1}{t_2} = \frac{2c\cos\left(\sin^{-1}\left(\frac{V_n}{c}\right)\right)}{d} = \frac{2c\sqrt{1-\frac{v_n^2}{c^2}}}{d} = \frac{2\sqrt{c^2 - v_n^2}}{d} \quad (5.70)$$

Isolating c^2:

$$\frac{1}{t_1} + \frac{1}{t_2} = \frac{2\sqrt{c^2 - v_n^2}}{d} \quad \Leftrightarrow \quad (5.71)$$

$$d\left(\frac{1}{t_1} + \frac{1}{t_2}\right) = 2\sqrt{c^2 - v_n^2} \quad \Leftrightarrow \quad (5.72)$$

$$\frac{d}{2}\left(\frac{1}{t_1} + \frac{1}{t_2}\right) = \sqrt{c^2 - v_n^2} \quad \Leftrightarrow \quad (5.73)$$

$$\frac{d^2}{4}\left(\frac{1}{t_1} + \frac{1}{t_2}\right)^2 = c^2 - v_n^2 \quad \Leftrightarrow \quad (5.74)$$

$$\frac{d^2}{4}\left(\frac{1}{t_1} + \frac{1}{t_2}\right)^2 + v_n^2 = c^2 \quad \Leftrightarrow \quad (5.75)$$

So far c has been treated as a constant. The speed of sound however, is not constant by varies with pressure and temperature. One expression valid for most applications(Kaimal and Finnigan, 1994, p. 216):

$$c^2 = 403T\left(1 + 0.32\frac{e}{p}\right) \tag{5.76}$$

Where T is the absolute temperature, e the water vapor pressure, and p the atmospheric pressure. "The term $\frac{e}{p}$ has little impact on the overall performance and is typically neglected"Sozzi and Favaron (1996). Inserting this expression into eq. (5.75):

$$\frac{d^2}{4}\left(\frac{1}{t_1} + \frac{1}{t_2}\right)^2 + v_n^2 = 403T \qquad \Leftrightarrow \tag{5.77}$$

$$T = \frac{d^2}{1612}\left(\frac{1}{t_1} + \frac{1}{t_2}\right)^2 + \frac{v_n^2}{403} \qquad \Leftrightarrow \tag{5.78}$$

The value of V_n is derived from the geometry of three sets of emitters/receivers in the sonicSozzi and Favaron (1996). All of the above is performed internally in the sonic anemometer, and the output consists of the x-, y-, and z-component of the wind speed, the vectorial sum, the wind direction and the temperature in degree Celsius.

In order to calculate the turbulence characteristics used in this study, cross-contamination of the wind-directions have to be avoided. The sonic theory thus far developed has assumed, that the sonic is perfectly leveled ant that the terrain is level as well. Since this is most often not the case, the data are treated in a streamline coordinate system instead of the sonic coordinate system. In order to align the data into this coordinate system a tilt correction algorithm is appliedWilczak et al. (2001). The fundamental assumption for this data transformation is that the turbulence is homogeneous such that there is no average vertical wind direction. The tilt correction algorithm follows this procedure(Løfstrøm[1], personal communication):

1. First the data points are transformed from the sonic coordinate system, to the ordinary right hand coordinate system.

2. A despiking procedure is applied. If $x_i - x_{i+1} > 5\sigma$ where x is a data point and i is a running index, the data point is discarded. Since the later calculated averages are not time averages, no interpolation between the data point before and after is made.

3. Next the average wind direction is calculated. This is done both as a scalar and a vector in order to handle wind directions around N, where an average between 360 ∘ and 0° is 180°.

4. A yaw rotation around the z-axis is applied such that the x-axis corresponds with the mean wind direction.

[1]Senior advisor/research meteorologist, Danish Center for Environment and Energy, Per Løfstrøm

5. A tilt rotation around the new y-axis is applied, such that the mean wind direction in the z-direction becomes 0 in agreement with the fundamental assumption.

6. Turbulence fluxes and moments are calculated.

The FORTRAN code implementing the above described algorithm, developed by Per Løfstrøm has been at disposal for the current project, but since it is used in a black box approach, it is not included in the report.

Cavity RingDown Spectrometer

In this section the physics of the Picarro G2203 Cavity RingDown Spectrometer is outlined. The section starts with an overview of the components of the instrument followed by a simple description of the working principles of the instrument known as the "photon-bullet" model of a cavity ringdown spectrometer. Afterwards a wave-description of the cavity and the formation of resonance modes in the cavity is presented, since the cavity constitutes the main element in the instrument. Lastly a series of technical details important for understanding the uncertainties in the results from the instrument are outlined.

An overview of the components comprising the CRDS is shown in figure 5.14. CRDS is a special type of absorption spectroscopy. In absorption spectroscopy light of a certain intensity is measured before and after the light has passed the sample, and the difference in intensity as a function of wavelength or frequency results from absorption in the sample. The absorption is then proportional to the concentration of absorbing material in the sample. In this way the concentration of the absorbing material in the sample can be determined by measuring the difference in intensity before and after passage of the sample.
In the Picarro G2203 instrument, the light is generated by a tunable[2] diode laser. The light then passes a wavelength monitor and one or more optical components which, as will be described below, match the wavelength and the cavity path length to each other in order to generate optical resonance in the cavity. The light the enters the cavity where it interacts with the atmospheric sample at low pressure, to avoid pressure broadening of the absorption lines, and then leaves the cavity to be measured by an optical detector.

The "photon-bullet" model of CRDS. As defined in section 6.2.2 radiation interacting with an absorbing medium of thickness s is weakened according to:

$$dI_\nu = -\alpha I_\nu ds \tag{5.79}$$

Where α is the absorption coefficient. Integrating both sides of the equation, assuming that α is independent of position, defining the incident intensity at $s = 0$ to be I_0, and replacing s with d yields what is known as Beer-Bouguer-Lambert law ((Liou, 2002, p. 28) and Lehmann et al. (2009)):

$$I = I_0 e^{-\alpha(\nu)d} \qquad \alpha(\nu) = N\sigma(\nu) \tag{5.80}$$

[2]Meaning that the wavelength of the radiation can be adjusted (Encyclopedia Britannica Online(1), 2012)

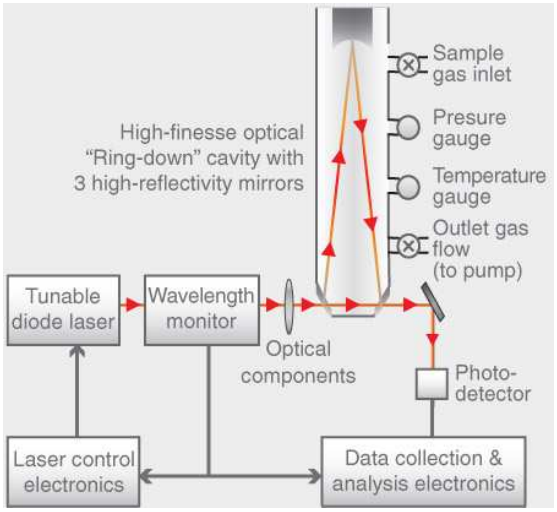

Figure 5.14: Schematic drawing of the components of the Picarro G2203 Cavity Ringdown Spectrometer. (Source: `www.picarro.com`)

Where N is the number density of the absorbing specie and $\sigma(\nu)$ is the absorption cross-section as a function of frequency.

The following description of a CRDS will be based in a simplified system as illustrated in fig. 5.15, consisting of a laser, two mirrors with reflectivity R and an oscilloscope connected to a computer. If the duration of the laser pulse width is shorter than the round-trip time, the signal exiting the cavity will consist of a series of discrete pulses. Imagining the mirrors to be without absorption and scattering losses, the transmission will be: $T = 1 - R$. For a light pulse leaving the laser source, passing through the first mirror, the cavity and the second mirror and ending up at the detector, the intensity registered by the detector will be:

$$I_0 = I_{\text{laser}} T^2 e^{-\alpha d} \tag{5.81}$$

Where d is the length of the cavity where the absorbing specie is present. The second pulse experiences to transmit the first mirror, pass the cavity, be reflected by the second mirror, pass the cavity again, be reflected by the first mirror, pass the cavity again and transmit through the second mirror. The intensity of this pulse will thus be:

$$I_1 = I_0 R^2 e^{-2\alpha d} \tag{5.82}$$

The intensity of pulse number n therefore becomes:

$$I_n = I_0 R^{2n} e^{-2n\alpha d} \tag{5.83}$$

The above equation can be rewritten as a function of time using the relationship $t = \frac{2nL}{c}$, where c is the speed of light in the medium and L is the distance between the mirrors. Using as well the relationship $R^{2n} = e^{2n\ln(R)}$ yields:

$$I(t) = I_0 e^{\frac{tc}{L}(\ln(R) - \alpha d)} \tag{5.84}$$

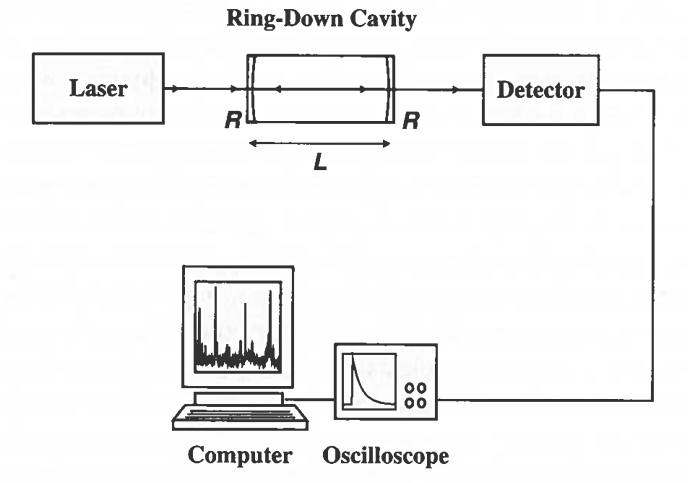

Figure 5.15: Sketch of a simplified model of a cavity ringdown spectrometer (Lehmann et al., 2009, p. 6).

Since the typical mirrors in a CRDS have a reflectivity close to 1, the approximation $\ln(R) = -(1 - R)$ can be used yielding:

$$\boxed{I(t) = I_0 e^{-\frac{tc}{L}(1-R+\alpha d)}} \tag{5.85}$$

As seen from eq. (5.85) the intensity of the light leaving the cavity is an exponentially decaying function with respect to time. It is also seen that the rate of the decay is proportional to the concentration of the absorbing specie within the cavity. To quantify the rate of the decay, the time from the first radiation strikes the detector to the radiation intensity has decayed to $1/e$ is termed the ring down time(τ) and is calculated as:

$$\tau = \frac{L}{c(1-R+\alpha d)} \tag{5.86}$$

Thus by measuring the ring down time the concentration of the specie within the cavity can be measured. In order to increase sensitivity, the ring down time is measured as a function of frequency across an absorption spectral line, and thus a range of absorptivity are measured giving a better signal-to-noise ratio (Lehmann et al., 2009).
"The simple description above (...) captures the essence of CRDS in most cases, but has made a number of simplifications. Most importantly, the bullet model ignores the interference of light in the cavity" (Lehmann et al., 2009, p. 10). Thus to understand the requirements for CRDS, a wave-approach has to be used, which will be introduced in the next section.

Cavity Optical Resonance The focus of this section will be the ringdown cavity. In order to be able to determine the concentration within the cavity, as described in the last paragraph, radiation has to build up in the cavity,

before it can decay according to a ringdown curve. Moreover the absorption cross-section(σ) and thus the ring down time (τ) are dependent on the radiation frequency. Thus in order to measure an unequivocal ring down time corresponding to a specific concentration, the radiation in the cavity has to have a narrow bandwidth[3]. Lastly, the more times the radiation "bounces" back and forth between the two mirrors, the more interaction with the gas sample will it have, and the smaller is the concentration detection limit of the instrument.

Axial resonance modes From classical optics, the time dependent part of an electric field of an electromagnetic plane wave is written as (Peatross and Ware, 2012, p. 46):

$$E(t) = E_0 \cos(\omega t + \phi) \tag{5.87}$$

Where E_0 is the amplitude of the oscillation, ω is the angular frequency of the oscillation and ϕ is an arbitrary constant phase term. Using Euler's formula the same expression can be written as:

$$E(t) = \mathrm{Re}\left\{\tilde{E_0} e^{-j\omega t}\right\} \tag{5.88}$$

Where Re means the real part of the equation, j is the imaginary number $j = \sqrt{-1}$ and $\tilde{E_0}$ is the complex amplitude defined as (Peatross and Ware, 2012, p. 47):

$$\tilde{E_0} = E_0 e^{i\phi} \tag{5.89}$$

In the following derivation the naming convention illustrated on fig. 5.16 will be used. Assuming that the incoming radiation is a steady-state sinusoidal optical signal, which is a very close approximation to most practical laser resonators, from which CRDS-cavities form a subset (Siegman, 1986, p. 413).
Modeling the mirrors of the cavity as a thin lossless dielectric slab with thickness L and index of refraction n and adjusting the optical thickness nL to be an odd number of quarter wavelengths, it can be shown, that the complex amplitude of the wave($\tilde{E}_t$) after passage of the mirror is (Siegman, 1986, p. 398–413):

$$\tilde{E}_t = j t_1 \tilde{E}_{\mathrm{inc}} \tag{5.90}$$

Where t_1 is the transmission coefficient of mirror 1, defined such that $t^2 + r^2 = 1$, where r is the reflection coefficient, and $\tilde{E}_{\mathrm{inc}}$ is the complex amplitude of the incoming radiation as illustrated on figure fig. 5.16. The complex amplitude of

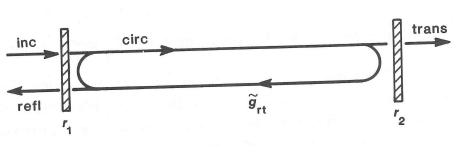

Figure 5.16: Illustration of the concepts used in the optical model of the cavity. The black lines represent radiation (Siegman, 1986, p. 414).

[3]Range of frequencies constituting the radiation (Encyclopedia Britannica Online(2), 2012)

the radiation just inside the input mirror is then the vector sum of the incoming radiation and the circulating radiation, which left this same point one round-trip time earlier($\tilde{E}_{\text{circ}}$). The total amplitude of the radiation inside the cavity is thus:

$$\tilde{E}_{\text{circ}} = jt_1\tilde{E}_{\text{inc}} + \tilde{g}_{\text{rt}}(\omega)\tilde{E}_{\text{circ}} \tag{5.91}$$

Where $\tilde{g}_{\text{rt}}(\omega)$ is the net round-trip gain representing the decrease in radiation as a result of the absorbing medium the radiation is passing in one round-trip. Referring to eq. (5.80) the amplitude of the radiation will be decreased due to absorption by $e^{-2\alpha d}$. Referring to eq. (5.88) the radiation will also be influenced by a propagation factor expressed by $e^{-j\omega t}$. This means that the amplitude of the circulating radiation after one complete round-trip will return to same point just inside mirror 1 with a net round-trip gain of (Siegman, 1986, p. 415):

$$\tilde{g}_{\text{rt}}(\omega) = r_1 r_2 e^{-2\alpha d - j\omega t} \tag{5.92}$$

Inserting this expression into eq. (5.91) yields:

$$\tilde{E}_{\text{circ}} = jt_1\tilde{E}_{\text{inc}} + r_1 r_2 e^{-2\alpha d - j\omega t}\tilde{E}_{\text{circ}} \tag{5.93}$$

Based in this expression the complex amplitude of the circulating signal in relationship to the incident signal outside the cavity can be calculated as follows:

$$\begin{aligned}
\tilde{E}_{\text{circ}} &= jt_1\tilde{E}_{\text{inc}} + r_1 r_2 e^{-2\alpha d - j\omega t}\tilde{E}_{\text{circ}} && \Leftrightarrow && (5.94)\\
\frac{\tilde{E}_{\text{circ}}}{\tilde{E}_{\text{inc}}} &= jt_1 + r_1 r_2 e^{-2\alpha d - j\omega t}\frac{\tilde{E}_{\text{circ}}}{\tilde{E}_{\text{inc}}} && \Leftrightarrow && (5.95)\\
1 &= jt_1\frac{\tilde{E}_{\text{inc}}}{\tilde{E}_{\text{circ}}} + r_1 r_2 e^{-2\alpha d - j\omega t} && \Leftrightarrow && (5.96)\\
1 - r_1 r_2 e^{-2\alpha d - j\omega t} &= jt_1\frac{\tilde{E}_{\text{inc}}}{\tilde{E}_{\text{circ}}} && \Leftrightarrow && (5.97)\\
\frac{\tilde{E}_{\text{circ}}}{\tilde{E}_{\text{inc}}} &= \frac{jt_1}{1 - r_1 r_2 e^{-2\alpha d - j\omega t}} && \Leftrightarrow && (5.98)
\end{aligned}$$

Using the fact, that the intensity of electromagnetic radiation is related to the amplitude of the radiation through $I_{\text{circ}} \equiv |\tilde{E}_{\text{circ}}|^2$, the circulating intensity in relation to the incoming radiation intensity as a function of angular frequency is plotted on fig. 5.17. The figure is generated assuming unit incident intensity, a round-trip absorption power loss of $2\alpha d = 2\%$ and symmetric mirror reflectivity ranging from $R = 0.7$ to $R = 0.98$. As is seen from fig. 5.17 the circulating intensity exhibits strong resonance peaks at $\omega t = 2\pi$. This means, that at certain radiation frequencies optical axial resonance will be generated in the cavity, whereas if the frequency of the incoming radiation is slightly off-axis, only limited radiation build-up will take place.

The frequencies where radiation buildup takes place is known as axial resonance modes and denominated by the letter q.

Transverse resonance modes The axial resonance frequencies presented in the last section was derived based on the plane wave-approximation. However, the electromagnetic radiation also has a transverse variation leading to a series of resonance modes, which will be introduced in this section, splitting the fundamental frequencies into tighter spaced sub-frequencies.

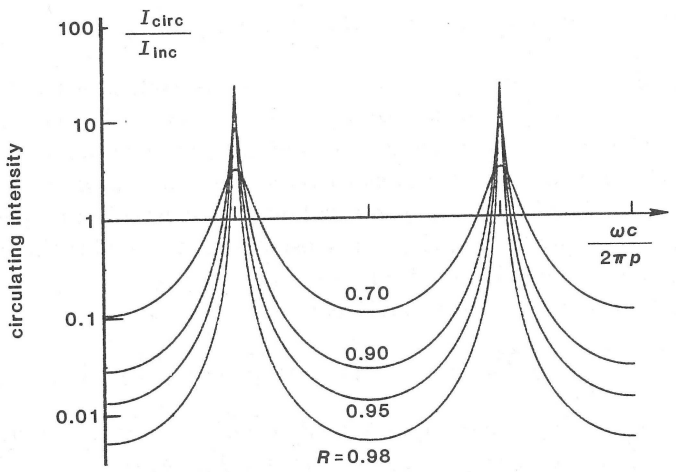

Figure 5.17: Graph of the relationship between the intensity of the circulating radiation(I_{circ}) and the intensity of the incoming radiation(I_{inc}). p is the perimeter of the round-trip and c is the speed of light in the medium (Siegman, 1986, p. 416).

To introduce transverse variations of the radiation a portion of the optical energy traveling in the $+z$ direction and contained within some short axial segment Δz within the cavity as illustrated on fig. 5.18 is considered. The segment of radiation or "slab" is chosen such that the axial thickness Δz is small compared to the length of the cavity but large compared to the optical wavelength. Writing up the E-field of such a radiation segment including transverse variation (Siegman, 1986, p. 560):

$$E(x,y,z) = \text{Re}\left\{\tilde{E}(x,y,z)e^{j(\omega t - kz)}\right\} \tag{5.99}$$

$$= \text{Re}\,|\tilde{E}(x,y,z)|e^{j(\omega t - kz)+j\phi(x,y,z)} \tag{5.100}$$

Where k is the propagation constant defined as $k = \frac{2\pi}{\lambda}$, where λ is the wavelength of the radiation. In the above equation the phase angle has been taken out of the complex amplitude. In this form, the plane-wave aspect of the wave is represented by the expression $e^{j(\omega t - kz)+j\phi(x,y,z)}$. This means, that the transverse intensity profile of the slab is given by $I(x,y,z) = |\tilde{E}(x,y,z)|^2$. Since the variation in the transverse beam profile with the z-coordinate is very slow compared to the factor e^{-jkz}, the transverse field pattern will only be considered with respect to the x and y coordinate(Siegman, 1986, p. 561). The transverse field pattern $\tilde{E}(x,y)$ will as a rule change with each revolution in the cavity as a result of diffraction, reflection and aperturing effects. To determine the transverse resonance modes of the cavity, solutions will be sought, where the slab will return one round trip later with exactly the same transverse field pattern. In mathematical terms, the propagation of such a slab of radiation will be represented by a propagation

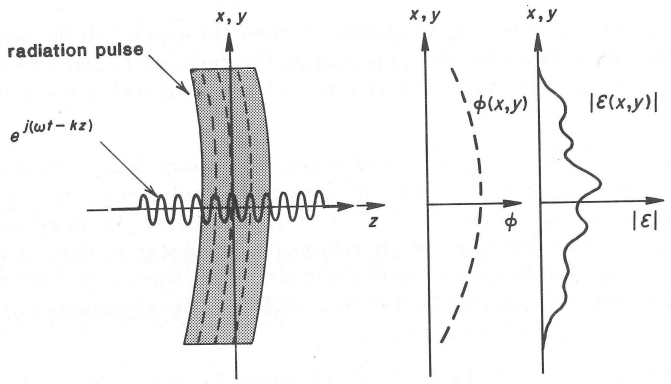

Figure 5.18: Illustration of the optical "slab" used for introducing the transverse resonance modes of an optical cavity (Siegman, 1986, p. 560).

integral as (Siegman, 1986, p. 565):

$$\tilde{E}^{(1)}(x,y) = e^{-jkp} \iint_{\substack{\text{Input}\\ \text{plane}}} \tilde{K}(x,y,x_0,y_0)\tilde{E}^{(0)}(x_0,y_0)dx_0dy_0 \tag{5.101}$$

Where $\tilde{E}^{(1)}(x,y)$ is the transverse field pattern after one round trip, k is the propagation constant, p is the length of one round trip, and the integral is over the transverse coordinates at the input plane. The function $\tilde{K}$ is called the propagation kernel, and works such that the field $\tilde{E}^{(1)}(x,y)$ can be obtained from the field one round trip earlier through the operation of the linear kernel $\tilde{K}(x,y,x_0,y_0)$. eq. (5.101) is called a linear operator equation (Siegman, 1986, p. 566). For a linear operator equation such as eq. (5.101), if there exist a set of eigensolutions, these eigensolutions will constitute the self-reproducing transverse eigenmodes of resonance. In mathematical terms this means that a set of solutions to eq. (5.101) exists satisfying:

$$\tilde{E}^{(1)}_{nm}(x,y) \equiv \iint_{\substack{\text{Input}\\ \text{plane}}} \tilde{K}(x,y,x_0,y_0)\tilde{E}^{(0)}_{nm}(x_0,y_0)dx_0dy_0 = \tilde{\gamma}_{nm}\tilde{E}^{(0)}_{nm}(x_0,y_0) \tag{5.102}$$

In order to find the eigensolutions of a given optical cavity, the „approach to finding the lowest-order resonator transverse modes is often called the "Fox and Li" approach, since it describes not only the real physical situation in an optical cavity, but also the numerical mode-calculation procedure (...). Fox and Li simulated the iterative round trips of a wavefront $\tilde{E}(x,y)$ in a resonator using numerical computation on a digital computer" (Siegman, 1986, p. 570).
The simplification made by only considering a slab of radiation is not influencing the transverse resonance modes in a cavity, since a continuous radiation is just a stream of slabs launched one after another "nose to tail"(Siegman, 1986, p. 569). The geometry of the intensity of the first few transverse modes of resonance is illustrated on fig. 5.19 and the frequency shifts from the axial modes of resonance is illustrated on fig. 5.20. This shows, that comparing the bandwidth of the laser, the cavity and the absorption line of the specie under assessment, that

care has to be taken only to activate one mode of resonance in the cavity in order to obtain an ubiquitous ring-down time and thereby limit the noise in the concentration detection.

In order for radiation to build up in the cavity the cavity, besides matching the cavity length and the radiation frequency to each other, the cavity have to be geometrically stable, meaning that radiation will not leak out of the cavity through the sides not covered by mirrors. This criteria can be described in mathematical terms using a matrix optics approach. Interested readers are referred to Busch et al. (1999).

Technical description of the Picarro G2203 Based in the theory presented in the preceding sections, the foundation is now laid for describing the details of the construction of the Picarro G2203. This paragraph is based on U.S. Patent 6,466,322 B1 (2002).

Based on the illustration of the working principles of the Picarro G2203 CRDS as illustrated on fig. 5.14 on 94 the light to be absorbed by the sample is emitted from a continuous wave laser in order for radiation to build up in the cavity. This is important in order to produce a clear measurable signal at the detector after passage of the cavity. Moreover it is important that the laser is able to reproduce light at the same frequency for every measurement, since several ringdown profiles are averaged for every concentration measurement data point. This is also easier obtained with a continuous wave laser as opposed to a pulsed laser.
To obtain a single axial and transverse resonance mode in the cavity, the radiation leaving the laser passes a pinhole and two lenses and in this way is directed into the cavity.
The cavity consists of three high reflectivity mirrors, such that only very narrow bandwidth radiation will generate resonance in the cavity. In order to match the cavity-roundtrip length to the frequency of the of the incoming laser such that only a single resonance mode is activated, one of the mirrors is attached to a piezo-electric transducer. Through tracking electronics the round trip length of the cavity is adjusted by perturbing the input voltage to the piezo-electric transducer.
When the radiation is leaving the cavity, it is measured by a photodetector. This photodetector is coupled to a threshold detector, which enacts the turnoff of the radiation and the recording of the ringdown curve as soon as the radiation within the cavity has reached a certain threshold. This threshold is set high enough for the preferred resonance mode to activate the signal, without the signal being activated from other resonance modes.
When the threshold detector level is reached the radiation is turned off fast

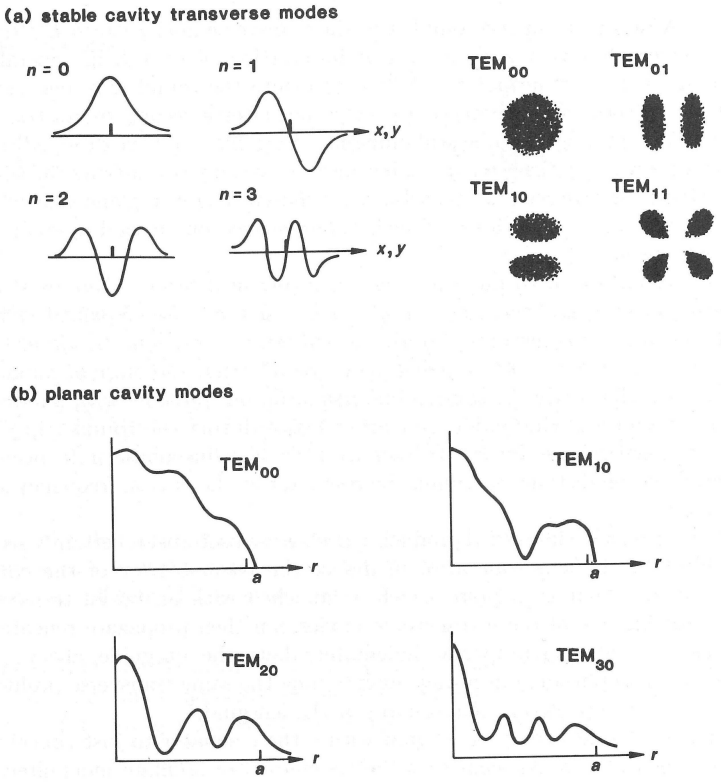

Figure 5.19: Intensity profiles of the first transverse resonance modes in a cavity. (a) a cavity where the radiation is not leaking out over the sides of the mirrors. (b) a cavity consisting of two spherical flat mirrors of radius s, with radiation leaking out of the cavity (Siegman, 1986, p. 564)

using an acusto-optic modulator[4]. Moreover ringdown sampling electronics are activated sampling the ringdown curve and fitting a straight line to the logarithm of the ringdown curve thus obtaining the ringdown time. This procedure is repeated a number of times and the ringdown time averaged to obtain a better signal to noise ratio. The whole process is repeated with a frequency shifted by $\Delta\nu$ in order to sample across a spectral feature of the absorbing specie. These datapoints are then fitted to "multiple known points across the target absorption line (...) [using a] proprietary multi-order fitting routine to get the most accurate fit for the line shape and hence its true peak height." (`http://www.picarro.com/technology/analyzer_performance_advantages`.

[4]An acusto-optic modulator works by sending sound waves through a crystal, that the electromagnetic radiation is passing as well. Sound waves traveling through a crystal causes a wave-pattern in the crystal density thus resulting in a wave-pattern in refractive index. Electromagnetic light is thus scattered on these wavefronts in the refractive index thus causing the light to change direction (McCarron, 2007).

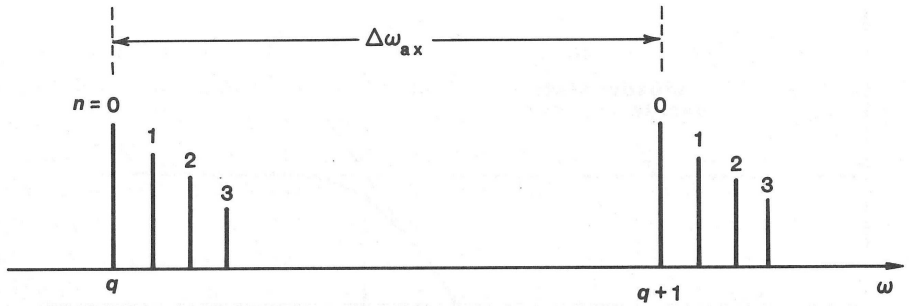

Figure 5.20: Frequency of the transverse modes in an optical resonator. q being the axial modes of resonance and n being the transverse modes of resonance. $\Delta\omega_{ax}$ is the angular frequency interval between the axial modes of resonance

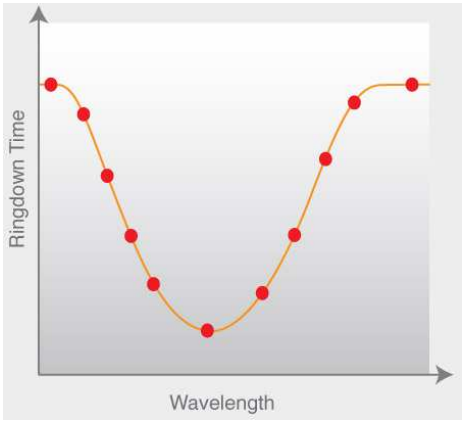

Figure 5.21: The ringdown time as a function of wavelength sampled across a spectral line of the absorbing specie. (Source: `www.picarro.com`)

5.2.3 Procedure and results

The field experiments were performed at November 26, 2012 in the afternoon. The wind direction as a function of time as measured with the sonic anemometer is shown in fig. 5.22. The presented wind direction is a 30-second average to reduce the amount of scatter in the graph. At the time of measurement, tank T-9805 was in a state of intermediate standing at a height of 17 meters and had been in the position for approximately 2 hours.
Two measurement time series were performed as illustrated in fig. 5.23 and fig. 5.24 respectively. Due to the lack of GPS-connectivity, the micrometeorological model, as described in section 5.2.1 was not used, and instead a trial-and-error approach was adopted. The first tracer release started at time 15.05, and measurements started approximately 10 minutes later. As can be seen from fig. 5.23 the background acetylene concentration is approximately zero. Due to the lack of position measurement, it is difficult to assess whether or not the measurements are inside or outside of the emission plume, and thus which data to include or

exclude from the analysis.
Based on a visual inspection of the graph from the first measurement series and the graph of the wind direction, it could look like the measurements are within the plume in the beginning of the time series, and as the wind direction is gradually turning south from around 16.20 the instrument is gradually becoming located outside the plume. The large fluctuations in the acetylene concentration in the beginning of fig. 5.24 could indicate that the instrument might be located close to the edge of the plume.
As seen from fig. 5.22 the wind direction was turning approximately 20-30° southerly around 16.30. This is also seen in fig. 5.23, as a marked drop in the acetylene concentration. In order to try to obtain more measurements, the CRDS was subsequently moved towards northwest as seen from the center of the tank. The results of the measurements taken at position 2 are shown in fig. 5.24. Again the time series is characterised by large fluctuations, probably indicating that the instrument is again at the fringe of the plume. Moreover, the methane concentration is continuously increasing during the measurement series unrelated to the change in acetylene concentration. The spike in the time series shortly after 15.30 correlates with the change in wind direction occurring at approximately the same time. One possible explanation to the increasing methane concentration could be an increase in background concentration as a result of decreasing average wind speed, however other nearby sources could also cause this effect.

No further measurements were take due to discontinued cooperation with DONG Oil Pipe.

Summing up, the small amount of available data combined with the large uncertainties related to position measurements and background levels the emissions must be deemed inconclusive.

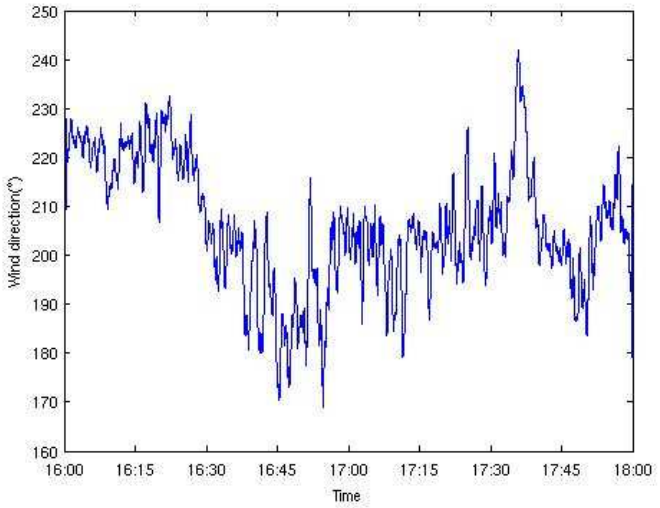

Figure 5.22: Wind direction during the field experiments.

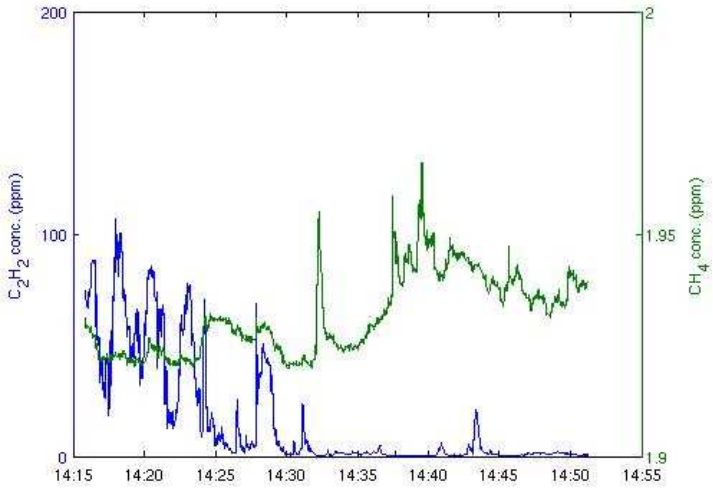

Figure 5.23: Results of first measurement series. Time values are one hour behind.

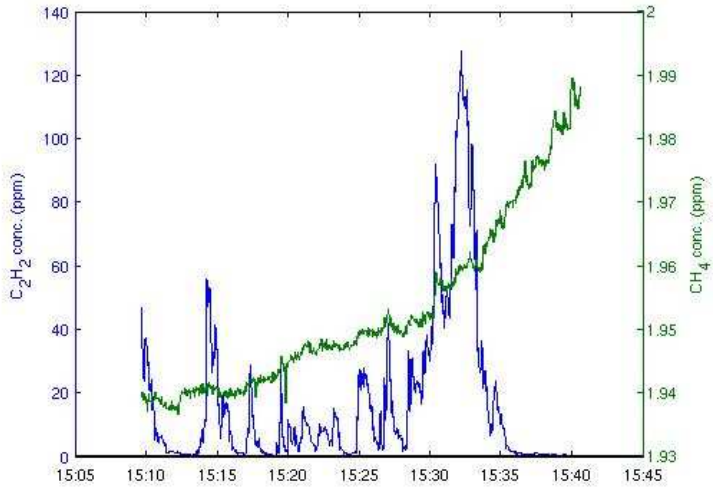

Figure 5.24: Results of second measurement series. Time values are one hour behind.

Chapter 6

Model

In this chapter, the modelling of the impact of the emission reduction is described. As described in chapter 3 the modelling consists of coupling a CTM to a 1DRCM. The structure of the chapter will follow this approach starting with a description of the DEHM model and the results following from this modelling, followed by a description of the 1DRCM model, and lastly followed by a description of the mechanisms to connect the two models.
The descriptions of the models start with an overall section, describing the important features of the models (e.g. the coordinate system) in mainly qualitative terms. For the DEHM model, this is the only description, since the model has been applied in a "black box"-approach in the present study. Moreover, explaining the details of the model would be quite extensive and make use of complicated mathematics, and this is therefore left out.
For the 1DRCM, a section describing the calculation of specific important quantities in the model has been added. These have been selected since a complete description of the model would be a project in itself, and because these quantities play a central role in relation to the aim of the present project.

6.1 DEHM

Based in the conceptual model illustrated in fig. 1.5 the DEHM model yields the concentrations as a function of the emissions. The DEHM model describes the atmospheric dispersion and chemical transformation of a given emission. In the following a brief overview of the central elements in the model will be given and the results of the modelling process presented.

6.1.1 Overall model description

The DEHM model is an Eulerian model. This means that it computes the change in concentration for a set of grid points fixed in space (as opposed to Lagrangian models, where an air parcel is moving along a trajectory). Eulerian models are as a rule advantageous when simulating dispersion on the large scale (Hertel and Brandt, 2009).
The simulation takes place on a 96x96 cell grid covering the northern hemisphere.

The projected coordinate system is a polar stereographic projection with the projected geoid matching the actual geoid best at 60° North.
The model runs in a nested mode with four nested grids. Nesting means that the model is divided into a subgrid with a higher spatial resolution covering a specific area of interest. The larger grid is then used as boundary conditions for the smaller grid. In the two-way nesting approach applied in the DEHM model, the finer resolution in the subgrids is achieved through a zooming capability. The grids of various resolution is as such coupled to each other online. The largest grid is covering the northern hemisphere and has a spatial resolution of $150km$. The second grid covers Europe and has a spatial resolution of $50km$, the third grid covers Northern Europe and has a spatial resolution of $16.67km$, the fourth grid covers Denmark and has a spatial resolution of $5.56km$. The coordinate system of the model is illustrated in fig. 6.1. The nesting technique is a way to improve the spatial resolution of the model, without extending the calculation time unreasonably (Frohn, 2004, p. 23). The model has a vertical resolution of 29 unequally spaced layers covering a total height of $\approx 15km$.
The atmospheric dispersion and chemical transformations are simulated solving the continuity equation and the chemical kinetics. The meteorology is generated using the MM5 model. The input data to this comes from National Centers for Environmental Protection (NCEP), USA.
The model has been run with a tagging representing the change in emission as a result of the installation of the degassing plant. The background data are thus the emissions after the installation of the degassing plant, and the background plus the tagged data represent the emissions before the installation of the degassing plant.
Tagging is a method to calculate changes in concentration as a result of changing emissions. Traditionally this is done running the model twice: once with the background emission and once with the changed emission. Lastly the differences between the model runs are determined from subtraction. Because modern Eulerian Chemical Transport Models are always subject to oscillations known as the Gibbs phenomenon, the subtraction method is not a very accurate way to simulate changes in emissions. This is due to the fact that the oscillations can be of the same order of magnitude as the changes in emissions. Using the tagging method, the concentration from the background emission and from the emission change are modelled in parallel leading to a larger precision. The tagging method is illustrated on fig. 6.2 (Brandt et al., 2012).
Modelling atmospheric chemistry is very calculation intensive due to the very large number of chemical species involved, and the even larger number of reaction pathways. The most accurate modelling would be solving the chemical kinetics explicitly for every single reaction, however, this would make calculation times incredible long. Instead a lumped scheme is used, where the chemical compounds are grouped according to certain properties. The inorganic atmospheric chemistry is reasonably well understood, and as such, developing an accurate lumping scheme for these reactions is possible at present. The organic atmospheric chemistry however, is much more complicated due to the large number of highly reactive hydrocarbons (Frohn, 2004, p. 39). The lumping scheme used in the DEHM model is the EMEP (European Monitoring and Evaluation Programme)

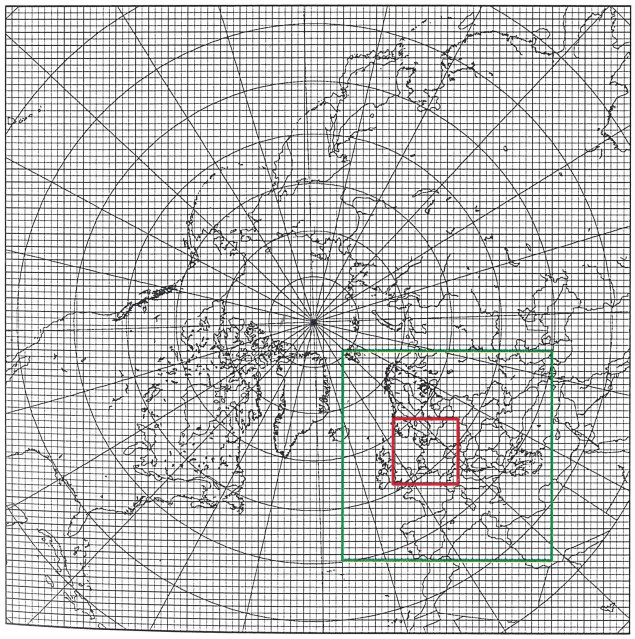

Figure 6.1: Illustration of the grid used in the DEHM model with the subgrid covering Europe marked with green and the subgrid covering Northern Europe marked with red(Frohn, 2004, p. 23).

scheme (Gross[1] , personal communication).

6.1.2 Model results

The seasonal development in the ground level concentration of methane is shown in figs. 6.3 to 6.6. The results are based on the tagged emission alone to illustrate the magnitude of the concentration change. The results of the change in methane emission is shown as a representative for the total emission, since the other species show similar results.
As can be seen, the installation of the degassing plant has entailed a decreased methane concentration of $\approx 10^{-4} ppmv$ for parts of Denmark and the surrounding countries.
Comparing the seasonal development as illustrated, there is no sign of concentration build-up or decrease. This is a result of the modelled tag-emission being static. Moreover, this shows that modelling the emission change as a result of the installation of the degassing plant as taking place January 1, 2010 is not influencing the resulting concentration change. The results are only shown for four months, but the results from the rest of the months confirm this conclusion.
Apart from the "main plume" that disperses approximately equally in all directions, it can be seen that the concentration plume is distributing the emission

[1] Allan Gross, professor Institute for Atmospheric Environment, National Center for Environment and Energy

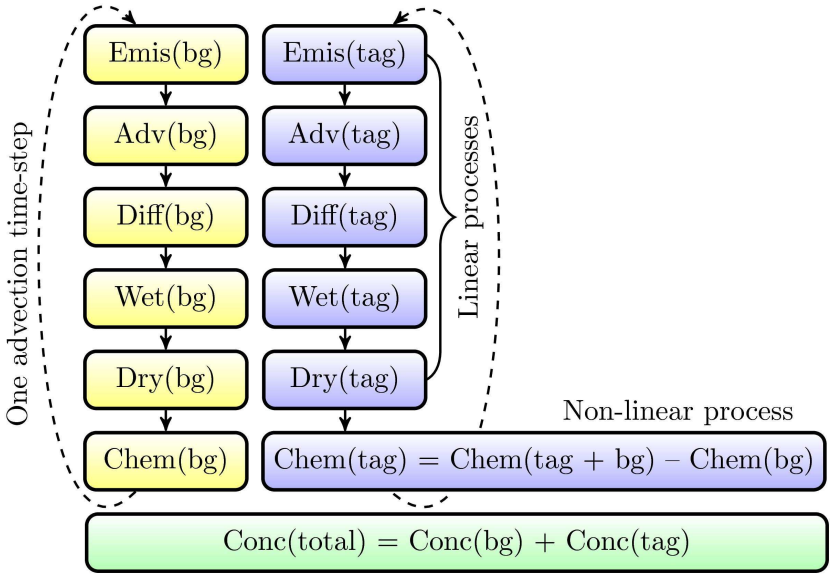

Figure 6.2: Schematic overview of the tagging method. The diagram shows that the concentration resulting from a specific source(tag) is modeled in parallel with the concentration resulting from the background(bg). The elements of a typical CTM is: Emission (Emis), advection(Adv), diffusion(Diff), wet deposition(Wet), dry deposition(Dry), and chemical conversion(Chem)Brandt et al. (2012).

in certain ”preferred directions’, yielding the ”plume tentacles” as seen on the maps. These are probably resulting from prolonged weather patterns with approximately constant wind direction.
At the edges of the plume, e.g. in the North Sea, there appears a wave-like phenomenon. This is a result of the previously mentioned Gibb’s phenomenon, and as such, is an artefact of the model and not of the emission change.
A few dark spots appear in the middle of the maps. These are results of computational errors somewhere in the data handling procedure.

In figs. 6.7 to 6.10 the same results as before are shown, however, the emission change has now been classified into 10 concentration classes. As can be seen, the emission change impact quite a large part of Europe, which is also the reason for the change in scale from the previous visualisation. The impact is of course largest close to the source, but the model predicts a change of $\approx 10^{-5} ppmv$ even far away into Eastern Europe.
This is a small change in absolute terms, and it is probably not possible to validate this modelling by measurements. However, this confirms that the DONG terminal is a large single source of emissions, and that the installation has entailed a noticeable decrease.
Looking at the temporal development, the spread of the plume is not equally large at all times of year. Since the emission is constant, this must be related to changing atmospheric conditions including changes in atmospheric dispersion and chemical removal pathways.

It appears from the visualisations in figs. 6.7 to 6.10 that the present modelling is not very influences by noise. The spline interpolation and the classification of course functions to rule out noise in the results, but noise doesn't appear to play a large role in figs. 6.3 to 6.6 either. If the results were influenced by noise, the visualisations would be characterised by a larger degree of randomness. This means that the noise level in the model must be smaller than the results.

The relative concentration changes for January 2010 for the respective chemical species included in the present analysis are shown in figs. 6.11 to 6.13. The concentrations are drawn using the same concentration color scheme, in order to visualise the differences in relative concentration. As can be seen, the methane concentration barely changes as a result of the installation of the degassing plant. This is because the atmospheric background concentration of methane is higher than for any of the other species included in the present study. As seen in fig. 6.12 the emission change causes a local change in the ethane concentration of approximately ten percent quickly being diluted to zero, and the same tendency is shown in fig. 6.13 although the dilution is slower. As can be seen, although the concentration change as a function of the installation of the DONG degassing plant in absolute magnitude is largest for methane and smaller for ethane and n-butane respectively, the relative change of the two NMVOCs is larger than for methane.

The height profiles of the emission as a function of latitude is illustrated in figs. 6.14 to 6.17. As can be seen, the largest change in emission, as a result of the installation of the degassing plant, occur near the ground. The similarity of the figures warrants the use of the ground level emission as a way to illustrate the results of the emission change. It is shown on the figures that the largest concentration changes appears within the lowermost 1000m.

Summing up, compared to the size of the model domain, the change in emission as a result of the installation of the DONG degassing plant is a small change. This is the reason, why the spatial effects are small as seen in all the figures. However, considering that the effects are caused by an emission reduction measure at one single plant, it indicates that widespread use of emission reduction technologies of similar magnitude to the DONG degassing plant, could have a potentially large effect especially with respect to NMVOCs.

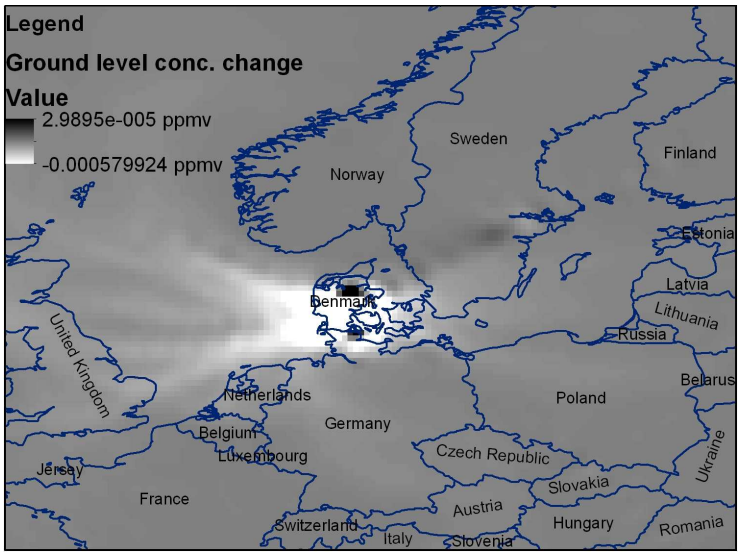

Figure 6.3: Methane monthly average ground level concentration change in January 2010. Data interpolated from the DEHM model second nest using the spline method and contrast stretched using two standard deviations.

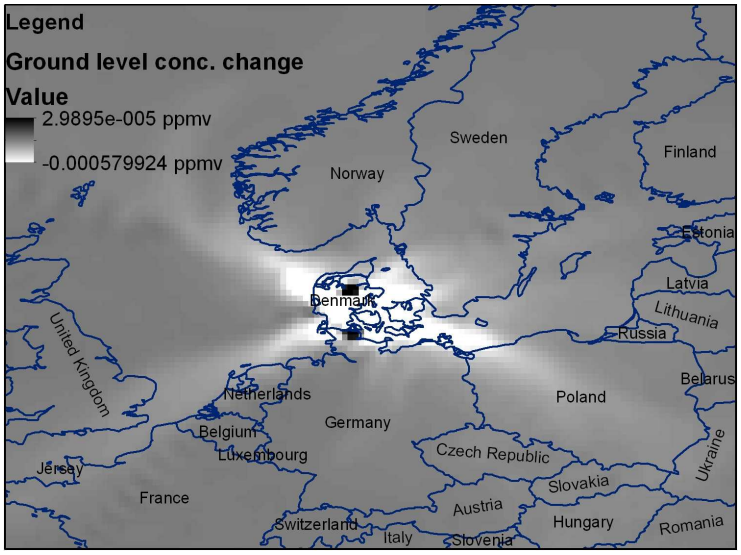

Figure 6.4: Methane monthly average ground level concentration change in April 2010. Data interpolated from the DEHM model second nest using the spline method and contrast stretched using two standard deviations.

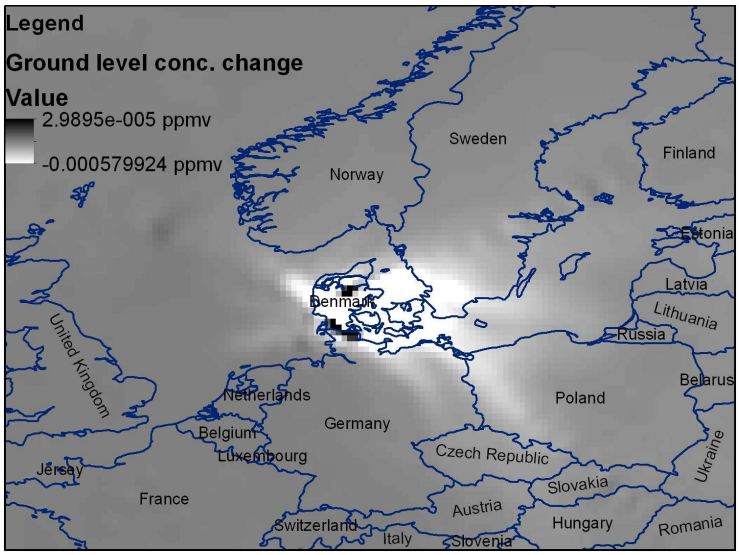

Figure 6.5: Methane monthly average ground level concentration change in July 2010. Data interpolated from the DEHM model second nest using the spline method and contrast stretched using two standard deviations.

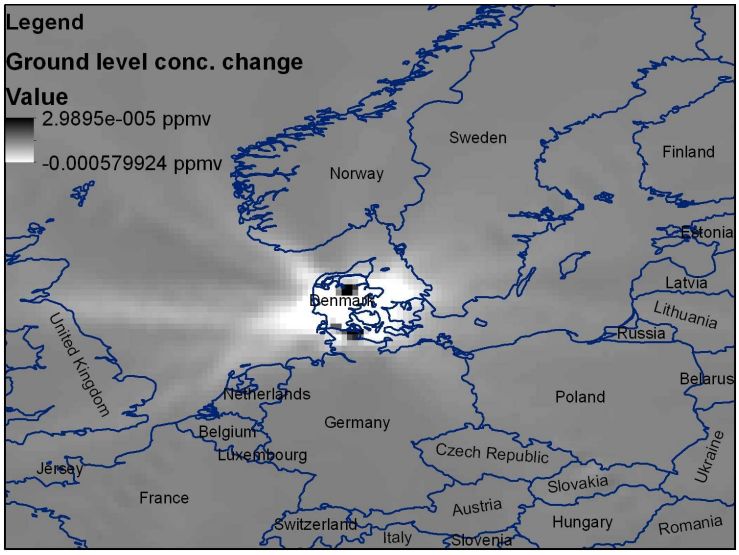

Figure 6.6: Methane monthly average ground level concentration change in October 2010. Data interpolated from the DEHM model second nest using the spline method and contrast stretched using two standard deviations.

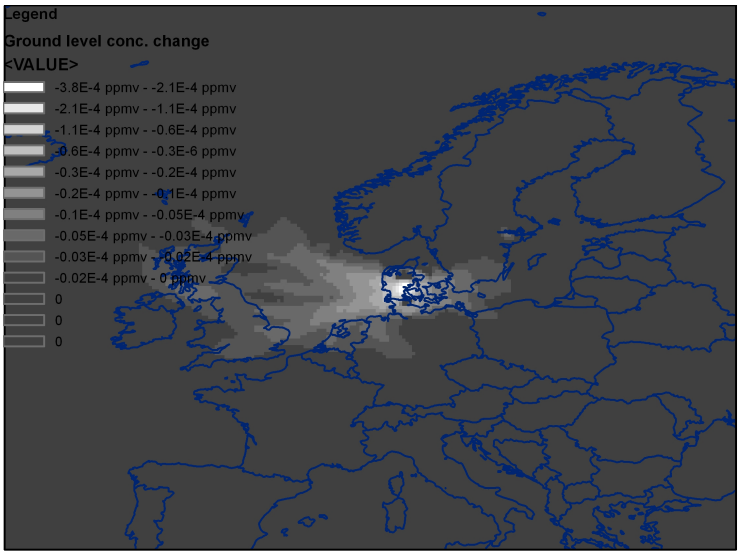

Figure 6.7: Methane monthly average ground level concentration change in January 2010. Data interpolated from the DEHM model second nest using the spline method and classified into 13 classes using the natural breaks method with the three classes representing values above 0 ppmv removed.

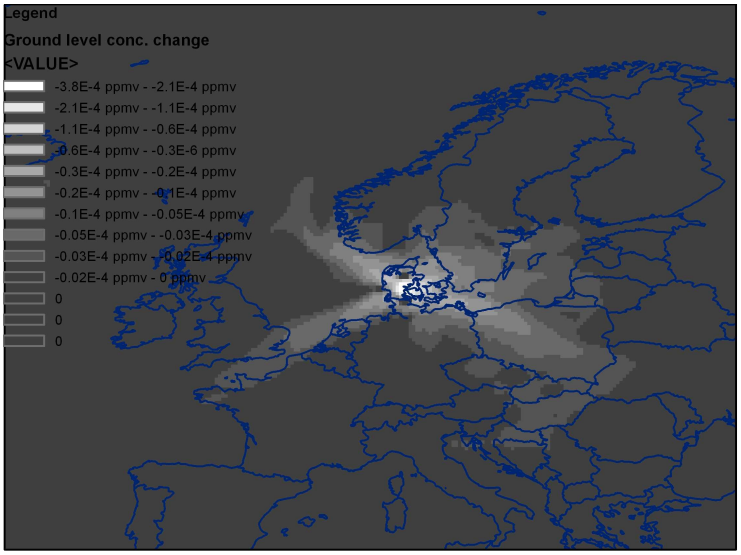

Figure 6.8: Methane monthly average ground level concentration change in April 2010. Data interpolated from the DEHM model second nest using the spline method and classified into 13 classes using the natural breaks method with the three classes representing values above 0 ppmv removed.

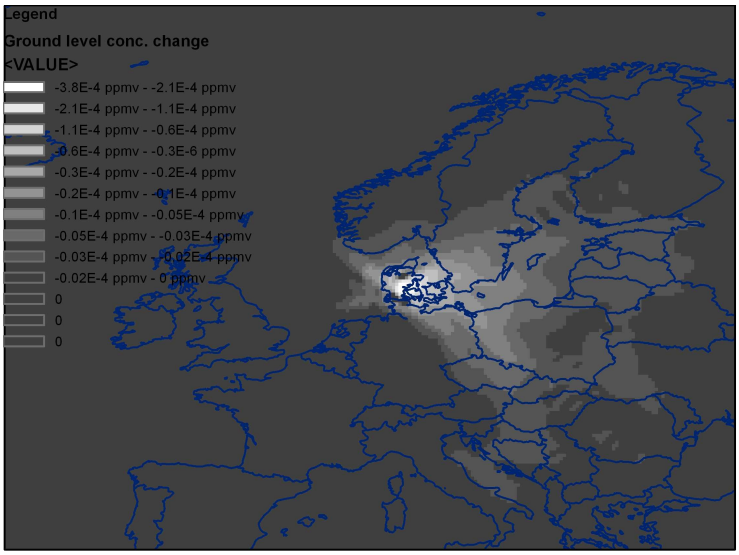

Figure 6.9: Methane monthly average ground level concentration change in July 2010. Data interpolated from the DEHM model second nest using the spline method and classified into 13 classes using the natural breaks method with the three classes representing values above 0 ppmv removed.

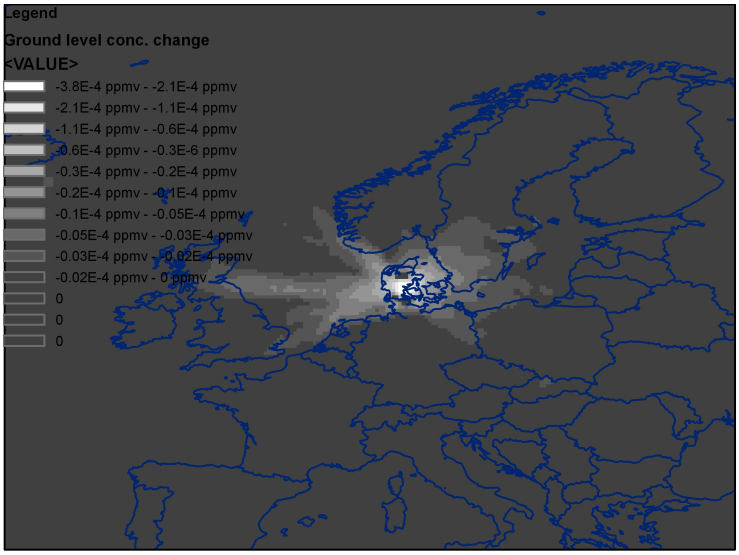

Figure 6.10: Methane monthly average ground level concentration change in October 2010. Data interpolated from the DEHM model second nest using the spline method and classified into 13 classes using the natural breaks method with the three classes representing values above 0 ppmv removed.

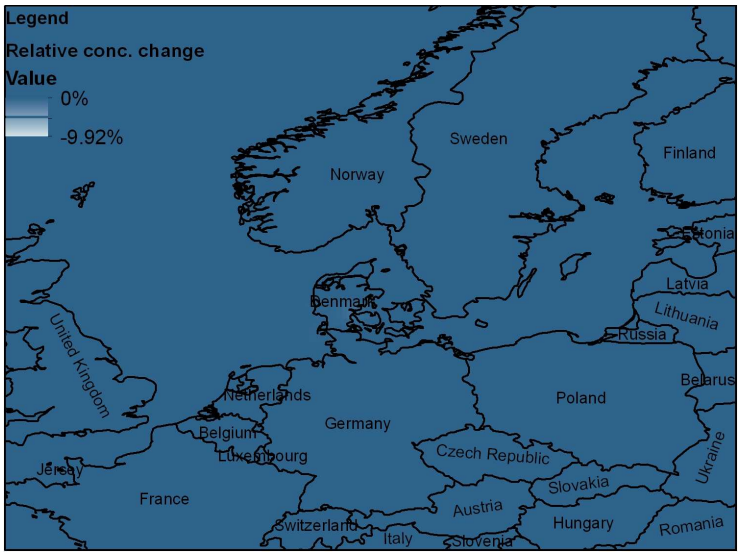

Figure 6.11: Methane monthly average ground level concentration change in January 2010. Data interpolated from the DEHM model second nest using the spline method. Units are percentages of tag-concentration relative to basis-concentration.

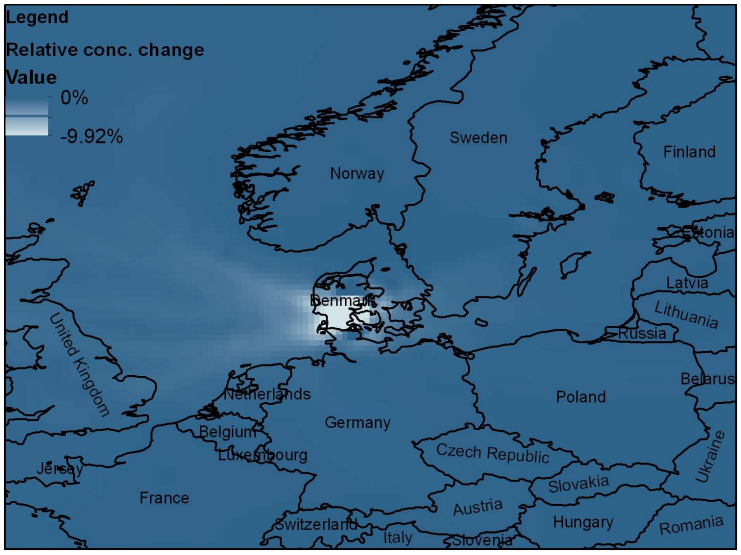

Figure 6.12: Ethane monthly average ground level concentration change in January 2010. Data interpolated from the DEHM model second nest using the spline method. Units are percentages of tag-concentration relative to basis-concentration.

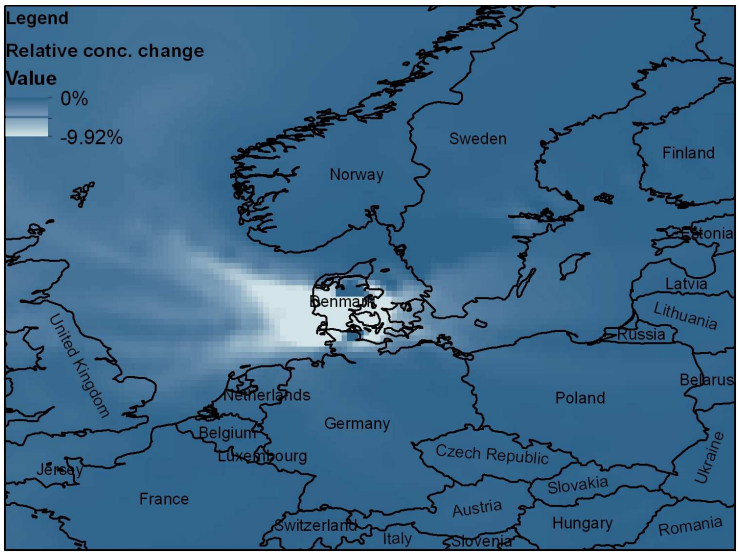

Figure 6.13: N-butane monthly average ground level concentration change in January 2010. Data interpolated from the DEHM model second nest using the spline method. Units are percentages of tag-concentration relative to basis-concentration.

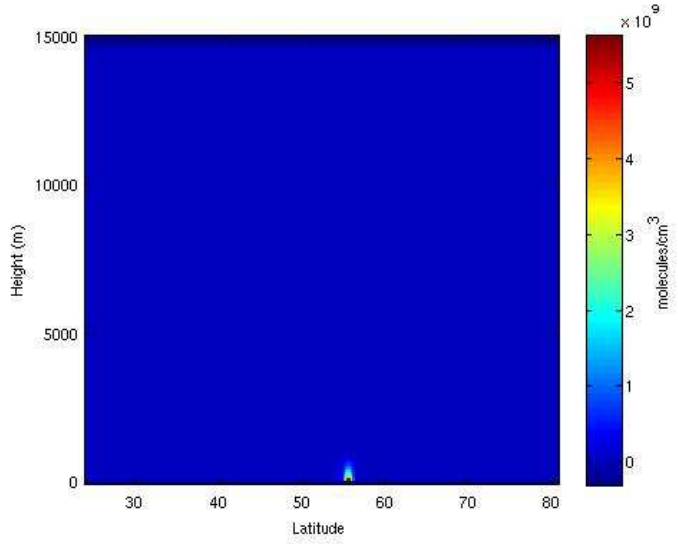

Figure 6.14: Height profile of the change in monthly average methane concentration for January 2010 as a function of latitude. The longitude is 9.50. Data interpolated from the DEHM model second nest using the spline method in the horisontal direction and linear interpolation in the vertical direction. Data are scaled to the full colormap.

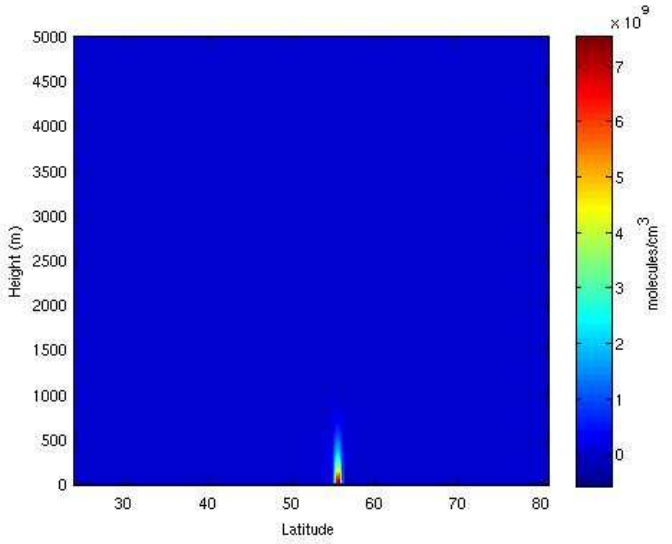

Figure 6.15: Height profile of the change in monthly average methane concentration for January 2010 as a function of latitude. The longitude is 9.50. Data interpolated from the DEHM model second nest using the spline method in the horisontal direction and linear interpolation in the vertical direction. Data are scaled to the full colormap.

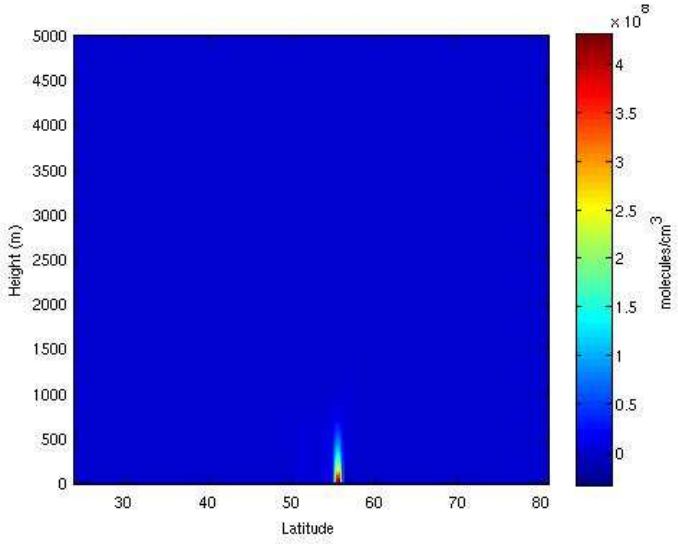

Figure 6.16: Height profile of the change in monthly average ethane concentration for January 2010 as a function of latitude. The longitude is 9.50. Data interpolated from the DEHM model second nest using the spline method in the horisontal direction and linear interpolation in the vertical direction.Data are scaled to the full colormap. Data are scaled to the full colormap.

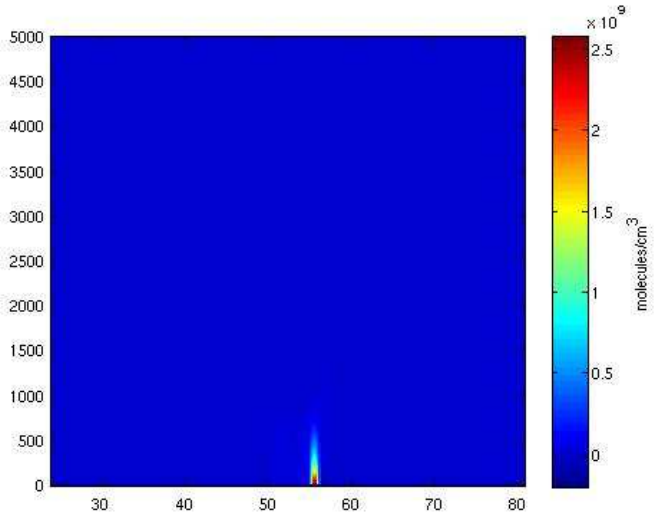

Figure 6.17: Height profile of the change in monthly average n-butane concentration for January 2010 as a function of latitude. The longitude is 9.50. Data interpolated from the DEHM model second nest using the spline method in the horisontal direction and linear interpolation in the vertical direction. Data are scaled to the full colormap.

6.2 1-D RCM

6.2.1 Overall model description

To calculate the change in radiative forcing as a result of the change in concentration as calculated with the DEHM model, the 1-D RCM model is used. The calculation procedure of the model is illustrated on figure 6.18.
The model describes the atmosphere as 18 plane parallel layers extending from the surface to a height of approximately 42km. The layers are numbered consecutively from the top of the atmosphere to the earth surface, such that the uppermost layer has number 1 and the layer representing the earth surface has number 19. Following the approach of (Manabe and Strickler, 1964, p. 368) the quantity σ is introduced in the following way:

$$pa_i = \sigma_i^2(3 - 2\sigma_i) \tag{6.1}$$

Where pa_i is the average pressure at the center of layer i relative to the earth surface pressure. The layer thicknesses are then defined such that σ is kept constant. Since there are 18 layers and the difference between the top of layer 1 and pa_1 and the difference between the earth surface at the bottom of layer 18 and pa_{18} is only half the difference between e.g. pa_1 and pa_2. This means that the pressure thickness of the layers has to be:

$$\sigma_0 = 0, \quad \sigma_1 = \tfrac{1}{36}, \quad \sigma_2 = \tfrac{3}{36}, \quad \sigma_4 = \tfrac{5}{36}, \quad \ldots, \quad \sigma_{18} = \tfrac{35}{36} \tag{6.2}$$

This is illustrated on figure 6.19. This layer thickness distribution is practical since it provides a high spatial resolution at the top of the atmosphere, where small absolute pressure differences correspond to large relative pressure differences and high spatial resolution near the earth's surface, where the boundary layer is modelled.
The earths surface is modelled as a layer of 100m of water as illustrated on figure 6.19. This represents a first attempt to represent the time it takes for the earth-atmosphere to come into equilibrium after an atmospheric perturbation (MacKay and Khalil, 1991).
The calculation of IR fluxes is described in section 6.2.2. The temperature change in a single time step as a result of radiative energy supplied to the individual layer is calculated using the first law of thermodynamics:

$$dU = dQ + dW \tag{6.3}$$

Since there is no external work done on the air mass in this system, and the energy supplied is in the form of radiation(F), the first law can be written as:

$$dU = dF \tag{6.4}$$

The radiative energy per unit volume per unit time for an individual layer is converted to thermal energy:

$$\rho c_p \tfrac{\Delta T}{\Delta t} \Delta z = F^-(z + \Delta z) + F^+(z) - F^+(z + \Delta z) - F^-(z) \tag{6.5}$$

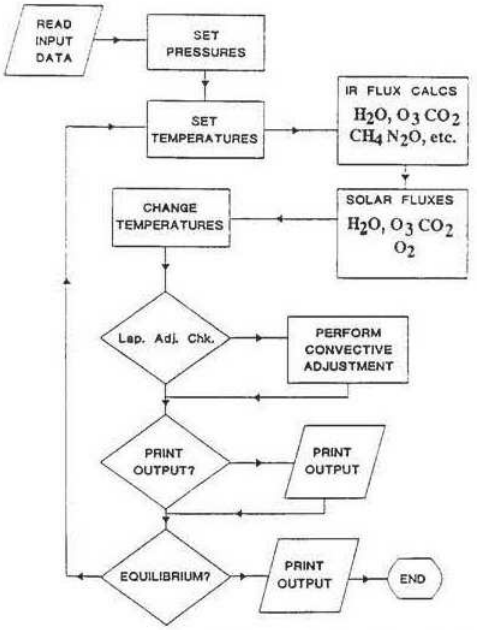

Figure 6.18: Flow diagram of the 1-D RCM modelMacKay and Khalil (1991).

Where ρ is the density of the individual layer, T is the temperature and t is the time. Rearranging to solve for the temperature change as a result of time and applying the hydrostatic equation:

$$\frac{\Delta T}{\Delta t} = \frac{1}{\rho c_p}\frac{\Delta F}{\Delta z} = \frac{g}{c_p}\frac{\Delta F}{\Delta P} \qquad \Delta P = -\rho g \Delta z \tag{6.6}$$

Where g is the gravitational constant. The temperature change as a result of solar radiation is calculated using a similar approach, where the infra-red flux is substituted by the net flux of solar energy. The two temperature changes are thus added and multiplied by the the time step to calculate the total temperature change of the individual layer. The change in surface temperature is likewise calculated according to:

$$c_w \rho h(\Delta T_{19}) = \left(F_{19}^{-} + A_{19} - \sigma(T_{19})^4\right)\Delta t \tag{6.7}$$

Where c_w is the specific heat of water, ρ is the density of water, h is the depth of the water layer, A is the net flux of solar energy, and σ is the Stefan-Boltzmann constant. The model includes an option for applying a convective adjustment, but since this is not used in this modelling approach it will not be explained here. The whole process is repeated until the change in integrated temperature over the whole model atmosphere is below some predefined small number (MacKay and Khalil, 1991).

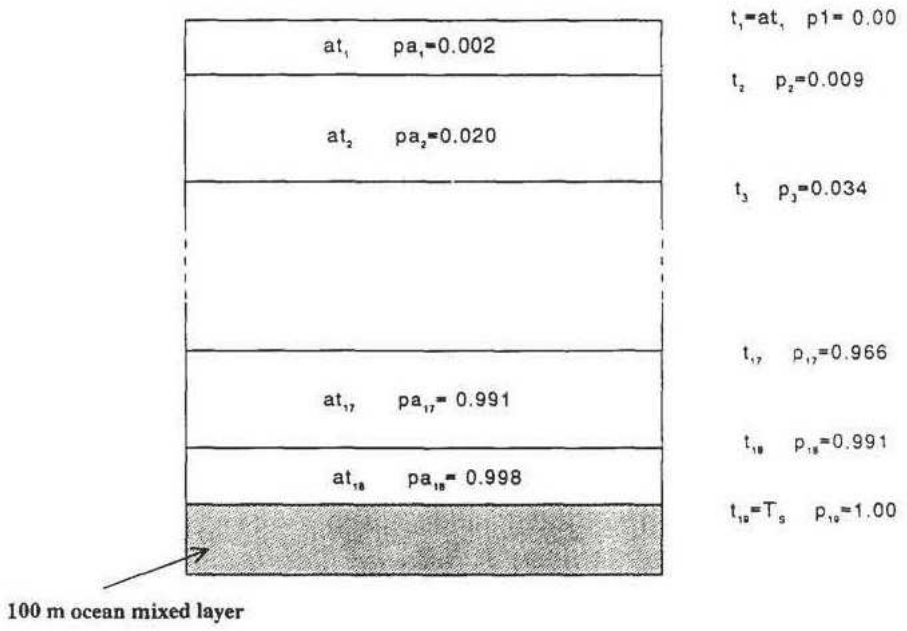

Figure 6.19: Illustration of the layers in the 1DRCM. Pressures are in units of atmospheres and at_i is the average temperature of layer i (MacKay and Khalil, 1991).

6.2.2 Calculation of selected quantities

Calculation of radiative forcing

In this section the calculation of radiative forcing as presented in MacKay and Khalil (1991) will be explained. The radiative forcing(F) is the change in net flux density of radiation at the tropopause after allowing stratospheric temperatures to adjust to radiative equilibrium. Therefore the following section will focus on calculating the upwards and downwards flux density.

General quantities. The following section is based on (Liou, 2002, p. 27–28). The intensity of a cylinder of radiation traversing a medium of thickness ds will be weakened by interaction with the matter according to:

$$dI_\lambda = -k_\lambda \rho I_\lambda ds \tag{6.8}$$

Where I_λ is the intensity of incoming radiation at wavelength λ, k_λ is the mass extinction cross section and ρ is the density of the medium. Since the medium itself has a temperature it will emit blackbody radiation which, along with scattering from all other directions into the pencil, will increase the intensity of the pencil's radiation. In analogy with the mass extinction cross section (k_λ) the source function coefficient (j_λ) of the medium is defined as:

$$dI_\lambda = j_\lambda \rho ds \tag{6.9}$$

Combining equation 6.8 and 6.9 to yield the general radiative transfer equation for the wavelength λ:

$$dI_\lambda = -k_\lambda \rho I_\lambda ds + j_\lambda \rho ds \tag{6.10}$$

Introducing the source function:

$$J_\lambda \equiv \frac{j_\lambda}{k_\lambda} \tag{6.11}$$

Inserting equation 6.11 into equation 6.10:

$$-\frac{1}{k_\lambda \rho}\frac{dI_\lambda}{ds} = I_\lambda - J_\lambda \tag{6.12}$$

The general solution. The model presented in MacKay and Khalil (1991) uses a plane-parallel description of the atmosphere. The plane-parallel coordinate system as illustrated on figure 6.20 is a spherical coordinate system with the origin located at the surface of the earth($z = 0$). Moreover variation in radiation intensity and atmospheric parameters are only permitted in the vertical direction. This means that absorption and emission will be symmetrical with respect to the azimuthal angle. Assuming that scattering is negligible rewriting equation 6.12 (Goody and Yung, 1989, p. 46):

$$-\zeta \frac{1}{k_\lambda \rho}\frac{dI_\lambda(z,\zeta)}{dz} = I_\lambda(z,\zeta) - J_\lambda(z,\zeta) \tag{6.13}$$

Where k_λ is now the mass absorption coefficient for the wavelength λ and $\zeta = cos(\theta)$. Assuming that the atmosphere in localized portions is in thermodynamic equilibrium, meaning that it has a uniform temperature and isotropic radiation, means that the source function(J_λ) can be substituted by the Planck intensity($B_\lambda(z) = B_\lambda(T(z))$):

$$-\zeta \frac{1}{k_\lambda \rho}\frac{dI_\lambda(z,\zeta)}{dz} = I_\lambda(z,\zeta) - B_\lambda(z) \tag{6.14}$$

Introducing the optical path($\vec{\tau_\lambda}$):

$$\vec{\tau}_\lambda(1,2) = \int_1^2 k_\lambda(s)\rho(s)ds \tag{6.15}$$

The derivative of the optical path is then (Liou, 2002, p. 124):

$$d\vec{\tau}_\lambda(1,2) = -k_\lambda \rho ds \tag{6.16}$$

Changing variable to $\vec{\tau}$ means that equation 6.14 for the geometry of figure 6.21 becomes:

$$\zeta \frac{dI(P',\vec{s})}{d\vec{\tau}_\lambda} = I_\lambda(P',\vec{s}) - J_\lambda(P',\vec{s}) \tag{6.17}$$

Multiplying both sides of equation 6.17 with $e^{-\vec{\tau}_\lambda}$ and integrating from P to P'' yields (Goody and Yung, 1989, p. 44):

$$I_\lambda(P,\vec{s}) = I_\lambda(P'',\vec{s})e^{-\vec{\tau}(P'',P)} + \int_0^{\vec{\tau}_\lambda(P'',P)} J_\lambda(P',\vec{s})e^{-\vec{\tau}_\lambda(P',P)}\frac{d\vec{\tau}_\lambda}{\zeta} \tag{6.18}$$

The optical depth of the position z is in the model (MacKay and Khalil, 1991) defined as:

$$\tau_\lambda = \int_z^{z''} k_\lambda(z')\rho(z')dz' \tag{6.19}$$

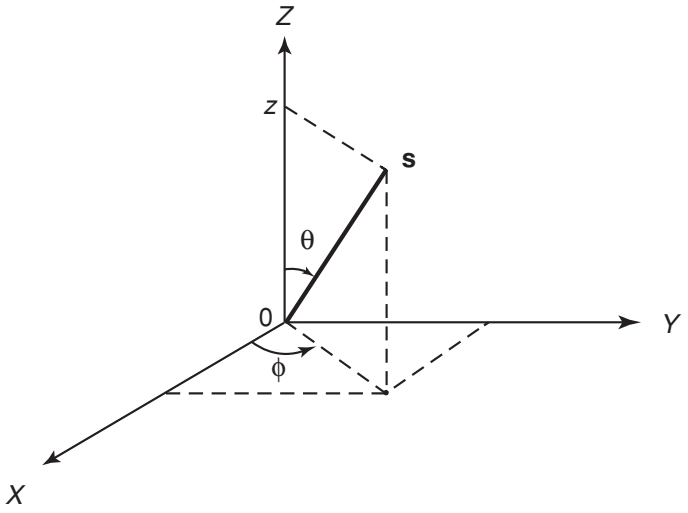

Figure 6.20: The coordinate system of a plane-parallel atmosphere, where z is the vertical direction and θ and ϕ denote respectively the zenith and azimuthal angles. s denote the position vector.(Liou, 2002, p. 31)

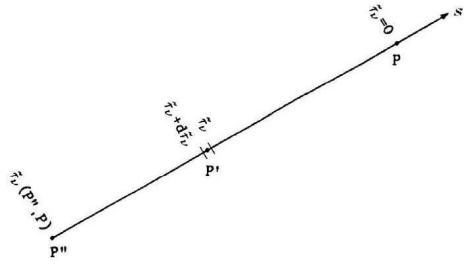

Figure 6.21: Path of integration.(Goody and Yung, 1989, p. 44)

This means, as can be seen from figure 6.22, that the relationship between optical depth and optical path will be:

$$\vec{\tau}_\lambda(1,2) = \frac{\tau(1,2)}{\zeta} \tag{6.20}$$

For the case of the plane-parallel atmosphere with the bottom of the top atmospheric layer located at $z = z_t$, the governing equation is 6.14, which is a first-order differential equation. Since the boundary conditions for upwards and downwards travelling radiation differ, two boundary conditions are required. For the upwards solution (I^+) the source function is the earth represented by a blackbody at $z = 0$ with temperature θ^* (Liou, 2002, p. 124):

$$I^+_\lambda(0,\zeta) = B_\lambda(\theta^*) \tag{6.21}$$

For the downwards solution (I^-) the source function is represented by a blackbody with the temperature at the top of the atmosphere (TOA). However, $B_\lambda(TOA) \cong$

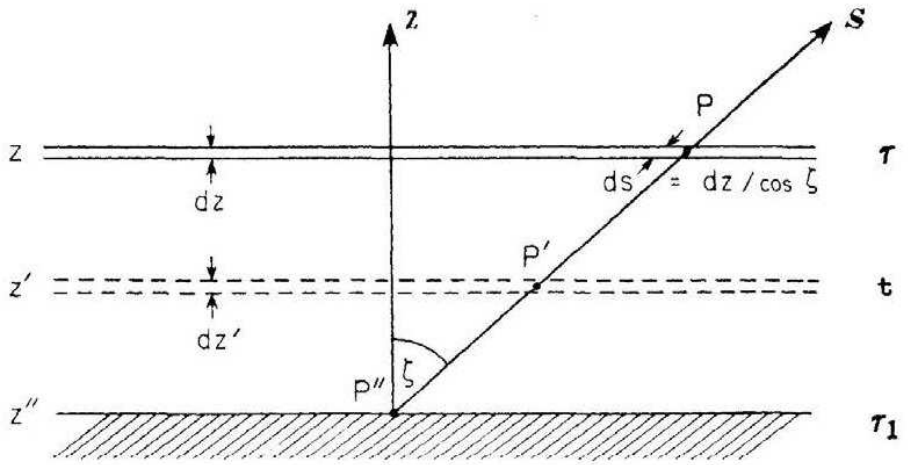

Figure 6.22: Geometry of the plane-parallel atmosphere (Goody and Yung, 1989, p. 46).

0 meaning that:

$$I_\lambda^-(z'', \zeta) = 0 \tag{6.22}$$

Substituting equation 6.20 into equation 6.18 and using the boundary conditions presented in equation 6.21 and 6.22 means the solution to the radiative transfer equation for respectively the upwards and downwards travelling radiation becomes:

$$I_\lambda^+(z, \zeta) = B_\lambda(\theta^*)e^{-\frac{\tau}{\zeta}} + \int_0^z B_\lambda(z')e^{-\frac{\tau}{\zeta}}\frac{dz'}{\zeta} \tag{6.23a}$$

$$I_\lambda^-(z, -\zeta) = \int_z^{z''} B_\lambda(z')e^{-\frac{\tau}{\zeta}}\frac{dz'}{\zeta} \tag{6.23b}$$

As defined by MacKay and Khalil (1991), the monochromatic transmission function is defined as:

$$T_\lambda(z, z') = e^{-\frac{\tau}{\zeta}} \tag{6.24}$$

$$\frac{dT_\lambda(z,z')}{dz'} = -\frac{1}{\zeta}e^{-\frac{\tau}{\zeta}} \tag{6.25}$$

In the model (MacKay and Khalil, 1991), $\frac{1}{\zeta}$ is approximated to the value 1.66, which is based in numerical computations. Inserting 6.24 and 6.25 in the solution for upwards and downwards travelling radiation results in:

$$I_\lambda^+(z, \zeta) = B_\lambda(\theta^*)T_\lambda(z, z') + \int_0^z B_\lambda(z')\frac{d}{dz'}T_\lambda(z, z')dz' \tag{6.26a}$$

$$I_\lambda^-(z, -\zeta) = \int_z^{z''} B_\lambda(z')\frac{d}{dz'}T_\lambda(z, z')dz' \tag{6.26b}$$

Since the radiative forcing (F) is the change in flux density, the intensities for the upwards and downwards radiation is integrated with respect to the azimuthal

and zenith angle and integrated over all wavelengths according to the following formula (Liou, 2002, p. 124–125):

$$F(z) = \int_0^\infty d\lambda \int_0^{2\pi} d\phi \int_0^1 I_\lambda(z, \pm\zeta)\zeta d\zeta \qquad \Updownarrow \qquad (6.27)$$

$$F(z) = 2\pi \int_0^\infty d\lambda \int_0^1 I_\lambda(z, \pm\zeta)\zeta d\zeta \qquad \Updownarrow \qquad (6.28)$$

$$(6.29)$$

Introducing the diffuse transmittance defined by:

$$T_\lambda^f(z) = 2\int_0^1 T\lambda(z, z')\zeta d\zeta \qquad (6.30)$$

Calculating the upwards and downwards flux and using the definition of the diffuse transmittance yields:

$$F^+(z) = \int_0^\infty d\lambda \left(\pi B_\lambda(\theta^*) T_\lambda^f(z, z') + \int_0^z \pi B_\lambda(z') \tfrac{d}{dz'} T_\lambda(z, z') dz' \right) \qquad (6.31a)$$

$$F^-(z) = \int_0^\infty d\lambda \left(\int_z^{z''} \pi B_\lambda(z') \tfrac{d}{dz'} T_\lambda^f(z, z') dz' \right) \qquad (6.31b)$$

Conversion from transmission to absorption. This section is based on MacKay and Khalil (1991). For the ease of calculation, the monochromatic absorption function is defined as:

$$A_\lambda = 1 - T_\lambda \qquad \Updownarrow \qquad (6.32)$$

$$\tfrac{dA_\lambda}{dz'} = \tfrac{dT_\lambda}{dz'} \qquad \Updownarrow \qquad (6.33)$$

Furthermore assuming that the atmospheric temperature T is constant above $z = z_t$ for the downwards radiation:

$$F^-(z) = \int_0^\infty d\lambda \left(\int_{z_t}^{z''} \pi B_\lambda(z') \tfrac{d}{dz'} A_\lambda^f(z, z') dz' + \int_z^{z_t} \pi B_\lambda(z') \tfrac{d}{dz'} A_\lambda^f(z, z') dz' \right) \Updownarrow \quad (6.34)$$

$$F^-(z) = \int_0^\infty d\lambda \left(\pi B_\lambda(z_t)\ A_\lambda^f(z, z') \Big|_{z_t}^\infty + \int_z^{z_t} \pi B_\lambda(z') \tfrac{d}{dz'} A_\lambda^f(z, z') dz' \right) \qquad \Updownarrow \quad (6.35)$$

$$F^-(z) = \int_0^\infty d\lambda \left(\pi B_\lambda(z_t) A_\lambda^f(z, \infty) - \pi B_\lambda(z_t) A_\lambda^f(z, z_t) \right.$$
$$\left. + \int_z^{z_t} \pi B_\lambda(z') \tfrac{d}{dz'} A_\lambda^f(z, z') dz' \right) \qquad \Updownarrow \quad (6.36)$$

Integrating the second integral by parts:

$$F^-(z) = \int_0^\infty d\lambda \left(\pi B_\lambda(z_t) A_\lambda^f(z, \infty) - \pi B_\lambda(z_t) A_\lambda^f(z, z_t) \right.$$
$$\left. + \int_z^{z_t} A_\lambda^f(z, z') \tfrac{d\left[\pi B_\lambda(z')\right]}{dz'} dz' + \pi B(z') A_\lambda^f(z, z') \Big|_z^{z_t} \right) \qquad \Updownarrow \quad (6.37)$$

$$F^-(z) = \int_0^\infty d\lambda \left(\pi B_\lambda(z_t) A_\lambda^f(z, \infty) - \pi B_\lambda(z_t) A_\lambda^f(z, z_t) \right.$$

$$+ \int_z^{z_t} A_\lambda^f(z,z') \tfrac{d[\pi B_\lambda(z')]}{dz'} dz' + \pi B(z_t) A_\lambda^f(z,z_t) - \pi B(z) A_\lambda^f(z,z)\Big) \quad \Updownarrow (6.38)$$

Since $A_\lambda^f(z,z) = 0$

$$F^-(z) = \int_0^\infty d\lambda \left(\pi B_\lambda(z_t) A_\lambda^f(z,\infty) - \pi B_\lambda(z_t) A_\lambda^f(z,z_t) + \int_z^{z_t} A_\lambda^f(z,z') \tfrac{d[\pi B_\lambda(z')]}{dz'} dz' + \pi B(z_t) A_\lambda^f(z,z_t)\right) \quad \Updownarrow (6.39)$$

$$\boxed{F^-(z) = \int_0^\infty d\lambda \left(\pi B_\lambda(z_t) A_\lambda^f(z,\infty) + \int_z^{z_t} A_\lambda^f(z,z') \tfrac{d[\pi B_\lambda(z')]}{dz'} dz'\right)} \quad (6.40)$$

Using a similar procedure it can be shown, that the upwards flux is calculated by:

$$\boxed{F^+(z) = \int_0^\infty d\lambda \left(\pi B_\lambda(0) + \int_0^z \pi A_\lambda^f(z,z') \tfrac{d[\pi B_\lambda(z')]}{dz'}\right) dz'} \quad (6.41)$$

This means that using equation 6.40 and 6.41 it is possible to calculate the change in flux density as a result of a perturbation in the atmospheric chemistry.

Calculation of the monochromatic absorption function.

In this section the calculation of the monochromatic absorption function (A_λ^f) is explained. The section will use CH_4 as an example, since CH_4 is one of the gases whose concentration is expected to change as a result of the installation of the degassing plant.
The monochromatic absorption function of CH_4 is modelled as an absorption band consisting of a number of absorption lines. As a start it is assumed that the lines do not overlap. If the width of the band is $N\delta$ and the band contains N lines with a mean spacing of δ. The equivalent width of line i (W_i) is the integral of the absorption of a single line over all frequencies (Goody and Yung, 1989, p. 129). This means, that the average absorption ($\bar{A}$) can be written as (Goody and Yung, 1989, p. 138):

$$\bar{A} = \frac{1}{N\delta} \sum_{i=1}^{N} W_i = \frac{\bar{W}}{\delta} \tag{6.42}$$

Where $\bar{W}$ is the mean equivalent width. Rewriting the mass extinction cross section (k_ν) as:

$$k_\nu = f(\nu)S \tag{6.43}$$

Where $f(\nu)$ is the line shape factor and S is the absorption line intensity defined as (Goody and Yung, 1989, p. 98):

$$S = \int k_\nu d\nu \tag{6.44}$$

Introducing the probability function $p(S)$ having the property that $p(S)dS$ is the fraction of lines having intensities between S and $S + dS$. Using this function and inserting the definitions of the monochromatic transmission function from eq. (6.24) on page 125 and eq. (6.19) on page 123 into eq. (6.32) on page 126 yields the following expression for the equivalent width:

$$\bar{W} = \int_0^\infty p(S) \int_{-\infty}^{\infty} 1 - e^{-Smf(\nu)} d\nu dS \tag{6.45}$$

Where m is the amount of absorbing material in appropriate units. Using the exponential distribution based on empirical arguments:

$$p(S) = \frac{1}{\sigma} e^{-\frac{S}{\sigma}} \tag{6.46}$$

Inserting this expression into eq. (6.45):

$$\bar{W} = \int_0^\infty \frac{1}{\sigma} e^{-\frac{S}{\sigma}} \int_{-\infty}^{\infty} 1 - e^{-Smf(\nu)} d\nu dS \tag{6.47}$$

Following the approach described in (Goody and Yung, 1989, p. 139), the order of integration is reversed and the integration for S is performed:

$$\bar{A} = \frac{1}{\delta}\int_{-\infty}^{\infty}\int_{0}^{\infty}\frac{1}{\sigma}e^{-\frac{S}{\sigma}}\left(1-e^{-Smf(\nu)}\right)dSd\nu \quad \Leftrightarrow \quad (6.48)$$

$$\bar{A} = \frac{1}{\delta}\int_{-\infty}^{\infty}\int_{0}^{\infty}\frac{1}{\sigma}e^{-\frac{S}{\sigma}}-\frac{1}{\sigma}e^{-\frac{S}{\sigma}}e^{-Smf(\nu)}dSd\nu \quad \Leftrightarrow \quad (6.49)$$

$$\bar{A} = \frac{1}{\delta}\int_{-\infty}^{\infty}\int_{0}^{\infty}\frac{1}{\sigma}e^{-\frac{S}{\sigma}}-\frac{1}{\sigma}e^{-\frac{S}{\sigma}-Smf(\nu)}dSd\nu \quad \Leftrightarrow \quad (6.50)$$

$$\bar{A} = \frac{1}{\delta}\int_{-\infty}^{\infty}\int_{0}^{\infty}\frac{1}{\sigma}e^{-\frac{S}{\sigma}}-\frac{1}{\sigma}e^{-S\left(\frac{1}{\sigma}+mf(\nu)\right)}dSd\nu \quad \Leftrightarrow \quad (6.51)$$

$$\bar{A} = \frac{1}{\delta}\int_{-\infty}^{\infty}\frac{1}{\sigma}\left[-\sigma e^{-\frac{S}{\sigma}}\right]_{0}^{\infty}-\frac{1}{\sigma}\left[\frac{1}{-\frac{1}{\sigma}-mf(\nu)}e^{-S\left(\frac{1}{\sigma}+mf(\nu)\right)}\right]_{0}^{\infty}d\nu \quad \Leftrightarrow \quad (6.52)$$

$$\bar{A} = \frac{1}{\delta}\int_{-\infty}^{\infty}\left[-e^{-\frac{S}{\sigma}}\right]_{0}^{\infty}-\left[\frac{1}{-1-m\sigma f(\nu)}e^{-S\left(\frac{1}{\sigma}+mf(\nu)\right)}\right]_{0}^{\infty}d\nu \quad \Leftrightarrow \quad (6.53)$$

$$\bar{A} = \frac{1}{\delta}\int_{-\infty}^{\infty}1+\frac{1}{-1-m\sigma f(\nu)}d\nu \quad \Leftrightarrow \quad (6.54)$$

$$\bar{A} = \frac{1}{\delta}\int_{-\infty}^{\infty}\frac{1+m\sigma f(\nu)}{1+m\sigma f(\nu)}+\frac{-1}{1+m\sigma f(\nu)}d\nu \quad \Leftrightarrow \quad (6.55)$$

$$\bar{A} = \frac{1}{\delta}\int_{-\infty}^{\infty}\frac{m\sigma f(\nu)}{1+m\sigma f(\nu)}d\nu \quad \Leftrightarrow \quad (6.56)$$

Inserting the expression for Lorentz line shape:

$$f(\nu) = \frac{\alpha_L}{\pi(\nu^2+\alpha_L^2)} \quad (6.57)$$

$$\bar{A} = \frac{1}{\delta}\int_{-\infty}^{\infty}\frac{\frac{m\sigma\alpha_L}{\pi\left(\nu^2+\alpha_L^2\right)}}{\left(1+\frac{m\sigma\alpha_L}{\pi\left(\nu^2+\alpha_L^2\right)}\right)}d\nu \quad \Leftrightarrow \quad (6.58)$$

$$\bar{A} = \frac{1}{\delta}\int_{-\infty}^{\infty}\frac{\frac{m\sigma\alpha_L}{\pi\left(\nu^2+\alpha_L^2\right)}}{\pi\left(\nu^2+\alpha_L^2\right)+\frac{\pi\left(\nu^2+\alpha_L^2\right)m\sigma\alpha_L}{\pi\left(\nu^2+\alpha_L^2\right)}}d\nu \quad \Leftrightarrow \quad (6.59)$$

$$\bar{A} = \frac{1}{\delta}\int_{-\infty}^{\infty}\frac{m\sigma\alpha_L}{\pi\left(\nu^2+\alpha_L^2\right)+m\sigma\alpha_L}d\nu \quad \Leftrightarrow \quad (6.60)$$

Using Mathematica computer algebra system to perform the integration:

$$\bar{A} = \frac{\alpha_L}{\delta}\left[\frac{m\sigma\tan^{-1}\left(\frac{\sqrt{\pi}\nu}{\sqrt{\alpha_L}\sqrt{\pi\alpha_L+m\sigma}}\right)}{\sqrt{\pi\alpha_L}\sqrt{\pi\alpha_L+m\sigma}}\right]_{-\infty}^{\infty} \quad \Leftrightarrow \quad (6.61)$$

$$\bar{A} = \frac{\alpha_L}{\delta}\frac{m\sigma\tan^{-1}\left(\frac{\sqrt{\pi}\nu}{\sqrt{\alpha_L}\sqrt{\pi\alpha_L+m\sigma}}\right)}{\sqrt{\pi\alpha_L}\sqrt{\pi\alpha_L+m\sigma}} \quad \Leftrightarrow \quad (6.62)$$

$$\bar{A} = \frac{\alpha_L}{\delta}\frac{m\sigma\pi}{\sqrt{\pi\alpha_L}\sqrt{\pi\alpha_L+m\sigma}} \quad \Leftrightarrow \quad (6.63)$$

$$\bar{A} = \frac{\alpha_L}{\delta}\frac{m\sigma\pi}{\sqrt{\pi^2\alpha_L^2+\pi\alpha_L m\sigma}} \quad \Leftrightarrow \quad (6.64)$$

$$\bar{A} = \frac{\alpha_L}{\delta} \frac{m\sigma\pi}{\sqrt{\pi^2\alpha_L^2 + 2\frac{\pi\alpha_L m\sigma}{2}}} \qquad \Leftrightarrow \qquad (6.65)$$

$$\bar{A} = \frac{\alpha_L}{\delta} \frac{m\sigma\pi}{\pi\alpha_L\sqrt{1+2\frac{m\sigma}{2\pi\alpha_L}}} \qquad \Leftrightarrow \qquad (6.66)$$

$$\bar{A} = \frac{\alpha_L}{\delta} \frac{2m\sigma\pi}{2\pi\alpha_L\sqrt{1+2\frac{m\sigma}{2\pi\alpha_L}}} \qquad \Leftrightarrow \qquad (6.67)$$

$$\bar{A} = \frac{2\pi y u_\sigma}{\sqrt{1+2u_\sigma}} \qquad y = \frac{\alpha_L}{\delta}, \qquad u_\sigma = \frac{\sigma m}{2\pi\alpha_L} \qquad (6.68)$$

Based on empirical data, Goody and Belton (1967) suggest a band model including overlap to be a function of the no-overlap solution. Goody and Belton (1967) states that "if $F(x) \to x$ as $x \to 0$ we are assured of correct results for short paths". This is because as the absorption decreases and the average line distance stays constant, the overlap will decrease and the no-overlap solution will be an acceptable approximation. Moreover "laboratory data for many bands (including the 15 μ CO_2 band) show a logarithmic dependence of band area upon path lengths for long paths" the above stated conditions "suggests a functional form" (Goody and Belton, 1967, p. 250):

$$\bar{A} = c \ln\left(1 + \frac{A(\text{no overlap})}{c}\right) \qquad (6.69)$$

Where c is a constant chosen to fit laboratory data. Changing nomenclature:

$$\bar{A} = 2\ln\left(1 + \frac{\sqrt{\beta}u}{\sqrt{u+4\beta}}\right) \qquad (6.70)$$

Based in a number of constraints (Cess and Tiwari, 1967, p. 245) suggests the following expression:

$$\bar{A} = 2\ln\left(1 + \frac{u}{2+\sqrt{u}\sqrt{1+\frac{1}{\beta}}}\right) \qquad (6.71)$$

This yields the following formulation used in the model:

$$\boxed{\bar{A} = 2A_0 \ln\left(1 + \frac{u}{\sqrt{4+u\left(1+\frac{1}{\beta}\right)}}\right)} \qquad (6.72)$$

6.2.3 Coupling between the models

To calculate the change in radiative forcing as a result of the installation of the DONG degassing plant, the DEHM model and the 1DRCM model have to be used together. The two model are thus coupled in an offline approach, meaning that the output from the DEHM model is used as input to the 1DRCM model, but that the 1DRCM does not feed back into the DEHM model. This is done on a point by point basis, such that for every data point in the DEHM model, a set of data are exported and subsequently imported into the 1DRCM. To connect the DEHM model with the 1DRCM model a range of parameters had to be converted from DEHM output to 1DRCM input. In the following, the calculation of the individual data are explained:

Time values: The 1DRCM model has an option to change the concentrations of ozone, carbon dioxide, methane, and nitrous oxide after specific time periods, as a way to simulate temporal climate changes. In this modelling, the time values are set at values larger than the run length, since the aim of this modelling is not to simulate temporal climate changes. The model is instead run once with the basis-concentrations from the DEHM model and once with the tag-concentrations from the DEHM model, and the results on the radiative forcing calculated from subtraction.

Temperature: The 1DRCM takes as input values the temperature for the 18 layers and the surface. A set of standard values are supplied with the model. Since the 1DRCM has a larger domain with respect to height, the original temperature input values are kept for the uppermost part of the model domain. For the lowermost part of the domain, the temperatures are calculated through a linear interpolation between the temperature values from DEHM for the two closest layers.

Ozone parameters: The atmospheric ozone distribution included in the model is the analytical expression taken from (Lacis and Hansen, 1974):

$$u(h) = \frac{a+ae^{-b/c}}{1+e^{h-b/c}} \tag{6.73}$$

Where $u(h)$ is the total ozone amount in cm at STP, a is the total ozone amount in a vertical column above ground, b is the height of the peak ozone concentration, and $a\left(1+e^{-b/c}\right)/4c$ is the peak ozone concentration. The input parameter to the 1DRCM in this case is only the value a, which is the Dobson unit taken from the DEHM model converted to the correct unit. The Dobson unit in the DEHM model is a climatological Dobson unit, and as such, is not influenced by the modelled change in emission. For simplicity the Dobson unit from the DEHM model is used anyway as a representative for a.

Solar constant: The solar constant divided by two is as a standard value set to $680.0^{kW}/_{m^2}$. This value is unchanged in the present model.

Solar zenith angle: The solar zenith angle for the individual data point is calculated as an average over the 24 values supplied by the DEHM model. The 1DRCM already includes a mechanism to compensate for day and night, and therefore only the positive values were included in the average.

Step size: The step size is as standard set to 0.9. This remains unchanged in the present modelling.

Low: The low value is the value to determine when radiative equilibrium is reached. It is as standard set to 0.0001k, which remains unchanged in the present modelling.

Run length: The run length is the "cut off" length, meaning that the model will terminate although radiative equilibrium has not been reached. This value is as standard set to 1200 days, but in order to obtain a total temperature change per iteration lower than 0.1k this value was gradually increased to 6000 days to strike a balance between approaching radiative equilibrium and a reasonable calculation time.

Critical lapse rate: Since the 1DRCM is run without the convective adjustment, this setting becomes unimportant.

Ocean depth: Although the it is stated in MacKay and Khalil (1991) that model uses 100m as ocean depth, the standard setting is 2.5m. This value remains unchanged in the present modelling.

Trace gas concentrations: The carbon dioxide concentration, nitrous oxide concentration, F-11 concentration and F-12 concentration are the 2005-values taken from (Forster et al., 2007, p. 141).

Methane concentration: The methane concentration is the column-average concentration of methane calculated from DEHM. In MacKay and Khalil (1991) the vertical profile of methane is stated to follow the one depicted in fig. 6.23. As can be seen from the figure, the CH_4-concentration is

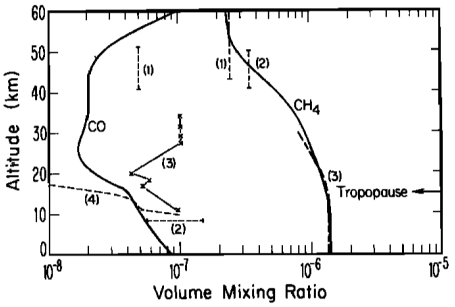

Figure 6.23: Vertical CO- and CH_4-concentration profile from (Crutzen, 1978). The solid curves represent the yearly average concentrations based on models. The numbers refer to measurements by: CH_4: 1, (Ehhalt et al., 1975), 2, (Ehhalt et al., 1975), 3, (Ehhalt et al., 1974), CO: 1, (Ehhalt et al., 1975), 2, (Seiler, 1974), 3, (Ehhalt et al., 1974), 4, (Goldman et al., 1973).

constant in the full domain of the DEHM model. This means that the used CH_4-concentration is the column-averaged CH_4-concentration.

NMVOC concentrations: In DEHM, the concentrations of n-butane are lumped concentrations. In order to calculate the concentration of the specific un-lumped species, certain assumptions have to be made. In the present modelling approach it is assumed that the distribution within the lumping groups follows the distribution in the emission. Since the chemical composition of the emission is unchanged in the tag-modelling compared to the basis-modelling, the composition distribution follows the composition distribution in the EMEP scheme. Moreover, it is assumed that the concentration distribution follows the distribution within the lumping group. If α_i is the NMVOC emission distribution factor for compound i, and β_i is the aggregation factor of specie i in a lumping group consisting of n species, the concentration of specie i in the lumping group $[HC]$ becomes:

$$[HC_i] = [HC]\frac{\alpha_i\beta_i}{\alpha_1\beta_1+\alpha_2\beta_2+...+\alpha_n\beta_n} \tag{6.74}$$

NMVOC center frequencies and band strengths: The NMVOC center frequencies and band strengths were calculated based on absorption spectra from NIST (National Institute of Standards and Technology) for ethane, propane, i-butane, i-pentane, and n-pentane and from (Bridgeman, 2013) for n-butane. The spectra were digitised using the program G3Data Graph Analyser as illustrated in creffig:G3. For each peak in the spectrum, the center was calculated as the average of the first and last data point constituting the peak, and the bad strength was calculated as the numerical integral over the absorption integrated over the peak. The numerical integral was performed with the *trapz* MatLab function.

Clouds: According to Christensen et al. (1996) the 1DRCM contains a programming error meaning that it behaves differently on different FORTRAN compilers. This means that the model yields "NaN" values for certain cloud settings. For this reason, the cloud fraction is set to zero, the cloud layer is set to 1, and the cloud optical depth is set to zero in order to rule out all effects of clouds.

Surface albedo: This value is taken from DEHM.

6.2.4 Model discussion

In order to obtain a reasonable calculation time lower levels for concentration changes between basis and tag for running the 1DRCM were set. Moreover, all data points with a value lower than $10^{-6}\frac{W}{m^2}$ were discarded as noise. This level was set since it approximately corresponds to the number of decimals assigned for the data type *real* in FORTRAN. The results of these two limitations were that no change in radiative forcing as a result of the installation of the degassing plant was detected. The cause of this would have to be looked further into.
If results of a magnitude smaller than $10^{-6}\frac{W}{m^2}$ should be detectable, the 1DRCM would need to be reprogrammed with the variable type *double precision* instead of *real*. This would however cause other problems, since uncertainties would result from lack of decimals in many of the numbers incorporated in the model. It would also be relevant to examine the radiative effect of concentration changes

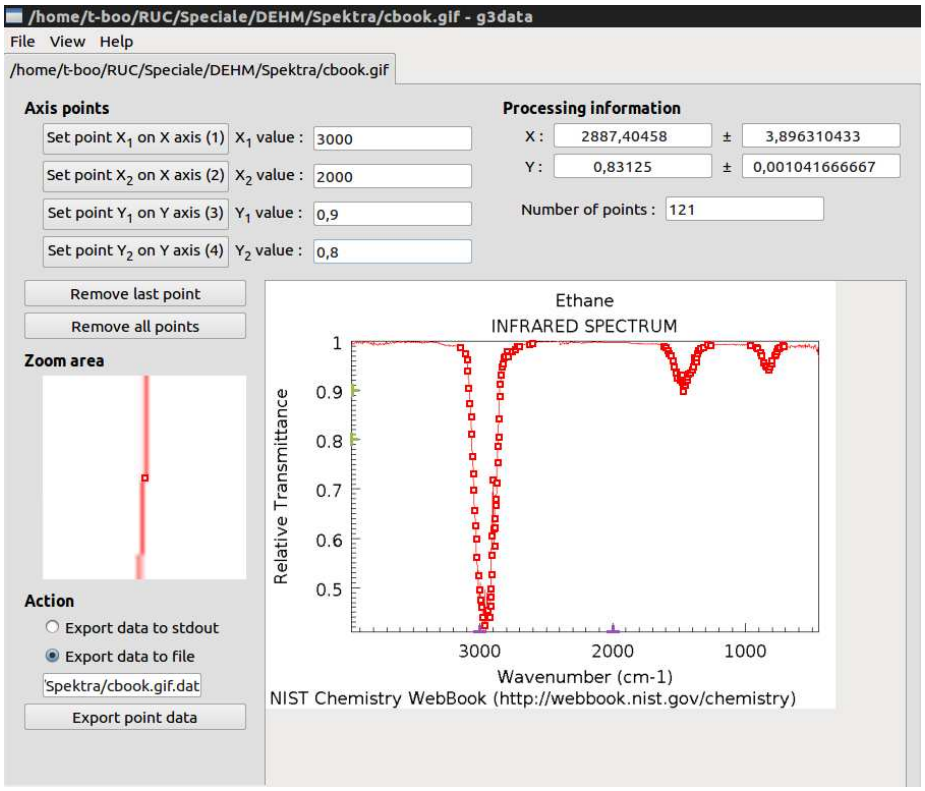

Figure 6.24: Screenshot of the program G3Data Graph Analyzer with the spectrum of ethane in the digitising progress.

of the NMVOCs alone, since it is not known how large concentration changes of these are required to cause a change in radiative forcing. This would influence the lower levels for which data points to include in the modelling. Lastly it would have to be looked into whether or not the 1DRCM with the input settings at all yields a realistic model atmosphere and how the equilibrium time is influenced by the various parameters.

Chapter 7

Technical analysis

As stated in section 3.4, the technical analysis will evaluate the technical performance of the degassing plant with respect to two parameters: the energy/production relationship and the availability. Both parameters will be determined empirically based on production data recorded for the Fredericia terminal and the degassing plant.

7.1 Energy/production relationship

As presented in section 3.4.1, the hypothesis of this section is that there has been a marked increase in the power consumption on the Fredericia oil terminal, as a result of the installation of the degassing plant.
Moreover, the trend in the power consumption is hypothesised to follow the trend in the amount of exported oil. The amount of exported oil, the amount of exported gas, and the power consumption on the Fredericia oil terminal, as a function of time from January 2002 to August 2012, is presented in fig. 7.1.
As can be seen, the power consumption is declining along with the oil export from 2002, reaching a local minimum around September 2008. After this point, the power consumption is increasing despite the continuing decline in the oil export.
The increase in power consumption happens at the same time as the degassing plant is starting to export gas, and as the gas export is increased, the power consumption increases as well.
A linear fit to the scatter plot of the power consumption vs oil export before and after the installation of the degassing plant is shown in fig. 7.2.
As described in section 2.2, the first offgas was exported in January 2009 with a gradual increase in the operational time during the spring of 2009. Moreover, in the first three months of operation the degasser was running at a pressure above atmospheric pressure, meaning that the efficiency was lower.
The "transition" period from January 2009 to July 2009 is therefore marked on fig. 7.2 and analysed separately. As can be seen, the best straight line through the data points has higher values after the installation of the degassing plant as compared to before the installation of the degassing plant, although there has been a lower throughput of oil as compared to the period before the installation

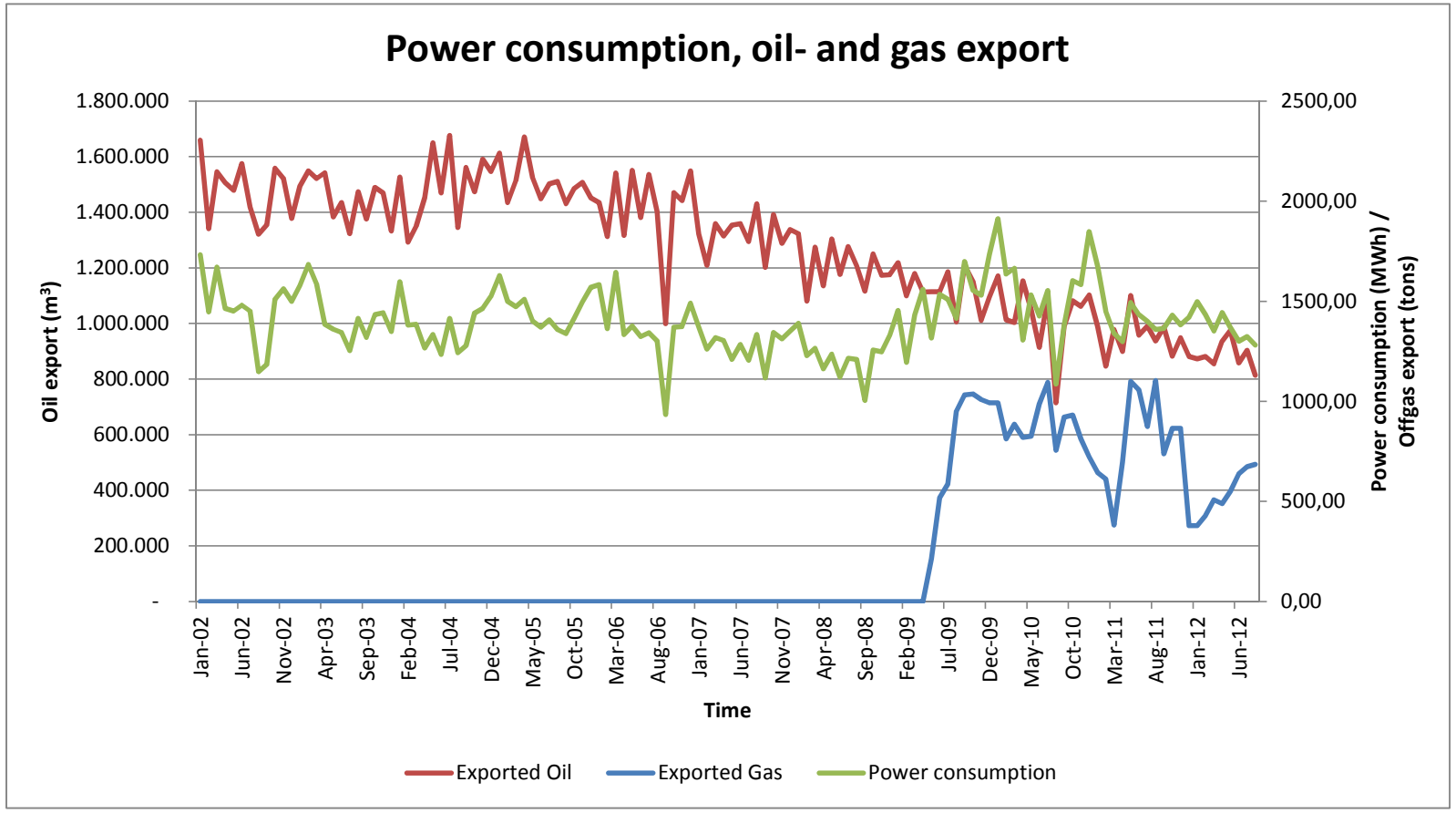

Figure 7.1: The oil exported from the Fredericia oil terminal, the gas exported from the Fredericia oil terminal, and the power consumption for the Fredericia oil terminal, plotted with monthly interval as a function of time. Data source: DONG Oil Pipe monthly report database.

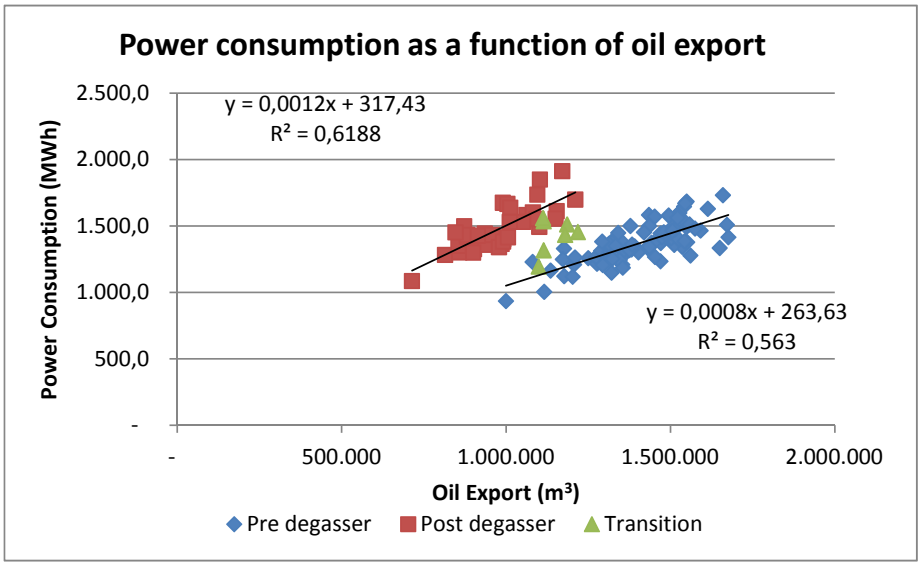

Figure 7.2: Scatter plot of the power consumption on the Fredericia oil terminal as a function of the oil export before installation, during commissioning, and after the installation of the degassing plant. For the period, before and after the installation of the degassing plant, a linear fit is performed, and the resulting equation is shown along with the coefficient of determination. Data source: DONG Oil Pipe monthly report database.

of the degassing plant. This means that the degassing plant has entailed a marked increase in the power consumption of the Fredericia oil terminal. The points representing the transition period are located in between the months representing post degasser and the months representing pre degasser. This justifies a separate analysis of these points.
The slope of the best fit line is slightly steeper for the dataset representing the period after the installation of the degassing plant, as compared to the dataset representing the period before. However, this is a small increase in absolute magnitude compared to the fact that the whole line is shifted upwards by $53.8MWh$.
It can also be seen that the coefficient of determination is approximately 0.563 for the dataset representing the period before the installation of the degassing plant and slightly higher for the dataset representing the period after the installation of the degassing plant. This shows that a significant amount of the variation in the power consumption can be explained by the variation in the oil export, but that there are other factors influencing the power consumption to a significant degree. This is natural, since the largest source of power consumption on the Fredericia oil terminal is the export pumps, transferring the oil from the storage tanks to the refinery or the harbour. The more oil passing through the terminal, the more time the export pumps will be in use, and the more power will be consumed.
To reduce the discrepancy between the fit and the data, a seasonal variation was hypothesised, based on a visual inspection of the residual between the fit and

the data of the time period before the installation of the degassing plant. The residual, between the linear fit and the dataset representing the period before the installation of the degassing plant, and the seasonal fit to the residual are shown in fig. 7.3. The fit was done using the MatLab function *fminsearch* with the prescribed form of the formula:

$$A\cos(\omega t + \phi)$$

Where A is the amplitude of the seasonal oscillation in MWh, ω is the angular frequency in radians calculated as $\frac{2\pi}{n}$, where n is the number of months since January 2002, and ϕ is a phase angle. The initial guess at the coefficients for the seasonal variation is presented in table 7.1.
The coefficients are estimated based on a visual inspection of the residual data. The fitted coefficients are presented in table 7.2. The coefficient of determination for the fit is 0.37 and, as such, not as good a fit as the straight line fit to the original data.
Nevertheless, the fit is not completely without resemblance to the data and, as such, is incorporated in the fit to the whole time series from 2002 to 2012. This is the case, because the fitted coefficient values are not too far from the initial guesses.
This can also be seen, since the Root Mean Square Error (RMSE), for the period before the installation of the degasser, is decreasing from $98.7MWh$ to $67.0MWh$ after adding the fitted seasonal variation to the straight line fit.
It was not considered whether the installation of the degassing plant had altered the seasonal variation, since the degassing plant has only been running for two and a half seasons, and fitting a seasonal variation to such a short time-series would be subject to considerable uncertainty.
The increase in power consumption in the winter months as fitted can be explained by the temperature dependence of the viscosity of the crude oil. As the temperature is increased the viscosity decreases, and more power is required to pump the oil.
For the transition period as illustrated in fig. 7.4, the correlation between power consumption and oil export is very poor. Instead a fit to the offgas export was performed, as illustrated in fig. 7.5, yielding a much better fit. The residual of the fit to the offgas export was subsequently fitted to the oil export with a reasonable coefficient of determination, as illustrated in fig. 7.6.
The fit to the power consumption as a function of time is shown in fig. 7.8.

As can be seen, the qualitative resemblance of the data points is good. For the period before the installation of the degassing plant, the fit tends to overestimate the power consumption slightly from September 2003 to June 2005 and again from October 2006 to August 2008. The projected power consumption without

A	100
ω	0.5235
ϕ	0

Table 7.1: Initial guess values for the fit to the seasonal variation in the residual.

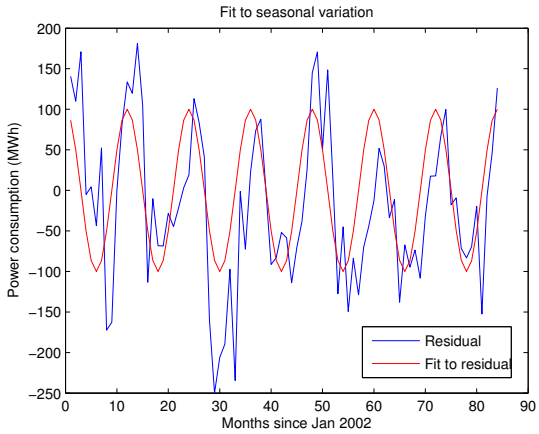

Figure 7.3: Seasonal variation fit to residual. Data source: DONG Oil Pipe monthly report database.

A	102.4167
ω	0.5251
ϕ	-0.6779

Table 7.2: Fitted coefficients to the seasonal variation in the residual.

the degassing plant is drawn on the graph as well as a diverging line at the point of installation of the degassing plant.

The power consumption of the degassing plant is subsequently calculated by subtracting the fitted power consumption without the degassing plant, taking into account both the effect of the oil export and the season, from the actual power consumption. This gives a monthly average power consumption of 435.1 MWh. Dividing through by the produced offgas gives $0.5897 \frac{MWh}{ton}$.
To evaluate the accuracy of the technical model, the residual between the fitted and the actual power consumption is shown in fig. 7.8. The trends in over- or under-prediction identified earlier are again visible in this graph. Apart from that, no temporal trend appears in the graph. Especially considering that the power consumption is fitted as a piecewise function, the fact that no noticeable change occurs in the curve of the residual at the points where the fitted formula change indicates a good fit. The histogram of the residual power consumption is shown in fig. 7.9. As can be seen, the histogram approximately resembles a normal distribution which indicates that the residuals of the power consumption are randomly distributed around the mean value. The mean value of the residuals is $-16.2MWh$ and the standard deviation is $66.8MWh$. This represents 1.2% and 4.9% respectively of the average monthly power consumption of $1374.2MWh$. The accuracy of the modelling is therefore concluded to be high.
When subtracting the fitted power consumption without the degassing plant from

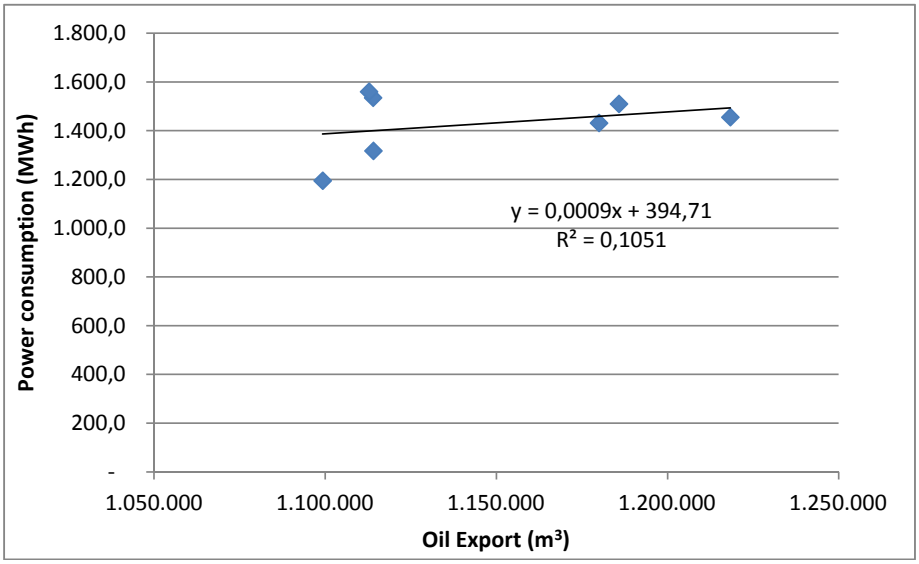

Figure 7.4: Power consumption as a function of oil export for the transition period. Data source: DONG Oil Pipe monthly report database.

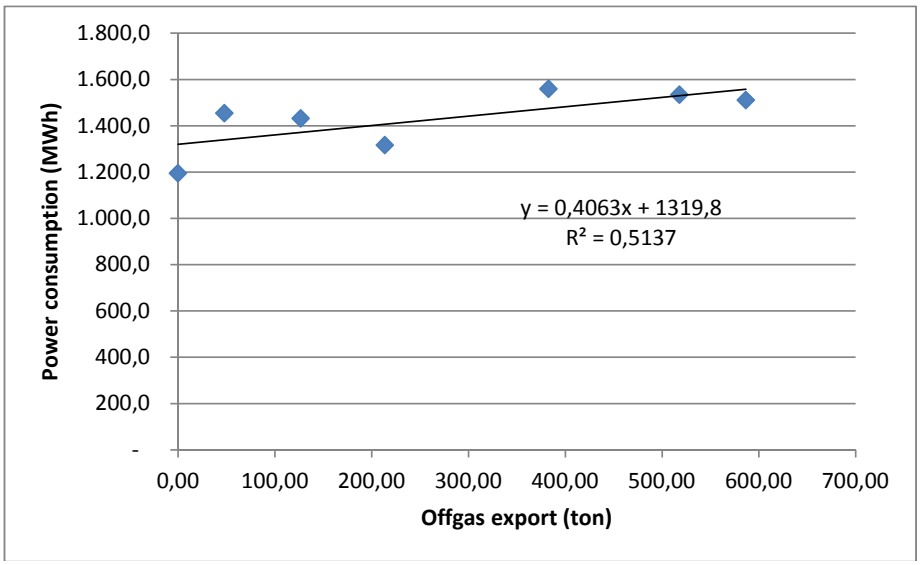

Figure 7.5: Power consumption as a function of offgas export for the transition period. Data source: DONG Oil Pipe monthly report database.

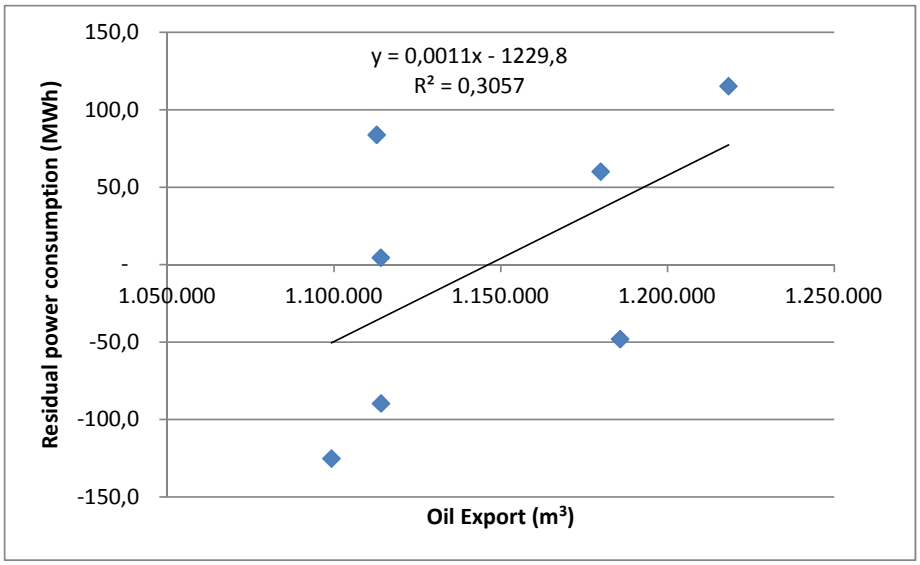

Figure 7.6: Residual power consumption as a function of ooil export for the transition period. Data source: DONG Oil Pipe monthly report database.

the actual measured power consumption the uncertainty of $66.8MWh$ is also the uncertainty of the fitted curve. This means that the uncertainty in the determined power consumption of the degassing plant becomes $\frac{66.8MWh}{435.1MWH} * 100\% \approx 15.4\%$. The same uncertainty is as well valid for the power consumption per ton offgas export. Comparing the average monthly power consumption from the above calculation to the modelled power consumption of $64.7kW \approx 47.24MWH/month$, as presented in section 2.2.4, the actual power consumption is about a factor of 9 greater than predicted before the installation of the degassing plant. As far as the author is aware, the power consumption per ton offgas is the first published number for this type of installation. Since the degassing plant is a kind of separator, it was examined whether energy efficiency figures for other types of separators was published, but this does not appear to be the case. It is therefore not possible to assess, whether or not the power consumption per ton offgas is a satisfactory performance.

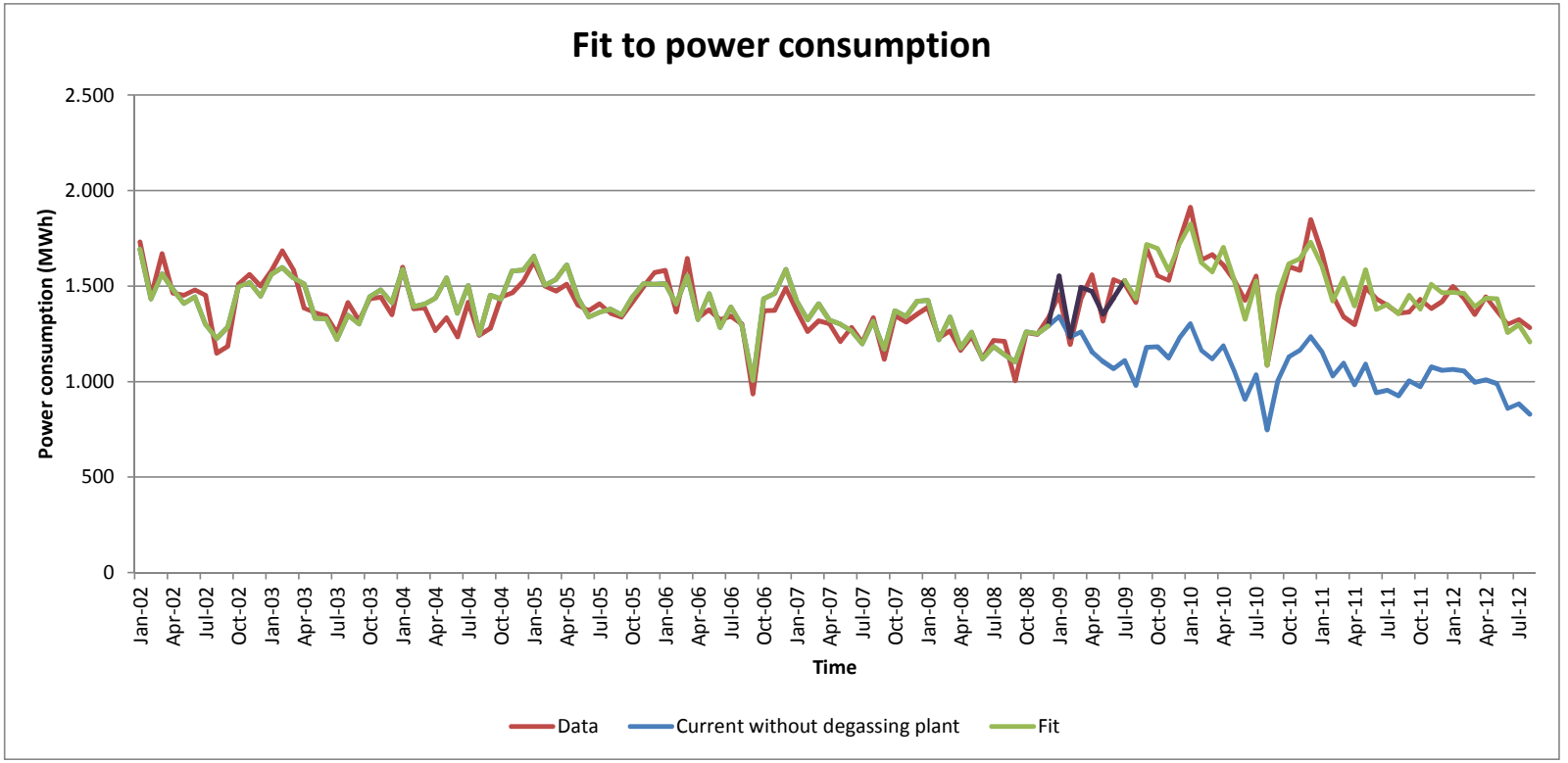

Figure 7.7: Fit to the power consumption on the Fredericia Oil Terminal and projection of power consumption without the degassing plant. The fit is made using the corresponding straight line fitted to the oil export plus the seasonal variation fitted to the period before the installation of the degassing plant. The projection is made in the same way as the fit, but without changing the straight line fit at the installation of the degassing plant. The fit to the transition period is marked with purple. Data source: DONG Oil Pipe monthly report database.

Figure 7.8: Residual power consumption as a function of time for the whole period under consideration. Data source: DONG Oil Pipe monthly report database.

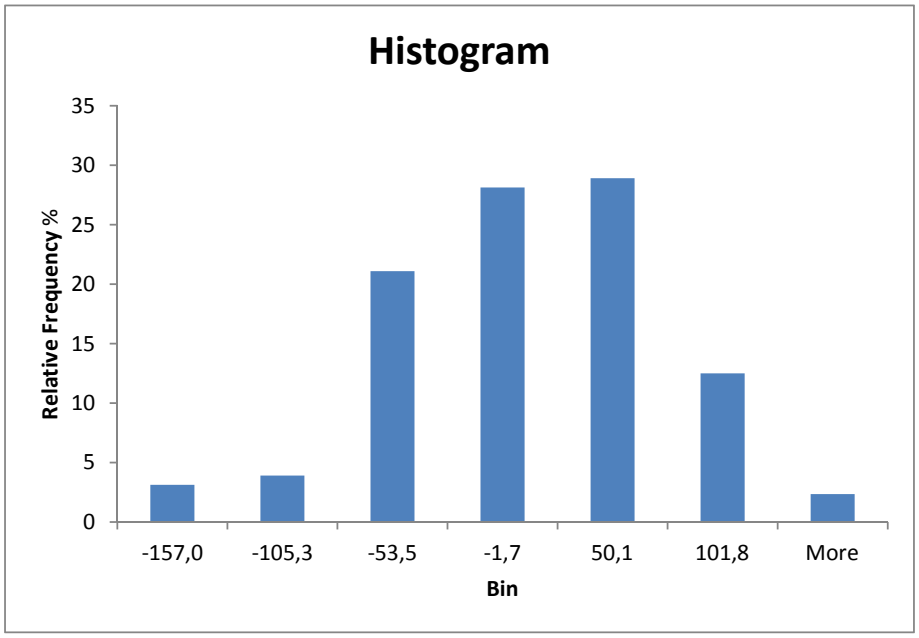

Figure 7.9: Histogram of the residual power consumption for the whole period under consideration. Data source: DONG Oil Pipe monthly report database.

7.2 Availability

In this section, the inherent availability of the DONG degassing plant and the uncertainties related to the inherent availability will be calculated. This is done by first setting up a definition of what constitutes a failure and what constitutes normal modes of operation followed by a calculation of respectively the MTBF and the MTTR. The uncertainties related to these quantities are calculated as well.

7.2.1 Description of the operational modes of the degassing plant

In order to compute the mean time between failure (MTBF), the definition of a failure has to be operational and unambiguous. In this case operational means that the definition of failure should relate to information which is available and complete. In this case unambiguous means that it should not be possible to question the results with respect to when the failure occurred and the duration of the failure.
Since there is no systematic recording of the failure of the degassing plant at a level of detail suitable for the present analysis, it was decided to construct a failure history based on available production data. As stated in section 2.1, the purpose of the degassing plant is to separate gas from the oil. Moreover, the environmental permit, as described in section 2.2.5, does not contain demands as to how much gas should be extracted. As such, the definition of failure

would be, "as soon as the power is cut from the plant". However, as described in section 3.4.1, there is no direct measurement of the power consumption of the degassing plant. The uptime therefore has to be defined based on the two available measurements: The offgas mass flow and the pressure in the degassing vessel.
Due to malfunctioning in the oxygen meters, meaning there was no control over the oxygen content of the exported gas and therefore a potential safety risk, the degassing pressure was, approximately the first three months, above one bara (Lund[1], personal communication). This means that the degassing plant was running in the period, however at lower efficiency. Therefore, the analysis below is performed twice, once for the first three months and once for the period after the first three months. The pressure in the degassing vessel over time is illustrated in fig. 7.10. Based on a visual inspection of fig. 7.10, the change, from a pressure above atmospheric to a vacuum, took place 1627 hours after the first gas export from the degassing plant, corresponding to 7 July 2009. It could be argued that the change in operating pressure did not happen instantaneously, but as a gradual change over the following period, but for simplicity this is ignored in the subsequent analysis. This is done, partly because determining the exact change, from a pressure above atmospheric pressure, to transition period, to vacuum, will be difficult due to the scatter in the data, and partly because the transition period is estimated to be short, compared to the period representing the normal mode of operation. The operational aim is to keep the pressure in the degassing vessel steady at 0.9 bara. The data in fig. 7.10, however shows significant problems achieving a constant pressure and a steady operation. This is a consequence of the variations in offgas content in the incoming crude oil.

A 3D histogram of the exported offgas vs degassing pressure is shown in fig. 7.11 on page 149. The figure shows a large amount of data in the area between roughly 15 $^{t}/_{hr}$ and 40 $^{t}/_{hr}$. Since this group of data is the vast majority of the measured values for the offgas export, this probably represents normal operations. One could hypothesise that the degassing plant had two modes of normal operation for the same pressure, one leading to approximately 20 $^{t}/_{hr}$ and one leading to approximately 30 $^{t}/_{hr}$ corresponding to the two peaks in the distribution. This could, however, also be a result of changes in the composition of the incoming crude oil stream (e.g. how much incoming oil is coming from which oil field) or some other unknown variable and would have to be looked further into in order to come up with a definitive explanation.
In the high end of the measured mass flow values there appears to be a peak in the histogram. It is smaller than the peaks representing ordinary mass flow but still a significant artefact of the graph. There appears to be no physical explanation connected to the degassing plant for this peak, since the pressure is not significantly different from the pressures describing the normal mode of operation. Either this represents situations with very volatile incoming oil, or it is an artefact of the technical system.
The last peak in the mass flow part of the histogram appears around zero $^{t}/_{hr}$. This is the situation when the degassing plant has failed. However, as can be

[1] Jakob Lund, Team Leader DONG Oil Pipe

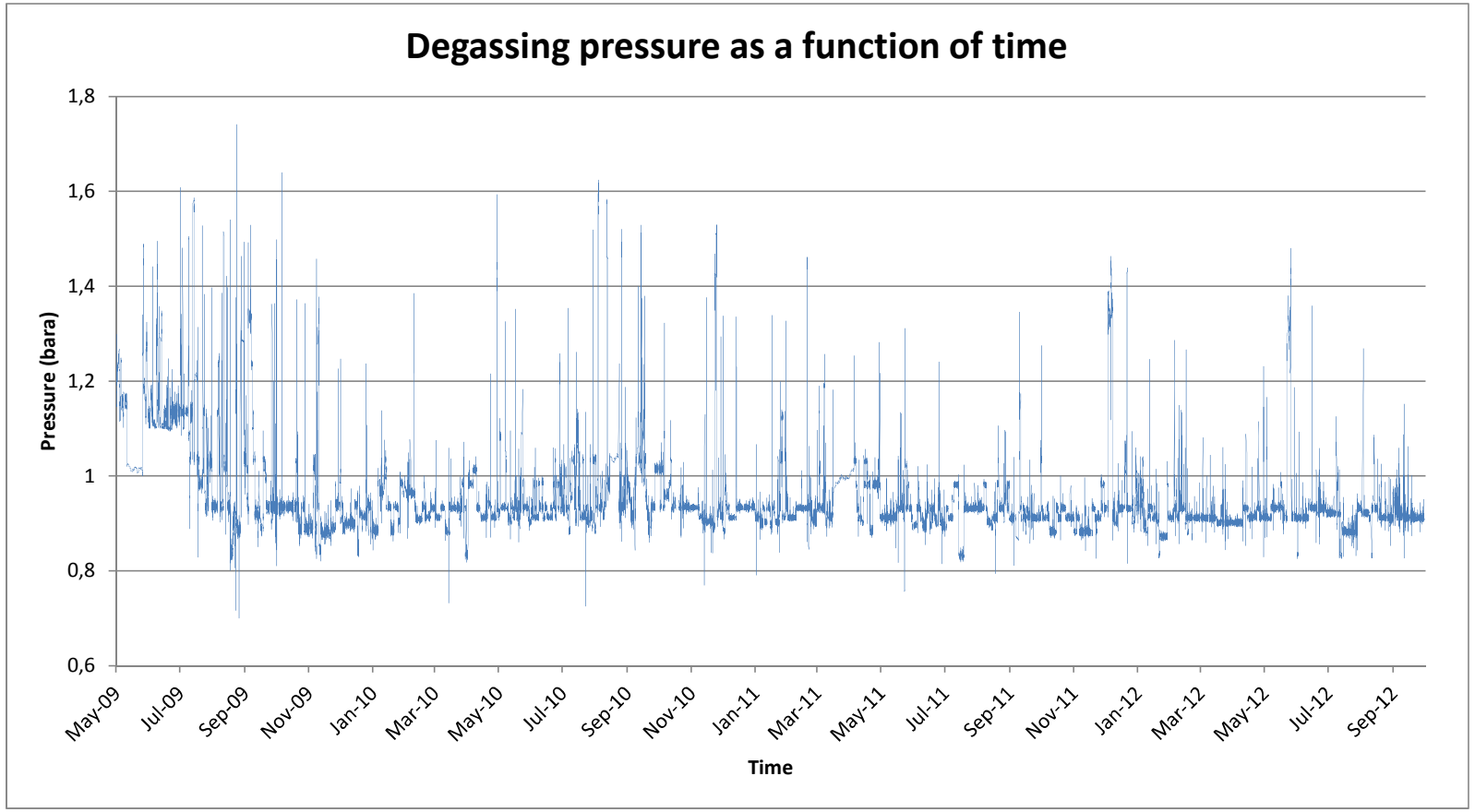

Figure 7.10: Pressure in the degassing vessel as a function of time with hourly resolution. Data source: DONG Oil pipe SCADA (Supervisory Control And Data Acquisition) system

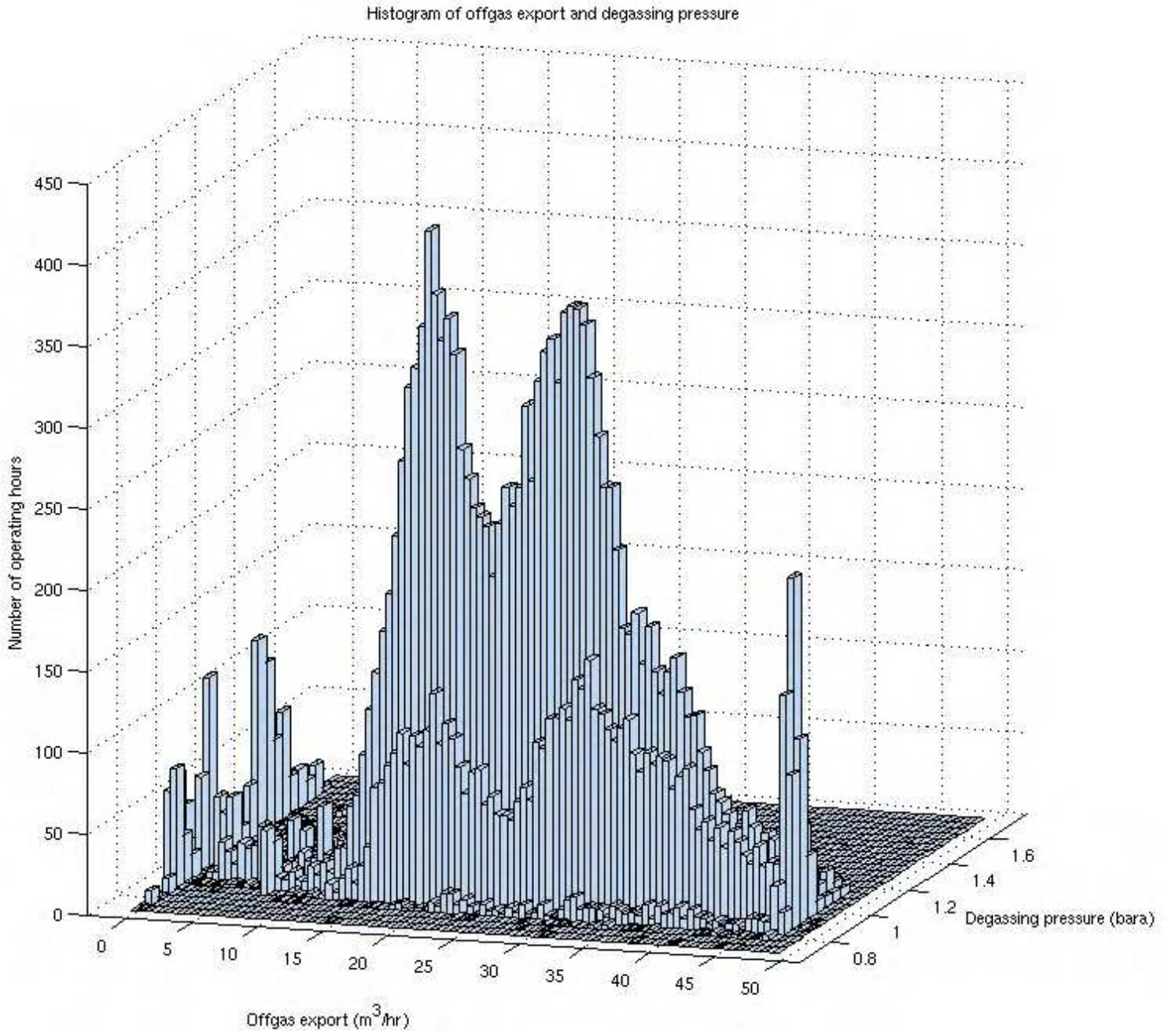

Figure 7.11: Histogram of offgas export vs. degassing pressure distributed in 100 bins for the mass flow and in 25 bins for the pressure. Original temporal resolution is one hour. Data source: DONG Oil Pipe SCADA system.

seen, although the exported offgas amount is approximately zero, a range of pressures is recorded. If the degassing plant fails, the exported offgas will go to zero, and the pressure will rise as a function of time signalised by the peak in the data at zero offgas export and high pressures. There will however also be situations where the mass flow will be approximately zero, but the degassing plant will be running if e.g. the mass flow meter has failed. In this case, the degassing plant is still running. The aim is thus to setup a failure criteria based on the available pressure and mass flow data, discriminating between running times and failure taking all of the above into account.

7.2.2 Definition of failure

The definition of failure based on the above analysis has to capture situations of almost zero offgas export and, what could be called "unusual pressure", in order to rule out situations where only the mass flow meter has failed. "Unusual pressure" in this context is defined as the opposite of "usual pressure", which is the pressure corresponding to normal operations. The normal operations pressure was defined as the pressure corresponding to normal operations mass flow. To determine this, the offgas export data was plotted as a histogram with 200 bins to get as precise as possible a determination of the spikes representing other operational modes of mass flow. The operational mode corresponding to almost no offgas export was manually determined to have an upper limit of 0.0140 $^t/_{hr}$, and the operational mode corresponding to very high mass flows was manually determined to have a lower limit of 46.640 $^t/_{hr}$, based on manual inspection of the histogram data. Data points corresponding to these two "unusual" operational modes were left out of the following analysis.
To determine the normal operations mass flow, the mean value(μ) and standard deviation(σ) of the remaining data points were computed resulting in $\mu = 26.4416^t/_{hr}$ and $\sigma = 9.0334^t/_{hr}$. The offgas export representing normal operations was then defined to be $\mu \pm \sigma$. Next, the time series was sorted such that data points with offgas export within the defined interval was included in the subsequent analysis. The mean value and standard deviation of the corresponding pressures were subsequently calculated yielding $\mu = 0.9307$bara and $\sigma = 0.0425$bara. Defining the pressure corresponding to the normal mode of operation in the same way as the offgas export means that the failure criteria will be offgas export below $0.0140^t/_{hr}$ and pressure above 0.9732bara.
The corresponding analysis was performed for the data representing the first three months yielding for the offgas export $\mu = 16.6364^t/_{hr}$ and $\sigma = 5,5667^t/_{hr}$ and for the corresponding pressure $\mu = 1.1535$bara and $\sigma = 0.0517$bara. This means that the failure criteria for the first three months is an offgas export below $0.0140^t/_{hr}$ and a pressure above 1.2052bara.

Based in the above two definitions, the time series from May 2009 to October 2012 was manually analysed for potential failures. If a data point was found to be within the failure criteria, it was examined as to whether outer circumstances could account for the measured values e.g. if the incoming flow to the Fredericia oil terminal was low in the same time period. This was done through manually searching through the electrolog for the corresponding period

and comparing with the data registered for the incoming flow to the terminal from the DONG Oil Pipe SCADA system. If an outer cause was found, the data points were not recorded as failures.
Moreover, the duration of the individual failures were determined by manually comparing the data series for offgas export and pressure. There is a lag time from a failure happening, until it can be detected in the production data. This is concluded since in most of the detected failures the mass flow starts to drop and the pressure starts to increase a while before reaching the failure criteria. The length of this time lag has not been investigated in this project, since the effect on the availability is assumed to be negligible. However, when a failure ends there sometimes happens to be a fluctuation around the failure criteria in either the offgas export, the pressure, or both. In the present project, the failure is defined as being over, when the degassing plant is operating outside the failure criteria and stays outside for a foreseeable time. This is especially important if two breakdowns have happened very close to each other. If both the pressure and the offgas export have been out of the failure criteria, they are classified as two failures. If only the pressure or the offgas export has been outside the failure criteria, it is counted as one long failure.

A total number of 52 failures was counted since the 1$^{\text{st}}$ of May 2009. These are listed in table 7.3 on page 152.

7.2.3 Calculation of MTBF

In order to determine the MTBF the following expression was used:

$$MTBF(t_1, t_2) = \frac{t_2 - t_1}{m(t_t, t_2)} \tag{7.1}$$

where $m(t_1, t_2) = E[N(t_2) - N(t_1)]$ is the expected change in number of failures over the time interval $[t_1, t_2]$. To determine $E[N(t_2) - N(t_1)]$ the failure data presented in table 7.3 were imported into MatLab, and a piecewise linear function was fitted to the cumulative number of failures as a function of time using the MatLab function *fminsearch*, following the approach described in Ebeling 1997, p. 31. The results are shown in fig. 7.12. The fitted piecewise linear function is:

$$E(t) = \begin{cases} 0.064t - 0.1683 & t < 3447\text{hrs} \\ 0.011t + 21.9050 & t > 3447\text{hrs} \end{cases} \tag{7.2}$$

Solving the fitted equations, for the total number of hours from 1 May 2009 subtracting the total hours of downtime, yields $E[N(t_2) - N(t_1))] = 54.1515$. This means:

$$MTBF = \frac{27901\text{hrs}}{54.1515} = 515.24\text{hrs} \approx 21\text{days} \tag{7.3}$$

As can be seen from fig. 7.12, the influence of the burn-in period (the period with low MTBF) is significant for the period under consideration. As time increases, the influence of this period will diminish.
The residual of the fit is shown in fig. 7.13. As can be seen, there appears to be no systematic trend in the residual, indicating that the data are randomly distributed around the fitted line. The same effect is seen in fig. 7.14, where

Failure date:	Operating hours	Failure duration (hrs)
27-05-2009	639	7
05-06-2009	857	2
08-06-2009	924	31
01-07-2009	1440	32
03-07-2009	1471	5
09-07-2009	1595	10
13-07-2009	1696	17
15-07-2009	1709	29
18-07-2009	1758	3
22-07-2009	1864	4
24-07-2009	1905	1
31-07-2009	2068	2
10-08-2009	2299	11
11-08-2009	2327	4
14-08-2009	2387	1
15-08-2009	2397	13
18-08-2009	2468	5
23-08-2009	2585	14
28-08-2009	2679	1
28-08-2009	2684	49
31-08-2009	2709	3
26-09-2009	3343	2
28-09-2009	3379	1
01-10-2009	3445	3
01-10-2009	3449	3
06-10-2009	3560	3
08-11-2009	4355	2
30-11-2009	4879	10
29-04-2010	8460	17
07-05-2010	8650	2
17-05-2010	8878	1
03-08-2010	10758	24
12-08-2010	10942	7
26-08-2010	11267	7
14-09-2010	11721	15
15-11-2010	13199	2
23-11-2010	13382	55
01-12-2010	13521	1
17-01-2011	14652	2
30-01-2011	14960	3
19-02-2011	15433	8
24-05-2011	17682	2
10-09-2011	20298	9
03-12-2011	22302	127
22-12-2011	22622	5
12-01-2012	23132	3
05-02-2012	23695	8
16-02-2012	23960	4
22-05-2012	26268	97
03-06-2012	26459	1
15-06-2012	26745	4
03-08-2012	27901	1

Table 7.3: Detected failures according to date, number of operating hours since 1st of May 2009, and duration in the time series from 1st of May 2009 to 1st of October 2012. Data source: DONG Oil Pipe SCADA system.

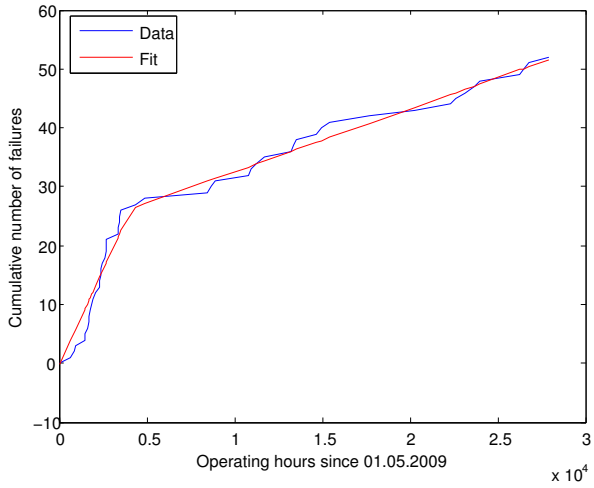

Figure 7.12: Cumulative number of failures as a function of operating hours since 1st of May 2009. Data source: DONG Oil Pipe SCADA system.

the histogram of the residual of the cumulative number of failures is drawn. The number of bins has been determined using Sturge's rule (Ebeling, 1997, p. 359):

$$k = [1 + 3.3 \log_{10}(n)] \tag{7.4}$$

Where k is the number of classes, n is the sample size, and $[x]$ means the integer part of x. The histogram resembles a normal distribution indicating that the data are randomly distributed around the fitted line. The mean value of the residual is -0.2115, and the standard deviation is 2.0223. This gives a relative error on the MTBF of $+3.9\%$ and -2.6%.

7.2.4 Calculation of MTTR

As can be seen from fig. 7.15, there is no significant trend in the time to repair a given failure. Therefore, the failures are treated as one homogeneous group of failures. The data are grouped into a histogram of six bins based on Sturge's rule.
Based on a visual inspection of the histogram, it was decided that the data follows an exponential distribution, described by the expression (Ebeling, 1997, p. 192): $e^{-\frac{t}{MTTR}}$. This expression was fitted using the MatLab function *fminsearch*. The result is shown in fig. 7.16. The fitted value yields: $MTTR = 22.8522$hrs. The uncertainties related to the fit are not evaluated due to the small number of data points.

7.2.5 Calculation of availability

Based on the above two calculations, the availability for the degassing plant can be calculated for the period under consideration using the equation:

$$A = \frac{\text{MTBF}}{\text{MTBF+MTTR}} \tag{7.5}$$

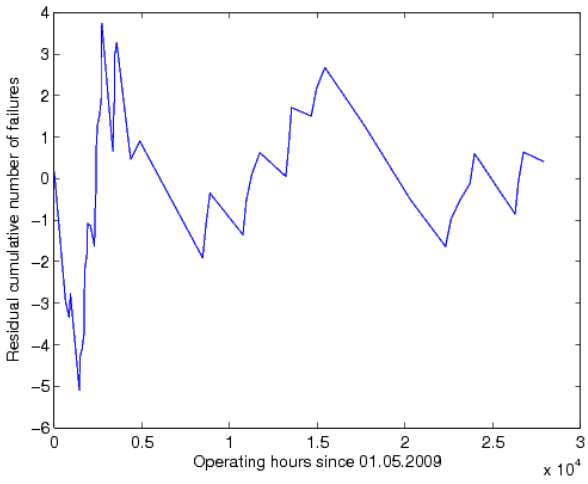

Figure 7.13: Residual cumulative number of failures as a function of operating hours since 1 May 2009. Data source: DONG Oil Pipe SCADA system.

Inserting the numbers:

$$A = \frac{515.24\text{hrs}}{515.24\text{hrs}+22.8522\text{hrs}} = 0.9575 \approx 95.75\% \tag{7.6}$$

Considering the above described uncertainties resulting from the fit of the MTBF, the result of the inherent availability becomes $95.75\% \pm 0.15\%$. This is lower than the expected availability of 98% as predicted before the installation of the degassing plant, as described in section 2.2.5. However, using the coefficient of the second part of the piecewise linear fit as the MTBF, the MTBF becomes $\approx$ 909hrs, and the availability becomes 97.5%, which is quite close to the predicted value before the installation of the plant. The degassing plant will approach this value as time goes, and as such, the availability must be concluded to be satisfactory.

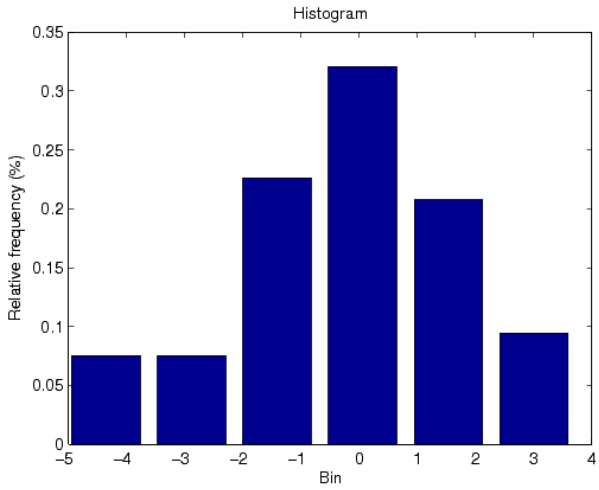

Figure 7.14: Histogram of residual of the cumulative number of failures. Data source: DONG Oil Pipe SCADA system.

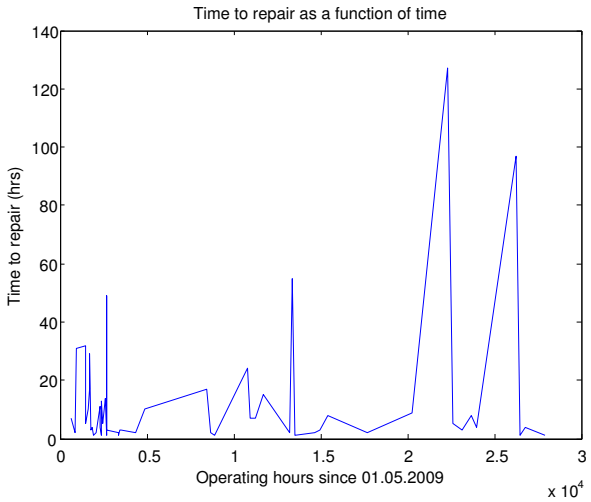

Figure 7.15: Time to repair an individual failure as a function of failure occurrence. Data source: DONG Oil Pipe SCADA system.

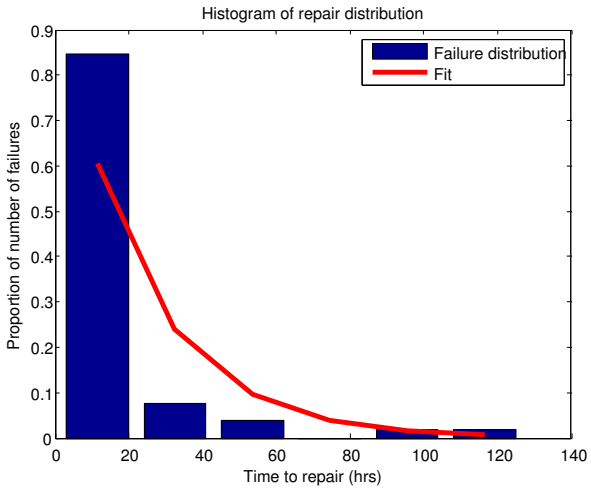

Figure 7.16: Repair time distribution and exponential fit. Data source: DONG Oil Pipe SCADA system.

Chapter 8

Cost-benefit analysis

In this chapter, the cost-benefit analysis of the DONG degassing plant will be described. As described in section 3.2, the analysis will analyse the consequences of the installation of the degassing plant in 2009 as seen from an economical perspective. This will be compared to a "business-as-usual"-scenario where all other things except for the degassing plant remain as expected. The chapter follows the structure for a CBA as described in Miljøministeriet (2010) starting with a consequence description, where the consequences of the installation of the degassing plant are described in physical units, followed by a section on valuation, where the valuation of the individual costs and benefits are described, followed by a section presenting the results and uncertainties of the analysis.

8.1 Consequence description

As described in section 3.2, a modified version of the consequence scheme, presented in (Miljøministeriet, 2010, p. 75), was used to generate an overview of the consequences of the DONG degassing plant in physical units. In the following list, the concrete representation of the various consequences is described. If there is no direct measure of the specific consequence, the calculation of the consequence is discussed. Since some of the calculations are quite lengthy, they are presented in separate subsections.

- Direct economic consequences:
  - Production of market transferred goods:
    - Solely nationally traded:
      - **Produced offgas:**
        The amount of produced offgas for the ex post part of the analysis is taken from the invoice for the offgas sent to Shell. The data are presented in chapter 7 in fig. 7.1. For the ex ante part of the analysis an average for the period August 2009 to August 2012 is calculated to 790.5t/month. The average is used since it has not been possible to find a suitable predictor variable for predicting the future amount of produced offgas.

This estimate is not changed in the uncertainty calculations since this would require increasing the item "Crude oil to gas" as well, and as such, almost cancel the effect.

- **Crude oil to gas:**
  Since a larger amount of offgas is retrieved from the oil than is saved in emissions, a certain amount of crude oil is converted to gas in the degassing plant. This amount is too small to measure in the flow meters located at the Fredericia Oil Terminal. Therefore, this amount is estimated by subtracting the avoided emission from the produced offgas. Since this is not a measured mass balance, but a mass balance pitched together from two independent calculations, in months of low offgas production the calculated avoided emission will be larger than the amount of exported offgas. In these months the item "crude oil to gas" is set to zero. For the best and worst case calculations, the calculated before and after emission are increased and decreased respectively with the uncertainties presented in Spectrasyne Ltd (2009). E.g. for the best case scenario, the emission before the installation of the degassing plant is increased by 5%, and the emission after the installation of the degassing plant is decreased by -15%.

* Internationally traded: None

– Use of factors of production:

* Labour:
  - **Operations of the degassing plant:**
    This is regulated by an agreement between DONG Oil Pipe A/S and Shell raffinaderiet, where the change in price for operating the terminal is agreed upon. For the present analysis, the amount is taken from the budget for the degassing plant and extrapolated using the GVA-deflator taken from Energistyrelsen (2011). Since this is an exact number taken from the accounts, this is not changed during the uncertainty calculations.
* Capital:
  - **Expenses for the construction of the degassing plant:**
    Since there is no direct recording of the expenses associated with the construction of the degassing plant, this amount is estimated from the annual accounts for DONG Oil Pipe. The item called "projects" is mainly dominated by the construction of the degassing plant in the years 2006 to 2009. It is possible that about 1% of the money was spent on other projects, but since this is a small amount, it is, for the present purpose, neglected. Since this number is taken from the accounts it is not changed for the uncertainty calculations.
  - **Power consumption:**
    This is, for the ex post analysis, based on the power consump-

tion calculated in chapter 7. For the ex ante analysis, the calculated average power consumption is used. For the uncertainty calculations, one standard deviation is respectively added or subtracted from the most likely value.

    - Nature (e.g. Agricultural land, forests, fishing waters): None
  - Use of raw materials:
    - Exhaustible resources (e.g. hydrocarbons and metals): None
    - Renewable resources (e.g. drinking water): None
  - Use of produced goods:
    - Solely nationally traded:
      - **Chemicals for water treatment:**
        As a result of the installation of the degassing plant, a larger amount of water is separated from the oil. This means that more chemicals are needed for the treatment of the waste water from the terminal. Since no direct measure of this increase exists, the amount of money spent on this is taken from the budget of the degassing plant and extrapolated using the GVA-deflator taken from Energistyrelsen (2011). Since this is an estimate, the range of possible uncertainties is highly unknown. Therefore, this item is not adjusted during the uncertainty calculations.
    - Internationally traded: None
  - Unilateral currency transfers (e.g. EU subsidies): None

- Direct environmental consequences:
  - Various kinds of environmental impacts (e.g. emissions, noise, physical impact):
    - **(Reduced) methane and NMVOC emission:**
      The methane and NMVOC emission has been reported in the environmental accounts for the oil terminal. It is reported as the measured emissions in 2002 and 2009 respectively as measured by Spectrasyne Ltd (2009), multiplied by the fraction of the transported oil in relation to the transported oil in the respective year. The reason for this way of calculating the emissions from the oil terminal is not clear to the author, since it has not been possible to find any official documentation on this calculation. Instead of using these figures, a new calculation of the emissions from the terminal based on Spectrasyne Ltd (2009) was performed. Since this calculation is lengthy it is described in section 8.1.1. The calculation of uncertainties related to this quantity is found under the item "Crude oil to gas".
  - The consequences of the environmental impact on the environment as a factor of production: None
  - The consequences of the environmental impact on the living conditions: Not assessed specifically, but included in the valuation of the emission in the form of unit prices.

- Indirect environmental consequences:
  - Production of inputs: Not included in the analysis due to lack of available information on this.
  - Avoided consequences from withdrawal of factors of production from other use: Not included in the analysis, since they are assessed to be small.

8.1.1 Calculation of the emissions from the Fredericia oil terminal

As explained in section 2.4.7, one of the central results in Spectrasyne Ltd (2009) is that the emission from an EFRT is dependent on the operational mode of the tank. In the following analysis this is assumed to be correct, as this is the fundamental assumption for the subsequent calculations. To calculate the emissions from the Fredericia Oil Terminal with and without the degassing plant, the hourly emission factors presented in fig. 2.6 was multiplied by the number of hours the respective tank spent in the respective operational mode, and the emissions were subsequently summed. The input data to this analysis were time series of the amount of oil in the respective tanks on hourly temporal resolution for the period November 1, 2007 to August 31, 2012 gathered from the DONG SCADA system. Hourly values with data-loss were excluded from the analysis. The hourly change in the amount of oil in a specific tank was calculated by subtracting one subsequent value from the other. The intervals classifying the operational mode of a specific tank were defined such that overlap was avoided. The classification criteria, used to classify the time series, are presented in table 8.1. The criteria for "Bottom dip" and "Top dip" were defined based on a visual inspection of the graph, representing a suitable interval of a time series for a specific tank. The criteria for "Filling" and "Rundown" were arbitrarily defined to be large enough to avoid including the fluctuations resulting from the automatic measurement equipment. The results of the classification are shown in table 8.2. The lease of Tank T53 from Shell started in July 2008, but doesn't

Tank:	Bottom dip:	Filling:	Top dip:	Rundown:	Intermediate static:
T9801	$X <= 5500$	$X > 100$	$X >= 43500$	$X < -100$	$[5500 < X < 43500]$
T9802	$X <= 5500$	$X > 100$	$X >= 43500$	$X < -100$	$[5500 < X < 43500]$
T9803	$X <= 5500$	$X > 100$	$X >= 43500$	$X < -100$	$[5500 < X < 43500]$
T9804	$X <= 5500$	$X > 100$	$X >= 43500$	$X < -100$	$[5500 < X < 43500]$
T9805	$X <= 5500$	$X > 100$	$X >= 43500$	$X < -100$	$[5500 < X < 43500]$
T9806	$X <= 5500$	$X > 100$	$X >= 43500$	$X < -100$	$[5500 < X < 43500]$
T67	$X <= 5000$	$X > 100$	$X >= 36500$	$X < -100$	$[5000 < X < 36500]$
T71	$X <= 5000$	$X > 100$	$X >= 39500$	$X < -100$	$[5000 < X < 39500]$
T53	$X <= 3500$	$X > 100$	$X >= 29000$	$X < -100$	$[3500 < X < 29000]$

Table 8.1: Criteria for the classification of the time series of the amount of oil in the respective tanks. For the modes "Bottom dip", "Top dip" and "Intermediate static" the unit is m^3. For the modes "Filling" and "Rundown" the unit is $^{m^3}/_{hr}$. The square brackets indicate an interval.

Year:	Bottom dip: (%)	Filling: (%)	Top dip: (%)	Rundown: (%)	Intermediate static: (%)	Total: (%)
2007	31.95	13.66	21.07	7.77	25.56	100.00
2008	32.70	13.01	21.85	7.19	25.25	100.00
2009	31.84	12.39	18.06	6.43	31.28	100.00
2010	28.25	11.93	23.21	5.63	30.98	100.00
2011	29.45	11.45	23.60	4.81	30.69	100.00
2012	22.03	12.10	22.20	5.27	38.41	100.00
Mean:	29.37	12.42	21.66	6.18	30.36	

Table 8.2: Percentage distribution of the operational modes based on all the tanks.

seem to influence the result of the classification. As can be seen, the amount of time the tanks spend in the respective operational modes is relatively static, with bottom dip, intermediate static, and top dip being the most dominant. The exception is 2012, where the amount of intermediate standing is noticeably larger than usual and bottom dip is noticeably smaller than usual. The reason for this is not quite apparent.
Comparison of the mean values from table 8.2 with the time factors from fig. 2.6 yields a smaller amount of time spent at bottom dip and a larger amount of time spent at intermediate static, compared to the data from Spectrasyne Ltd (2009). This might be because of differences in the definitions of bottom dip and intermediate static respectively, but since the definitions used in Spectrasyne Ltd (2009) are not presented in the report, it is difficult to compare. Another explanation might be changes in maintenance of the tanks in the studied period, however this would require a more careful examination. This variation in time factors, however only changes the average hourly emission for a tank by a few percent.

The constancy of the distribution is surprising, since there has been a steady decline in the amount of transported oil over the studied period, which intuitively would lead to an increase in bottom dip and intermediate static and a decrease in top dip. A possible explanation why this is not the case, is the possibility of a comparative decrease in the frequency of the ships arriving at the harbour to export the oil. To confirm this, a more careful examination is however needed.

The calculated emission for the period, where the degassing plant has been exporting (some) offgas, is graphed in fig. 8.1. The marked drop that appears in May 2009 is caused by the change in emission factors. For simplicity, the emission factors are changed at 1 May 2009, but as described in chapter 7, the commissioning of the degassing plant was very gradual and, as such, the drop should not be as steep as presented in the graph. A combination of the availability analysis presented in chapter 7 and the present analysis would probably have been able to give a better picture of the transition, but then a new set of emission factors representing the period of over pressure in the vessel would also be needed.
The graph also shows that since the installation of the degassing plant the

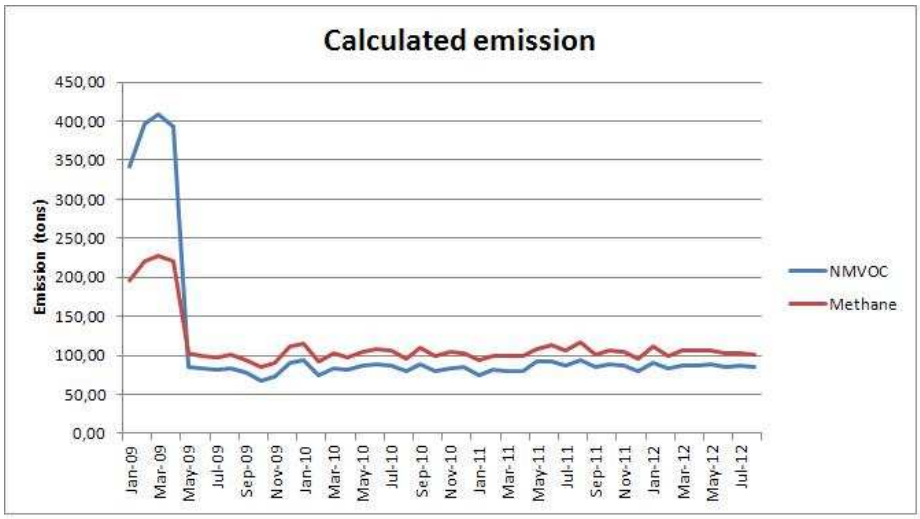

Figure 8.1: Calculated monthly emission for the period where the degassing plant has exported offgas. The calculation is based on the classification performed in the present report.

emissions from the Fredericia Oil Terminal have been very stable, in line with the numbers presented in table 8.2. In this graph, the reduction of 79% for VOC and 53% for methane, as presented by Spectrasyne Ltd (2009), is clearly visible. For the basis scenario without the degassing plant, the calculated emissions are shown in fig. 8.2. They show a slightly increasing trend.

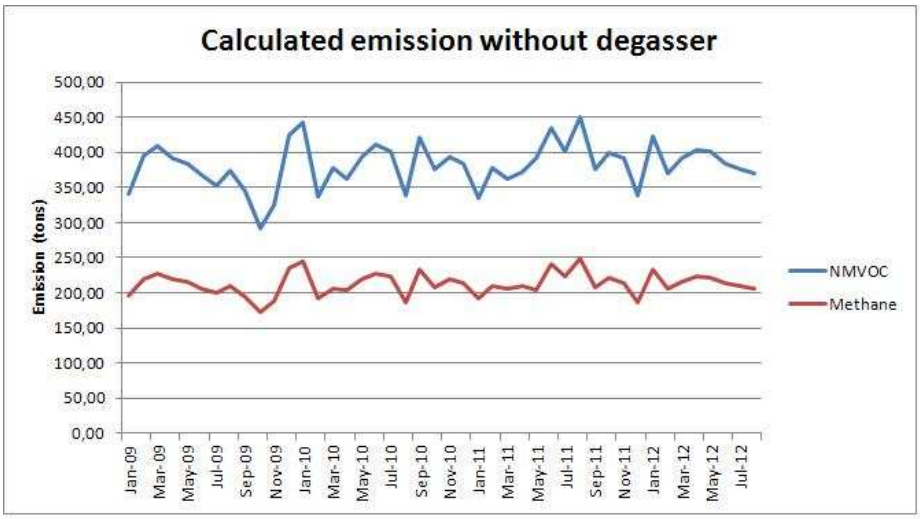

Figure 8.2: Calculated monthly emission for the period where the degassing plant has exported offgas with the emission factors from 2002. The calculation is based on the classification performed in the present report.

8.2 Valuation

The valuation used in the analysis follows the practice described in Miljøministeriet (2010). In the following, the data sources for the valuation of the individual analysis elements are described in the same order as for the consequence description, for ease of comparison:

- Direct economic consequences
  - Production of market transferred goods
    - Solely nationally traded:
      - **Produced offgas:**
        For the ex post analysis the offgas price without VAT from the invoice for the offgas sent to Shell is used. For the ex ante analysis the natural gas price from Energistyrelsen (2011) under the category "at plant" is used. Since Energistyrelsen (2011) is calculating in volume, and the offgas meter at the plant measures in weight, the density of methane is used for conversion. To convert from real price to nominal price the GVA-deflator is used. The calculated price for the year 2012 per ton offgas is compared to the offgas price from the invoice and they are concluded to be approximately equal. This ensures the validity of the calculation.
      - **Crude oil to gas:**
        This item is valuated using the oil price from the DONG Oil Pipe monthly report for the ex post analysis and the numbers from Energistyrelsen (2011) for the ex ante analysis.

Since the crude oil to gas is calculated as a cost, and the full amount of offgas is calculated as a benefit, this corresponds to valuating this element by the difference between the oil- and the gas price.

- Use of factors of production:
  - Labour:
    - **Operations of the degassing plant:**
      Valuation presented under the consequence description.
  - Capital:
    - **Expenses for the construction of the degassing plant:**
      Valuation presented under the consequence description.
    - **The power consumption:**
      For the ex post analysis the price of the power consumption is taken from the electricity bill for the Fredericia Oil Terminal including electricity duties, but without VAT. For the ex ante analysis the power price is taken from Energistyrelsen (2011) for the category "at company", multiplied by the GVA-deflator to convert to nominal prices. For the duties a linear interpolation based on the projections until year 2015 presented in Energistyrelsen (2011) was performed and the results added to the calculated price.
- Use of produced goods:
  - Solely nationally traded:
    - **Chemicals for water treatment:**
      Valuation presented under the consequence description.

- Direct environmental consequences:
  - Various kinds of environmental impacts (e.g. emissions, noise, physical impact):
    - **(Reduced) methane and NMVOC emission:**
      Since the valuation of this element i lengthy it is described in a separate section. The calculation can be found in 8.2.1.

The values given in Energistyrelsen (2011) are not changed during the uncertainty calculations. This is due to the fact that no estimate of the uncertainties in the numbers presented exist (personal communication with the Danish Energy Agency).

8.2.1 Valuation of change in emissions

Miljøministeriet (2010) does not present direct valuation of environmental benefits for Denmark. Instead the Danish Center for Environment and Energy (previously the National Environmental Research Institute) has published a compilation of prices for the Ministry of Environment in Andersen and Strange (2003). In Andersen and Strange (2003) it is stated that almost all socioeconomic analyses, performed within the environmental area, use the prices from Finansministeriet

(2001). In (Finansministeriet, 2001, p. 113) the unit price for the release of one Kg of VOC is set to DKK 50 in year 2000 prices, regardless of whether the emission comes from energy production or transport. The validity of this estimate is reviewed in Andersen and Strange (2003):
The uncertainty of this estimate is presented in (Finansministeriet, 2001, p. 152). In the table of uncertainties however, there appears two categories: One called "VOC" and one called "HC" (HydroCarbons) with two different set of prices attached to them. VOC is still priced by DKK 50 regardless of the source, but HC is priced as DKK 56 for energy production and DKK 21 for transport. The source of the unit price for HC is stated to be Larsen (1996). For VOC the source is stated to be Lawaetz (2001) that again refers to Larsen (1996). Larsen (1996) however, refers to Trafikministeriet (1997) (finished in 96) where, based on a german and a swedish study, the price of HC/VOC is presented. Trafikministeriet (1997) has however not supplied enough information to find the actual fundamental studies that the prices are based on.
In Larsen (1996) the two studies presented in Trafikministeriet (1997) are compared, and since the damage costs for HC and SO_2 are approximately equal, the marginal health damages from these two types of emissions are assumed to be equal. Since the publication of Larsen (1996), new estimates for the damage costs of SO_2 has been made, and these are included in Finansministeriet (2001). However, the price of HC/VOC has not likewise been updated. The cause of this is not explained in Finansministeriet (2001). The new numbers for SO_2 are DKK 34 – DKK 35 per Kg for energy production and DKK 44 – DKK 77 per Kg for emissions from traffic.
More surprising is it that in Finansministeriet (2001) two different prices are stated for respectively HC and VOC since, with regards to emissions to air, it is exactly the same (Andersen and Strange, 2003). This is also surprising considering that the estimate sources are apparently the same, and there is neither any explanation given to this in Finansministeriet (2001).
One of the newest studies on valuation of air emissions are the "External Costs of Transport" presented in respectively Danish Ministry of Transport (2004a), Danish Ministry of Transport (2004b) and Danish Ministry of Transport (2004c). In (Danish Ministry of Transport, 2004a, p. 25) the results of the european BeTa (Benefit Tables) study are presented yielding a unit cost for HC for Copenhagen at 7200 Euro per ton which approximately matches the price presented in Andersen and Strange (2003). However, in the footnote on the same page in Danish Ministry of Transport (2004a) it is stated:

> "The BeTa-value for HC for Denmark appears very high. It is more than twice the value for the second highest value among the EU-15 countries whereas the Danish value for other pollutants is in the lower end of the range. The authors have been addressed about this and they have verified the value but no explanation has been given for the high value."

In other words a critique of the earlier presented values are raised in Danish Ministry of Transport (2004a). This continues in (Danish Ministry of Transport, 2004b, p. 23), where it is stated that the exposure factor used in the BeTa study for Copenhagen is higher than for all other countries and that "this seems to be

a clear mistake". Instead an estimate of the unit price for HC is presented being DKK 3 – DKK 6 per Kg emission in year 2000 prices.
Concluding, there seems to be quite a bit of ambiguity about the unit price for HC/VOC. Due to the lack of consistency between the results of the different studies, a "most likely" price cannot be defined, and for the subsequent analysis only "best case" and "worst case" estimates will be given using the values DKK 3 and DKK 77 per ton VOC emission in year 2000 prices. These prices are subsequently converted to nominal prices using the GVA-deflator from Energistyrelsen (2011).

Apart from the effect on human health and crop yield, the emission of VOC to the atmosphere also has an effect on the climate. This effect is calculated using the CO_2-quota price as predicted in Energistyrelsen (2011), multiplied by the net duty factor, converted to nominal values using the GVA-deflator also from Energistyrelsen (2011). To account for the release of respectively methane and NMVOC, the numbers were multiplied by the global warming potential taken from Forster et al. (2007) for methane and from Collins et al. (2002) for some of the NMVOCs.

8.3 Results

8.3.1 Scenario A - Technology Assessment

The scenario A is called "technology evaluation", because it has a time perspective corresponding to the lifetime of the degassing plant itself. This means that the scenario represents the economical effect of the "technology itself".

The perspective of the users of the oil pipe

Seen from the users of the oil pipe, there has been an increase in the expenses due to the installation of the degassing plant resulting from e.g. the construction of the degassing plant and the power consumption. Moreover, there has been some earnings due to sale of offgas. Seen from the users of the oil pipe's perspective, the more gas that would otherwise have evaporated to the atmosphere that are now generating an income in the form of offgas sale, the less they have to pay for their oil transport. When crude oil is converted to gas, as when more gas is taken out of the oil in the degassing plant than would otherwise have evaporated to the atmosphere, this means a slight quality degradation of the oil and slightly less oil for sale. Therefore, the interest of the users of the oil pipe is to sell the gas for approximately the same price as the oil.

Most likely scenario: The costs and benefits, seen from the perspective of the users of the oil pipe with a time horizon corresponding to the lifetime of the degassing plant, are shown on table 8.3 and table 8.4. The results are shown on table 8.5. As can be seen on table 8.3, the costs are dominated by the construction, the power consumption and the crude oil to gas. However, there is a link between the crude oil to gas and the offgas export such that if the offgas export increases, the crude oil to gas conversion increases as well. It is probably not unreasonable to expect the construction costs of a "prototype" like the DONG degassing plant to occupy quite a large part of the costs. Moreover, discounting means that the construction costs that occur in the beginning of the plant lifetime have comparatively larger weight than the benefits that occur over a longer time period as illustrated on table 8.4. The value of the crude oil to gas is a representation of the fact that approximately half of the offgas export is in reality crude oil being converted to gas. However, as stated in section 8.1.1 and section 2.4.7, this is a result of a calculation based on a set of measurements, and as such, subject to uncertainties. Moreover, these numbers are not tantamount to the technical possibillity of actually retrieving this oil. The annual flow through the Fredericia Oil Terminal is approximately $12.000.000m^3$ of crude oil corresponding to roughly 10.000.000 tons. Since the crude oil to gas is roughly 54.000 tons, this corresponds to 0.5% of the annual throughput, which is in the same order of magnitude as the uncertainty on the flow meters at the terminal. Therefore, it is not possible to measure this "loss" of crude oil. Comparing the result of kr. 18.217.000 from table 8.5, which is the result of the most likely scenario, to fig. 2.4 on page 22, it is highly surprising that the most likely result is expected to be positive, where it was assumed to be negative at the installation of the plant. This shows that the degassing plant

probably both improves the environment and the economy for the users of the oil pipe.

Year:	Construction:	Power consumption:	Chemicals:	Maintenance:	Crude oil to gas:	Operation:	Total:	Present value:
Number:	1	2	3	4	5	6	7	8
2006	kr. 3.712.000,00						kr. 3.712.000,00	kr. 3.712.000,00
2007	kr. 34.001.000,00						kr. 34.001.000,00	kr. 32.615.000,00
2008	kr. 53.844.000,00						kr. 53.844.000,00	kr. 49.543.000,00
2009	kr. 9.986.000,00	kr. 3.434.000,00	kr. 90.000,00	kr. 499.999,85	kr. 7.937.000,00	kr. 547.000,00	kr. 22.494.000,00	kr. 19.854.000,00
2010		kr. 6.320.000,00	kr. 90.000,00	kr. 1.366.049,68	kr. 13.153.000,00	kr. 837.000,00	kr. 21.766.000,00	kr. 18.428.000,00
2011		kr. 5.730.000,00	kr. 90.000,00	kr. 939.413,65	kr. 15.017.000,00	kr. 858.000,00	kr. 22.634.000,00	kr. 18.382.000,00
2012		kr. 6.577.000,00	kr. 92.000,00	kr. 819.000,00	kr. 9.942.000,00	kr. 877.000,00	kr. 18.307.000,00	kr. 14.261.000,00
2013		kr. 7.184.000,00	kr. 93.000,00	kr. 1.075.000,00	kr. 15.438.000,00	kr. 897.000,00	kr. 24.688.000,00	kr. 18.448.000,00
2014		kr. 7.399.000,00	kr. 95.000,00	kr. 1.103.000,00	kr. 15.713.000,00	kr. 917.000,00	kr. 25.227.000,00	kr. 18.082.000,00
2015		kr. 7.423.000,00	kr. 97.000,00	kr. 1.128.000,00	kr. 15.799.000,00	kr. 938.000,00	kr. 25.385.000,00	kr. 17.454.000,00
2016		kr. 7.458.000,00	kr. 99.000,00	kr. 1.150.000,00	kr. 16.140.000,00	kr. 959.000,00	kr. 25.806.000,00	kr. 17.020.000,00
2017		kr. 7.712.000,00	kr. 101.000,00	kr. 1.172.000,00	kr. 16.484.000,00	kr. 981.000,00	kr. 26.451.000,00	kr. 16.734.000,00
2018		kr. 7.769.000,00	kr. 103.000,00	kr. 1.195.000,00	kr. 16.827.000,00	kr. 1.003.000,00	kr. 26.897.000,00	kr. 16.323.000,00
2019		kr. 8.025.000,00	kr. 105.000,00	kr. 1.219.000,00	kr. 17.376.000,00	kr. 1.026.000,00	kr. 27.752.000,00	kr. 16.155.000,00
2020		kr. 8.238.000,00	kr. 108.000,00	kr. 1.244.000,00	kr. 17.935.000,00	kr. 1.049.000,00	kr. 28.574.000,00	kr. 15.955.000,00
2021		kr. 8.091.000,00	kr. 110.000,00	kr. 1.270.000,00	kr. 18.473.000,00	kr. 1.073.000,00	kr. 29.017.000,00	kr. 15.542.000,00
2022		kr. 8.401.000,00	kr. 112.000,00	kr. 1.296.000,00	kr. 19.017.000,00	kr. 1.097.000,00	kr. 29.923.000,00	kr. 15.374.000,00
2023		kr. 8.719.000,00	kr. 114.000,00	kr. 1.325.000,00	kr. 19.610.000,00	kr. 1.122.000,00	kr. 30.890.000,00	kr. 15.224.000,00
2024		kr. 8.368.000,00	kr. 117.000,00	kr. 1.353.000,00	kr. 20.200.000,00	kr. 1.147.000,00	kr. 31.185.000,00	kr. 14.743.000,00
Total:	kr. 101.543.000,00	kr. 116.848.000,00	kr. 1.616.000,00	kr. 18.157.000,00	kr. 255.061.000,00	kr. 15.328.000,00	kr. 508.553.000,00	kr. 353.849.000,00

Table 8.3: Cost for the most likely scenario seen from the perspective of the users of the oil pipe. The scenario is Scenario A, where the time horison is the same as the lifetime of the degassing plant.

Year:	Offgas export:	Saved 5%-element:	Total:	Present value:
Number:	9	10	11	12
2006				
2007				
2008				
2009	kr. 15.126.000,00	kr. 397.000,00	kr. 15.523.000,00	kr. 13.701.000,00
2010	kr. 28.900.000,00	kr. 658.000,00	kr. 29.558.000,00	kr. 25.025.000,00
2011	kr. 34.172.000,00	kr. 751.000,00	kr. 34.923.000,00	kr. 28.362.000,00
2012	kr. 29.379.000,00	kr. 151.000,00	kr. 29.530.000,00	kr. 23.004.000,00
2013	kr. 34.156.000,00		kr. 34.156.000,00	kr. 25.523.000,00
2014	kr. 35.108.000,00		kr. 35.108.000,00	kr. 25.165.000,00
2015	kr. 35.674.000,00		kr. 35.674.000,00	kr. 24.528.000,00
2016	kr. 36.558.000,00		kr. 36.558.000,00	kr. 24.111.000,00
2017	kr. 37.451.000,00		kr. 37.451.000,00	kr. 23.693.000,00
2018	kr. 38.345.000,00		kr. 38.345.000,00	kr. 23.270.000,00
2019	kr. 39.682.000,00		kr. 39.682.000,00	kr. 23.100.000,00
2020	kr. 41.044.000,00		kr. 41.044.000,00	kr. 22.918.000,00
2021	kr. 42.411.000,00		kr. 42.411.000,00	kr. 22.716.000,00
2022	kr. 43.795.000,00		kr. 43.795.000,00	kr. 22.501.000,00
2023	kr. 45.297.000,00		kr. 45.297.000,00	kr. 22.324.000,00
2024	kr. 46.800.000,00		kr. 46.800.000,00	kr. 22.125.000,00
Total:	kr. 583.898.000,00	kr. 1.957.000,00	kr. 585.855.000,00	kr. 372.066.000,00

Table 8.4: Benefits for the most likely scenario seen from the perspective of the users of the oil pipe. The scenario is Scenario A, where the time horison is the same as the lifetime of the degassing plant.

Number:	Text:	Value:
12	Total present value benefits:	kr. 372.066.000,00
8	Total present value costs:	kr. 353.849.000,00
13	Net present value:	kr. 18.217.000,00

Table 8.5: Summary of costs and benefits for the most likely scenario seen from the perspective of the users of the oil pipe with a time horison corresponding to the lifetime of the degassing plant.

Best case/Worst case scenario: For the best case scenario, only the costs are presented on table 8.6 and the results are presented on table 8.7, since the benefits are unchanged from the most likely scenario. As can be seen, the power consumption and the crude oil to gas have been reduced contributing in total 53 millions to the result. The crude oil to gas has been reduced by assuming that the numbers presented by Spectrasyne Ltd (2009) are off by the maximum uncertainties in favor of increasing the effect of the degassing plant. Due to the limited information in Spectrasyne Ltd (2009), it is hard to assess the validity of this assumption. For the worst case scenario, as presented in table 8.8 and table 8.9, the two items are changed from the most likely scenario to the maximum uncertainties against the effect of the degassing plant yielding a deficit of 45 mio. Especially since the uncertainties presented in Spectrasyne Ltd (2009) are assymetrical around 0, it makes a large effect on the result, if the emission before the installation was 15% lower than measured. Since the most likely scenario is positive and is located closer to the best case scenario than the worst case scenario, the result is probably positive, but since there is no probabillity distribution related to the uncertainties from Spectrasyne Ltd (2009), it is not possible to know for sure. None of the numbers are, however, significantly different from zero. This means that seen from the users of the oil pipe's perspective the economics of the installation of the degassing plant is probably close to break even.
Dividing the capital expenses of the most likely scenario of kr. 585.855.000,00 by an average oil transport of 12 mio. m^3 of oil for the time from the construction of the degassing plant start to the end of the technology lifetime, yields an average extra expenditure of kr. 2.6 per m^3 transported crude oil.

Year:	Construction:	Power consumption:	Chemicals:	Maintenance:	Crude oil to gas:	Operation:	Total:	Present value:
Number:	1	2	3	4	5	6	7	8
2006	kr. 3.712.000,00						kr. 3.712.000,00	kr. 3.712.000,00
2007	kr. 34.001.000,00						kr. 34.001.000,00	kr. 32.615.000,00
2008	kr. 53.844.000,00						kr. 53.844.000,00	kr. 49.543.000,00
2009	kr. 9.986.000,00	kr. 2.263.000,00	kr. 90.000,00	kr. 499.999,85	kr. 6.955.000,00	kr. 546.949,32	kr. 20.341.000,00	kr. 17.953.000,00
2010		kr. 4.165.000,00	kr. 90.000,00	kr. 1.366.049,68	kr. 11.502.000,00	kr. 836.537,06	kr. 17.960.000,00	kr. 15.206.000,00
2011		kr. 3.776.000,00	kr. 90.000,00	kr. 939.413,65	kr. 13.076.000,00	kr. 858.021,16	kr. 18.739.000,00	kr. 15.218.000,00
2012		kr. 4.334.000,00	kr. 92.000,00	kr. 819.000,00	kr. 6.608.000,00	kr. 877.000,00	kr. 12.730.000,00	kr. 9.917.000,00
2013		kr. 4.735.000,00	kr. 93.000,00	kr. 1.075.000,00	kr. 12.820.692,00	kr. 897.000,00	kr. 19.622.000,00	kr. 14.663.000,00
2014		kr. 4.876.000,00	kr. 95.000,00	kr. 1.103.000,00	kr. 13.049.000,00	kr. 917.000,00	kr. 20.040.000,00	kr. 14.364.000,00
2015		kr. 4.892.000,00	kr. 97.000,00	kr. 1.128.000,00	kr. 13.121.000,00	kr. 938.000,00	kr. 20.176.000,00	kr. 13.872.000,00
2016		kr. 4.915.000,00	kr. 99.000,00	kr. 1.150.000,00	kr. 13.404.000,00	kr. 959.000,00	kr. 20.527.000,00	kr. 13.538.000,00
2017		kr. 5.082.000,00	kr. 101.000,00	kr. 1.172.000,00	kr. 13.689.000,00	kr. 981.000,00	kr. 21.026.000,00	kr. 13.302.000,00
2018		kr. 5.120.000,00	kr. 103.000,00	kr. 1.195.000,00	kr. 13.974.000,00	kr. 1.003.000,00	kr. 21.395.000,00	kr. 12.984.000,00
2019		kr. 5.288.000,00	kr. 105.000,00	kr. 1.219.000,00	kr. 14.430.000,00	kr. 1.026.000,00	kr. 22.069.000,00	kr. 12.847.000,00
2020		kr. 5.429.000,00	kr. 108.000,00	kr. 1.244.000,00	kr. 14.894.000,00	kr. 1.049.000,00	kr. 22.724.000,00	kr. 12.689.000,00
2021		kr. 5.332.000,00	kr. 110.000,00	kr. 1.270.000,00	kr. 15.341.000,00	kr. 1.073.000,00	kr. 23.126.000,00	kr. 12.387.000,00
2022		kr. 5.537.000,00	kr. 112.000,00	kr. 1.296.000,00	kr. 15.793.000,00	kr. 1.097.000,00	kr. 23.835.000,00	kr. 12.246.000,00
2023		kr. 5.746.000,00	kr. 114.000,00	kr. 1.325.000,00	kr. 16.285.000,00	kr. 1.122.000,00	kr. 24.592.000,00	kr. 12.120.000,00
2024		kr. 5.514.000,00	kr. 117.000,00	kr. 1.353.000,00	kr. 16.775.000,00	kr. 1.147.000,00	kr. 24.906.000,00	kr. 11.774.000,00
Total:	kr. 101.543.000,00	kr. 77.004.000,00	kr. 1.616.000,00	kr. 18.157.000,00	kr. 211.717.000,00	kr. 15.328.000,00	kr. 425.363.000,00	kr. 300.950.000,00

Table 8.6: Cost for the best case scenario seen from the users perspective with a time horison corresponding to the lifetime of the degassing plant.

Number:	Text:	Value:
12	Total present value benefits:	kr. 372.066.000,00
8	Total present value costs:	kr. 300.948.000,00
13	Net present value:	kr. 71.116.000,00

Table 8.7: Results of the best case scenario seen from the perspective of the users of the oil pipe and with a time horison corresponding to the lifetime of the degassing plant.

Year:	Construction:	Power consumption:	Chemicals:	Maintenance:	Crude oil to gas:	Operation:	Total:	Present value:
Number:	1	2	3	4	5	6	7	8
2006	kr. 3.712.000,00						kr. 3.712.000,00	kr. 3.712.000,00
2007	kr. 34.001.000,00						kr. 34.001.000,00	kr. 32.615.000,00
2008	kr. 53.844.000,00						kr. 53.844.000,00	kr. 49.543.000,00
2009	kr. 9.986.000,00	kr. 4.605.000,00	kr. 90.000,00	kr. 499.999,85	kr. 8.832.000,00	kr. 546.949,32	kr. 24.560.000,00	kr. 21.677.000,00
2010		kr. 8.475.000,00	kr. 90.000,00	kr. 1.366.049,68	kr. 15.976.000,00	kr. 836.537,06	kr. 26.744.000,00	kr. 22.642.000,00
2011		kr. 7.684.000,00	kr. 90.000,00	kr. 939.413,65	kr. 17.506.000,00	kr. 858.021,16	kr. 27.077.000,00	kr. 21.990.000,00
2012		kr. 8.820.000,00	kr. 92.000,00	kr. 819.000,00	kr. 12.471.000,00	kr. 877.000,00	kr. 23.079.000,00	kr. 17.979.000,00
2013		kr. 9.634.000,00	kr. 93.000,00	kr. 1.076.000,00	kr. 19.258.000,00	kr. 897.000,00	kr. 30.958.000,00	kr. 23.133.000,00
2014		kr. 9.922.000,00	kr. 95.000,00	kr. 1.103.000,00	kr. 19.601.000,00	kr. 917.000,00	kr. 31.638.000,00	kr. 22.678.000,00
2015		kr. 9.954.000,00	kr. 97.000,00	kr. 1.128.000,00	kr. 19.709.000,00	kr. 938.000,00	kr. 31.826.000,00	kr. 21.883.000,00
2016		kr. 10.001.000,00	kr. 99.000,00	kr. 1.150.000,00	kr. 20.134.000,00	kr. 959.000,00	kr. 32.343.000,00	kr. 21.331.000,00
2017		kr. 10.342.000,00	kr. 101.000,00	kr. 1.173.000,00	kr. 20.562.000,00	kr. 981.000,00	kr. 33.159.000,00	kr. 20.978.000,00
2018		kr. 10.418.000,00	kr. 103.000,00	kr. 1.195.000,00	kr. 20.990.000,00	kr. 1.003.000,00	kr. 33.709.000,00	kr. 20.457.000,00
2019		kr. 10.761.000,00	kr. 105.000,00	kr. 1.220.000,00	kr. 21.675.000,00	kr. 1.026.000,00	kr. 34.787.000,00	kr. 20.250.000,00
2020		kr. 11.047.000,00	kr. 108.000,00	kr. 1.244.000,00	kr. 22.372.000,00	kr. 1.049.000,00	kr. 35.820.000,00	kr. 20.001.000,00
2021		kr. 10.850.000,00	kr. 110.000,00	kr. 1.270.000,00	kr. 23.044.000,00	kr. 1.073.000,00	kr. 36.347.000,00	kr. 19.468.000,00
2022		kr. 11.266.000,00	kr. 112.000,00	kr. 1.296.000,00	kr. 23.722.000,00	kr. 1.097.000,00	kr. 37.493.000,00	kr. 19.263.000,00
2023		kr. 11.693.000,00	kr. 114.000,00	kr. 1.325.000,00	kr. 24.462.000,00	kr. 1.122.000,00	kr. 38.716.000,00	kr. 19.081.000,00
2024		kr. 11.221.000,00	kr. 117.000,00	kr. 1.353.000,00	kr. 25.198.000,00	kr. 1.147.000,00	kr. 39.036.000,00	kr. 18.454.000,00
Total:	kr. 101.543.000,00	kr. 156.693.000,00	kr. 1.616.000,00	kr. 18.157.000,00	kr. 315.512.000,00	kr. 15.328.000,00	kr. 608.849.000,00	kr. 417.135.000,00

Table 8.8: Worst case scenario costs seen from the perspective of the users of the oil pipe with a time horison corresponding to the lifetime of the degassing plant.

Number:	Text:	Value:
12	Total present value benefits:	kr. 372.066.000,00
8	Total present value costs:	kr. 417.135.000,00
13	Net present value:	kr. -45.069.000,00

Table 8.9: Results of the worst case scenario seen from the perspective of the users of the oil pipe with a time horison corresponding to the lifetime of the degassing plant.

The societal perspective

Seen from the societal perspective, it is relevant to know, whether or not the continued use of this technology should be encouraged. One of the decision parameters in this is whether the use of the technology generates a net present value, and how certain it is that the technology will generate a net present value. Moreover, the interest of the society is to obtain as large a reduction as possible at a price as small as possible.

Seen from the societal perspective, the results, as presented in tables 8.10 to 8.15, are very much dominated by the large span in unit costs for the emission of VOC yielding results between kr. 86.000.000 and kr. 4.600.000.000. As such, the economical effect of the installation of the degassing plant is generating a net societal benefit no matter the unit price of VOC. However, the large span in the results are reflecting the large span in the unit prices, which makes the assessment of the size of the benefit impossible. For the best case scenario the total capital expenses divided by the total emission reduction yields an emission reduction price of kr. 4500/ton. For the worst case scenario, the equivalent calculation yields kr. 4700/ton. These numbers are for VOC including methane. For NMVOC, the equivalent numbers are respectively kr. 6200/ton and kr. 6400/ton. Comparing this to the reduction measures suggested in Illerup et al. (2002), where the cheapest reduction measure, car painter switching to water based paint, has a price of kr. 126.000/ton emission reduction, the degassing plant must be considered to be a very cheap emission reduction measure.

Year:	Construction:	Power consumption:	Chemicals:	Maintenance:	Crude oil to gas:	Operation:	Total:	Present value:
Number:	1	2	3	4	5	6	7	8
2006	kr. 3.712.000,00						kr. 3.712.000,00	kr. 3.712.000,00
2007	kr. 34.001.000,00						kr. 34.001.000,00	kr. 31.482.000,00
2008	kr. 53.844.000,00						kr. 53.844.000,00	kr. 46.163.000,00
2009	kr. 9.986.000,00	kr. 3.434.000,00	kr. 90.000,00	kr. 499.999,85	kr. 7.937.000,00	kr. 547.000,00	kr. 22.494.000,00	kr. 17.856.000,00
2010		kr. 6.320.000,00	kr. 90.000,00	kr. 1.366.049,68	kr. 13.153.000,00	kr. 837.000,00	kr. 21.766.000,00	kr. 15.999.000,00
2011		kr. 5.730.000,00	kr. 90.000,00	kr. 939.413,65	kr. 15.017.000,00	kr. 858.000,00	kr. 22.634.000,00	kr. 15.404.000,00
2012		kr. 6.577.000,00	kr. 92.000,00	kr. 819.000,00	kr. 9.942.000,00	kr. 877.000,00	kr. 18.307.000,00	kr. 11.537.000,00
2013		kr. 7.184.000,00	kr. 93.000,00	kr. 1.075.000,00	kr. 15.438.000,00	kr. 897.000,00	kr. 24.688.000,00	kr. 14.405.000,00
2014		kr. 7.399.000,00	kr. 95.000,00	kr. 1.103.000,00	kr. 15.713.000,00	kr. 917.000,00	kr. 25.227.000,00	kr. 13.629.000,00
2015		kr. 7.423.000,00	kr. 97.000,00	kr. 1.128.000,00	kr. 15.799.000,00	kr. 938.000,00	kr. 25.385.000,00	kr. 12.699.000,00
2016		kr. 7.458.000,00	kr. 99.000,00	kr. 1.150.000,00	kr. 16.140.000,00	kr. 959.000,00	kr. 25.806.000,00	kr. 11.953.000,00
2017		kr. 7.712.000,00	kr. 101.000,00	kr. 1.172.000,00	kr. 16.484.000,00	kr. 981.000,00	kr. 26.451.000,00	kr. 11.344.000,00
2018		kr. 7.769.000,00	kr. 103.000,00	kr. 1.195.000,00	kr. 16.827.000,00	kr. 1.003.000,00	kr. 26.897.000,00	kr. 10.681.000,00
2019		kr. 8.025.000,00	kr. 105.000,00	kr. 1.219.000,00	kr. 17.376.000,00	kr. 1.026.000,00	kr. 27.752.000,00	kr. 10.204.000,00
2020		kr. 8.238.000,00	kr. 108.000,00	kr. 1.244.000,00	kr. 17.935.000,00	kr. 1.049.000,00	kr. 28.574.000,00	kr. 9.728.000,00
2021		kr. 8.091.000,00	kr. 110.000,00	kr. 1.270.000,00	kr. 18.473.000,00	kr. 1.073.000,00	kr. 29.017.000,00	kr. 9.147.000,00
2022		kr. 8.401.000,00	kr. 112.000,00	kr. 1.296.000,00	kr. 19.017.000,00	kr. 1.097.000,00	kr. 29.923.000,00	kr. 8.734.000,00
2023		kr. 8.719.000,00	kr. 114.000,00	kr. 1.325.000,00	kr. 19.610.000,00	kr. 1.122.000,00	kr. 30.890.000,00	kr. 8.349.000,00
2024		kr. 8.368.000,00	kr. 117.000,00	kr. 1.353.000,00	kr. 20.200.000,00	kr. 1.147.000,00	kr. 31.185.000,00	kr. 7.804.000,00
Total:	kr. 101.543.000,00	kr. 116.848.000,00	kr. 1.616.000,00	kr. 18.157.000,00	kr. 255.061.000,00	kr. 15.328.000,00	kr. 508.553.000,00	kr. 270.830.000,00

Table 8.10: Cost for the best case scenario seen from the societal perspective. The scenario is Scenario A, where the time horison is the same as the lifetime of the degassing plant.

Year:	Offgas export:	Saved 5%-element:	Avoided emission damage costs:	Total:	Present value:
Number:	9	10	11	12	
2006					
2007					
2008					
2009	kr. 15.126.000,00	kr. 397.000,00	kr. 386.967.000,00	kr. 402.490.000,00	kr. 319.510.000,00
2010	kr. 28.900.000,00	kr. 658.000,00	kr. 574.393.000,00	kr. 603.951.000,00	kr. 443.922.000,00
2011	kr. 34.172.000,00	kr. 751.000,00	kr. 573.785.000,00	kr. 608.708.000,00	kr. 414.276.000,00
2012	kr. 29.379.000,00	kr. 151.000,00	kr. 588.523.000,00	kr. 618.053.000,00	kr. 389.478.000,00
2013	kr. 34.156.000,00		kr. 594.059.000,00	kr. 628.215.000,00	kr. 366.557.000,00
2014	kr. 35.108.000,00		kr. 609.883.000,00	kr. 644.991.000,00	kr. 348.469.000,00
2015	kr. 35.674.000,00		kr. 624.518.000,00	kr. 660.192.000,00	kr. 330.260.000,00
2016	kr. 36.558.000,00		kr. 637.499.000,00	kr. 674.057.000,00	kr. 312.219.000,00
2017	kr. 37.451.000,00		kr. 650.716.000,00	kr. 688.167.000,00	kr. 295.143.000,00
2018	kr. 38.345.000,00		kr. 664.064.000,00	kr. 702.409.000,00	kr. 278.936.000,00
2019	kr. 39.682.000,00		kr. 678.422.000,00	kr. 718.104.000,00	kr. 264.045.000,00
2020	kr. 41.044.000,00		kr. 692.856.000,00	kr. 733.900.000,00	kr. 249.864.000,00
2021	kr. 42.411.000,00		kr. 707.693.000,00	kr. 750.104.000,00	kr. 236.464.000,00
2022	kr. 43.795.000,00		kr. 722.481.000,00	kr. 766.276.000,00	kr. 223.669.000,00
2023	kr. 45.297.000,00		kr. 738.879.000,00	kr. 784.176.000,00	kr. 211.938.000,00
2024	kr. 46.800.000,00		kr. 754.936.000,00	kr. 801.736.000,00	kr. 200.634.000,00
Total:	kr. 583.898.000,00	kr. 1.957.000,00	kr. 10.199.674.000,00	kr. 10.785.529.000,00	kr. 4.885.387.000,00

Table 8.11: Benefits of the best case scenario seen from the societal perspective with a time horison corresponding to the lifetime of the degassing plant.

Number:	Text:	Value:
12	Total present value benefits:	kr. 4.885.384.000,00
8	Total present value costs:	kr. 270.830.000,00
13	Net present value:	kr 4.614.557.000,00

Table 8.12: Result for best case scenario seen from the societal perspective with a time horison corresponding to the lifetime of the degassing plant.

Year:	Construction:	Power consumption:	Chemicals:	Maintenance:	Crude oil to gas:	Operation:	Total:	Present value:
Number:	1	2	3	4	5	6	7	8
2006	kr. 3.712.000,00						kr. 3.712.000,00	kr. 3.712.000,00
2007	kr. 34.001.000,00						kr. 34.001.000,00	kr. 31.482.000,00
2008	kr. 53.844.000,00						kr. 53.844.000,00	kr. 46.163.000,00
2009	kr. 9.986.000,00	kr. 4.605.000,00	kr. 90.000,00	kr. 499.999,85	kr. 8.832.000,00	kr. 546.949,32	kr. 24.560.000,00	kr. 19.497.000,00
2010		kr. 8.475.000,00	kr. 90.000,00	kr. 1.366.049,68	kr. 15.976.000,00	kr. 836.537,06	kr. 26.744.000,00	kr. 19.658.000,00
2011		kr. 7.684.000,00	kr. 90.000,00	kr. 939.413,65	kr. 17.506.000,00	kr. 858.021,16	kr. 27.077.000,00	kr. 18.428.000,00
2012		kr. 8.820.000,00	kr. 92.000,00	kr. 819.000,00	kr. 12.471.000,00	kr. 877.000,00	kr. 23.079.000,00	kr. 14.544.000,00
2013		kr. 9.634.000,00	kr. 93.000,00	kr. 1.076.000,00	kr. 19.258.000,00	kr. 897.000,00	kr. 30.958.000,00	kr. 18.064.000,00
2014		kr. 9.922.000,00	kr. 95.000,00	kr. 1.103.000,00	kr. 19.601.000,00	kr. 917.000,00	kr. 31.638.000,00	kr. 17.093.000,00
2015		kr. 9.954.000,00	kr. 97.000,00	kr. 1.128.000,00	kr. 19.709.000,00	kr. 938.000,00	kr. 31.826.000,00	kr. 15.921.000,00
2016		kr. 10.001.000,00	kr. 99.000,00	kr. 1.150.000,00	kr. 20.134.000,00	kr. 959.000,00	kr. 32.343.000,00	kr. 14.981.000,00
2017		kr. 10.342.000,00	kr. 101.000,00	kr. 1.173.000,00	kr. 20.562.000,00	kr. 981.000,00	kr. 33.159.000,00	kr. 14.221.000,00
2018		kr. 10.418.000,00	kr. 103.000,00	kr. 1.195.000,00	kr. 20.990.000,00	kr. 1.003.000,00	kr. 33.709.000,00	kr. 13.386.000,00
2019		kr. 10.761.000,00	kr. 105.000,00	kr. 1.220.000,00	kr. 21.675.000,00	kr. 1.026.000,00	kr. 34.787.000,00	kr. 12.791.000,00
2020		kr. 11.047.000,00	kr. 108.000,00	kr. 1.244.000,00	kr. 22.372.000,00	kr. 1.049.000,00	kr. 35.820.000,00	kr. 12.195.000,00
2021		kr. 10.850.000,00	kr. 110.000,00	kr. 1.270.000,00	kr. 23.044.000,00	kr. 1.073.000,00	kr. 36.347.000,00	kr. 11.458.000,00
2022		kr. 11.266.000,00	kr. 112.000,00	kr. 1.296.000,00	kr. 23.722.000,00	kr. 1.097.000,00	kr. 37.493.000,00	kr. 10.944.000,00
2023		kr. 11.693.000,00	kr. 114.000,00	kr. 1.325.000,00	kr. 24.462.000,00	kr. 1.122.000,00	kr. 38.716.000,00	kr. 10.464.000,00
2024		kr. 11.221.000,00	kr. 117.000,00	kr. 1.353.000,00	kr. 25.198.000,00	kr. 1.147.000,00	kr. 39.036.000,00	kr. 9.769.000,00
Total:	kr. 101.543.000,00	kr. 156.693.000,00	kr. 1.616.000,00	kr. 18.157.000,00	kr. 315.512.000,00	kr. 15.328.000,00	kr. 608.849.000,00	kr. 314.771.000,00

Table 8.13: Worst case scenario costs seen from the societal perspective with a time horison corresponding to the lifetime of the degassing plant.

Year:	Offgas export:	Saved 5%-element:	Avoided emission damage cost:	Total:	Present value:
Number:	9	10	11	12	
2006					
2007					
2008					
2009	kr. 15.126.000,00	kr. 397.000,00	kr. 10.419.000,00	kr. 25.942.000,00	kr. 20.594.000,00
2010	kr. 28.900.000,00	kr. 658.000,00	kr. 17.592.000,00	kr. 47.150.000,00	kr. 34.657.000,00
2011	kr. 34.172.000,00	kr. 751.000,00	kr. 17.423.000,00	kr. 52.346.000,00	kr. 35.626.000,00
2012	kr. 29.379.000,00	kr. 151.000,00	kr. 16.596.000,00	kr. 46.126.000,00	kr. 29.067.000,00
2013	kr. 34.156.000,00		kr. 16.865.000,00	kr. 51.021.000,00	kr. 29.770.000,00
2014	kr. 35.108.000,00		kr. 17.707.000,00	kr. 52.815.000,00	kr. 28.534.000,00
2015	kr. 35.674.000,00		kr. 18.508.000,00	kr. 54.182.000,00	kr. 27.104.000,00
2016	kr. 36.558.000,00		kr. 19.268.000,00	kr. 55.826.000,00	kr. 25.858.000,00
2017	kr. 37.451.000,00		kr. 20.040.000,00	kr. 57.491.000,00	kr. 24.657.000,00
2018	kr. 38.345.000,00		kr. 20.821.000,00	kr. 59.166.000,00	kr. 23.496.000,00
2019	kr. 39.682.000,00		kr. 21.686.000,00	kr. 61.368.000,00	kr. 22.565.000,00
2020	kr. 41.044.000,00		kr. 22.570.000,00	kr. 63.614.000,00	kr. 21.658.000,00
2021	kr. 42.411.000,00		kr. 23.212.000,00	kr. 65.623.000,00	kr. 20.687.000,00
2022	kr. 43.795.000,00		kr. 23.858.000,00	kr. 67.653.000,00	kr. 19.747.000,00
2023	kr. 45.297.000,00		kr. 24.565.000,00	kr. 69.862.000,00	kr. 18.882.000,00
2024	kr. 46.800.000,00		kr. 25.267.000,00	kr. 72.067.000,00	kr. 18.035.000,00
Total:	kr. 583.898.000,00	kr. 1.957.000,00	kr. 316.397.000,00	kr. 902.252.000,00	kr. 400.937.000,00

Table 8.14: Benefits of worst case scenario seen from the societal perspective with a time horizon corresponding to the lifetime of the degassing plant.

Number:	Text:	Value:
12	Total present value benefits:	kr. 400.937.000,00
8	Total present value costs:	kr. 314.771.000,00
13	Net present value:	kr 86.166.000,00

Table 8.15: Results of the worst case scenario seen from the societal perspective with a time horison corresponding to the lifetime of the degassing plant

The new societal discount rate

In the previous section, the calculations were made with the nominal discount rate of 8% published by the ministry of finance. However, according to Energistyrelsen (2011) a real discount rate of 5% should be used. Moreover, it is stated in the government platform (Regeringen, 2011) that the discount rate should be further lowered. Therefore, Scenario A has been calculated again, seen from the societal perspective, with a real discount rate of 3% corresponding to a nominal discount rate of 5%. As before, a best case and a worst case scenario are calculated due to the large span in the unit costs for VOC. The results are respectively presented in tables 8.16 to 8.18 and tables 8.19 to 8.21.

As in the previously presented case for the societal perspective, there is a large span in the results due to the large span in the unit cost for VOC. Decreasing the discount rate increases the weight of the benefits occurring later in the project lifetime in relation to the costs occurring early in the project lifetime. As seen from the tables, this increases the project's net present value making the project even more recommendable from a societal point of view.

Year:	Construction:	Power consumption:	Chemicals:	Maintenance:	Crude oil to gas:	Operation:	Total:	Present value:
Number:	1	2	3	4	5	6	7	8
2006	kr. 3.712.000,00						kr. 3.712.000,00	kr. 3.712.000,00
2007	kr. 34.001.000,00						kr. 34.001.000,00	kr. 32.382.000,00
2008	kr. 53.844.000,00						kr. 53.844.000,00	kr. 48.838.000,00
2009	kr. 9.986.000,00	kr. 3.434.000,00	kr. 90.000,00	kr. 499.999,85	kr. 7.937.000,00	kr. 547.000,00	kr. 22.494.000,00	kr. 19.431.000,00
2010		kr. 6.320.000,00	kr. 90.000,00	kr. 1.366.049,68	kr. 13.153.000,00	kr. 837.000,00	kr. 21.766.000,00	kr. 17.907.000,00
2011		kr. 5.730.000,00	kr. 90.000,00	kr. 939.413,65	kr. 15.017.000,00	kr. 858.000,00	kr. 22.634.000,00	kr. 17.734.000,00
2012		kr. 6.577.000,00	kr. 92.000,00	kr. 819.000,00	kr. 9.942.000,00	kr. 877.000,00	kr. 18.307.000,00	kr. 13.661.000,00
2013		kr. 7.184.000,00	kr. 93.000,00	kr. 1.075.000,00	kr. 15.438.000,00	kr. 897.000,00	kr. 24.688.000,00	kr. 17.545.000,00
2014		kr. 7.399.000,00	kr. 95.000,00	kr. 1.103.000,00	kr. 15.713.000,00	kr. 917.000,00	kr. 25.227.000,00	kr. 17.075.000,00
2015		kr. 7.423.000,00	kr. 97.000,00	kr. 1.128.000,00	kr. 15.799.000,00	kr. 938.000,00	kr. 25.385.000,00	kr. 16.363.000,00
2016		kr. 7.458.000,00	kr. 99.000,00	kr. 1.150.000,00	kr. 16.140.000,00	kr. 959.000,00	kr. 25.806.000,00	kr. 15.843.000,00
2017		kr. 7.712.000,00	kr. 101.000,00	kr. 1.172.000,00	kr. 16.484.000,00	kr. 981.000,00	kr. 26.451.000,00	kr. 15.465.000,00
2018		kr. 7.769.000,00	kr. 103.000,00	kr. 1.195.000,00	kr. 16.827.000,00	kr. 1.003.000,00	kr. 26.897.000,00	kr. 14.977.000,00
2019		kr. 8.025.000,00	kr. 105.000,00	kr. 1.219.000,00	kr. 17.376.000,00	kr. 1.026.000,00	kr. 27.752.000,00	kr. 14.717.000,00
2020		kr. 8.238.000,00	kr. 108.000,00	kr. 1.244.000,00	kr. 17.935.000,00	kr. 1.049.000,00	kr. 28.574.000,00	kr. 14.432.000,00
2021		kr. 8.091.000,00	kr. 110.000,00	kr. 1.270.000,00	kr. 18.473.000,00	kr. 1.073.000,00	kr. 29.017.000,00	kr. 13.958.000,00
2022		kr. 8.401.000,00	kr. 112.000,00	kr. 1.296.000,00	kr. 19.017.000,00	kr. 1.097.000,00	kr. 29.923.000,00	kr. 13.708.000,00
2023		kr. 8.719.000,00	kr. 114.000,00	kr. 1.325.000,00	kr. 19.610.000,00	kr. 1.122.000,00	kr. 30.890.000,00	kr. 13.477.000,00
2024		kr. 8.368.000,00	kr. 117.000,00	kr. 1.353.000,00	kr. 20.200.000,00	kr. 1.147.000,00	kr. 31.185.000,00	kr. 12.958.000,00
Total:	kr. 101.543.000,00	kr. 116.848.000,00	kr. 1.616.000,00	kr. 18.157.000,00	kr. 255.061.000,00	kr. 15.328.000,00	kr. 508.553.000,00	kr. 334.183.000,00

Table 8.16: Cost for the best case scenario seen from the societal perspective. The scenario is Scenario A, where the time horison is the same as the lifetime of the degassing plant. The used discount rate is in this case 5% nominally.

Year:	Offgas export:	Saved 5%-element:	Avoided emission damage costs:	Total:	Present value:
Number:	9	10	11	12	
2006					
2007					
2008					
2009	kr. 15.126.000,00	kr. 397.000,00	kr. 386.967.000,00	kr. 402.490.000,00	kr. 347.686.000,00
2010	kr. 28.900.000,00	kr. 658.000,00	kr. 574.393.000,00	kr. 603.951.000,00	kr. 496.872.000,00
2011	kr. 34.172.000,00	kr. 751.000,00	kr. 573.785.000,00	kr. 608.708.000,00	kr. 476.939.000,00
2012	kr. 29.379.000,00	kr. 151.000,00	kr. 588.523.000,00	kr. 618.053.000,00	kr. 461.204.000,00
2013	kr. 34.156.000,00		kr. 594.059.000,00	kr. 628.215.000,00	kr. 446.461.000,00
2014	kr. 35.108.000,00		kr. 609.883.000,00	kr. 644.991.000,00	kr. 436.555.000,00
2015	kr. 35.674.000,00		kr. 624.518.000,00	kr. 660.192.000,00	kr. 425.566.000,00
2016	kr. 36.558.000,00		kr. 637.499.000,00	kr. 674.057.000,00	kr. 413.813.000,00
2017	kr. 37.451.000,00		kr. 650.716.000,00	kr. 688.167.000,00	kr. 402.357.000,00
2018	kr. 38.345.000,00		kr. 664.064.000,00	kr. 702.409.000,00	kr. 391.128.000,00
2019	kr. 39.682.000,00		kr. 678.422.000,00	kr. 718.104.000,00	kr. 380.826.000,00
2020	kr. 41.044.000,00		kr. 692.856.000,00	kr. 733.900.000,00	kr. 370.669.000,00
2021	kr. 42.411.000,00		kr. 707.693.000,00	kr. 750.104.000,00	kr. 360.813.000,00
2022	kr. 43.795.000,00		kr. 722.481.000,00	kr. 766.276.000,00	kr. 351.040.000,00
2023	kr. 45.297.000,00		kr. 738.879.000,00	kr. 784.176.000,00	kr. 342.133.000,00
2024	kr. 46.800.000,00		kr. 754.936.000,00	kr. 801.736.000,00	kr. 333.138.000,00
Total:	kr. 583.898.000,00	kr. 1.957.000,00	kr. 10.199.674.000,00	kr. 10.785.529.000,00	kr. 6.437.200.000,00

Table 8.17: Benefits of best case scenario seen from the societal perspective with a time horison corresponding to the lifetime of the degassing plant. The used discount rate is in this case 5% nominally.

Number:	Text:	Value:
12	Total present value benefits:	kr. 6.437.200.000,00
8	Total present value costs:	kr. 334.183.000,00
13	Net present value:	kr. 6.103.017.000,00

Table 8.18: Result for best case scenario seen from the societal perspective with a time horison corresponding to the lifetime of the degassing plant. The used discount rate is in this case 5% nominally.

Year:	Construction:	Power consumption:	Chemicals:	Maintenance:	Crude oil to gas:	Operation:	Total:	Present value:
Number:	1	2	3	4	5	6	7	8
2006	kr. 3.712.000,00						kr. 3.712.000,00	kr. 3.712.000,00
2007	kr. 34.001.000,00						kr. 34.001.000,00	kr. 32.382.000,00
2008	kr. 53.844.000,00						kr. 53.844.000,00	kr. 48.838.000,00
2009	kr. 9.986.000,00	kr. 4.605.000,00	kr. 90.000,00	kr. 499.999,85	kr. 8.832.000,00	kr. 546.949,32	kr. 24.560.000,00	kr. 21.216.000,00
2010		kr. 8.475.000,00	kr. 90.000,00	kr. 1.366.049,68	kr. 15.976.000,00	kr. 836.537,06	kr. 26.744.000,00	kr. 22.002.000,00
2011		kr. 7.684.000,00	kr. 90.000,00	kr. 939.413,65	kr. 17.506.000,00	kr. 858.021,16	kr. 27.077.000,00	kr. 21.216.000,00
2012		kr. 8.820.000,00	kr. 92.000,00	kr. 819.000,00	kr. 12.471.000,00	kr. 877.000,00	kr. 23.079.000,00	kr. 17.222.000,00
2013		kr. 9.634.000,00	kr. 93.000,00	kr. 1.076.000,00	kr. 19.258.000,00	kr. 897.000,00	kr. 30.958.000,00	kr. 22.001.000,00
2014		kr. 9.922.000,00	kr. 95.000,00	kr. 1.103.000,00	kr. 19.601.000,00	kr. 917.000,00	kr. 31.638.000,00	kr. 21.414.000,00
2015		kr. 9.954.000,00	kr. 97.000,00	kr. 1.128.000,00	kr. 19.709.000,00	kr. 938.000,00	kr. 31.826.000,00	kr. 20.515.000,00
2016		kr. 10.001.000,00	kr. 99.000,00	kr. 1.150.000,00	kr. 20.134.000,00	kr. 959.000,00	kr. 32.343.000,00	kr. 19.856.000,00
2017		kr. 10.342.000,00	kr. 101.000,00	kr. 1.173.000,00	kr. 20.562.000,00	kr. 981.000,00	kr. 33.159.000,00	kr. 19.387.000,00
2018		kr. 10.418.000,00	kr. 103.000,00	kr. 1.195.000,00	kr. 20.990.000,00	kr. 1.003.000,00	kr. 33.709.000,00	kr. 18.770.000,00
2019		kr. 10.761.000,00	kr. 105.000,00	kr. 1.220.000,00	kr. 21.675.000,00	kr. 1.026.000,00	kr. 34.787.000,00	kr. 18.448.000,00
2020		kr. 11.047.000,00	kr. 108.000,00	kr. 1.244.000,00	kr. 22.372.000,00	kr. 1.049.000,00	kr. 35.820.000,00	kr. 18.092.000,00
2021		kr. 10.850.000,00	kr. 110.000,00	kr. 1.270.000,00	kr. 23.044.000,00	kr. 1.073.000,00	kr. 36.347.000,00	kr. 17.484.000,00
2022		kr. 11.266.000,00	kr. 112.000,00	kr. 1.296.000,00	kr. 23.722.000,00	kr. 1.097.000,00	kr. 37.493.000,00	kr. 17.176.000,00
2023		kr. 11.693.000,00	kr. 114.000,00	kr. 1.325.000,00	kr. 24.462.000,00	kr. 1.122.000,00	kr. 38.716.000,00	kr. 16.892.000,00
2024		kr. 11.221.000,00	kr. 117.000,00	kr. 1.353.000,00	kr. 25.198.000,00	kr. 1.147.000,00	kr. 39.036.000,00	kr. 16.220.000,00
Total:	kr. 101.543.000,00	kr. 156.693.000,00	kr. 1.616.000,00	kr. 18.157.000,00	kr. 315.512.000,00	kr. 15.328.000,00	kr. 608.849.000,00	kr. 392.843.000,00

Table 8.19: Worst case scenario costs seen from the societal perspective with a time horison corresponding to the lifetime of the degassing plant. The used discount rate is in this case 5% nominally.

Year:	Offgas export:	Saved 5%-element:	Avoided emission damage cost:	Total:	Present value:
Number:	9	10	11	12	
2006					
2007					
2008					
2009	kr. 15.126.000,00	kr. 397.000,00	kr. 10.419.000,00	kr. 25.942.000,00	kr. 22.410.000,00
2010	kr. 28.900.000,00	kr. 658.000,00	kr. 17.592.000,00	kr. 47.150.000,00	kr. 38.790.000,00
2011	kr. 34.172.000,00	kr. 751.000,00	kr. 17.423.000,00	kr. 52.346.000,00	kr. 41.014.000,00
2012	kr. 29.379.000,00	kr. 151.000,00	kr. 16.596.000,00	kr. 46.126.000,00	kr. 34.420.000,00
2013	kr. 34.156.000,00		kr. 16.865.000,00	kr. 51.021.000,00	kr. 36.260.000,00
2014	kr. 35.108.000,00		kr. 17.707.000,00	kr. 52.815.000,00	kr. 35.747.000,00
2015	kr. 35.674.000,00		kr. 18.508.000,00	kr. 54.182.000,00	kr. 34.926.000,00
2016	kr. 36.558.000,00		kr. 19.268.000,00	kr. 55.826.000,00	kr. 34.272.000,00
2017	kr. 37.451.000,00		kr. 20.040.000,00	kr. 57.491.000,00	kr. 33.614.000,00
2018	kr. 38.345.000,00		kr. 20.821.000,00	kr. 59.166.000,00	kr. 32.946.000,00
2019	kr. 39.682.000,00		kr. 21.686.000,00	kr. 61.368.000,00	kr. 32.545.000,00
2020	kr. 41.044.000,00		kr. 22.570.000,00	kr. 63.614.000,00	kr. 32.129.000,00
2021	kr. 42.411.000,00		kr. 23.212.000,00	kr. 65.623.000,00	kr. 31.566.000,00
2022	kr. 43.795.000,00		kr. 23.858.000,00	kr. 67.653.000,00	kr. 30.993.000,00
2023	kr. 45.297.000,00		kr. 24.565.000,00	kr. 69.862.000,00	kr. 30.481.000,00
2024	kr. 46.800.000,00		kr. 25.267.000,00	kr. 72.067.000,00	kr. 29.945.000,00
Total:	kr. 583.898.000,00	kr. 1.957.000,00	kr. 316.397.000,00	kr. 902.252.000,00	kr. 532.058.000,00

Table 8.20: Benefits of worst case scenario seen from the societal perspective with a time horizon corresponding to the lifetime of the degassing plant. The used discount rate is in this case 5% nominally.

Number:	Text:	Value:
12	Total present value benefits:	kr. 532.058.000,00
8	Total present value costs:	kr. 392.843.000,00
13	Net present value:	kr 139.215.000,00

Table 8.21: esults of the worst case scenario seen from the societal perspective with a time horison corresponding to the lifetime of the degassing plant. The used discount rate is in this case 5% nominally.

8.3.2 Scenario B – Hejre

For the Hejre scenarios, the time horison has been shortened to end at the commissioning of the Hejre field in 2015. The costs and benefits are the same as for Scenario A, therefore only the results are presented. When decommissioning the degassing plant before the end of the technological life, as is the case in this scenario, a scrap value can be attached to the plant. This is, however, not included in the present analysis, since it is difficult to estimate a reliable scrap value of the plant.
Seen from the perspective of the users of the oil pipe as presented in table 8.22, table 8.23, and table 8.24, the project will generate a deficit in all cases. Seen from the societal perspective as presented in table 8.25 and table 8.26, the project has a very wide outcome range depicting the variation in unit costs for one ton VOC emission, but with a larger deficit in the worst case scenario. This is again a function of the costs incurring early in the project lifetime and the benefits incurring later in the project lifetime. As the project lifetime is shortened, the deficit will increase. Using the same arguments as for Scenario A, it could be likely that the project would end up close to zero since none of the results are significantly different from zero. This is, however, again subject to uncertainty.

Text:	Value:
Costs:	
Construction:	kr. 101.543.000,00
Power consumption:	kr. 36.644.000,00
Chemicals:	kr. 550.000,00
Maintenance:	kr. 5.803.000,00
Crude oil to gas:	kr. 77.200.000,00
Operation:	kr. 4.933.000,00
Total costs:	kr. 226.673.000,00
Present value:	kr. 193.325.000,00
Benefits:	
Offgas export:	kr. 176.841.000,00
Saved 5%-element	kr. 1.957.000,00
Total benefits:	kr. 178.798.000,00
Present value:	kr. 140.780.000,00
Net Present Value:	kr. -52.545.000,00

Table 8.22: Results of the most likely scenario seen from the perspective of the users of the oil pipe with a time horison ending at the end of 2014.

Text:	Value:
Costs:	
Construction:	kr. 101.543.000,00
Power consumption:	kr. 24.149.000,00
Chemicals:	kr. 550.000,00
Maintenance:	kr. 5.803.000,00
Crude oil to gas:	kr. 64.011.000,00
Operation:	kr. 4.933.000,00
Total costs:	kr. 200.989.000,00
Present value:	kr. 173.191.000,00
Benefits:	
Offgas export:	kr. 176.841.000,00
Saved 5%-element	kr. 1.957.000,00
Total benefits:	kr. 178.798.000,00
Present value:	kr. 140.780.000,00
Net Present Value:	kr. -32.411.000,00

Table 8.23: Results of the best case scenario seen from the perspective of the users of the oil pipe with a time horison ending at the end of 2014.

Text:	Value:
Costs:	
Construction:	kr. 101.543.000,00
Power consumption:	kr. 49.140.000,00
Chemicals:	kr. 550.000,00
Maintenance:	kr. 5.803.000,00
Crude oil to gas:	kr. 93.644.000,00
Operation:	kr. 4.933.000,00
Total costs:	kr. 255.613.000,00
Present value:	kr. 215.969.000,00
Benefits:	
Offgas export:	kr. 176.841.000,00
Saved 5%-element	kr. 1.957.000,00
Total benefits:	kr. 178.798.000,00
Present value:	kr. 140.780.000,00
Net Present Value:	kr. -75.189.000,00

Table 8.24: Results of the worst case scenario seen from the perspective of the users of the oil pipe with a time horison ending at the end of 2014.

Text:	Value:
Costs:	
Construction:	kr. 101.543.000,00
Power consumption:	kr. 36.644.000,00
Chemicals:	kr. 550.000,00
Maintenance:	kr. 5.803.000,00
Crude oil to gas:	kr. 77.200.000,00
Operation:	kr. 4.933.000,00
Total costs:	kr. 226.673.000,00
Present value:	kr. 170.187.000,00
Benefits:	
Offgas export:	kr. 176.841.000,00
Saved 5%-element	kr. 1.957.000,00
Avoided emission damage costs:	kr. 3.327.615.000,00
Total benefits:	kr. 3.506.413.000,00
Present value:	kr. 2.282.215.000,00
Net Present Value:	kr 2.112.028.000,00

Table 8.25: Results of the best case scenario seen from the societal perspective with a time horison ending at the end of 2014.

Text:	Value:
Costs:	
Construction:	kr. 101.543.000,00
Power consumption:	kr. 49.140.000,00
Chemicals:	kr. 550.000,00
Maintenance:	kr. 5.803.000,00
Crude oil to gas:	kr. 93.644.000,00
Operation:	kr. 4.933.000,00
Total costs:	kr. 255.613.000,00
Present value:	kr. 188.639.675,00
Benefits:	
Offgas export:	kr. 176.841.000,00
Saved 5%-element	kr. 1.957.000,00
Avoided emission damage costs:	kr. 96.602.000,00
Total benefits:	kr. 275.400.000,00
Present value:	kr. 178.248.000,00
Net Present Value:	kr -10.391.675,00

Table 8.26: Results of the worst case scenario seen from the societal perspective with a time horison ending at the end of 2014.

8.4 Chapter summary

The CBA presented in this chapter has analysed the economical effect of the installation of the degassing plant seen from the perspective of the users of the oil pipe and the societal perspective and for the technological lifetime of the plant and for an artificially shortened lifetime due to the commissioning of the Hejre field.
The results show that for the users of the oil pipe, the installation of the degassing plant is probably roughly a break even project, since the net present value for the most likely case, the best case, and the worst case is small compared to the total earnings and expenses of the project. From the societal perspective, the project generates a net present value whose size depends on the used discount rate. However, the size of the net present value is very variable depending on the chosen unit price for VOC. This fact stirrers the line of the results meaning that the uncertainties related to the net present value seen from the societal perspective are larger than the results. With respect to the Hejre scenario, the project generates a deficit in most cases, since the artificially shortened lifetime reduces the earnings that the project will have time to generate. This is, however, to be compared to the even larger incomes generated from oil production from the field, and as such, the deficit resulting from early scrapping of the degassing plant probably represents a very humble amount in comparison.

Chapter 9

Conclusion

The aim of the project was to evaluate the environmental, technical and economical performance of the DONG degassing plant. Due to the small number of measurements obtained in the present project, it is not possible to conclude on the performance with respect to emission reductions. Spectrasyne Ltd (2009) reported a reduction of 79% for NMVOC and 53% for methane, however, as described in section 2.4 these numbers are also subject to uncertainties.
In chapter 6 the impact of the emission change was modelled using DEHM and 1DRCM. It was shown, that the emission reduction had caused a corresponding concentration reduction of up to $10^{-4} ppm$, with the major concentration reduction in the vicinity of Fredericia, but also with a noticeable impact on parts of Northern Europe.
In chapter 7 the energy per to offgas produced was calculated to $0.5897 {}^{MWh}/_{ton}$ and the inherent availability was calculated to approximately 96% approaching 98% over time. The energy consumption was much higher than expected before the installation of the degassing plant. The expected availability predicted before the installation of the degassing plant was 98%, and apart from the burn-in failures, this appears to be fulfilled.
In chapter 8 a cost-benefit analysis with the users of the oil pipe and the society respectively as stakeholders. It was shown that the degassing plant as a technology would have resulted in roughly "break even" for the users in case it had been in use for the full lifetime. Moreover, it was shown that the installation of the degassing plant had generated a net benefit to the society, however the magnitude of this was inconclusive due to the large uncertainties related to the unit price of VOC.

Bibliography

Adler, M. and E. A. Posner (2009). New foundations of cost-benefit analysis: A reply to Professors Sinden, Kysar and Driesen. *Regulation & Governance 3*, 72–83.

Adler, M. D. and E. A. Posner (2006). *New Foundations of Cost-Benefit Analysis*. Harvard University Press.

Alfke, G., G. Bunch, G. Crociani, D. Dando, M. Fontaine, P. Goodsell, A. Green, W. Hafker, G. Isaak, J. Marvillet, B. Poot, H. Sutherland, A. van der Rest, J. van Oudenhoven, T. Walden, E. Martin, and H. Schipper (1999, January). Best Available Techniques to Reduce Emissions from Refineries – Part II Air Pollution. Technical report, CONCAWE Air and Water Quality Management group.

American Society of Mechanical Engineers (1971). *Fluid Meters* (Sixth edition ed.). American Society of Mechanical Engineers.

Andersen, M. S. and N. Strange (2003). Miljøøkonomiske beregningspriser. Forprojekt, Faglig rapport fra DMU nr. 459, Danmarks Miljøundersøgelser. `http://www2.dmu.dk/1_viden/2_publikationer/3_fagrapporter/rapporter/FR459.PDF`.

API (1990, December). Measurement of BTEX Emission Fluxes from Refinery Wastewarer Impoundments Using Atmospheric Tracer Techniques. Technical Report 4518, American Petroleum Institute.

Atmospheric Studies Group (2012). Website. `http://www.src.com/calpuff/calpuff1.htm`.

Basse, E. M. (2007). Eu's miljøkvalitets- og procesnormer. In E. M. Basse (Ed.), *Miljøretten 4 – Forurenende anlæg og processer*, pp. 35–178. Jurist- og Økonomforbundets Forlag.

Betalingsbekendtgørelsen (2010). Bekendtgørelse om betaling for transport af råolie og kondensat. `https://www.retsinformation.dk/Forms/R0710.aspx?id=132748`.

Brandt, J., J. D. Silver, L. M. Frohn, C. Geels, A. Gross, A. B. Hansen, K. M. Hansen, G. B. Hedegaard, C. A. Skjøth, H. Villadsen, A. Zare, and J. H. Christensen (2012, June). An integrated model study for Europe and North America using the Danish Eulerian Hemispheric Model with focus on intercontinental transport. *Atmospheric Environment 53*, 156–176.

Bridgeman, A. J. (2013). webpage. School of Chemistry, the University of Sydney, `http://assign3.chem.usyd.edu.au/spectroscopy/infrared_spectrum.php?res=high&molecule=butane`.

Busch, K. W., A. Hennequin, and M. A. Busch (1999). Introduction to Optical Cavities. In K. W. Busch and M. A. Busch (Eds.), *Cavity-Ringdown Spectroscopy –An Ultratrace-Absorption Measurement Technique*, pp. 20–34. Blackwell Publishing.

Carlsen, A. (2009). Health impacts. In J. Fenger and J. C. Tjell (Eds.), *Air Pollution – From a Local to a Global Perspective*, pp. 329–358. Polyteknisk Forlag.

Cess, R. D. and S. N. Tiwari (1967). Infrared Radiative Energy Transfer in Gases. *Advances in Heat Transfer 8*, 229–283.

Cetin, E. (2002). Ambient Volatile Organic Compound (VOC) Concentrations Around A Petrochemical Plant. Master's thesis, Graduate School of Natural and Applied Sciences, Dokuz Eylul University.

Cetin, E., M. Odabasi, and R. Seyfioglu (2003). Ambient volatile organic compound (VOC) concentrations around a petrochemical complex and a petroleum refinery. *The Science of the Total Environment 312*, 103–112.

Chang, L.-S. and S.-U. Park (2004). Direct radiative forcing due to anthropogenic aerosols in East Asia during April 2001. *Atmospheric Environment 38*, 4467–4482.

Chang, R. (2008). *General Chemistry*. McGraw Hill.

Christensen, L. K., M. BIlde, S. B. Andersen, and A. Gross (1996). Afløsningsopgave i forbindelse med studiekreds om strålingstransport i forårssemestret 1996.

Christensen, M. (2005, August). DONG råolieterminal Degassing Projekt. Notat. Internal document provided by DONG Oil Pipe.

Christensen, M. (2006, April). Miljøgodkendelse af degassing anlæg på dongs råolieterminal, vejlbyvej 28, 7000 fredericia, matr.nr. 294 fredericia kobbeljorde og 101 vejlby, fredericia jorder, som tillæg til miljøgodkendelse af 17. august 2000. Miljøgodkendelse. Internal document provided by DONG Oil Pipe.

Clemmensen, B., S. Pedersen, and K. R. Dirckinck-Holmfeld (2007). *Environmental Policy – Legal and Economic Instruments*. The Baltic University Press.

Collins, W. J., R. G. Derwent, C. E. Johnson, and D. S. Stevenson (2002). The oxidation of organic compounds in the troposphere and their global warming potentials. *Climatic Change 52*, 453–479.

COWI (2006). *DONG Oil Pipe A/S – Degassing Plant – Basic Design and Engineering Package*. COWI.

Crane Co (1999). *Flow of Fluids Through Valves, Fittings and Pipe* (Metric Edition – SI Units ed.). Crane Co.

Crutzen, P. J. (1978). The Impact of the Chlorocarbon Industry on the Ozone Layer. *Journal of Geophysical Research 83*, 345–363.

Danish Ministry of Transport (2004a, July). *External Costs of Transport – 1st Report – Review of European Studies*. Danish Ministry of Transport. `http://www.trm.dk/~/media/Files/Publication/English/1stReport.pdf`.

Danish Ministry of Transport (2004b, July). *External Costs of Transport – 2nd Report – Marginal external cost matrices for Denmark*. Danish Ministry of Transport. http://www.trm.dk/~/media/Files/Publication/English/2ndReport.pdf.

Danish Ministry of Transport (2004c, July). *External Costs of Transport – 3rd Report – Total external costs of road and rail transport in Denmark*. Danish Ministry of Transport. http://www.trm.dk/~/media/Files/Publication/English/3rdReport.pdf.

Dayton, B. B. (1998). Kinetic Theory of Gases. In J. M. Lafferty (Ed.), *Foundations of Vacuum Science and Technology*. John Wiley & Sons, Inc.

DONG Oil Pipe (2010, December). Driftsrapport. Technical report, DONG Oil Pipe.

DONG Oil Pipe (2012, January). Månedsrapport. Technical report, DONG Oil Pipe.

Ebeling, C. E. (1997). *Reliability and Maintainability Engineering*. The McGraw-Hill Companies, Inc.

Ehhalt, D., L. E. Heidt, R. H. Lueb, and N. Roper (1974). Vertical profiles of CH_4, H_2, CO, N_2O, and CO_2 in the stratosphere. In *Proceedings of the Third Conference of CLAP*, Volume Rep. DOT-TSC-OST-74-15, pp. 153–160. Clim. Impact Assessment Program, Washington, D.C. Cited by Crutzen (1978).

Ehhalt, D. H., L. E. Heidt, R. H. Lueb, and E. A. Martell (1975). Concentrations of CH_4, CO, CO_2, H_2, H_2O and N_2O in the Upper Stratosphere. *Journal of the Atmospheric Sciences 32*(1), 163–169.

Eklund, B. (1999). Comparison of line- and point-source releases of tracer gases. *Atmospheric Evnironment 33*, 1065–1071.

Encyclopedia Britannica Online(1) (2012, October). laser. Encyclopædia Britannica Online. http://www.britannica.com.molly.ruc.dk/EBchecked/topic/330874/laser.

Encyclopedia Britannica Online(2) (2012, October). bandwidth. Encyclopædia Britannica Online. http://www.britannica.com.molly.ruc.dk/EBchecked/topic/51642/bandwidth.

Energistyrelsen (2011, April). Forudsætninger for samfundsøkonomiske analyser på energiområdet, april 2011. http://www.ens.dk/da-DK/Info/TalOgKort/Fremskrivninger/beregningsforudsatninger/Documents/Foruds%C3%A6tninger%20for%20samfunds%C3%B8konomiske%20analyser%20p%C3%A5%20energiomr%C3%A5det%202011.pdf.

Energistyrelsen (2011). Tillægsblad om kalkulationsrente, levetid og reference til vejledning i samfundsøkonomiske analyser på energiområdet, energistyrelsen, april 2005 (beregningseksempler revideret juli 2007),. Notat. http://www.ens.dk/da-DK/Info/TalOgKort/

Fremskrivninger/analysemetode/Documents/Till%C3%A6gsblad%20om%20kalkulationsrente%20til%20vejledning.pdf.

Finansministeriet (2001, February). *Miljøpolitikkens økonomiske fordele og omkostninger*. Finansministeriet. http://www.fm.dk/publikationer/2001/miljoepolitikkens-oekonomiske-fordele-og-omkostninger/download/~/media/Files/Publikationer/2008/Download/miljpoli.ashx.

Fingas, M. F. (1996). *The Evaporation of Crude Oil and Petroleum Products*. Ph. D. thesis, Department of Natural Resources Sciences, McGill University, Montreal.

Forster, P., V. Ramaswamy, P. Artaxo, T. Berntsen, D. W. Fahey, J. Haywood, J. Lean, D. C. Lowe, G. Myhre, J. Nganga, R. Prinn, G. Raga, M. Schulz, and R. V. Dorland (2007). Changes in Atmospheric Constituents and in Radiative Forcing. In S. Solomon, D. Qin, M. Manning, Z. Chen, M. Marquis, K. Averyt, M.Tignor, and H. Miller (Eds.), *Climate Change 2007: The Physical Science Basis. Contribution of Working Group I to the Fourth Assessment Report of the Intergovernmental Panel on Climate Change.*, pp. 129–234. Cambridge University Press.

Frohn, L. M. (2004). *A Study of long-term high-resolution air pollution modelling*. Ph. D. thesis, Niels Bohr Institute for Astronomy, Physics and Geophysics, University of Copenhagen and Ministry of Environment, National Environmental Research Institute.

Fuglestvedt, J. S., T. K. Berntsen, O. Godal, R. Sausen, K. P. Shine, and T. Skodvin (2003). Metrics of climate change: Assessing radiative forcing and emission indices. *Climatic Change 58*, 267–331.

Fuglestvedt, J. S., K. P. Shine, T. Berntsen, J. Cook, D. S. Lee, A. Stenke, R. B. Skeie, G. J. M. Velders, and I. A. Waitz (2010). Transport Impact on Atmosphere and Climate: Metrics. *Atmospheric Environment 44*, 4648–4677.

Galle, B. (1999). *Development and Application of Methods based on DOAS and FTIR Absorption Spectroscopy for Atmospheric Research*. Doctoral thesis, Institutionen för experimentell fysik, Chalmers University of Technology.

Goldman, A., D. G. Murcray, F. H. Murcray, W. J. Williams, J. N. Brooks, and C. M. Bradford (1973). Vertical distribution of CO in the atmosphere. *Journal of Geophysical Research 78*(24), 5273–5283.

Goody, R. and M. J. S. Belton (1967). Radiative Relaxation Times for Mars. *Planetary and Space Science 15*, 247–256.

Goody, R. M. and Y. L. Yung (1989). *Atmospheric Radiation – Theoretical Basis*. Oxford University Press.

Gullick, J., R. Smyllie, and R. Collitt (2005, May). VOC Emissions in the Fredericia Area. Technical report, Entec UK Limited and Tractebel Gas Engineering.

Hansen, S. G. Hejre – dong energy's største udbygning og et centralt knudepunkt. Webpage. http://www.dongenergy.com/da/forretningsaktiviteter/exploration_and_production/aktiviteter_fordelt_paa_lande/pages/hejre.aspx.

Hatzianestis, J., P. Kalabokas, J. Bartzis, and N. Mimikos (1996). Concentration levels of hydrocarbons in the atmosphere of the Athens basin. In *Proceedings of the International Conference on Protection and Rehabilitation of the Environment III*, pp. 320–327. as cited in Kalabokas et al. (2001).

Hertel, O. and J. Brandt (2009). Air pollution modelling. In J. Fenger and J. C. Tjell (Eds.), *Air Pollution – From a Local to a Global Perspective*, pp. 293–326. Polyteknisk Forlag.

Higgins, J. and R. Johnstone (2001). Initial Report on Site Investigation Findings of Tanks T-9801/06, Tk-67 & Tk-71 at A/S Dansk Shell Fredericia Refinery. Technical report, Motherwell Bridge Engineering Limited.

Hodges, W. (2009). Functional modelling and mathematical models: A semantic analysis. In A. Meijers (Ed.), *Philosophy of Technology and Engineering Sciences*, pp. 655–692. Elsevier B.V.

Hougaard, K. (2012, July). TillÆg til miljØgodkendelse for: Dong oil pipe a/s, råolieterminalen i fredericia, vejlbyvej 20, 7000 fredericia. Miljøgodkendelse. http://www.mst.dk/Virksomhed_og_myndighed/Annoncering_decentral_administration/Jylland/2012/juli/ODE_DONG_OilPipe_Raaolieterminal_afgoerelse_9jul12.htm.

Illerup, J. B., K. Birr-Pedersen, M. H. Mikkelsen, M. Winther, S. Gyldenkærne, H. G. Bruun, and J. Fenhann (2002). Projection Models 2010. Danish emissions of SO_2, NO_x, NMVOC and NH_3. Technical report, National Environmental Research Institute, Denmark. NERI Technical Report nr. 414. http://www2.dmu.dk/1_viden/2_Publikationer/3_fagrapporter/rapporter/FR414.pdf.

Jackson, M. M. (2006). Organic liquid storage tanks volatile organic compounds (VOCs) emissions, dispersion and risk assessment in developing countries: The case of Dar-Es-Salaam City, Tanzania. *Environmental Monitoring and Assessment 116*, 363–382.

Jensen, S. (2012). Fw: Gorm produktion olie fra en brønd til land. E-mail communication. Production Support, Mærsk Olie og Gas A/S.

Jones, F. E. (1992). *Evaporation of Water*. Lewis Publishers.

Jonson, G. M. J. E., J. Bartnicki, F. Stordal, and K. P. Shine (2002). Role of spatial and temporal variations in the computatiom of radiative forcing due to suplhate aerosols: A regional study. *Wuarterly Journal of the Royal Meteorological Society 128*, 973–989.

Jovanovic, J., M. Jovanovic, A. Jovanovic, and V. Marinovic (2010). Introduction of cleaner production in the tank farm of the Pancevo Oil Refinery, Serbia. *Journal of Cleaner Production 18*, 791–798.

Kaimal, J. C. and J. J. Finnigan (1994). *Atmospheric Boundary Layer Flows*. Oxford University Press.

Kalabokas, P. D., J. Hatzianestis, J. G. Bartzis, and P. Papagiannakopoulos (2001). Atmospheric concentrations of saturated and aromatic hydrocarbons around a Greek oil refinery. *Atmospheric Environment 35*, 2545–2555.

Lacis, A. A. and J. E. Hansen (1974). A Parameterization for the Absorption of Solar Radiation in the Earth's Atmosphere. *Journal of the Atmospheric Sciences 31*, 118–133. `http://journals.ametsoc.org/doi/pdf/10.1175/1520-0469%281974%29031%3C0118%3AAPFTAO%3E2.0.CO%3B2`.

Lamb, B. K., J. B. McManus, J. H. Shorter, C. E. Kolb, B. Mosher, R. C. Harriss, E. Allwine, D. Blaha, T. Howard, A. Guenther, R. A. Lott, R. Siverson, H. Westberg, and P. Zimmerman (1995). Development of Atmospheric Tracer Methods To Measure Methane Emissions from Natural Gas Facilities and Urban Areas. *Environmental Science and Technology 29*, 1468–1479.

Larsen, I. (2010). Danmarks olie- og gasproduktion – og udnyttelse af undergrunden. Technical report, Energistyrelsen.

Larsen, M. (1996). Transportens eksterne effekter. Technical report, Det økonomiske råd.

Lawaetz, H. (2001). Omkostninger og miljøgevinster ved emissionsreduktioner. Technical report, Energistyrelsen. `http://www.ens.dk/graphics/Publikationer/Energipolitik/Omkostninger_og_miljoegevinster.pdf`.

Lehmann, K. K., G. Berden, and R. Engeln (2009). An Introduction to Cavity Ring-Down Spectroscopy. In G. Berden and R. Engeln (Eds.), *Cavity Ring-Down Spectroscopy – Techniques and Applications*, pp. 1–26. Blackwell Publishing.

Lin, T.-Y., U. Sree, S.-H. Tseng, K. H. Chiu, C.-H. Wu, and J.-G. Lo (2004). Volatile organic compound concentrations in ambient air of Kaohsiung petroleum refinery in Taiwan. *Atmospheric Environment 38*, 4111–4122.

Liou, K. N. (2002). *An Introduction to Atmospheric Radiation*. Academic Press.

Livesey, R. G. (1998). Flow of Gases Through Tubes and Orifices. In J. M. Lafferty (Ed.), *Foundations of Vacuum Science and Technology*. John Wiley & Sons, Inc.

Livesey, R. G. (2004). Solution methods for gas flow in ducts through the whole pressure regime. *Vacuum 76*, 101–107.

MacKay, R. M. and M. A. K. Khalil (1991). Theory and development of a one dimensional time dependent radiative convectice climate model. *Chemosphere 22*(3–4), 383–417.

Maersk Olie og Gas A/S (2012). Separationsprincipper – Gorm Basic Production. PowerPoint Presentation. Mærsk Olie og Gas A/S.

Manabe, S. and R. F. Strickler (1964). Thermal Equilibrium of the Atmosphere with a Convective Adjustment. *Journal of the Atmospheric Sciences 21*, 361–385.

McCarron, D. J. (2007). A Guide to Acusto-Optic Modulators. Course material for the course in Atomic and Molecular Physics at Durham University. `http://massey.dur.ac.uk/resources/slcornish/AOMGuide.pdf`.

Miljøministeriet (2010). *Samfundsøkonomisk vurdering af miljøprojekter*. Miljøministeriet. `http://www.mst.dk/Publikationer/Publikationer/2010/01/978-87-92548-71-9.htm`.

Miljøstyrelsen - Stab & Strategi (2005). Samfundsøkonomiske analyser: Problemstillinger og diskussioner. Webpage. `http://www.mst.dk/Virksomhed_og_myndighed/Gron_strategi/Miljoeoekonomi/Samfunds\T1\okonomiske+analyser/Analyser_og_rapporter/09050101.htm`.

Moe, M. (2011). *Miljøret*. Karnov Group.

Morvay, Z. K. and D. D. Gvozdenac (2008). *Applied Industrial Energy and Environmental Management*. John Wiley and Sons Ltd.

Myhre, G., N. Bellouin, T. F. Berglen, T. K. Berntsen, O. Boucher, A. Grini, I. S. A. Isaksen, M. Johnsrud, M. I. Mishchenko, F. Stordal, and D. Tanré (2007). Comparison of the radiative properties and direct radiative effect of aerosols from a global aerosol model and remote sensing data over ocean. *Tellus 59B*, 115–129.

Myhre, G., A. Grini, J. M. Haywood, F. Stordal, B. Chatenet, D. Tanré, J. K. Sundet, and I. S. A. Isaksen (2003). Modeling the radiative impact of mineral dust during the Saharan Dust Experiment (SHADE) campaign. *Journal of Geophysical Research 108*(D18, 8579). DOI: 10.1029/2002JD002566.

NASA (2008, September). RCM Guide – Reliability-Centered Maintenance Guide. Technical report, National Aeronautics and Space Administration. `http://wbdg.org/ccb/NASA/GUIDES/rcmguide.pdf`.

Nassar, R. H. (2012). Minimizing tank's still pipes movement. Presentation at Storage Terminal Operators Conference and Exhibition, Rotterdam, Netherlands.

NEC-bekendtgørelsen (2011). Bekendtgørelse om emissionslofter for svovldioxid, nitrogenoxider, flygtige organiske forbindelser og ammniak. `https://www.retsinformation.dk/forms/R0710.aspx?id=139538`.

Nielsen, M., O.-K. Nielsen, M. Plejdrup, and K. Hjelgaard (2010). Danish emission inventories for stationary combustion plants – inventories until 2008. Technical report, National Environmental Research Institute, University of Aarhus, Denmark.

Paulauskiene, T., V. Zabukas, and P. Vaitiekunas (2009). Investigation of volatile organic compound (VOC) emission in oil terminal storage tank parks. *Journal of Environmental Engineering and Landscape Management 17*(2), 81–88.

Peatross, J. and M. Ware (2012, March). *Physics of Light and Optics*. Brigham Young University.

Plejdrup, M. S. (2012, Accessed April 2012). Fugitive Emissions from Fuels. Webpage. http://www.dmu.dk/luft/emissioner/reportingsectors/fugitiveemissions/.

Poulsen, T. L. (2008). Ren luft til alle – indsats overfor luftforurening. Governmental strategy. http://www.mst.dk/NR/rdonlyres/A6D17706-2F26-4683-AA8E-387497E4BB52/0/Renlufttilalleindsatsoverforluftforurening14062008.pdf.

Ramaswamy, V., O. Boucher, J. Haigh, D. Hauglustaine, J. Haywood, G. Myhre, T. Nakajima, G. Y. Shi, and S. Solomon (2001). Radiative Forcing of Climate Change. In J. T. Houghton, Y. Ding, D. J. Griggs, M. Noguer, P. J. van der Linden, X. Dai, K. Maskell, and C. A. Johnson (Eds.), *Climate Change 2001: The Scientific Basis. Contribution of Working Group I to the Third Assessment Report of the Intergovernmental Panel on Climate Change.*, pp. 349–416. Cambridge University Press.

Rappenglück, B., P. Fabian, P. Kalabokas, L. G. Viras, and I. C. Ziomas (1998). Quasi-continous measurements of non-methane hydrocarbons (NMHC) in the Greater Athens area during MEDCAPHOT-TRACE. *Atmospheric Environment 32*(12), 2103–2121.

Reed, M., Øistein Johansen, P. J. Brandvik, P. Daling, A. Lewis, R. Fiocco, D. Mackay, and R. Prentki (1999). Oil Spill Modelling towards the Close of the 20^{th} Century: Overview of the State of the Art. *Spill Science & Technology Bulletin 5*(1), 3–16.

Regeringen (2011). Et Danmark der står sammen. Regeringsgrundlag. http://www.stm.dk/publikationer/Et_Danmark_der_staar_sammen_11/Regeringsgrundlag_okt_2011.pdf.

Rudd, H. J. and N. A. Hill (2001, August). Measures to Reduce Emissions of VOCs during Loading and Unloading of Ships in the EU. Technical Report B4/3040/99/116755/MAR/D3 Issue 2, European Comission – Directorate General Environment.

Rørledningsloven (2011). Bekendtgørelse af lov om etablering og benyttelse af en rørledning til transport af råolie og kondensat. https://www.retsinformation.dk/Forms/R0710.aspx?id=138659.

Seiler, W. (1974). The cycle of atmospheric CO. *Tellus 26*(1–2), 116–135.

Seinfeld, J. H. and S. N. Pandis (2006). *Atmospheric Chemistry and Physics*. John Wiley and Sons.

Shell (1995). Operating agreement between Dansk Olierør A/S and A/S Dansk Shell Terminal Facilities at Fredericia, Denmark.

Siegman, A. E. (1986). *Lasers*. University Science Books.

Sinden, A., D. A. Kysar, and D. M. Driesen (2009). Cost-benefit analysis: New foundations on shifting sand. *Regulation & Governance 3*, 48–71.

Sleigh, P. A. and I. M. Goodwill (1998). Section 1: Fluid Flow in Pipes. Course note to CIVE 2400: Fluid Mechanics 2.2, University of Leeds.

Smith, V. H. (1990). *The Economics of Technology*. Research Foundation of State University of New York. `http://www.math.dartmouth.edu/~mqed/NLA/EconomTech/EconomTech.phtml`.

Smyllie, R. (2003, February). Fredericia Terminal Emissions Study – Legislative Review. Technical report, Entec UK Limited.

Smyllie, R., R. Collitt, and J. Gullick (2005, July). DONG Terminal Degassing Plant Operating Pressure Review. Technical report, Entec UK Limited and Tractebel Gas Engineering.

Smyllie, R., I. Rogerson, P. Akehurst, T. Hall, I. Johnson, H. Isalski, and R. Collitt (2003, February). Emissions Reduction Study at the Fredericia Crude Oil Terminal. Technical report, Entec UK Limited and Tractebel Engineering.

Sozzi, R. and M. Favaron (1996). Sonic anemometry and thermometry: theoretical basis and data-processing software. *Environmental Software 11*(4), 259–270.

Spectrasyne Ltd (2002). A VOC emission survey of the DONG Crude Oil Storage facility, Fredericia, denmark. Technical report, Spectrasyne Ltd.

Spectrasyne Ltd (2009). Fugitive Hydrocarbon Emission Survey of 8 Crude Oil Storage Tanks at DONG Fredericia. Technical report, Spectrasyne Environmental Surveying.

Tekada, K., A. I. Tekada, J. Bryant, and A. Clegg (2007, September). Systematic review of the impact of emissions from aviation on current and future climate. Technical Report AFM 07/08, University of Southampton – School of Engineering Sciences Aerospace Engineering AFM.

the European IPPC Bureau (2001, September). Integrated Pollution Prevention and Control Draft Best Available Technique (BAT) on Emissions from Storage. Technical report, European Comission.

the European IPPC Bureau (2002, February). IPPC Reference Document on Best Available Techniques in Common Waste Water and Waste Gas Treatment/Management Systems in the Chemical Sector. Technical report.

the European IPPC Bureau (2003a, February). Integrated Pollution Prevention and Control – Reference Document on Best Available Techniques for Mineral Oil and Gas Refineries. Technical report, European Comission. `http://eippcb.jrc.es/reference/BREF/ref_bref_0203.pdf`.

the European IPPC Bureau (2003b, July). Integrated Pollution Prevention and Control – Reference Document on the General Principles of Monitoring. Technical report, European Comission. http://eippcb.jrc.es/reference/BREF/ref_bref_0203.pdf.

the European IPPC Bureau (2006). Integrated Pollution Prevention and Control – Reference Document on Best Available Techniques on – Emissions from Storage. Technical report, European Comission. http://eippcb.jrc.es/reference/BREF/esb_bref_0706.pdf.

Thoma, E. D., S. A. Thorneloe, R. R. Segall, R. B. Green, G. R. Hater, R. A. Hashmonay, M. T. Modrak, M. J. Chase, and C. D. Goldsmith (2008, June). Development of EPA OTM 10 for Landfill Applications, Interim Report. In *Proceedings of the 101st Annual Conference of the Air & Waste Management Association, Portland OR*.

Trafikministeriet (1997). *Samfundsøkonomisk omkostningseffektivitet i transportsektoren*. Trafikministeriet.

US DoD ESTCP (2008, September). ESTCP Cost and Performance Report - Optical Remote Sensing Method to Determine Strength of Non-point Sources. Technical Report SI-0214, U.S. Department of Defence – Environmental Security Technology Certification Program.

U.S. Environmental Protection Agency (1995). Compilation of Air Pollutant Emission Factors – Volume 1: Stationary Point and Area Sources. Technical report, Office Of Air Quality Planning and Standards, U.S. Environmental Protection Agency.

US EPA (2007, February). Evaluation of Fugitive Emissions Using Ground-Based Optical Remote Sensing Technology. Technical Report EPA/600/R-07/032, United States Environmental Protection Agency.

U.S. Patent 6,466,322 B1 (2002, October). SWEPT CONTINOUS WAVE CAVITY RING-DOWN SPECTROSCOPY. United States Patent. http://www.google.com/patents/US6466322.

Valks, P. J. M. and G. J. M. Velders (1999). The present-day and future impact of NO_x emissions from subsonic aircraft on the atmosphere in relation to the impact of NO_x surface sources. *Annals Geophysicae 17*, 1064–1079.

Van Vactor, S. A. (2010). *Introduction to the Global Oil & Gas Business*. PennWell Corporation.

Vandevoorde, D. (1998, April). The Maximal Rectangle Problem. http://www.drdobbs.com/database/the-maximal-rectangle-problem/184410529.

Weatherill, S. (2010). *Cases and Materials on EU Law* (9th Edition ed.). Oxford University Press.

Wilczak, J. M., S. P. Oncley, and S. A. Stage (2001). Sonic Anemometer Tilt Correction Algorithms. *Boundary-Layer Meteorology 99*, 127–150.

Williams, J. and R. Koppmann (2007). Volatile organic compounds in the atmosphere: An overview. In R. Koppmann (Ed.), *Volatile Organic Compounds in the Atmosphere*, pp. 1–32. Blackwell Publishing.

Winther, M. (2008). Danish emission inventories for road transport and other mobile sources – inventories until year 2006. Technical report, National Environmental Research Institure, University of Aarhus, Denmark.

Ørum Nielsen, N. (2008). *Operational User Guide – DONG Degassing unit 9600*. Nielsen Senior Consult.

Index

Appendix A

Beskrivelse af opstilling til måling af emission fra en olietank

Dato: 14-09-12

A.1 Overordnet måle-princip

Forsøget bygger på den fremgangsmåde der i terminologien kaldes tracer-release. Målemetoden er en indirekte målemetode, som er velegnet til måling af kilder med diffus emission. I den videnskabelige literatur er metoden anvendt til emissionsmålinger af f.eks. lossepladser, marker og gylletanke. Metoden er valgt pga. sine lave omkostninger og sine lave krav til ikke mindst antallet af måleinstrumenter.
Metoden består i at den emission af gas man gerne vil måle (i dette tilfælde metan(CH_4), som repræsentation for den samlede emission af flygtige organiske forbindelser) spores ("trace" på engelsk) vha. en sporgas som ikke findes i emissionen i forvejen. Der laves altså et kunstigt udslip af spor-gas (i dette tilfælde acetylen (C_2H_2)) til atmosfæren. Herefter måles koncentrationen af både emissions-gas og sporgas samtidig i en vis afstand fra kilden som illustreret på figur A.1. Det er så antagelsen, at under tidsligt gennemsnitlige statiske forhold, gælder følgende sammenhæng:

$$\frac{Q_{CH_4}}{Q_{C_2H_2}} = \frac{C_{CH_4}}{C_{C_2H_2}}$$

Hvor Q_x er emissionen af stof x til atmosfæren, og C_x er koncentrationen af stof x til atmosfæren. Da de to koncentrationer måles og emissionen af sporstoffet er kontrolleret, kan den gennemsnitlige emission af emission-gassen bestemmes ved beregning. Det er vigtigt at sikre en god opblanding af emissions-gas og spor-gas for at få gode resultater. Derfor er det vigtigt at geometrien af spor-gas-udslippet så præcist som muligt matcher geometrien af emissions-gas-udslippet.
Sporgassen acetylen er valgt på baggrund af at det anvendte måleinstrument (Picarro G2203 Cavity Ring Down Spectrometer) er designet til samtidig måling

af metan og acetylen. Desuden oplyser producenten at acetylen som sporstof har følgende fordele:

- Molarmassen af acetylen er 26, hvilket er tæt på atmosfærisk luft. Det betyder at gassen ikke har nogen naturlig tendens til at stige til vejrs eller deponere på jorden, men transporteres med vinden.
- Den atmosfæriske halveringstid er ca. 13 dage, hvilket betyder at stoffet i denne sammenhæng er kemisk inert, dvs. den kemiske nedbrydning af stoffet forløber meget langsomt. Desuden betyder denne nedbrydningstid at gassen ikke er en nævneværdig klimagas, og emmission af denne gas giver derfor ikke problemer med myndighederne.

Desuden findes acetylen ikke i udslippet af flygtige organiske forbindelser fra tanken i forvejen (jvf. tidligere foretaget undersøgelse af Spectrazyne), hvilket gør det velegnet som sporstof.

A.2 Opstilling

Princippet i forsøgsopstillingen er illustreret på figur A.2. I det følgende gennemgås de enkelte elementer i opstillingen i den rækkefølge, som spor-gassen oplever dem på sin vej fra gasflasken til atmosfæren.
Kilden til gassen er en gruppe af enkeltstående gasflasker. Der skal til forsøget anvendes 9 flasker á 6.4kg (40L). Dette er beregnet ud fra at AGA oplyser at det maksimale flow fra en sådan flaske er 1000l/t v. 15 $°C$. Under antagelse af at forsøget kan gennemføres på 14 dage ved 8 timers arbejde om dagen, hvor der kan lukkes gas ud i halvdelen af tiden skal der anvendes ca. 40 kg. acetylen. For at forhindre at der undervejs løbes tør for gas, er det påkrævede antal flasker ganget med 1.5. Ovenstående beregning skal udelukkende forstås som en måde at estimere mængden af anvendt gas og ikke som en faktuel beskrivelse af forsøgets udførelse. En beskrivelse af fremgangsmåden er præsenteret længere nede.
Foruden ovenstående mængde acetylen leveres også et nitrogen-batteri, hvor højtryksslangen kobles på således at systemet kan "skylles igennem" med nitrogen før og efter at forsøgene går i gang.
Batteriet placeres på vej nr. 28 som vist på vedhæftede tegning "Tegning2.pdf". Efter aftale med Shell bestilles batteriet af Shell, for at udnytte den allerede eksisterende aftale mellem Shell og AGA. Shell sørger desuden for placering af batteriet, samt udstyring af batteriet med blink el. lign. i overensstemmelse med procedurene. Fra batteriet løber en AGA højtryksslange, som muliggør flaskeskift, til et stativ designet og fremstillet på RUC, som udgør holder til lovpligtig flammespær, reduktionsventil og AGA 85-30 flammespær. Gassen passerer herefter en lovpligtig flammespær, en reduktionsventil og en flammespær. Ventilenheden er tegnet på figur A.3, fitting imellem reduktionsventil og flammespær er tegnet på figur A.4 og en foreløbig tegning af ventilenheden samt stativet til ventilenheden er vist på figur A.5 Herefter løber gassen ind i hovedslangen.
Shell sørger for det værktøj, der lever op til sikkerhedsforeskrifterne, der skal bruges til betjening af udstyret herunder flaskeskift. I tilfælde af brand skal det være muligt hurtigt at kappe forbindelsen til gassen således at gasflaskerne ikke

er "bundet fast" med slangen. Shell sørger for værktøj (kniv, tang el. lign.) til dette formål.
Udgangstrykket indstilles ved at prøve sig frem således at der opnås et flow der er stort nok til at signalet kan detekteres i den påkrævede afstand fra tanken og samtidig ikke større end påkrævet for at opnå ovennævnte signal. Dette sker naturligvis under hensyntagen til at det beregnede flow ikke overstiger 1000l/t, som er det maksimale flow der må lukkes ud fra en enkelt acetylen gasflaske ifølge DS/INF 111.
Hovedslangen er en 19mm AGA acetylen-slange. Shell undersøger ledningsevnen af hovedslangen og sørger for jordforbindelse eller lignende såfremt dette er påkrævet. For at forebygge faldskader ved trappen til tanken, placeres hovedslangen under kabelgennemføring når den passerer tværs over trappen. Kabelgennemføringen er vist på figur A.6–A.7.

Hovedslangen fastgøres til trappen til taget af tanken med messingtråd ved trappens fæstninger til tanken, som vist på vedhæftede "Tegning1.pdf". Hovedslangen monteres af Shell. På tank-gauging-platformen fastgøres hovedslangen til et styrerør som indikeret på vedhæftede "Tegning3.pdf". På flydetaget fastgøres hovedslangen ligeledes til et styrerør som er fastgjort til flydetaget som indikeret på vedhæftede "Tegning3.jpg". Styrerørne designes, fremstilles og monteres af Shell.
På flydetaget ved foam-dam'en kobles hovedslangen til et T-stykke som vist på figur A.8–A.10. T-stykket med tilhørende flammespær er vist på figur A.11. De enkelte elementer er tegnet på figur A.12–A.15. T-stykket og fittings fremstilles af RUCs mekaniske værksted. T-stykket fastgøres til flydetaget med to 30kg magneter samt tilhørende beslag som vist på figur A.16. T-stykket og flammespærene placeret i beslagene til fastgørelse som kan ses på figur A.17. Beslagene til fastgørelse af T-stykke med tilhørende flammespær fremstilles af RUCs mekaniske værksted. I hver side af T-stykket fastgøres en flammespær samt en 8mm fordeler-acetylen-slange efter samme mekanisme som fastgørelsen af hovedslangen. Fordelerslangerne og T-stykke monteres af Shell. Disse kobles herefter til en udblæser-enhed efter samme mekanisme som tilkoblingen af hovedslangen, således at de 20 udblæsere kommer til at sidde i to halvcirkler lige indenfor foam dam'en rundt langs kanten af flydetaget. For enden af hver halvcirkel placeres en udblæser med en prop, som vist på figur A.25. Udblæser-enhederne fastgøres ligeledes til flydetaget med magneter. Udblæser-enheden og enkelt-dele er tegnet på figur A.18 til figur A.24. På hver enkelt tegning er beskrevet, hvilket materiale det enkelte element er fremstillet af. Udblæser-enheden designes og produceres på RUCs mekaniske værksted. Udblæser-enheden samles og monteres af Shell.

A.3 Fremgangsmåde

Forsøget gennemføres af RUC-studerende og DONG-ansat Thor-Bjørn Ottosen (THOTT) og DTU-studerende Jakob G. Mønster (JAGM). Inden forsøget igangsættes har både THOTT og JAGM gennemgået Shell sikkerhedskursus (er allerede gennemført). Ved arbejde på terminalen er THOTT og JAGM iført antistatisk tøj, sikkerhedssko med ankelbeskyttelse, sikkerhedshjelm og

sikkerhedsbriller, samt relevant udstyr i relation til H_2S. Desuden er relevante tilladelser såsom arbejds- og køretilladelse inhentet inden forsøget går i gang.
Inden selve målingen af emissionen fra tanken foretages en undersøgelse af om der skulle ligge forstyrrende kilder til acetylen (f.eks. svejseværksteder o.lign.) i nærheden af tank 9805 og som kan forstyrre målingerne fra tanken. Denne undersøgelse foretages ved at måleapparatet køres en runde på terminalen i en bil, som leveres af DONG. Bilen køres af JAGM. Under kørslen suger måleapparatet atmosfærisk luft ind igennem bilens vindue via en slange og analyserer den for metan og acetylen. Datablad for måleapparatet Picarro G2203 CRDS er vedlagt. Måleapparatet får strøm fra to stk 12 V, 110 Ah Marine/fritid batterier som sidder i serie. De to batterier er forbundet til en 1000 W converter, der laver de 12V DC om til 110/220V AC. I tilfælde af forstyrrende kilder i nærheden tilstræbes målingerne foretaget når der ikke er nærliggende acetylen-emission f.eks. om aftenen/natten.
Inden målingen af emissionen fra tanken kontrolleres det fra tank-gauging platformen at der ikke er opstået knuder o. lign. på slangen. Set-up'et kobles herefter til nitrogen-batteriet og der lukkes nitrogen igennem systemet i en periode lang nok til at alle slangerne er fyldte.
Selve emissions-målingen foretages ved at måleapparatet placeres på DONGs mark nord for terminalen i en afstand på 100-200m fra tank-kanten. Måleapparatet tændes. Herefter kobles hovedslangen til gasflasken og der åbnes for gas-flowet ved det rigtige tryk. Efter en rum tid som afgøres ved at prøve sig frem lukkes for gas-flowet igen. Under hele processen er der kontakt imellem personen ved gasflaske-batteriet og personen ved måleinstrumentet på marken nord for terminalen vha. walkie-talkies udleveret af Shell. Det tænkes som hovedregel at JAGM er placeret ved måleapparatet og THOTT er placeret ved gasflaske-batteriet. En hypotetisk data-serie er afbilledet på figur A.26. Ved tiden t_1 åbnes for spor-gassen. Afstanden imellem t_1 og t_2 afgøres af hvor hurtigt det pneumatiske setup fyldes med acetylen, samt vindhastigheden der afgør hvor hurtigt spor-gassen transporteres fra tanken til måleinstrumentet. Som tommelfingerregel er det tidsinterval aftanden fra tanken til måleinstrumentet divideret med vindhastigheden. Ved t_3 lukkes for spor-gassen. Afstanden mellem t_1 og t_3 er tænkt som 10 minutter. Brugbare måle-data er i tidsintervallet t_2 til t_4. Hvis, baseret på inspektion af de opnåede måledata, intervallet t_2 til t_4 ikke er langt nok til at opnå brugbare data, kan intervallet hvor spor-gassen frigives (t_1 til t_3) forlænges.
Efter at der igen er lukket for gas-flowet kobles måleapparatet til en skærm og et tastatur i bilen på marken nord for terminalen, hvorefter dataenes kvalitet vurderes.
Hvis de opnåede data vurderes gode kan proceduren med undtagelse af undersøgelsen af baggrundskilder samt inspektion fra tank-gauging platformen, gentages for at verificere de opnåede data. Undersøgelsen af baggrundskilder vil kun blive gentaget ved omslag i de meteorologiske forhold som målt ved klimamast på DONGs mark nord for terminalen. Hvis de opnåede data ikke vurderes tilfredsstillende kan prodecuren med undtagelse af undersøgelsen af baggrundskilder samt inspektion fra tank-gauging platformen, gentages med en ny placering af måleinstrumentet. Dette gentages indtil tilfredsstillende resultater er opnået og verificeret eller et på forhånd aftalt antal timer er gået. Det forventes

at hver måling inklusiv tilkobling og frakobling af hovedslange, inspektion fra tank-gauging platformen og vurdering af data kan gennemføres på en time. Når der ikke foretages flere målinger resten af dagen kobles nitrogen-batteriet til igen og på samme måde som før målingerne lukkes der gas igennem systemet.
Når de første tilfredsstillende målinger er taget vil de følgende målinger blive koordineret med Shell drift og i forhold til vejrudsigten, da målingerne kun kan foretages ved vind fra vest-sydvestlig retning, for at foretage målinger i alle fem operationelle tilstande på tanken (Bottom Dip, Filling, Top Dip, Static, Rundown). Disse målinger vil blive foretaget efter samme fremgangsmåde som beskrevet ovenfor.
Når disse målinger er foretaget på tilfredsstillende vis vil Shell drift blive bedt om at bypasse degassing-anlægget i en periode, hvorefter de samme målinger som med degassing-anlægget vil blive foretaget efter samme fremgangsmåde som ovenfor, således at emissionerne fra tanken igen måles i alle fem operationelle tilstande. Under måling med bypass af degassing-anlæg måles døgnet rundt for at sikre at perioden med bypass af degassing-anlægget bliver så kort som muligt. proceduren for bypass af degasser foreslås at være som følger:

1. Tank 9805 tømmes inden bypass af degasseren. Det er vigtigt for målingerne at der ikke er rester af afgasset olie i tanken.

2. Degasseren settes i bypass.

3. Tank 9805 fyldes med ikke-afgasset olie. Dette tager tilpas lang tid til at det skulle være muligt (ved den rigtige vindretning) at få foretaget en eller flere gode målinger af tanken.

4. Top dip (tanken er helt fuld). Ved dialog med driften, er vi klar med målesystemet når tanken når sit fyldningspunkt. En eller flere målinger foretages afhængig af forholdene. Når målingerne er taget eller den afsatte tid er opbrugt, gives besked til driften.

5. Tømning af tanken påbegyndes. Målinger foretages som ved fyldning.

6. Efter dialog med driften stoppes tømningen af tanken undervejs, således at tilstanden Intermediate standing kan måles. Dette foretages på samme måde som Top dip.

7. Herefter fortsætter tømningen af tanken. Afhængig af om det er lykkedes at foretage gode målinger ved første halvdel af tømningen tages evt. flere målinger her.

8. Når tanken igen er tom foretages målinger af tilstanden Bottom dip, efter samme princip som Top dip og Intermediate standing.

Maksimal degasser nedetid: 72 timer, evt. kortere afhængig af hvor let det går med at måle Top dip, Intermediate standing og Bottom dip. Senest 72 timer efter start af bypass af degasser startes degasseren op igen. I denne periode kan der evt. udføres vedligehold på degasseren.

A.4 Forhold under gennemførsel af målinger

Acetylen er en stærkt brændbar gas. Antændelsesgrænsen for acetylen er 2,5% (volumen). For at afgøre størrelsesforholdene, beregnes koncentrationen af acetylen i volumet over tank-taget ved tank-taget helt i bund, under antagelse af god opblanding i hele volumet og ingen opblanding med den overliggende atmosfære. Dette er udregnet som et worst-case scenarie. Volumet over tank-taget er ca. $35000m^3$. Ved en release-rate på 0,2g/s for alle udblæsere på en gang og en målingsvarighed på 10 minutter, hvilket har været designkriteriet for målingen, frigives der 120g acetylen. Vha. idealgas-ligningen beregnes volumen af denne mængde for et tryk på en atmosfære og en temperatur på $20°C$ til $0{,}110m^3$. Dette medfører at koncentration på ca. $3 \cdot 10^{-4}$% (volumen) altså langt under antændelsesgrænsen. Ydermere vil der ikke blive foretaget målinger under vindstille forhold, da der kræves vind for at transportere gassen fra tanken til måleinstrumentet. Dette forhold betyder at der vil ske en vis opblanding i tanken med ren atmosfærisk luft, og dermed vil koncentrationerne blive endnu lavere.

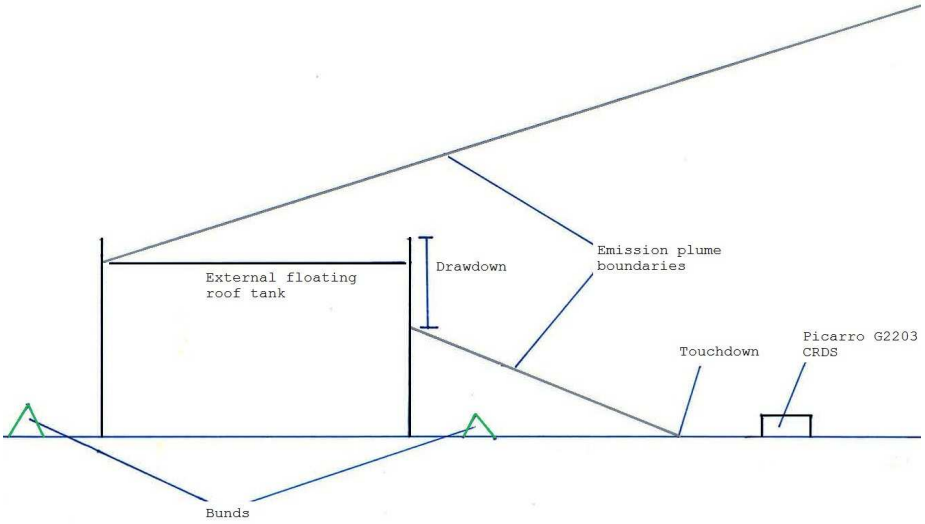

Figure A.1: Illustration af emissionen fra tanken og placeringen af måleinstrumentet. Tegningen er ikke målfast.

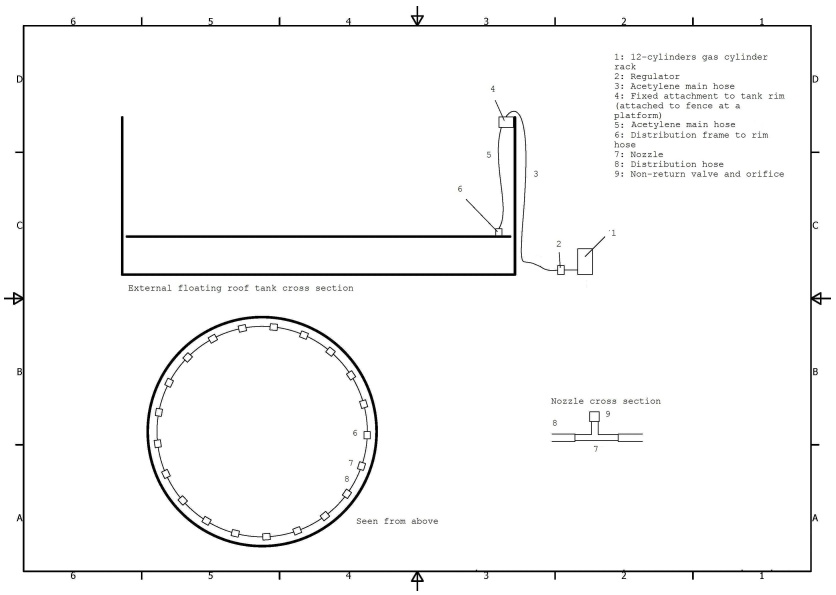

Figure A.2: Illustration af princippet i det kontrollerede udslip. Tegning er ikke målfast.

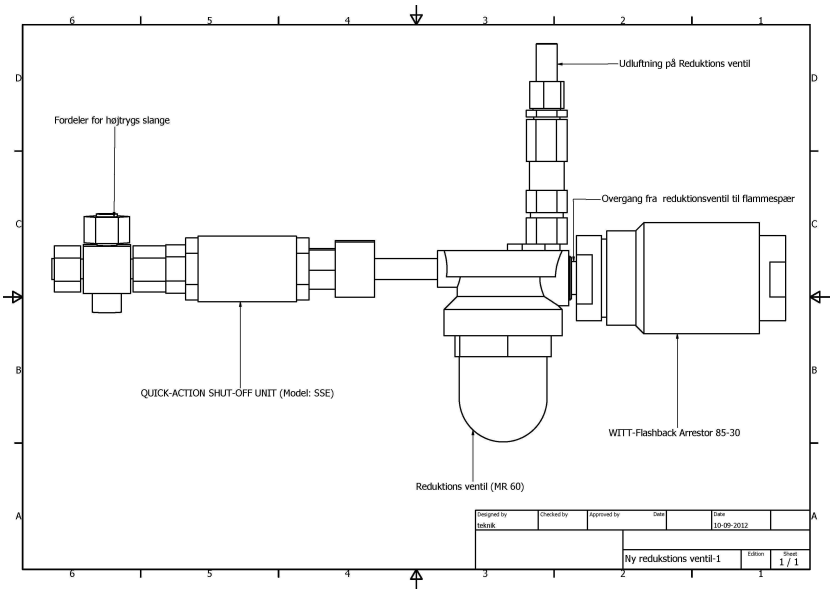

Figure A.3: Tegning af lovpligtig flammespær, reduktionsventil og flammespær

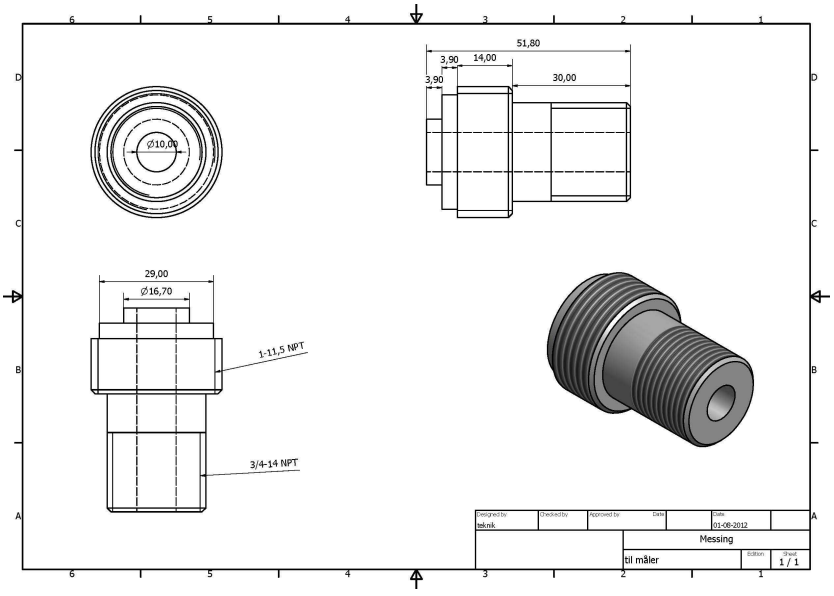

Figure A.4: Tegning af overgangen fra reduktionsventil til flammespær.

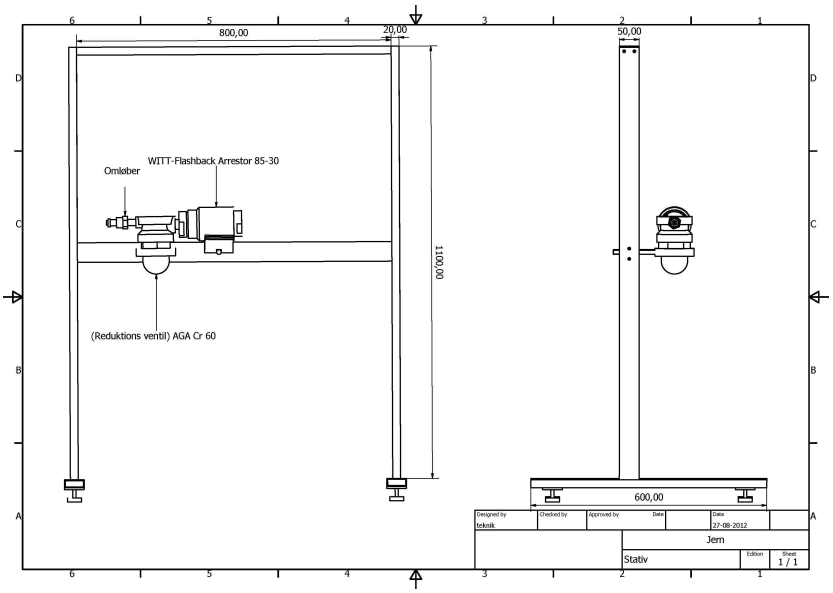

Figure A.5: Foreløbig tegning af stativ der holder ventil-assembliet. Stativet vil blive modificeret således at den nye ventilenhed tegnet på figur A.3 kan fastgøres.

Figure A.6: Fotografi af kabelgennemføring af gummi til forebyggelse af faldskader. Stållinealen er 60cm lang.

Figure A.7: Fotografi af kabelgennemføring. Højden er ca. 10cm.

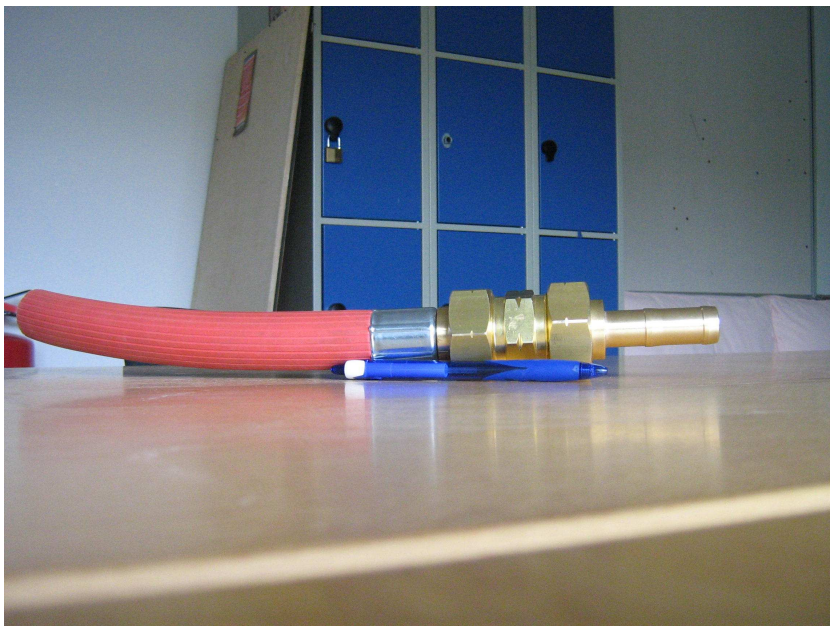

Figure A.8: Fotografi af fastgørelse af slange til T-Stykke og udblæsere.

Figure A.9: Fotografi af fastgørelse af slange til T-Stykke og udblæsere.

Figure A.10: Fotografi af fastgørelse af slange til T-Stykke og udblæsere.

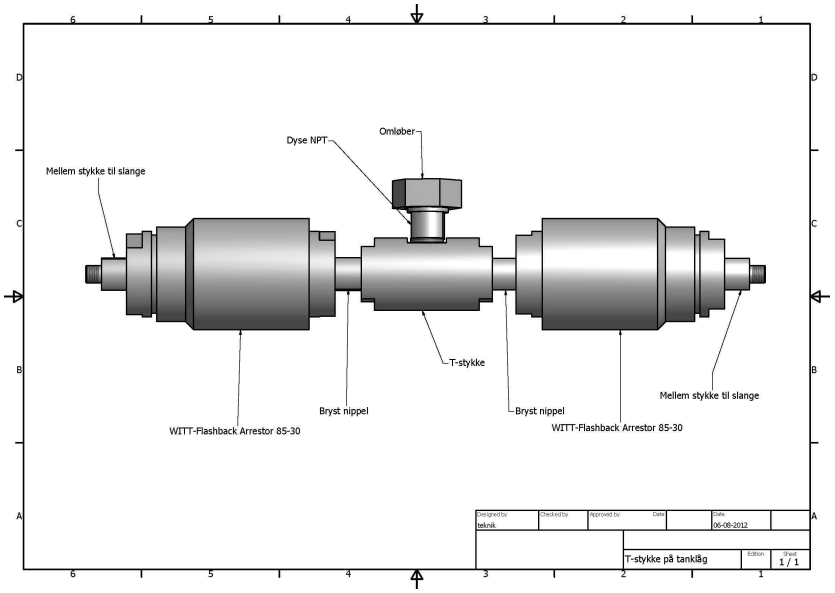

Figure A.11: Tegning af T-stykke med tilhørende flammespær og fittings.

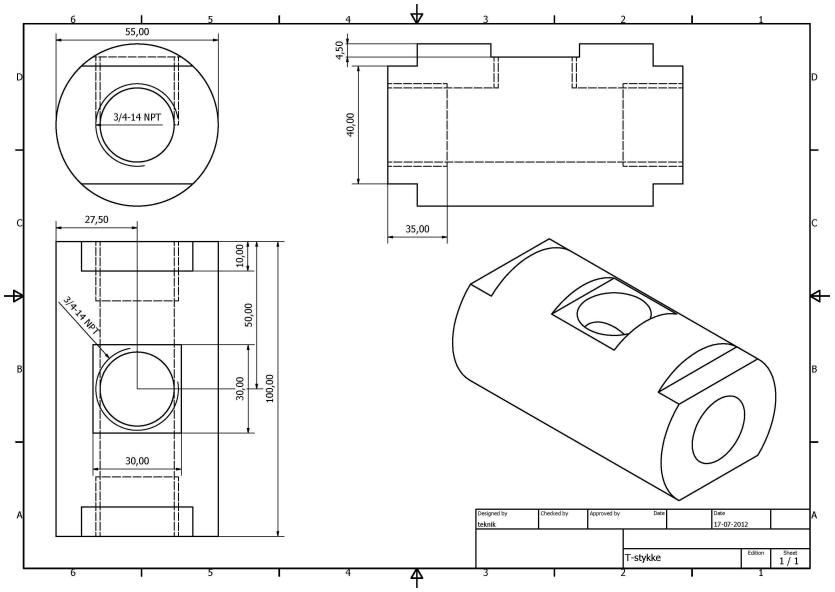

Figure A.12: Tegning af T-stykke. Materialet er messing.

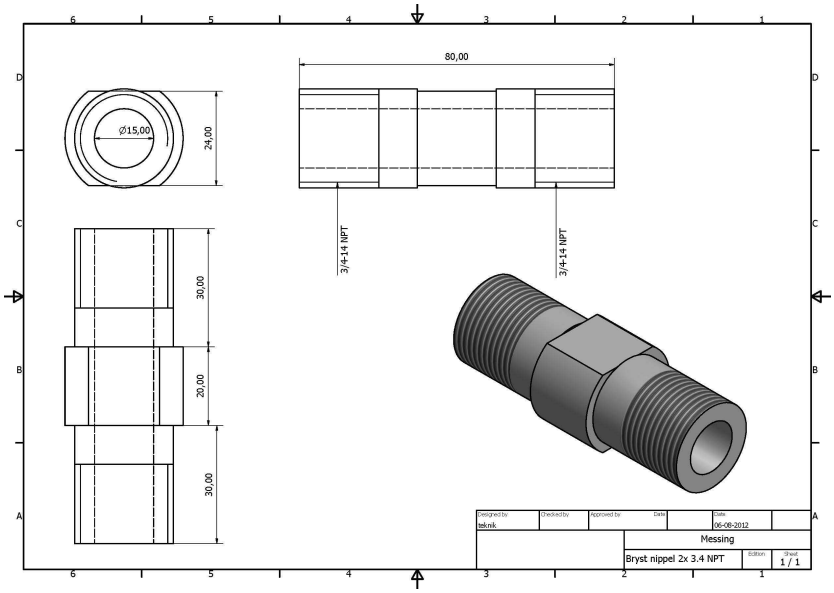

Figure A.13: Tegning af fitting mellem T-stykke og flammespær

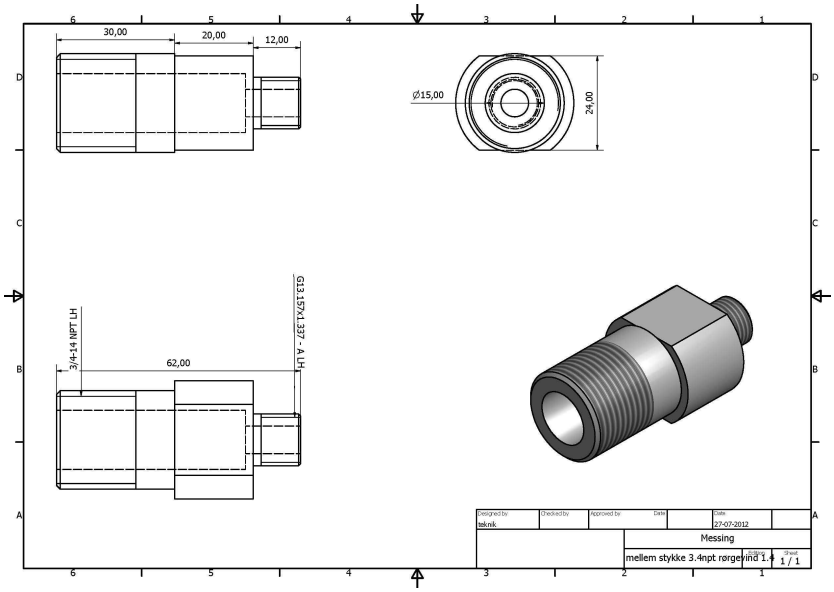

Figure A.14: Tegning af fitting mellem flammespær og fordelerslange

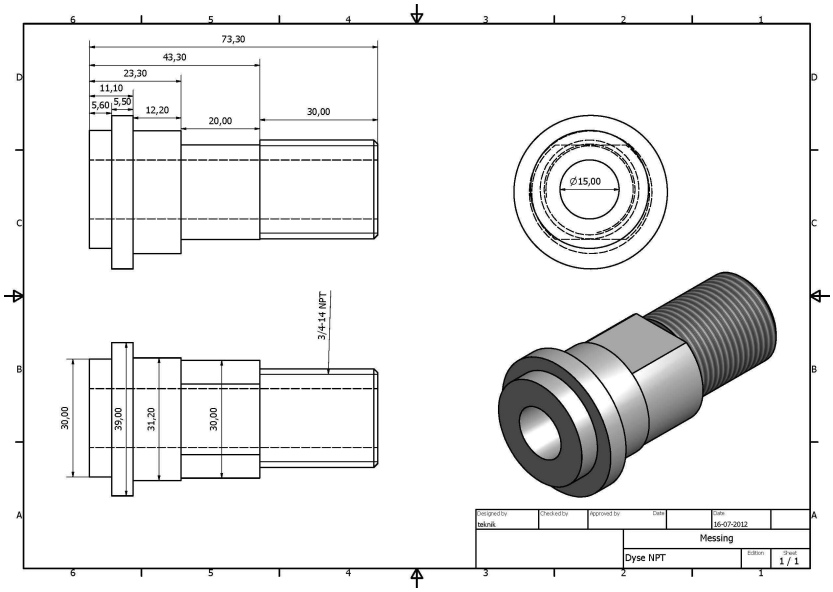

Figure A.15: Tegning af fitting mellem T-stykke og hovedslange

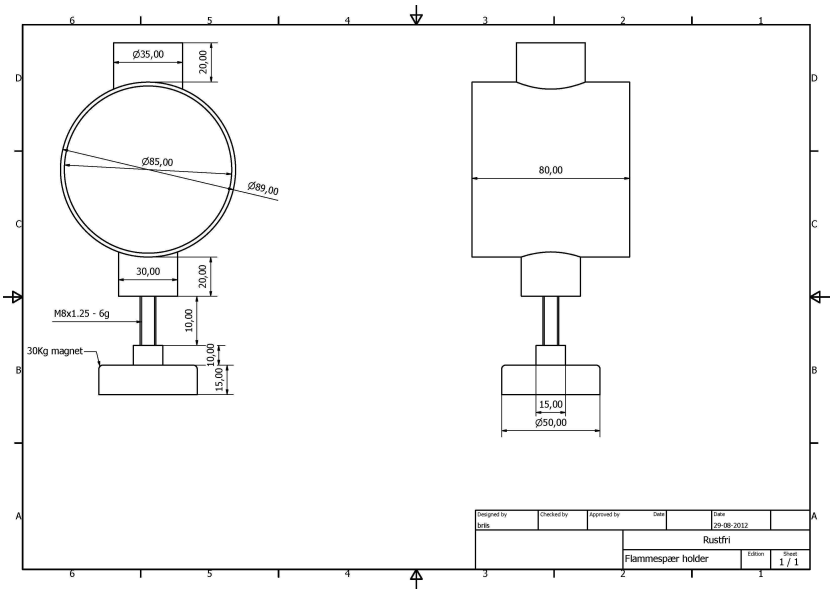

Figure A.16: Magnet og beslag til fastgørelse af T-stykke med tilhørende flammespær. Der anvendes to af disse til fastgørelsen.

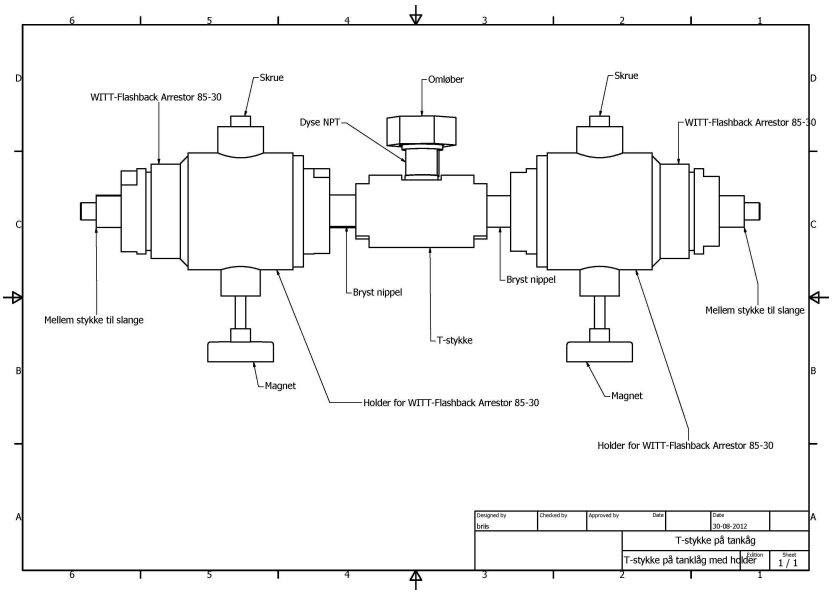

Figure A.17: T-stykke og flammespær placeret i holder til fastgørelse på flydetag.

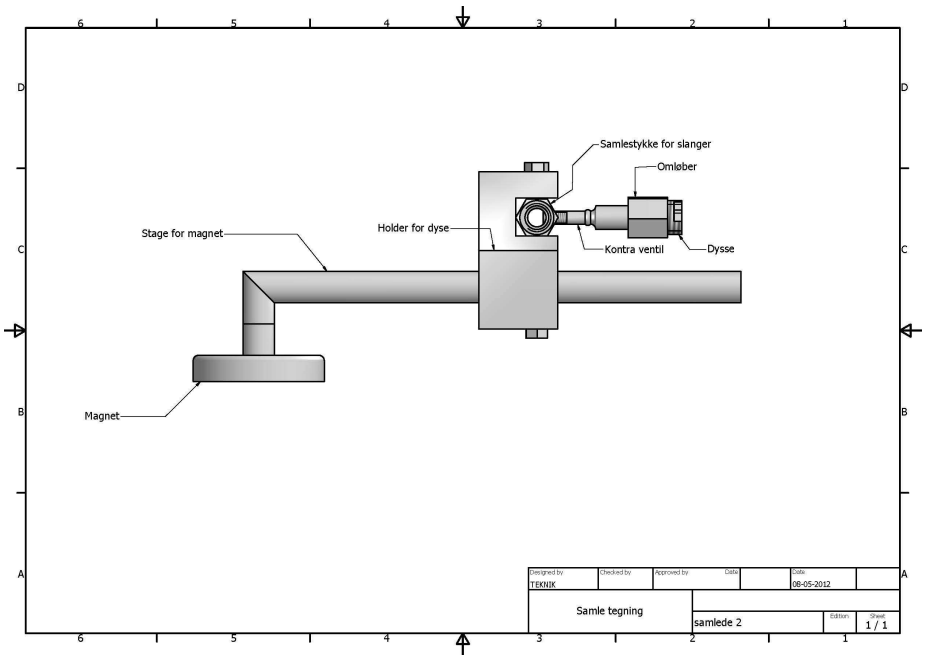

Figure A.18: Tegning af den samlede udblæser.

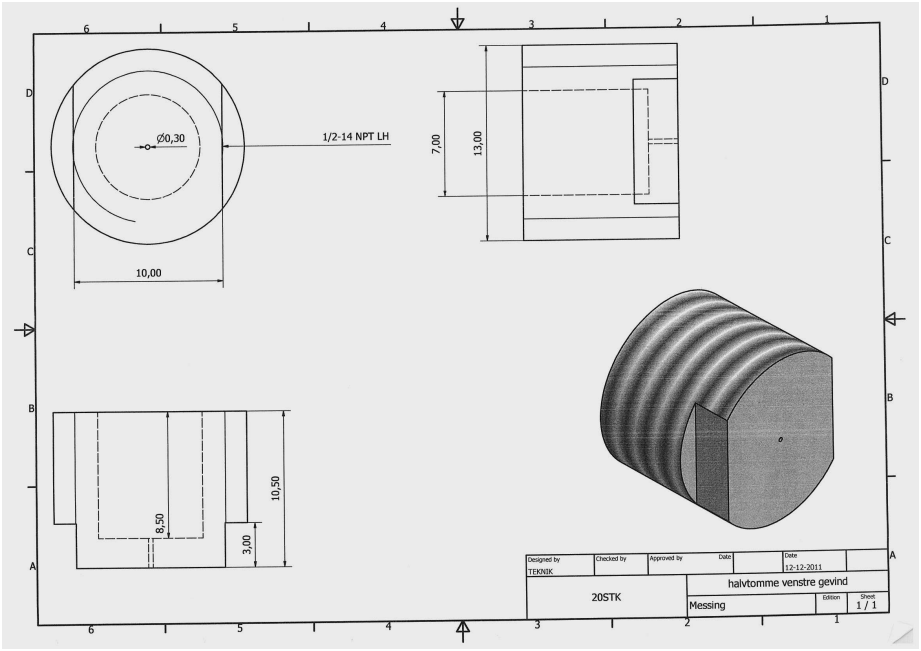

Figure A.19: Tegning af dysen.

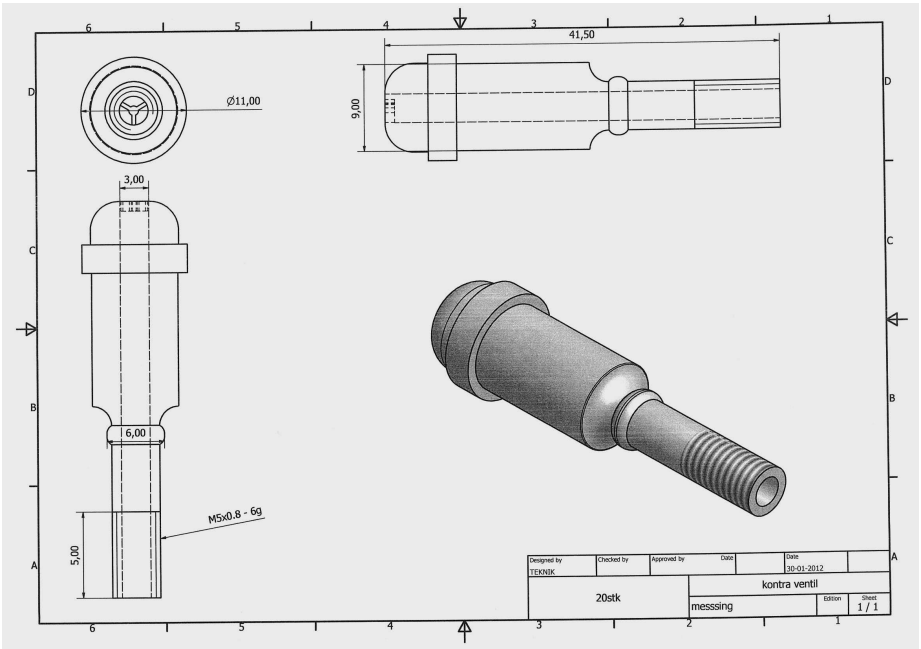

Figure A.20: Tegning af kontraventilen.

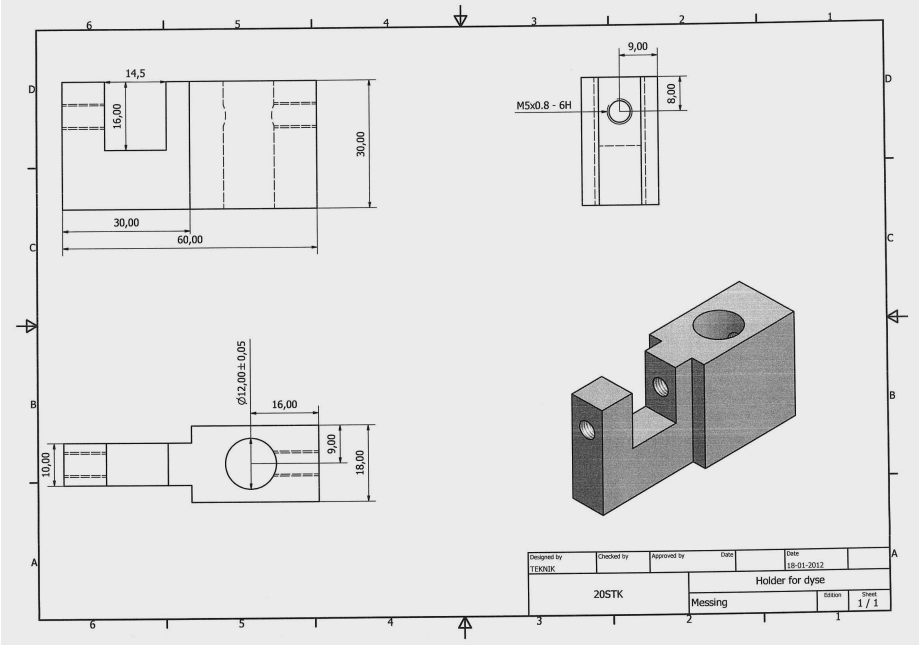

Figure A.21: Tegning af holderen.

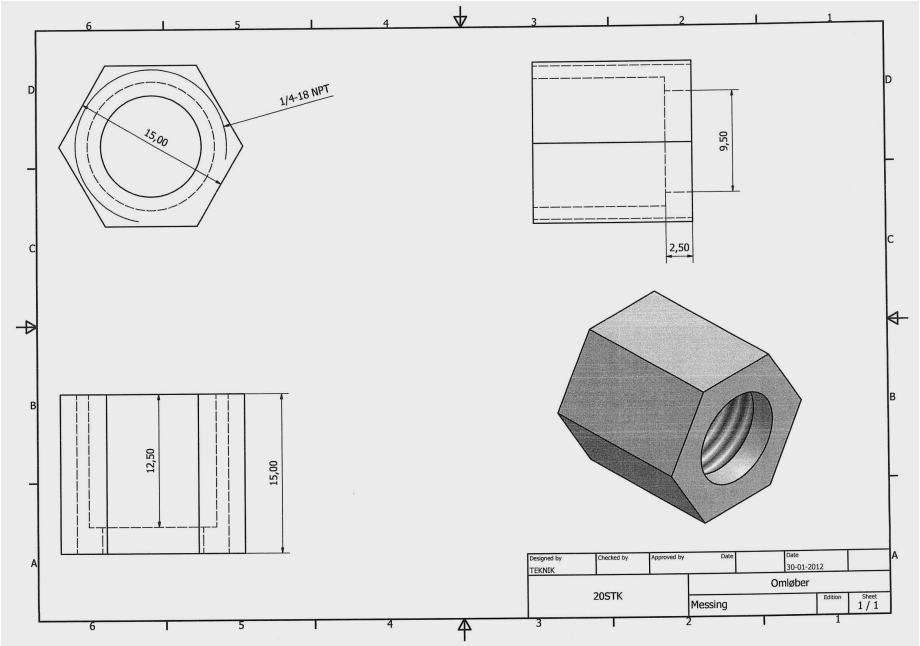

Figure A.22: Tegning af omløber.

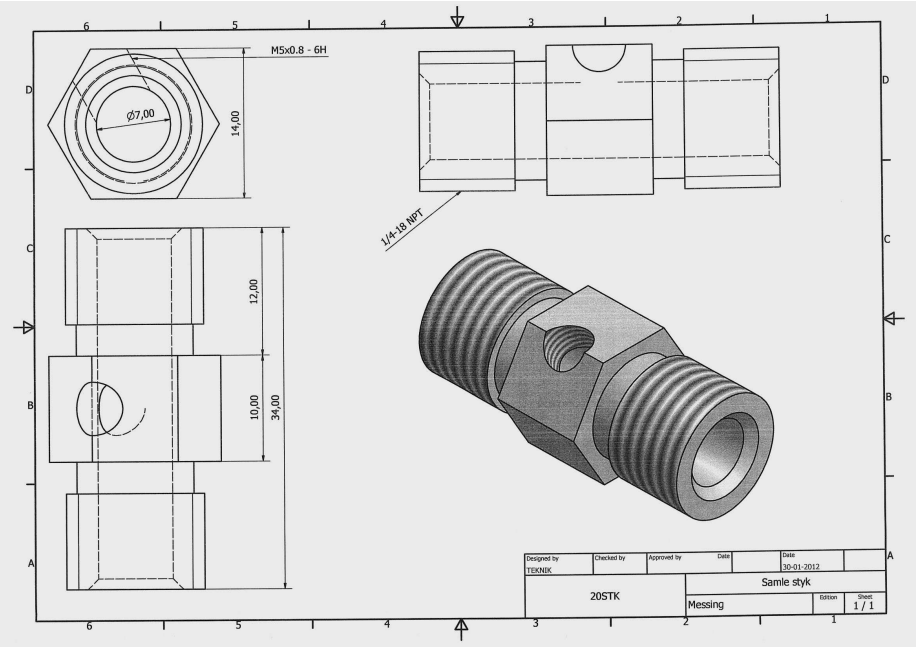

Figure A.23: Tegning af samlestykke.

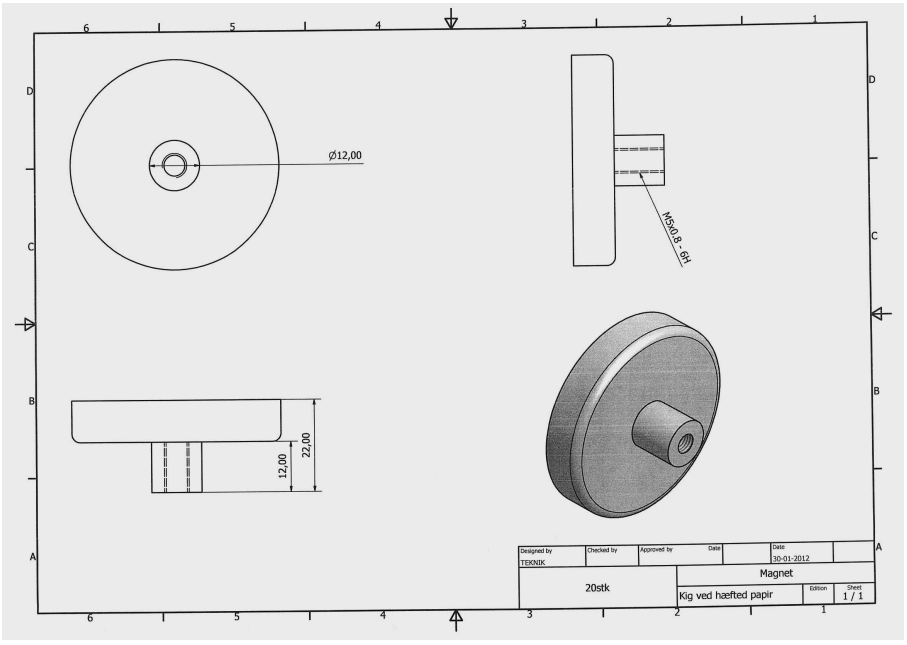

Figure A.24: Tegning af magnet. Beskrivelse af magnet findes i vedhæftede katalog fra Bakker Magnetics side 33. Modellen hedder BM 31.030 og forhandles af Hindsbro Magneter APS, Sdr. Ringvej 32, 4000 Roskilde, tlf.: 46351788.

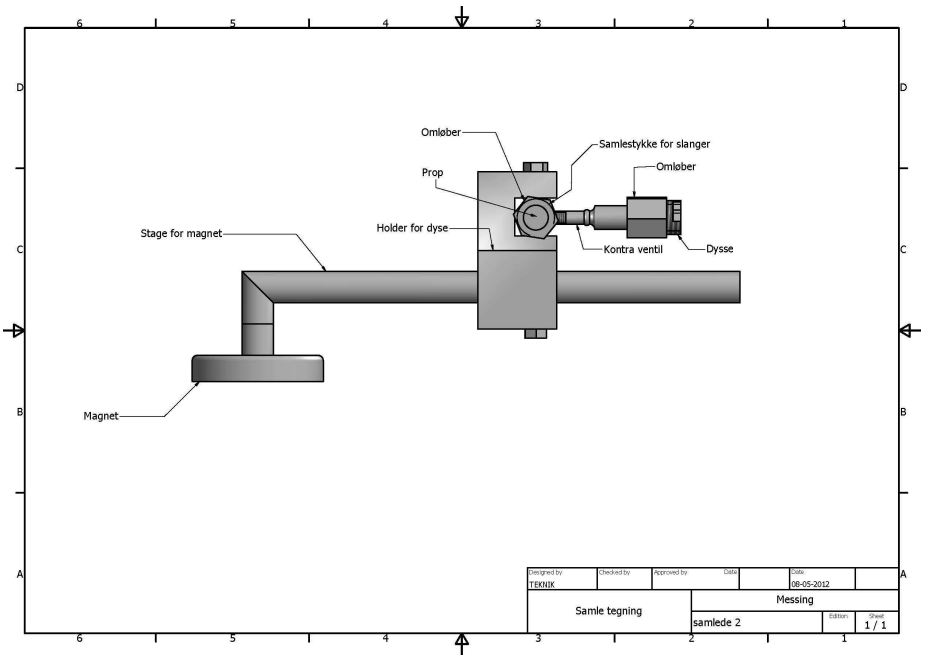

Figure A.25: Tegning af udblæser for enden af hver halvcirkel.

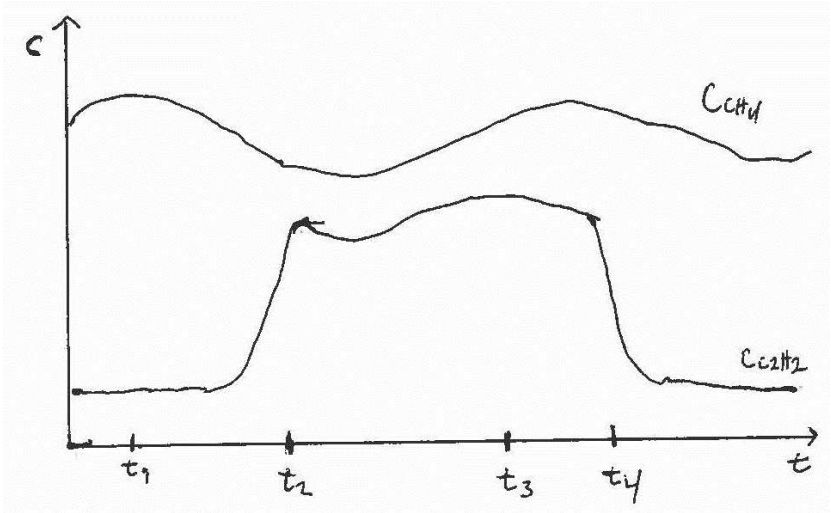

Figure A.26: Hypotetiske data for en måleserie. X-aksen er tiden og y-aksen er koncentrationen af henholdsvis metan og acetylen. Data er ikke målfast.